University of Stavanger

FACULTY OF SCIENCE AND TECHNOLOGY

MASTER'S THESIS

Study program/specialization: **Petroleum Engineering/ Drilling Technology**	Spring/Autumn semester, 2021 Open
Author: **Hallvard Titlestad**	***Hallvard Titlestad*** (Signature of author)
Supervisor(s): **Mesfin Belayneh**	
Title of master's thesis: ***Effect of nano-SiO_2 , nano-Al_2O_3 , MWCNT and FA on properties of Portland G-class cement***	
Credits: 30	
Keywords: Portland Cement Nanoparticles SiO_2 Al_2O_3 MWCNT UCS UCS Modelling Rheology Heat of Hydration Varying curing ages Fly ash Nanoparticles Bond Strength	Number of pages: **142** + Supplemental material/other: **62** (Appendix) 15/06/2021, Stavanger

Abstract

Cement is an important element in oil and gas wells, as it provides structural integrity and acts a barrier to prevent unwanted leakages in the well. According to NORSOK D-010 standard, properties of cement are required to be impermeable, ductile, resistant to corrosive substances and non-shrinking [1]. However, a well integrity survey in the North Sea Continental Shelf (NCS) conducted by PSA (2006) showed that 10.67% of reported well integrity issues were associated with cement related failures [2]. Furthermore, a survey in Alberta, found that approximately 14490 wells suffered from gas migration issues originating from poor cement jobs [3]. In fact, a survey conducted in 2001, found that primary cements jobs had a failure rate of roughly 15% [4]. Additionally, in 2010, a survey found that 20% of detected well integrity issues were due to poor zonal isolation and annular integrity, likely as a result of cement failures [5]. These surveys show that cement as a barrier material does not maintain lifelong well integrity, which does not satisfy the regulatory requirements.

Nanotechnology (1-100nm) is a growing technology that seeks to introduce novel and superior properties which could create innovative solutions for conventional technologies and engineering problems across several fields of studies. The application of nanotechnology in the petroleum industry has also shown promising results. Therefore, in this thesis, the impact of nanoparticles and fly ash on neat G-class cement has been investigated. A total of five different experimental designs were formulated, which were cured for 3, 7 and 28 days. Nanoparticles and FA as additives exhibited predominantly favourable results in several of the tested properties of neat G-class cement. SiO_2 nanoparticles exhibited high early strength with 23,27% and 26,95% UCS improvement after 3 and 7 days. A binary blend of Al_2O_3 and SiO_2 nanoparticles yielded 26,64% UCS increase after 28 days. Small concentrations of FA gave a 21,24% UCS improvement after 28 days of curing. A ternary blend of nanoparticles and fly ash mixed with SiO_2 also provided improved properties of neat G-class cement after 28 days of curing. The empirical uniaxial compressive strength (UCS) vs compressional wave velocity (Vp) model developed from measured data in this thesis, has shown quite good predictions of UCS.

Acknowledgments

Firstly, I would like to express my gratitude to my supervisor Mesfin Belayneh Agonafir for his mentoring and counselling during this thesis as his advice and assistance has been invaluable. Not only is he highly knowledgeable and available from early mornings to late evenings, but he is also highly passionate of educating others. He goes the extra mile in order to teach his vast knowledge to his students by always prioritizing his students before himself.

Secondly, I would like to thank the University of Stavanger for letting me utilize their laboratory equipment and supplying me with required materials to conduct the experimental portion of this thesis. Their thorough handling of HSE information before using any lab equipment and infection control has been commendable. As a result, this thesis has for the most part been unaffected by the ongoing pandemic.

Finally, I would extent my gratitude towards family and friends who always provided motivation in times of need throughout the semester.

Table of content

List of figures

List of tables

List of equations

Nomenclature

A= Cross-sectional area, mm^2

E = Young's modulus, MPa

F_{max} = Max load applied before failure, N

G = Shear modulus, GPa

K = Bulk modulus, GPa

M = P-wave-modulus, GPa

M_w = Mass wet (after submersion in water), g

M_d = Mass dry (before submersion in water), g

ΔM = Change in mass, %

R = Resilience, J/m^3

Vp = Compressional wave velocity, m/s

ρ = Density of the given cement plug, kg/m^3

$\Delta\sigma$ = change in stress, MPa

$\Delta\varepsilon$ =change in strain, dimensionless

σ_y = Uniaxial compressive strength at yield point, Pa

ε_y = Strain at yield point, dimensionless

τ = Shear stress, $lb_f/100ft^2$

τ_c = Casson yield stress, $lb_f/100ft^2$

μ_c = Casson plastic viscosity, $lb_fs/100ft^2$

γ = Shear rate, Sec^{-1}

Abbreviations

API = The American Petroleum Institute

ASV = Annular Safety Valve

ASTM = American Society for Testing and Materials

DAQ = Data Acquisition Software

EOR = Enhanced Oil Recovery

FA = Fly Ash

HPHT = High Pressure High Temperature

ID = Inner Diameter

ISO = International Organization of Standardization

MWCNT = Multiwalled Carbon Nanotubes

MK = Metakaolin

NCS = Norwegian Continental Shelf

NP = Nanoparticle(s)

OD = Outer Diameter

OPC = Ordinary Portland Cement

PSA = Petroleum Safety Authority

PV = Plastic Viscosity

P&A = Plug and Abandonment

RPM = Rotations Per Minute

SCP = Sustained Casing Pressure

SCVF = Surface Casing Vent Flow

SF = Silica Fume

TB= Test batch

TM= Test matrix

UCA= Ultrasonic cement analyser

UCS = Uniaxial Compressive Strength

w/b = Water to binder

WBM = Water-Based Mud

WCR = Water to Cement Ratio

WOC = Wait on Cement

wt% = Weight percent

YP = Yield Point

%bwoc = Percent by weight of cement

%bwob = Percent by weight of binder

1 Introduction

Portland G-class cement is commonly used for oil and gas well construction and for plug and abandonment operations. The primary functions are generally to ensure well integrity and prevent undesired fluid leaks to reach the surface. However, well integrity surveys show that conventional cement exhibits failures and does not fully satisfy the regulatory requirements from NORSOK D-010. This suggests the need for improvements to G-class cement as it is the most abundantly used well cement. Therefore, this thesis presents an experimental study regarding the effects regarding various nanoparticles and fly ash as additives to 0.44 WCR neat G-class cement. The properties of the cement were characterized through destructive- and non-destructive experiments. Moreover, the literature studies on the application of nanotechnology with regards to cement along with the theory to characterize the cement properties are presented. Additionally, an empirical model was developed from the recorded test data, which can be used to estimate uniaxial compressive strength (UCS) of cement from the compressional wave velocity (Vp).

1.1 Background and motivation

The primary objective of any oil and gas well is to extract hydrocarbons from the reservoir in a safe and economical manner. For this, the well should be properly designed and constructed making sure that the well maintain long term structural integrity. Figure 1.1 shows a sketch of typical well construction comprises of conductor casing, surface casing, intermediate casing, production casing, a liner and surrounding cement. The structural elements of the well in general should be designed to carry operational loading such as temperature and pressure in order to withstand various failure mechanisms such as collapse, burst, corrosion and deformation

In NORSOK D-010 well integrity is defined as "*Application of technical, operational and organisational solutions to reduce risk of uncontrolled formation fluids throughout the lifecycle of a well"* [1]. Additionally, in NORSOK D-010, cement has the following regulatory requirements [1].

Listed below:

- Impermeable
- Non-shrinking

- Provide long term integrity
- Ductile – able to withstand mechanical loads and impact
- Ensure bonding to steel
- Resistant to corrosive substances

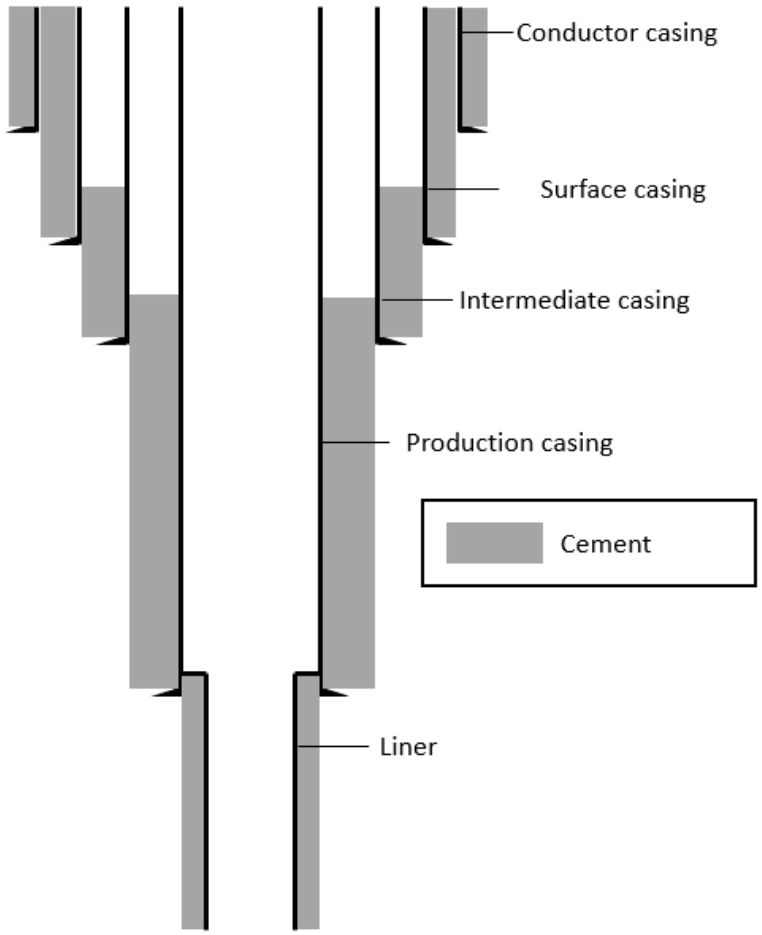

Figure 1.1 Typical well construction and the primary cement job

In terms of well integrity, cement is primarily used to seal the spacing found between the formation and casing, also called the annulus. The objective with this is to support the casing and restrict fluid from flowing in the annular space between the casing and formation, thus improving zonal isolation in the well and creating a hydraulic seal. This is referred to as the primary cement job and is done by pumping cement slurry into the wellbore in such a way that the slurry travels up the annular space between casing and formation and harden there. The primary cementing procedure is paramount, and if it is unsuccessful, a remedial cement job ought to commence to ensure well integrity [4].

To further establish the importance of cement in a well, one must comprehend that cement has many utilizations within a well. In NORSOK D-010 cement is regarded as both a primary and a secondary well barrier. However, which role the cement plays as barrier is dependent upon the state of the well. During normal operations, it is regarded as a secondary barrier. However, in some cases the liner cement acts a primary barrier, i.e., during a temporary P&A operation, where X-mas tree and BOP is removed [1]. A barrier is an element which will prevent unwanted flow from a potential source. As there always should be at least two barriers in place, some barriers are primary preventors, while others are secondary. Furthermore, cement aids with corrosion protection for the casing, which is done by shielding the steel casing from harsh fluids and gases such as H_2S, brine and CO_2, increasing the longevity of the well.

Cement can also be employed in other well operations such as P&A, well intervention and well completion. One such usage is to cement a section such that the cement acts as a plug between zones in the wellbore. This can be done both temporarily or permanently depending on the well operation. Currently, during a permanent plug and abandonment operation, cement is commonly used as the material for plugging as its cheap and relatively abundant. Arguably, it may not be the best suited plugging material, especially with respect to perpetuity, for reasons which will be introduced shortly. Figure 1.2 shows how cement could be utilized in a permanent P&A operation.

As mentioned before, wellbores are subjected demanding environmental conditions such as high temperatures, high pressures, and fluids and gases that cause corrosion both presented naturally and introduced operationally. Temperature and pressure in the well are often widely different based on the operation and phase in the lifecycle of a well. Ultimately, fluctuations in pressure and temperature can cause the casing and cement sheath to expand and contract differently, which can crack the cement due to stresses introduced by the fluctuations. This is often referred to as cracking. Of equal importance, is the term debonding, which describes when either the casing-cement or cement-formation debond. Essentially, a failure between cement and casing/formation interface. There are several factors which might be the source of debonding [4].

Listed below:

- Cement shrinkage over time
- Stimulation operations, such as intentional fracturing

- Gradual pressure depletion as the well is produced
- Thermal and pressure fluctuations
- Subsidence resulting in casing movement

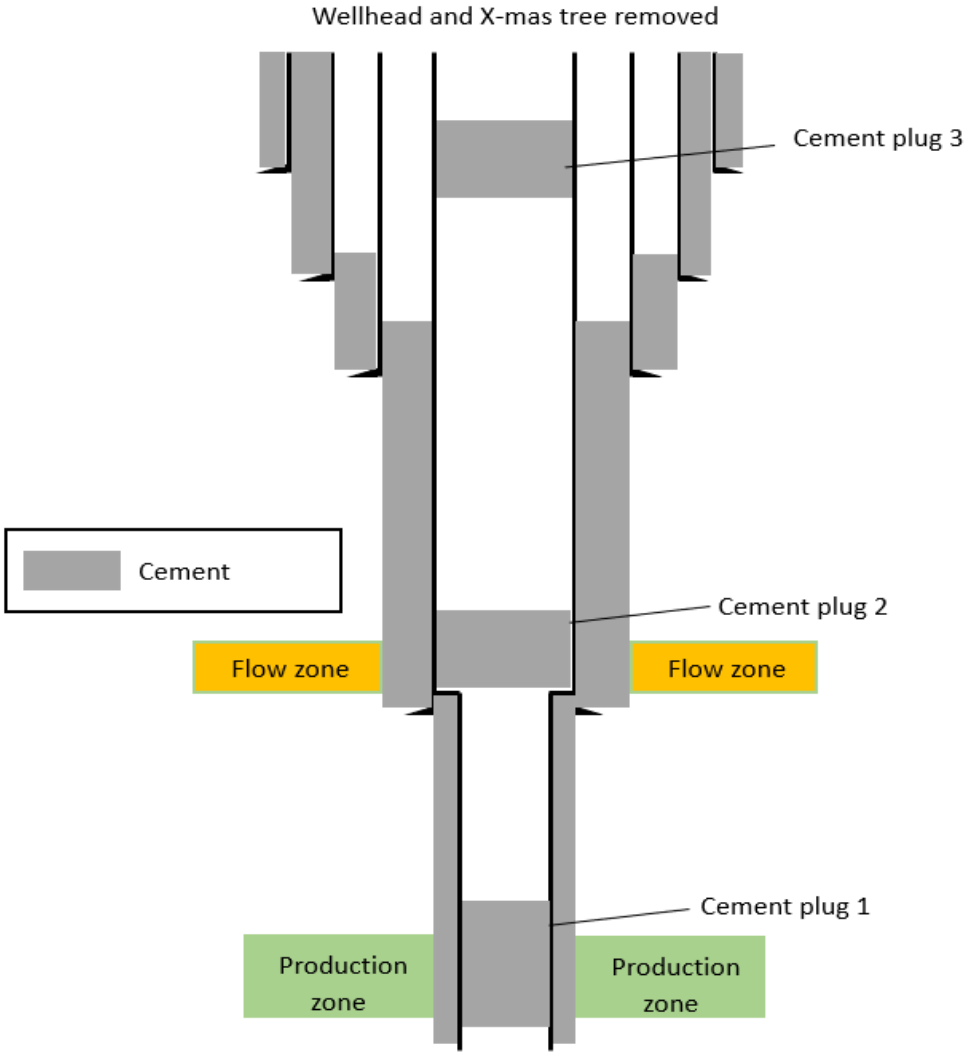

Figure 1.2 Cement plugs in a permanent plug and abandonment scenario

These scenarios listed are hard to avoid during the lifespan of a well. Additionally, a third term can be introduced which also can compromise cement integrity. Often called shear failure, which usually manifests as an absolute failure of the cement sheath. This is frequently a result of stress escalation around the wellbore, primarily caused by movements or vibrations. Subsidence as the reservoir depletes or self-inflicted vibrations during well operations may cause cement shear failure [4].

The common denominator of debonding, shear failure and cracking are that the cement integrity is impaired, thus resulting in a compromised well integrity. If the cement succumbs to the challenging environment posed by the demanding well environment, migration pathways might be formed in the cement, where fluids and gases can leak through, which can result in severe ramifications.

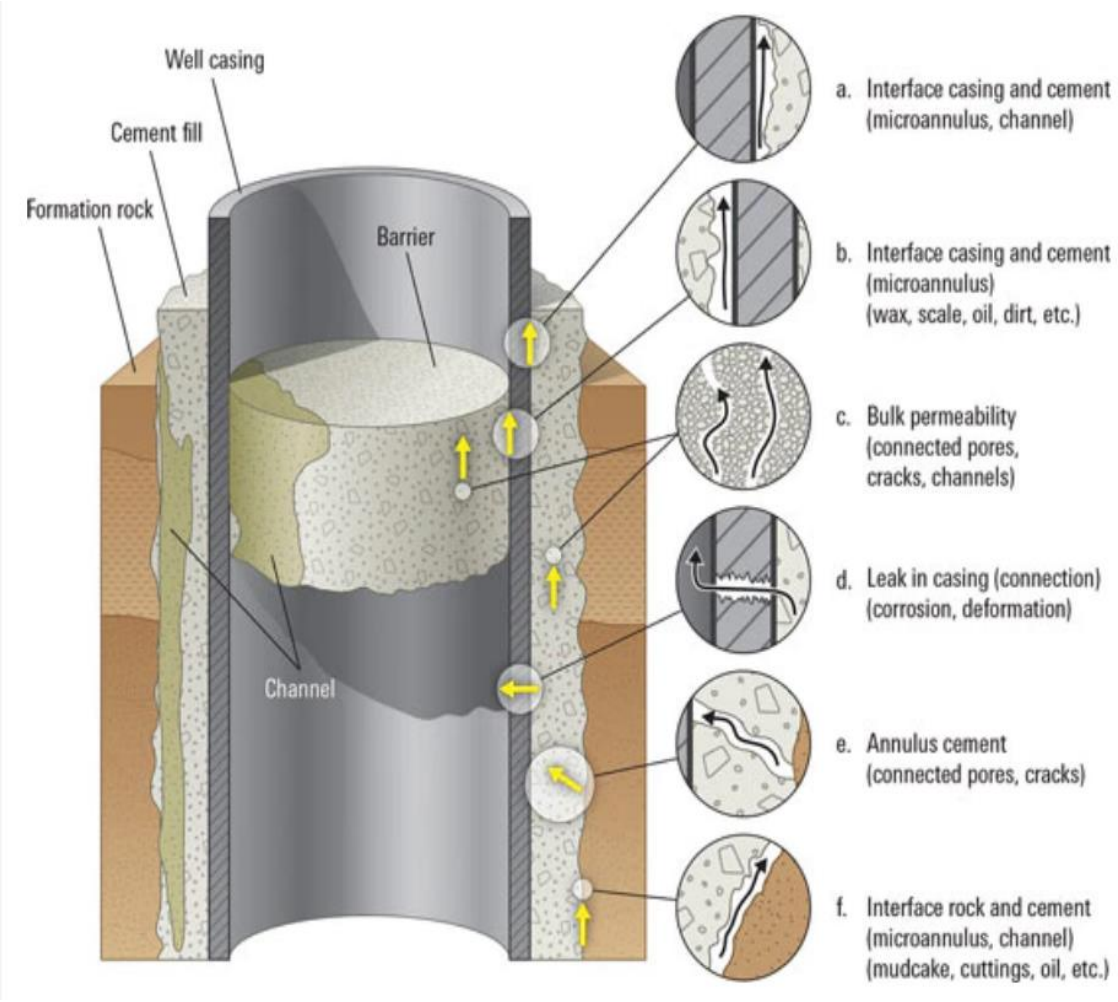

Figure 1.3 Potential leakage pathways present in compromised cement [6]

Figure 1.3 illustrates how the terms introduced above can cause failure in the cement sheath, it is observed that (a), (b), (f) are leakage paths likely originated from poor debonding between interfaces. In addition, (c), (e) could be a result of fractured cement. Finally, (d) is caused by casing failure by the likes of corrosion or deformation.

Furthermore, several surveys have found that cement failures are one of the most prevalent causes for diminished well integrity. According to "*Well-Integrity Issues Offshore Norway*" by Aadnøy and Vignes (2008) [2] it was found that 75 wells out of 406 wells were subject to well integrity issues.

Figure 1.4 displays causes for compromised well integrity from the survey. From figure 1.4, it is observed that 38,67% of cases of well integrity problems were due to tubing related issues, whereas 12% was caused by ASV issues and 10.67% by casing and cement related problems, respectively. The main culprits of the cement related issues were leaks in the annulus due to poor bonds between the formation and the casing. Furthermore, leaks were also discovered in through micro annulus in the cement [2]. Of the reported casing related issues, it is likely some of the blame could be put on cement failures, as leakages through cement can cause casing issues, such as sustained casing pressure (SCP).

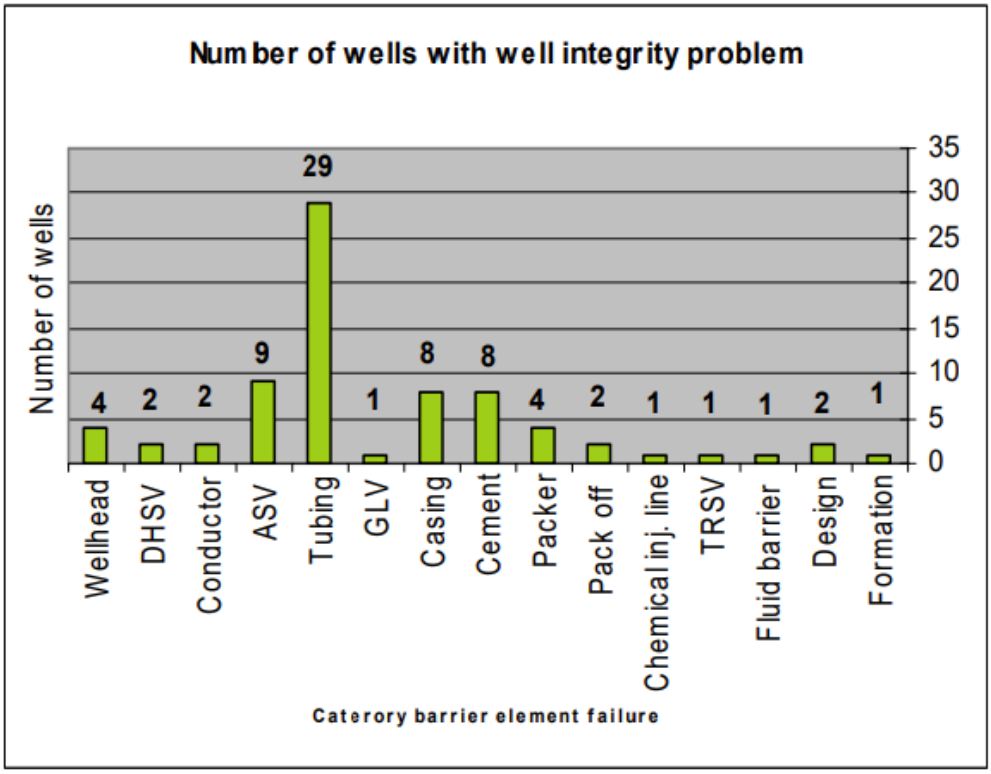

Figure 1.4 Exhibits well integrity issues of 75 NCS wells [2].

Another survey conducted by US Minerals Management Service found that 6650 out of 14927 wells surveyed was affected by SCP [4]. This is a superfluous and persistent casing pressure, which reoccurs if bled down [7]. One of the most prevalent reasons for SCP is leakage of gas or fluids during the primary cement job. More severe cases of SCP can shorten the lifespan of a well and pose HSE risks [4].

EUB (Energy and Utilities Board) in Alberta, Canada is in possession of data from 315 000 oil and gas wells. And from these 315 000 wells, it is estimated that approximately 4,6% of the wells has experienced issues regarding SCVF (Sustained casing vent flow) and GM (gas

migration). Furthermore, the study stated that majority of these issues occurred at shallower depths and poor cementing in the upper sections were to blame for some of these instances [3].

Moreover, in 2011, Ken Feather presented "*Better Well integrity*" on behalf of Archer, where he showed figure 1.5. The presented data was based on a OTM and Archer market survey in 2010 done about well integrity and performance failures. Based on this figure it is observed that failures in annular integrity and zonal isolation were present in 20% of the cases which had experienced well integrity and performance failures [5]. Although, the presentation does not specifically mention cement failures, its within good reason to assume that of the 20% failures caused by poor zonal isolation and annular integrity, cement is one of the main culprits. Corrosion was also an issue experienced in 14% of the cases. Cement likely played a role here as well, as it can contribute to this issue by not protecting adequately against corrosive elements in the wellbore.

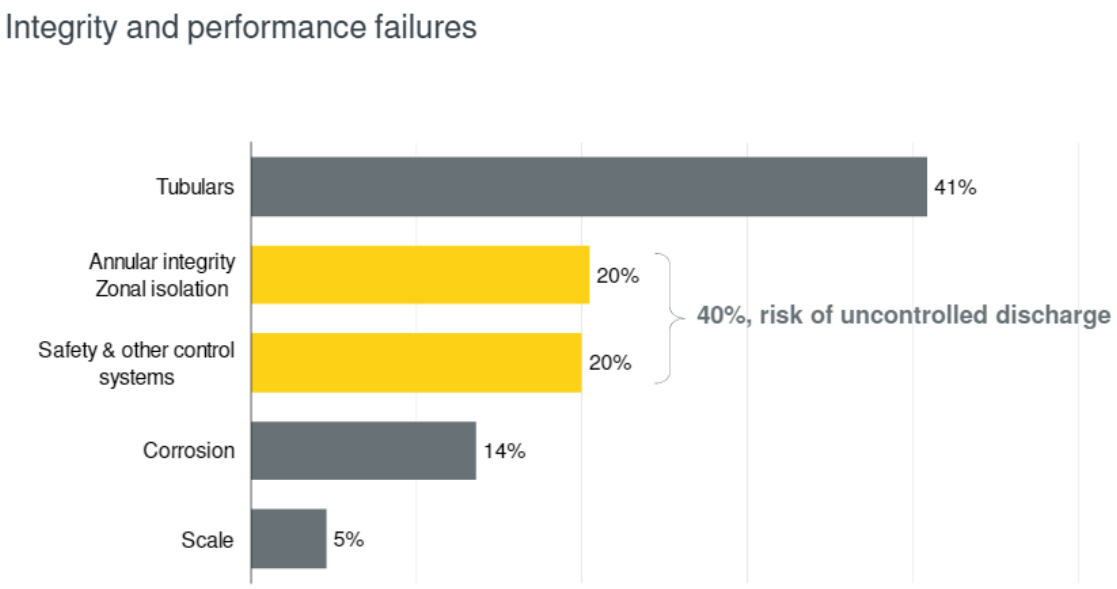

Figure 1.5 Failures affecting well performance from OTM and Archer market survey [5].

The surveys introduced all indicates that loss of well integrity is recurrent and cement contributes noteworthy to the issue. Severe leakages from a well, could have significant environmental ramifications and be the root of sustained personnel injuries and worst-case loss of human life. Aside from this, loss of cement integrity can lead to diminished production from the well, reduced lifespan of the well, expensive remedial operations and possible fines by governmental agencies depending on the severity of the case. Improving cement composition will help to mitigate the amount of well integrity issues, by reducing the cases where the root is cement related problems.

Even though, the petroleum industry may not seem like the hottest topic currently, due to the increased focus and awareness around climate, environment and sustainability of our energy sources. Whether we like it or not, the petroleum industry is still the largest supplier of energy, as can be seen from figure 1.6. It is observed that oil amounts to 33,1%, coal to 27% and natural gas to 24,2% of the primary energy shares. In total, oil and gas garner 57,3% of the world's energy share and will likely remain this way for the many years to come. Therefore, well integrity is a global issue as oil and gas wells are the highest supplier of energy. Conclusively, as cement is an integral part in the well integrity equation, and it plays an essential role to continue the fuel our rising energy consumption.

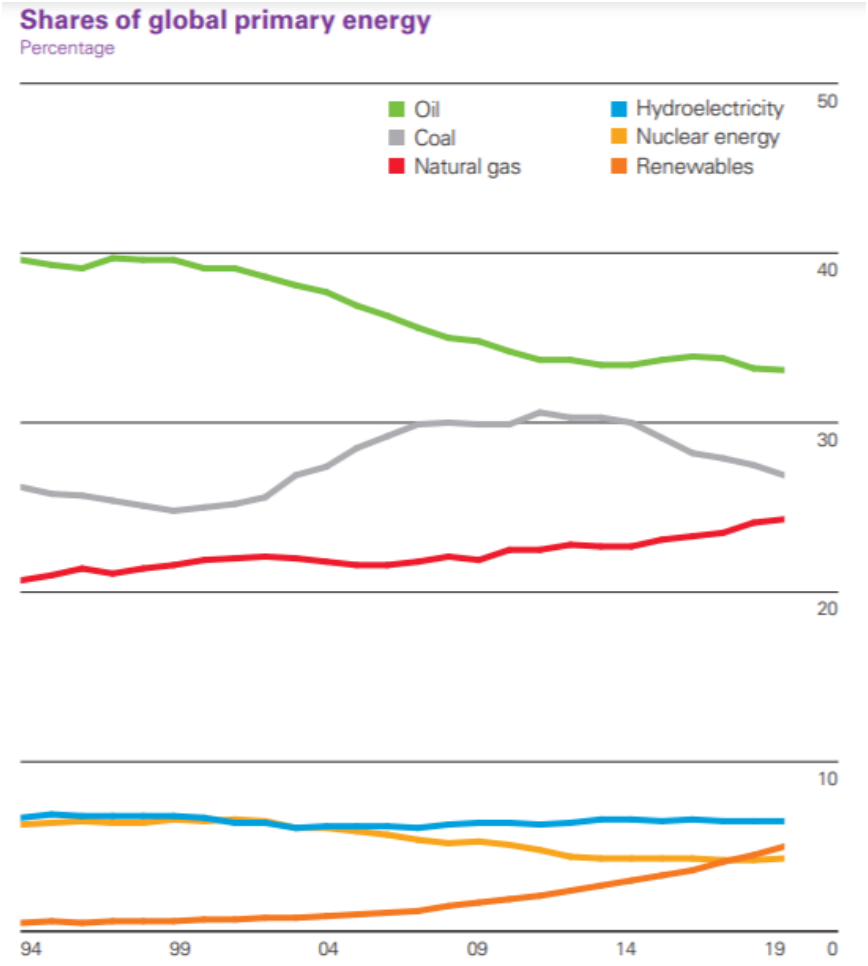

Figure 1.6 Global primary energy shares for 2019 [8].

1.2 Problem statement and research questions

Cement is used abundantly for the well construction and as a plugging material in P&A operations, as it remains one of the only viable options for these applications. However, as presented in section 1.1, among the well integrity issues, cement failure is recorded at a significantly high rate. Cement failure can result in structural failure and also cause reservoir

fluids to leak to the surface. This suggests that the well cements do no satisfy all the criteria defined by the NORSOK D-010 standard. Ultimately, the material properties of cement need to be improved.

In the recent years, the application of nanoparticles in the petroleum industry has shown impressive results for applications such as well cementing, drilling fluids, and EOR. However, nanoparticle applications in the petroleum industry are not fully developed for commercial usage, and it is still in the research and development phase. This thesis will investigate the effects of the selected nanoparticles and fly ash on 0.44 WCR G-class cement. The research questions to be addressed are:

- How will various nanoparticles and fly ash affect mechanical, elastic, rheological and thermal properties of neat G-class cement?
- How does a binary and ternary nanoparticle blend compare to the effects of a single nanoparticle system in neat G-class cement?
- What are the effects of fly ash as a standalone additive and in a blend with a nanoparticle on the neat G-class cement?

1.3 Overview and research methods

In addition to examine the questions in section 1.2, the thesis will also cover the following topics:

- Literature study on the effects of nanoparticles
- Experimentally investigate:
    - Impact of single SiO_2 on G-class cement
    - Impact of binary blend of SiO_2 and Al_2O_3 on G-class cement
    - Impact of ternary blend of SiO_2 and Al_2O_3 and MWCNT on G-class cement
    - Impact of fly ash on G-class cement
    - Impact of fly ash mixed with SiO_2 on G-class cement
- Empirical modelling of uniaxial compressive strength (UCS) vs compressional wave velocity (Vp)

Figure 1.7 presents a complete overview of this MSc thesis, whereas Figure 1.8 depicts overview of the literature study.

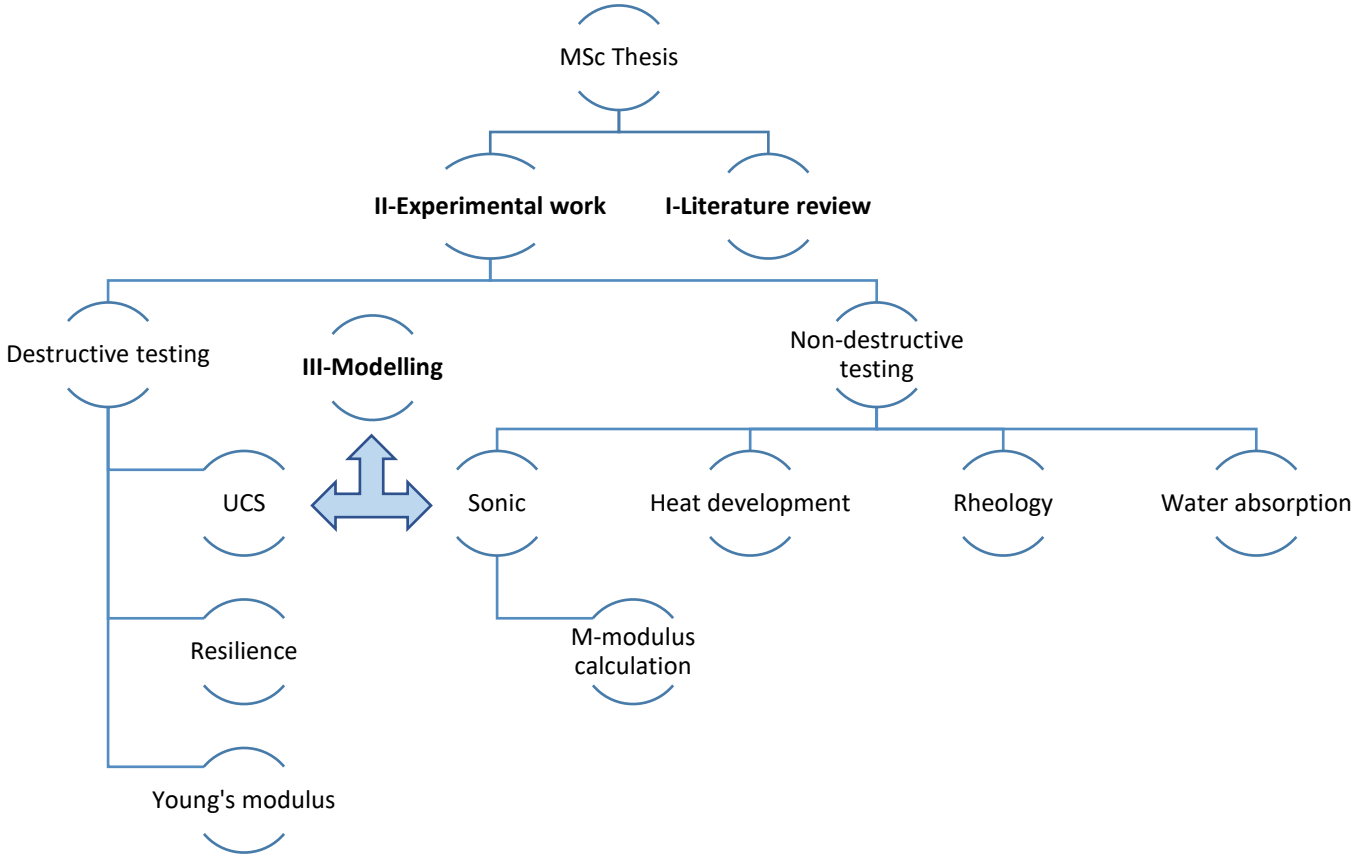

Figure 1.7 Overview of MSc Thesis

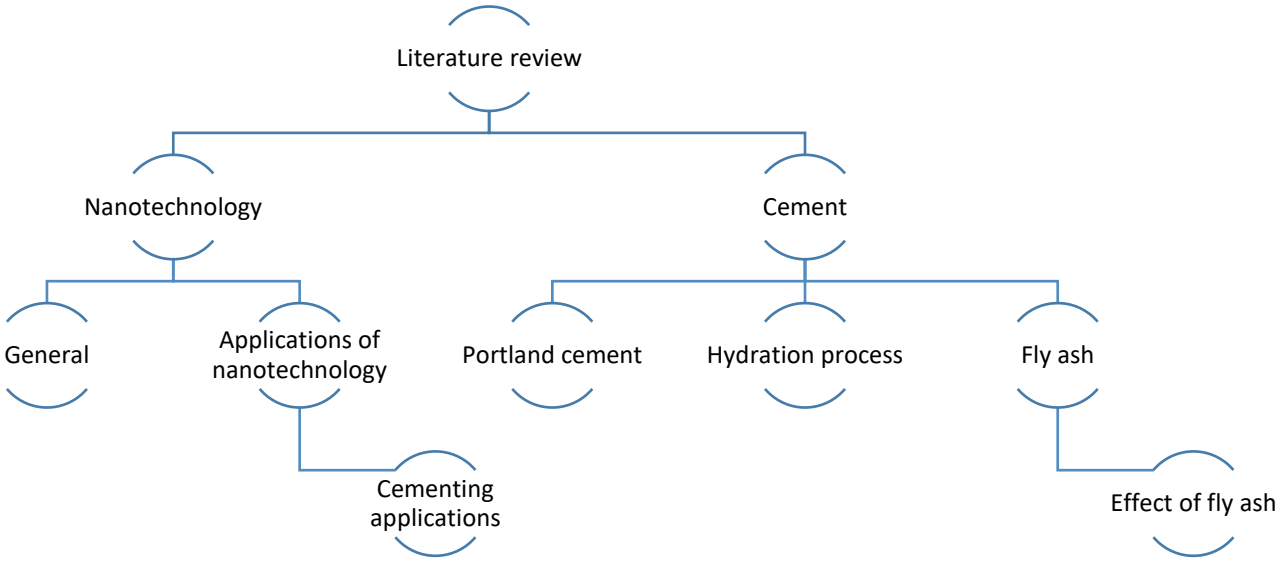

Figure 1.8 Overview of literature study

2 Literature study

The following section aims to provide theoretical background with a literature study of relevant materials utilized in the experimental works of this thesis.

2.1 Cement

The term cement is often analogous with the construction industry. However, cement is utilized abundantly by many industries, and can be found almost everywhere. In fact, concrete is the most used building material in the world, and the main constituent of concrete is cement, which plays the role of the binding material. Ordinary Portland Cement or OPC, is the most prevalent type of cement in the world as it is relatively affordable. In the petroleum industry, OPC is the most widespread binding material used in oil and gas wells in terms of amount produced. Portland cement in oil and gas wells will undoubtably be exposed different conditions than it would have in construction applications, which prompts the usage of varying additives in order to improve the cement properties to combat the demanding environments [4].

OPC is defined as a hydraulic cement and what this entails is that the cement set and mature by hydrating, meaning that it acquires and develops compressive strength when in contact with water. Portland cement inhabits a concoction of desirable properties for well cementing applications. It can set amid both air or water, and the hardened product is practically insoluble in water. Furthermore, its strength development is predictable and relatively quick, and the cured cement has low permeability, which makes it great for sealing off annulus in a wellbore [4]. Couple these properties with its abundance and relative economic viability, and it is straightforward to comprehend why Portland cement is used so abundantly in the petroleum industry.

Portland cement is a fine powder which is manufactured by pulverizing clinker. The term clinker describes nodules with varying diameters of 5-25mm, which is a result of sintering material in the rotary kiln, a device which is utilized in cement plants. Furthermore, the clinker consists of 4 main minerals, Alite, Belite, Tricalcium Aluminate and Tetra calcium aluminate-ferrite [9]. It follows that the raw materials used to make OPC contains apt amounts of calcium, silica, alumina, and iron compounds, thus various raw materials can create OPC clinker as long as they meet the required quantity, seen in table 2.1.

Oxide Composition	Cement Notation	Common Name	Concentration (wt%)
$3CaO \cdot SiO_2$	C_3S	Alite	55–65
$2CaO \cdot SiO_2$	C_2S	Belite	15–25
$3CaO \cdot Al_2O_3$	C_3A	Aluminate	8–14
$4CaO \cdot Al_2O_3 \cdot Fe_2O_3$	C_4AF	Ferrite phase	8–12

Table 2.1 The composition of OPC Clinker [4]

Hydration of cement occurs when water and the cement powder encounter each other, thus an exothermic chemical reaction commences. Portland cement is a mixture where its ingredients are anhydrous, which means that they contain no water. Quickly after water and cement are in contact, a gelatinous substance develops, which is often referred to as calcium silicate hydrate (C-S-H) gel. Subsequently, the C-S-H gel is accompanied by the precipitation of hexagonal plates consisting of calcium hydroxide, CH. As the hydration process advances, the C-S-H gel grows between adjacent cement grains and incorporates the other constituents present in the cement thus resulting in the creation of a rigid structure [10]. In hardened cement, approximately 65% of the final product is made up of C-S-H gel, whereas the hexagonal plates consisting of CH only makes up somewhere around 15-20% [4].

In the Portland cement clinker, the main constituents all react differently to the hydration process and will exhibit different hydration kinetics. The silicates, C_3S and C_2S, are the most prevalent in the Portland cement mixture and have the following idealized chemical reaction [4]. Seen below:

Equation 2.1

$$2C_3S \rightarrow C_3S_2H_3 + 3CH$$

$$2C_2S + 4H \rightarrow C_3S_2H_3 + CH$$

Notably, in the C-S-H gel the C:S and H:S ratios vary based on a handful of factors such as aging, presence of additives, temperature, and the concentration of calcium in the aqueous phase. Consequently, this means that C-S-H gel does not have the identical make up of $C_3S_2H_3$, hence why the chemical reactions, eq. 2.1, are considered idealized [4].

When first in contact with water, the silicate phases will undergo a succinct induction phase where there is low reactivity, and the rheology of the cement slurry does not change remarkably.

After this brief phase, the hydration process will recommence. However, C_3S hydrates quicker than C_2S due to the large quantity difference, as the clinker consists of 55-65wt% of C_3S, whereas only 15-25wt% of C_2S. Even though the C-S-H phase of C_2S is almost identical to that of C_3S, the vast amount of C_3S presented initiates an enormous and rapid formation of C-S-H gel. Hence why the rapid C_3S hydration is predominantly accountable for the initial strength and set of the cement. While C_2S is often associated with final strength of the cement as it takes longer to hydrate. The difference in hydration time can be observed in figure 2.1. Ultimately, C_3S hydration is often used as a model for the hydration behaviour for Portland cement, when considering all the other constituents [4].

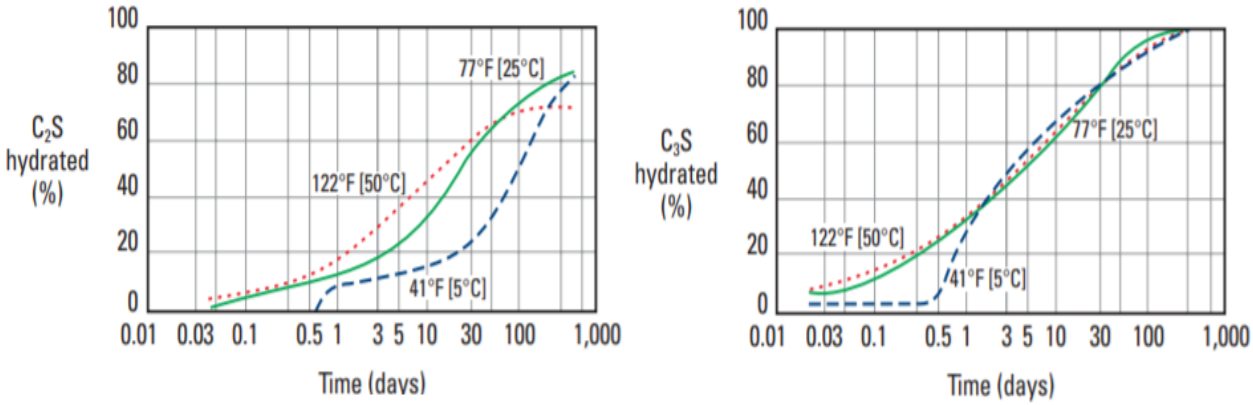

Figure 2.1 Hydration time for C_2S vs C_3S [4]

Furthermore, the hydration process of Portland cement can be categorized in five stages. Figure 2.2 exhibits the heat evolution during the different stages of hydration [4]. In order of appearance during the hydration process:

- I: Preinduction period
- II: Induction period
- III: Acceleration period
- IV: Deacceleration period
- V: Diffusion period

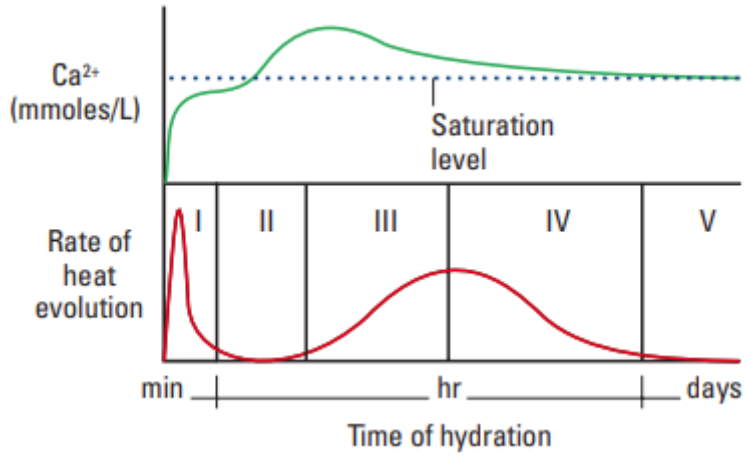

Figure 2.2 Hydration stages and heat development [4]

2.1.1 Factors affecting hydration process

From beginning to end of the Portland cement hydration process, there is a sustained solidification of the cement slurry until a completely rigid product. The hydration is a complex chemical process, where the reactants present in the cement powder all react at differing rates. There are also several variables that affect the hydration process when factoring in all constituents of the cement and not only C_3S hydration which often can act as a model. Some factors which might affect the hydration process are listed below [4]:

- Volume changes during setting
- Temperature effects
- Aging effects
- Surface area effects

As water and cement powder react, they undergo an absolute volume depletion caused by the density difference between the initial reactants and the hydrated mixture, where the hydrated mixture is denser. Despite this reduction in absolute volume, the external volume experience insignificant difference. Consequently, the outcome is often that the porosity of the cement matrix is increased. In context of a wellbore this could lead to reduced zonal isolation, as fluid migration might be more prevalent.

Furthermore, it has been found that the temperature at which the hydration occurs, carries a significant impact on the hydration rate of the cement and stability of the hydration products.

Temperature greatly enhances the hydration and setting time, as depicted in figure 2.3. However, there is a downside to this. With longer curing periods, complete hydration can be obstructed if exposed to high curing temperatures, thus ultimately reducing the compressive strength of the cement. Incomplete hydration is believably due to the development of a thick layer of C-S-H gel which surrounds and blocks available C_3S surfaces from fully hydrating. Resulting in that curing temperatures exceeding 40°C should be avoided in order to prevent any obstruction of complete hydration [4].

Additionally, during storage in sacks or silos, the performance of the Portland cement might be diminished if the cement is exposed over longer periods of time to the atmosphere and/or high temperatures. Some of the side effects of this exposure might manifest as decreased compressive strength and increased thickening time. Additionally, the surface area or fineness of the cement is given as cm^2/g, or surface area to per unit of mass, and can vary from one cement manufacturer to another. Slurry rheology, pumpability, hydration rate can all vary based on the surface area of the cement grains [11]. Furthermore, compressive strength is also often thought to become greater with finer cement particles. Cements with higher fineness has a large surface area per unit mass and are generally considered to perform better, hence why finer cement particles are also more expensive [4].

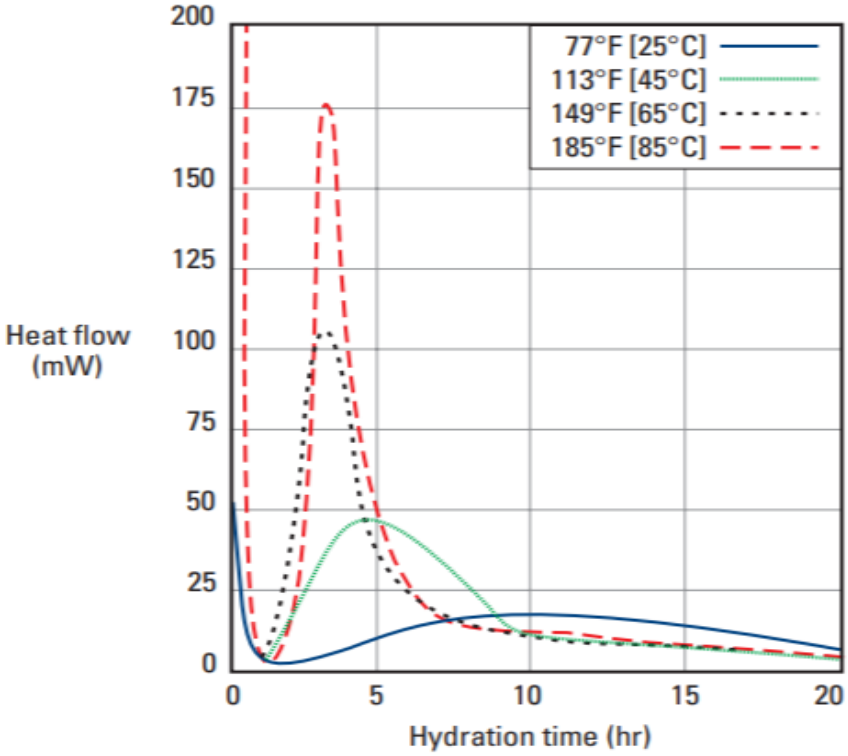

Figure 2.3 Temperature (heat flow) effects with regards to time [4]

2.1.2 Classification of Portland cement

Due to Portland cements being used in so many industries, they are often exposed to different environments, and as a result they are manufactured with different properties based on their intended application. Furthermore, in order to ensure consistency in performance and properties, and to help distinguish between different types of cements, classification systems has been introduced. This enables cement manufacturers, to meet specific criteria which are based on the intended application of the final product. As a result, there are several classification systems available. The two most common classification systems for the petroleum industry are the API classification system as it is used by the ISO standard and the classification system of ASTM [4]. Table 2.2 exhibits the API classification system

API Classification	
Classes	**Intended Usage and Grade**
Class A	Used when no special properties are needed. Grade: O
Class B	Used when moderate sulphate resistance or high sulphate resistance is essential. Grade: MSR and HSR
Class C	Used when conditions demand high early strength. Grade: O, MSR and HSR
Class D, E, F	Used when moderate pressure and temperature conditions must be met. Rarely seen in use today, due to their usage of inadequate retarders Grade: MSR and HSR
Class G and H	Termed the "Basic Well Cement". By far the most used today in the petroleum industry. Grade: MSR and HSR

Table 2.2 Overview of API classes and intended usage. Created with information from Nelsen and Guillot (2006) [4].

Well conditions as temperature and pressure varies based on their depth in the well.. Essentially, meaning that the classes are categorized based on the expected well conditions that the cement will be subjected to. Furthermore, the API classification system has eight classes, A through H, and the classes provide different grades of sulphate resistance, ordinary (O), moderate sulphate

resistance (MSR) and high sulphate resistance (HSR) [4]. By a significant margin, API Classes G and H are the most used ones in well environments, however other classes are also used albeit in different scenarios. For instance, C – class cement is utilized when high early strength is required, thus it has a more niche use than class G/H.

2.1.3 Additives in Portland Cement

To further tailor the Portland cement to fit the demanding conditions it will inevitably face in the well, usage of additives in the cement is common practice. They modify the performance and properties to meet specific requirements required for well operations. Additives are often aimed at generally improving the cement with properties like, rapid strength development, longevity of the cement or improving zonal isolation. Additives can come in both solid forms and liquid and while there are hundreds of additives utilized for well cementing practices, they are often subdivided into eight larger categories [4].

Listed below:

1. Accelerators – Reduces setting time and increase the compressive strength with respect to time
2. Retarders – Delays setting time of the cement slurry
3. Extenders – Lowers the density and/or reduces the quantity of cement per unit of volume of set product
4. Weighting agents – Increases density
5. Dispersals – Reduces viscosity of the cement slurry
6. Fluid-loss agents – Additives that control leakage in aqueous phase of a cement system to the formation
7. Lost-circulation agents – Additives that control lost fluid to weak or fractured formation
8. Speciality additives – Miscellaneous additives, such as anti-foam etc

2.2 Fly Ash

Fly ash is defined as the residue of pulverized coal that has been incinerated, typically at a coal power plant. The ash usually solidifies as rough spherical shapes, as they are suspended in flue gases, hence why fly ash also is called flue ash. Additionally, the ash has roughly the same surface area as Portland cements. Fly ashes consist of several minerals, however the most

prevalent are alumina, silica, iron oxide, magnesia, lime and alkalis. In addition, the composition and properties of fly ash tends to vary due based on the coal source and coal plant efficiencies. Resulting in that the specific gravity of the ash can differ [4].

Interestingly, fly ash is a pozzolanic material. This is often defined as a substance that are aluminous, siliceous or a combination between both. A pozzolanic material, when isolated, possessed no cementitious abilities. However, in contact with moisture, a pozzolanic material will react chemically with calcium hydroxide which will result in the creation of substances which inhabits cementitious abilities [12]. This prompts the question if this could enhance regular OPC when used in conjunction with it, or even be used to create potential replacement materials, as geopolymers, which eventually could replace cement.

ASTM has classified fly ash into three classes of fly ash, N, C and F. Typically, class C of fly ash contains a smaller amount of silica, are made from lignite or subbituminous coals. Additionally, class C has around 50% of pozzolanic compounds, whereas class F and N has around 70%. Furthermore, F and N class fly ash are made predominantly from anthracite and bituminous coals. As a result, Class F and N is the most pozzolanic, whilst type C does not entirely fit the description of a pozzolanic material. To summarize, class F and N are pozzolanic, and have approximately no cementitious ability alone, whilst class C is somewhat pozzolanic and can inhabit self-cementitious abilities [4].

As alluded to, a fairly new technology has emerged in the recent years, where fly ash used in combination with an alkaline reactant and water to create something called a geopolymer, which is a cementitious substance. Geopolymers can be created in conjunction with other materials other than fly ash, such as slag or clays. Additionally, one enormous benefit to this substance is that it is considered more environmentally friendly, compared to cement. This is because fly ash is a biproduct of other processes, and therefore exist in abundance, while also being the main constituent of geopolymers. Ultimately, geopolymers are considered as more sustainable when compared with regular cement. As it stands currently, geopolymers have some distinct drawbacks, but do possess potential, and could be utilized with further development [13].

2.3 Nanotechnology

Everything in our world is constructed by atoms, arranged in various ways forming a vast quantity of molecules. The ability to make changes at atomic and molecular scale could have a tremendous impact for further technological progression and innovation. A practical definition of nanotechnology is "*The design, characterization, production, and application of structures,*

devices, and systems by controlled manipulation of size and shape at the nanometre scale (atomic, molecular, and macromolecular scale) that produces structures, devices, and systems with at least one novel/superior characteristic or property" from Bawa et al. (2005) [14].

As the definition states nanotechnology aims to make enhancements or introduce novelty in the form of a property or characteristic, to fuel innovation in technology by modifications done at a scale of 1 to 100 nanometre (10^{-9}). Utilization of nanomaterials for industrial, science and engineering applications are becoming more frequent, as the novelty/enhancements nanoparticles potentially can introduce along with their capability of providing new viable solutions to existing technical challenges, make them sought after. With further research, nanotechnology can become widespread, and make further appearances in fields as medicine, agriculture, energy technologies, textile and electrical technologies among more. Figure 2.4 shows applications of nanotechnology in various industries. Industries and disciplines that do research and study nanotechnology, will benefit directly from their own research, but also indirectly benefit from research conducted by fellow industries also researching nanotechnology, as it is believed that nanotechnology will play a pivotal role in a lot of industries in the future [15].

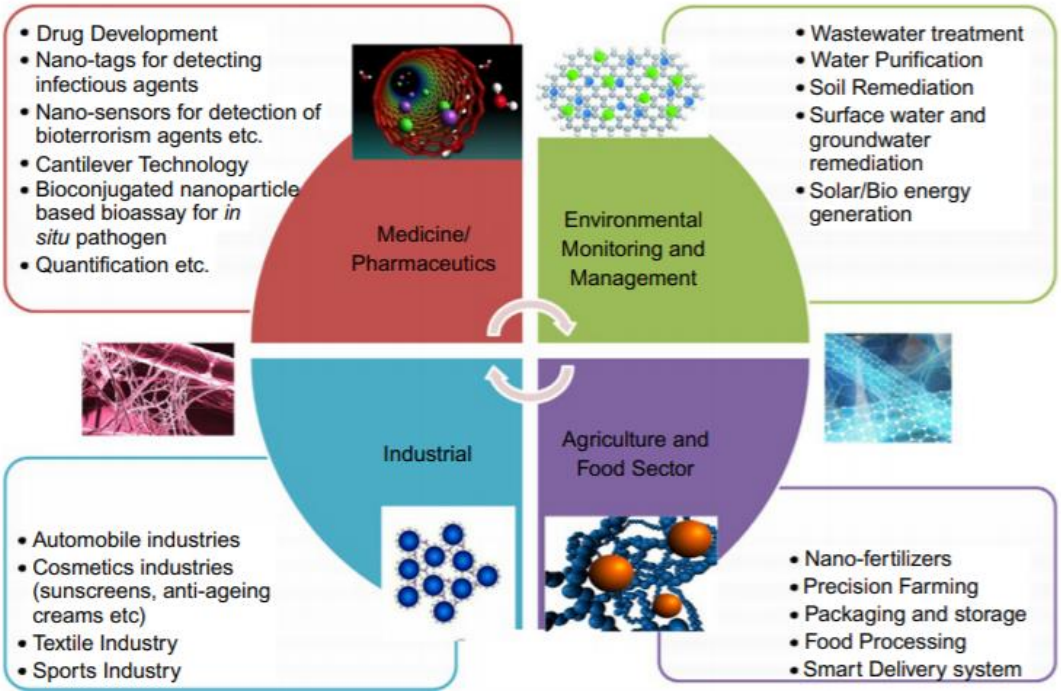

Figure 2.4 Shows several applications of nanotechnology in various fields [16]

The creation of synthetic nanomaterials is primarily done with two methods. The first approach is called the top-down method and is in layman terms the same as what an ice sculptor would do to an ice block, starting with a large chunk, and slowly and precisely sculpting the block into the desired shape. The nanomaterial is manufactured through etching the source material via mechanical processes, often by ball milling or lithography, until the desired result. Whereas, the second approach is called bottom-up, and as the name implies, is the opposite of top-down. In this method the nanomaterial is built from the ground and up, atom by atom, usually via chemical synthesis or aerosol techniques. This method is more complex and time consuming, however it allows for more control over the end result and [15], [17]. Figure 2.5, provides an illustration of what the approaches look like.

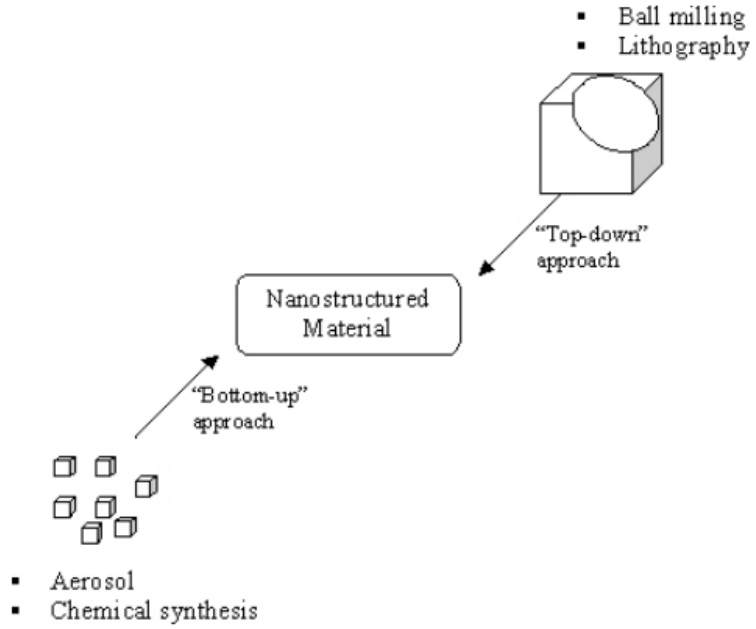

Figure 2.5 Top down and Bottom up approaches to manufacture nanomaterials [17].

2.3.1 Nanotechnology in the petroleum industry

The petroleum industry has also indulged in nanotechnology, where investments have been made to further research nanotechnology, develop it and to find applications where nanomaterials can enhance the current operations in the petroleum industry. Some of the most prevalent applications is in well cementing, drilling fluids, well stimulation and enhanced oil recovery (EOR). Nanoparticles for instance, has some distinctive characteristics which make them attractive. The incredible small size of the nanoparticle provides a very large surface area to volume ratio. This can result in improved reactivity and/or interaction with adjacent surfaces.

Their size also enables them flow easily and access tight and small pore spaces, which can be beneficial in a number of ways, in drilling fluids and fracturing fluids [18]. Additionally, it is believed that nanoparticles can access and fill/block pores in cement, making the cement matrix more refined.

Furthermore, nanotechnology have acted as fertile soil for creative minds in the petroleum industry, by imagining various ways the technology might be utilized to improve the industry. Figure 2.6 exhibits some applications where nanotechnology can bring innovative solutions. Recently, publications with nanoparticle related applications in the petroleum industry has experienced a rampancy in the later years, as depicted in figure 2.7. Most of the research into nanotechnology is still on a laboratory scale, where the results are often favourable. On the contrary, nanotechnology still for the most part lacking proper utilization in the field. More research has to commence to investigate nanomaterials before nanotechnology can be used in commercial well operations. [19].

Figure 2.6 Potential uses for nanotechnology in the petroleum industry [19].

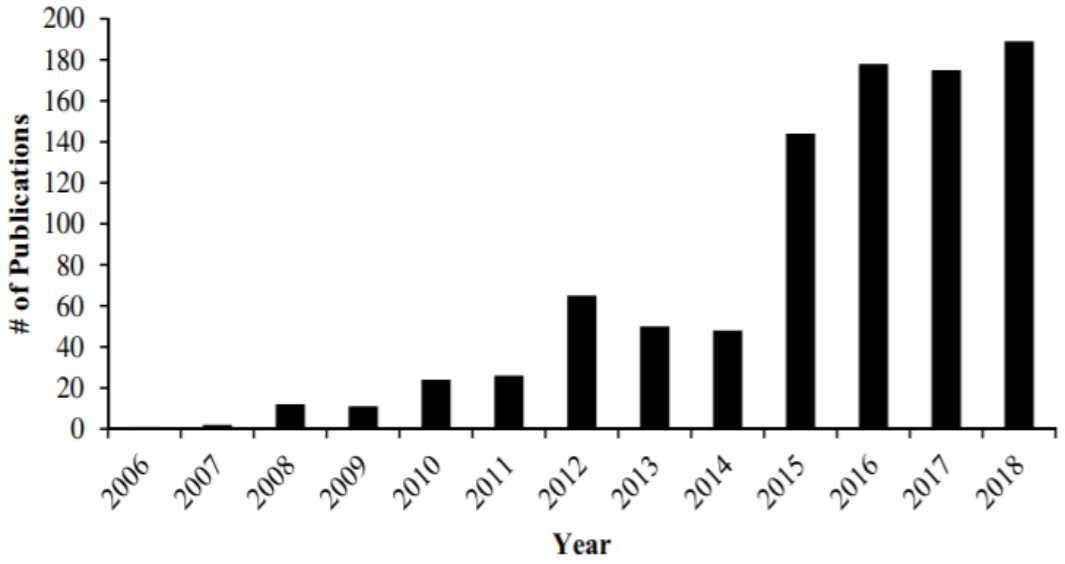

Figure 2.7 Depicts number of related publications of NP usage in the petroleum industry with respect to time [18].

2.3.2 Effect of nanoparticles on cementing applications

Nanoparticles are no stranger to being experimented with in well cements. Well cement testing has become more frequent in the later years as research has indicated that nanoparticles may yield significant improvements. These improvements can come in differing abilities, such as mechanical improvements due to microstructure refinement, accelerating setting time, improving early and/or late strength development. Also, other properties such as enhancing fluid loss and decreasing shrinkage among more can be improved upon. In the following the effect SiO_2, Al_2O_3 and MWCNT on the cement application will be reviewed. The main reason is that these particles are also be tested in this thesis work, but with different combinations.

2.3.2.1 SiO_2 nanoparticles as an additive for cementing applications

A study done by Patil and Deshpande (2012) [20] utilized SiO_2 nanoparticles as additives in cement, where the resulting effect of the silica nanoparticles on the cement were examined. The SiO_2 nanoparticles had a particle size of 5-7nm and was dispersed. The slurries were also mixed based on the API classifications and premium H-class cement was used for the testing. Conclusively, the results showed that nano-SiO_2 significantly improved the compressive strength, especially early strength. To better display the effects of the SiO_2 nanoparticles, micron sized silica was tested as well. The variance between micron and nano size was staggering, as micron had a rate of 160 psi/hr while nano had 460 psi/hr, resulting in that nano-SiO_2 was the first to achieve a compressive strength of 500 psi and had far higher 24-hour compressive strength, compared to the reference specimen and the specimen with micron silica,

as can be seen in table 2.3. This could help to reduce wait on cement time (WOC), and normal well operations could commence quicker.

TABLE 1—EFFECT OF NANOSILICA ON COMPRESSIVE STRENGTH[a]

Latex (gal/sk)	Silica	Retarder (gal/sk)	Time to 500 psi (hr:min)	UCA Strength Rate of Strength Development (psi/hr)	24-hr Strength (psi)
1.5	0	0.05	23:05	172	690
1.5	Micron sized silica	0.05	21:45	160	610
1.5	Nanosilica	0.05	13:29	460	2203

[a]Premium Class H cement, defoamer 0.05 gal/sk, stabilizer 0.2 gal/sk, dispersant 0.143 gal/sk, density 16.4 lbm/gal, Yield 1.1 ft^3/sk.

TABLE 3—FLUID LOSS RESPONSE WITH FLUID LOSS ADDITIVE[a]

Latex (gal/sk)	Nano Silica (gal/sk)	Fluid Loss Additive (% bwoc)	API Fluid Loss (mL/30 min)
1.5	0	0	52
1.5	0.2	0	34
1.5	0	0.5	38
1.5	0.2	0.5	22

[a]Premium Class H cement, defoamer 0.05 gal/sk, 0.2 gal/sk, dispersant 0.143 gal/sk, Density 16.4 lb/gal, Yield 1.1 ft^3/sk

Table 2.3 Compressive strength (top table) and fluid loss (bottom table) from Patil and Deshpande (2012) [20].

The study also found that nano silica had significant effects on fluid loss, both as a standalone additive and when used in conjunction with other fluid loss additives. This suggest that SiO_2 contains some synergistic abilities. Additionally, it was believed that the promising impact of nano-SiO_2 was due to its effects on the C-S-H gel formation, essentially accelerating the formation of the gelatinous substance. Furthermore, it was thought that nano-SiO_2 also acted as a filler in the cement matrix. In conclusion, nano-SiO_2 also exhibited some synergistic abilities as they worked well with other additives used in the fluid loss and compressive strength experiments [20].

Already in 2003, a study was conducted by Li et al. (2003) [21] where they utilized nano-Fe_2O_3 and nano-SiO_2 as additives to cement mortar. They believed that the cement mortar would leave structural defects in the form of pore spaces, where the added nanoparticles would have room to ameliorate the regular cement mortar, by filling and blocking some of these the pore spaces. OPC was used as the binder, along with a water-reducing agent, a defoamer, and sand. Both nanoparticles were dispersed, Fe_2O_3 at 0.25 wt% and SiO_2 at 0.5 wt%.

They created cubes of the cement mortar which were cured for 7 and 28 days at room temperature. Furthermore, 3, 5, 10%bwoc was used as the nanoparticle concentrations, respectively. A-1 was reference sample, whereas sample A-2 to A-4 utilized nano-Fe_2O_3 and A-5 to A-7 included nano-SiO_2. Table 2.4 and 2.5 show the compressive strength and flexural strength of the tested specimens.

Compressive strengths of specimens

Mixture no.	Compressive strength at the 7th day		Compressive strength at the 28th day	
	Target (MPa)	Enhanced extent (%)	Target (MPa)	Enhanced extent (%)
A-1	17.6	0	28.9	0
A-2	21.4	22.7	36.4	26.0
A-3	20.6	16.7	33.1	14.5
A-4	21.1	20.0	30.0	3.7
A-5	18.6	5.7	32.9	13.8
A-6	21.3	20.1	33.8	17.0
A-7	21.3	20.1	36.4	26.0

Table 2.4 Compressive results from Li et al. (2003) [21]

Flexural strengths of specimens at the 28th day

Mixture no.	A-1	A-2	A-3	A-5	A-6
Flexural strength (MPa)	4.90	5.77	6.04	5.84	6.23
Enhanced extent (%)	0	17.76	23.26	19.18	27.14

Table 2.5 Flexural strength from Li et al. (2003) [21]

Both tables show that all SiO_2 and Fe_2O_3 dosages increased compressive strength compared to the reference value, for every curing age. Significant improvements were also made to the flexural strength. Conclusively, the study found that both nanoparticles improved the compressive strengths and flexural strengths compared to the reference sample for all cases, as depicted in table 2.4 and 2.5 [21].

Another research executed by Jalal et al. (2011) [22] was aimed at investigating the impact of micron-SiO_2 and nano-SiO_2 on high performance self-compacting concrete (HPSCC). Mechanical, rheological, durability and microstructural properties were all investigated in this study. Micron- and nano- SiO_2 was tested individually, as well as a blend of both. Concentrations were 10%bwoc for micron silica, 2%bwoc for nano silica and the blend contained 10bwoc% of micron + 2%bwoc for nano silica. Additionally, three different binder contents were utilized, 400 kg/m^3, 450 kg/m^3 and 500 kg/m^3. The amount of added silica was subtracted from the binder content, such that cement + added silica equalled either 400kg/m^3, 450kg/m^3 or 500kg/m^3. This ensured a constant w/b ratio of 0.38. Samples were created in a cubic mould which were removed after the initial curing of 48 hours. Following this, the

samples were put in water at a temperature of 20°C where they cured until test day. Curing times for this study were 3,7,28 and 90 days where the average of two samples were used in the results [22].

No	Concrete ID	Compressive strength (Mpa)			
		3 days	7 days	28 days	90 days
1	HPSCC400	27.8	36.4	51.8	53.1
2	HPSCC450	27.8	36.4	52	53
3	HPSCC500	32.5	40.2	52.5	53.2
4	HPSCC400NS2%	29.2	44.3	71.3	75.9
5	HPSCC450NS2%	31.8	44.1	80.4	85.3
6	HPSCC500NS2%	36.2	49.1	82.1	86.1
7	HPSCC400MS10%	36.1	48.7	56.5	58.1
8	HPSCC450MS10%	33.4	42.8	58.3	59.3
9	HPSCC500MS10%	34.3	43.9	63.4	65.1
10	HPSCC400MS10NS2%	40.3	59	78.8	82.4
11	HPSCC450MS10NS2%	38.7	50.1	83.5	89.9
12	HPSCC500MS10NS2%	41	52.3	87.9	92.1

Table 2.6 Compressive results from Jalal et al. (2011) [22]

No	Concrete ID	Splitting tensile strength (Mpa)			
		3 days	7 days	28 days	90 days
1	HPSCC400	2.1	2.9	3.6	3.9
2	HPSCC450	2.2	2.7	4.5	4.6
3	HPSCC500	2.8	3.7	4.7	4.8
4	HPSCC400NS2%	2	3	3.7	4.4
5	HPSCC450NS2%	2.1	3.1	4.5	4.8
6	HPSCC500NS2%	2.3	3.6	4.7	4.9
7	HPSCC400MS10%	2.3	3.1	3.7	4.3
8	HPSCC450MS10%	2.4	3.2	4.3	4.6
9	HPSCC500MS10%	2.5	3.7	4.7	4.8
10	HPSCC400MS10NS2%	2.5	3.4	4.8	4.9
11	HPSCC450MS10NS2%	2.6	3.8	4.9	5.1
12	HPSCC500MS10NS2%	2.9	3.7	4.8	5.3

Table 2.7 Splitting tensile results from Jalal et al. (2011) [22]

From tables 2.6 and 2.7, both sizes of SiO_2, nano, micron or in a blend, had a primarily positive impact on the mechanical properties of HPSCC. Interestingly, for compressive at curing age of 28 and 90 days, the specimens which included nano-SiO_2, either as a standalone additive or in a blend seems to achieve far superior results when compared to micron alone. It was concluded that the addition of micron- and nano-SiO_2 improved mechanical properties remarkably. The study also suggested that the improvement was due to an accelerated C-S-H gel formation, similarly to what Patil and Deshpande (2012) found.

Furthermore, the paper also found other interesting results. Water and capillary absorption testing found that the addition of SiO_2 demonstrated a notable reduction in water absorption and capillary absorption. Scan Electron Microscope (SEM) micrographs seem to indicate that when silica was added it resulted in a refined microstructure with smaller pores [22]. The water and capillary results likely reflect this as well, an improved cement matrix would believably attribute to less water absorption and capillary absorption.

Finally, in 2006 Shih et al. [23] carried out a study where they used nano-SiO_2 as cement additive. Four different concentrations of nano-SiO_2 were dispersed in water and added to ASTM Type I C150 standard Portland cement with the aim of examining the mechanical and microstructural impact. The nanoparticles had an average spherical diameter of 20nm and were cured for 7, 14, 28, and 56 days in cylindrical moulds. Furthermore, the water to cement ratio (WCR) was kept constant at 0.55 for all samples created, and dosages of nano silica utilized were 0.0, 0.2, 0.4, 0.6, 0.8wt%, with the first dosage being used as reference samples.

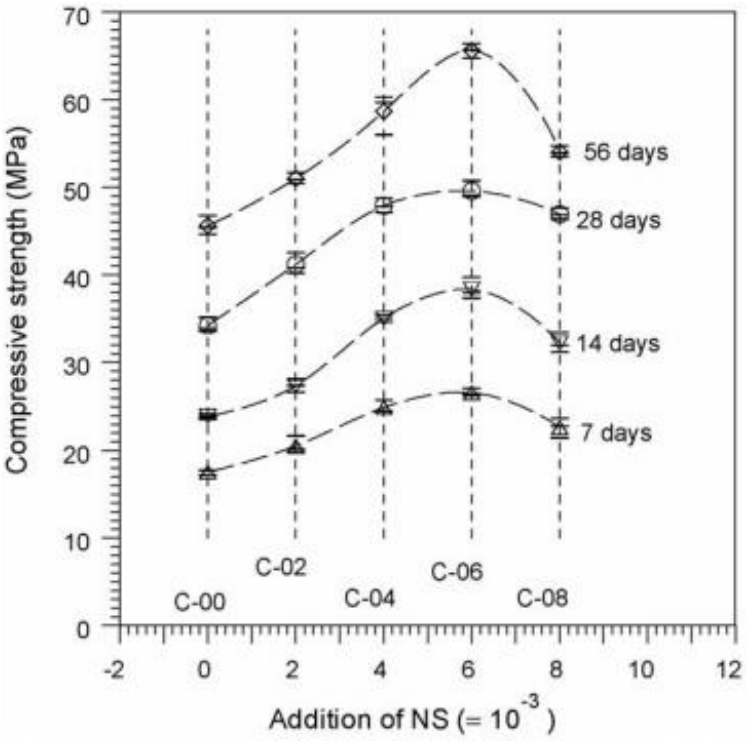

Figure 2.8 Compressive strength results from Shih et al. (2006) [23].

Figure 2.8 shows that the compressive strength increased with higher dosages of nano silica increased for every curing age until the dosage reached 0.6wt% of SiO_2. Afterwards, diminishing returns were experienced with 0.8wt%, which resulted in worse compressive strengths. Additionally, when compared to the reference sample the biggest increase was 60.6% found after 14 days, and the runner up was 43,8% after 56 days, both occurred at 0.6wt% of

nano-SiO_2. The highest compressive strength recorded was 65,62 MPa, which occurred with 0.6wt% after 56 days of curing. It is clear that SiO_2 nanoparticles had a profound impact on compressive strength.

Moreover, the BET (Braunauer-Emmett-Teller) test conducted in this study provided data that indicated denser microstructure for the cement samples which included nano-SiO_2 when compared to reference specimens. Additionally, the NMR (Nuclear Magnetic Resonance) test conducted, exhibited that samples with nano-SiO_2 acquires stronger bonding and were more stable. Essentially, nano-SiO_2 provided significantly superior UCS values for every curing age, along with higher stability, stronger bonding and more refined microstructure within the specimens with nano-SiO_2 [23].

Another study conducted by Isfahani et al. (2016) [24] investigated the effect of SiO_2 nanoparticles on compressive strength and durability properties in concrete. Nano-SiO_2 were added in dosages of 0, 0.5, 1.0, 1.5%bwoc and had an average particle size of 20nm. Interestingly, the study also conducted the experiments with different w/b ratios of 0.65, 0.55 and 0.50, in order to determine what impact this would have on the added SiO_2 nanoparticles. The concrete was cured in cubes, in a moist environment for 7 and 28 days.

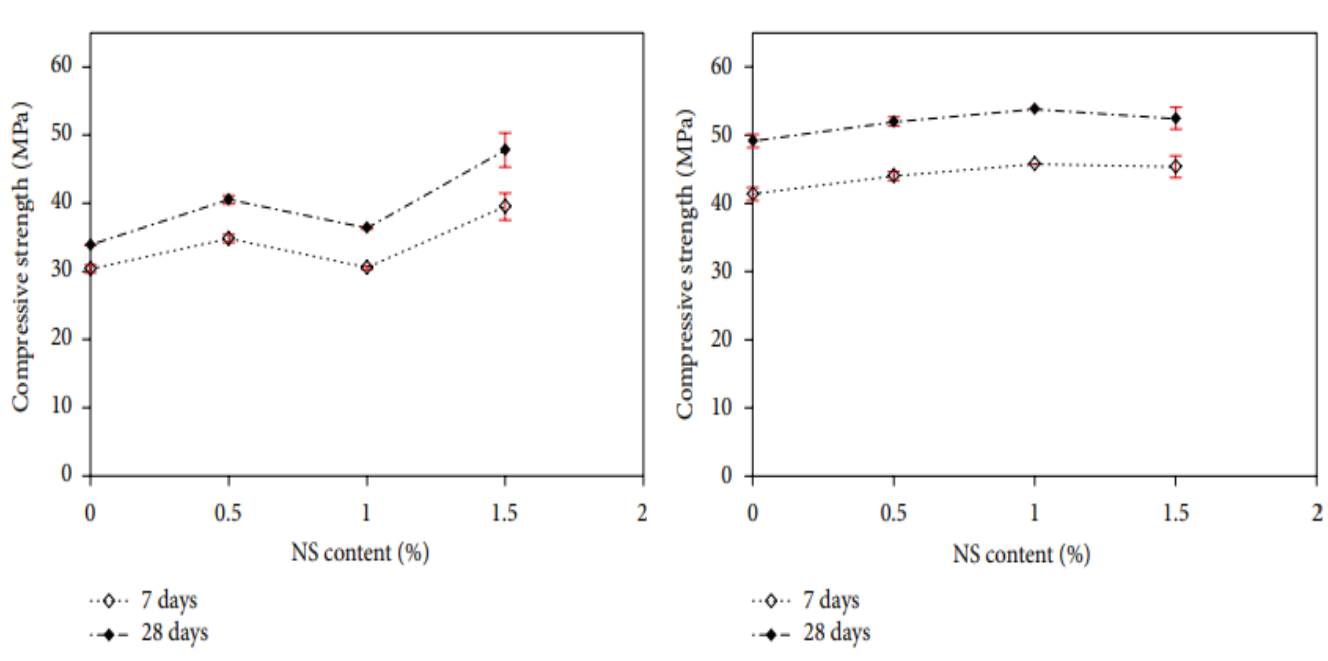

Figure 2.9 Compressive strength from the study conducted by Isfahani et al. (2016) [24].

Figure 2.9 displays the compressive results achieved for the w/b ratio of 0.65 (left) and 0.55 (right). The majority of specimens with added SiO_2 nanoparticles exhibits an increased compressive strength compared to the reference specimen. The w/b ratio of 0.65 seems to yield

larger improvements for the optimal dosages, whereas with the w/b ratio of 0.55, the improvements seem more grounded. The best compressive strength improvement from w/b ratio of 0.65 was 41%, while the best result from 0.55 w/b ratio was 6,5%. Additionally, figure 2.10 depicts the compressive strength results with a w/b ratio of 0.5, and it is observed that specimens with nano-SiO_2 provided mostly adverse results, as almost all values are below the reference value. Conclusively, the w/b ratio seems to have a profound impact on the effect of nano-SiO_2 with regards to compressive strengths as adverse compressive strength was exhibited with a low w/b ratio [24].

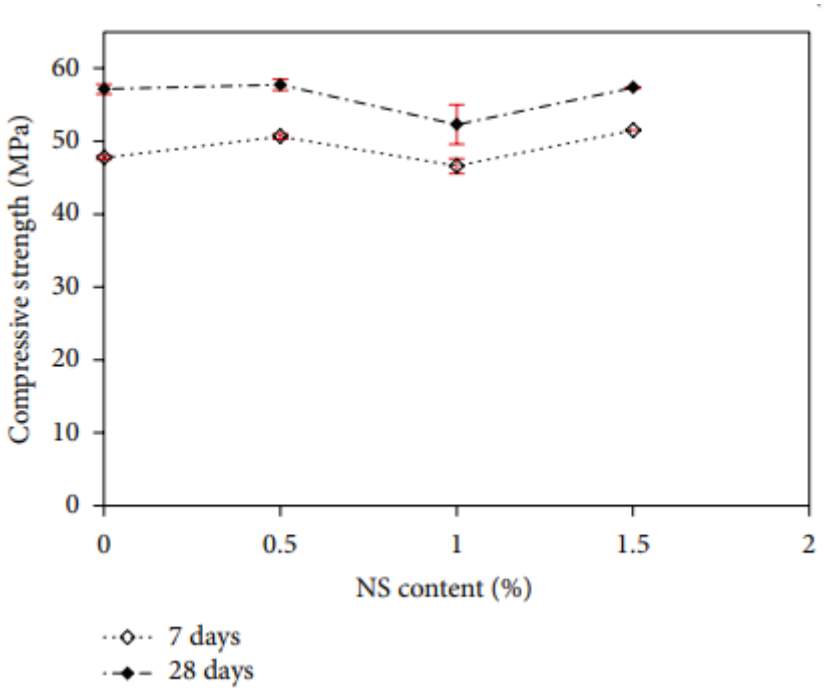

Figure 2.10 Compressive strength with a w/b ratio of 0.5 [24].

2.3.2.2 Al_2O_3 nanoparticles as an additive for cementing applications

In 2011, Nazari and Riahi (2011) [25] carried out a study where they examined the physical, mechanical, and thermal properties of cured concrete, containing Al_2O_3 nanoparticles. The binder used for the experiments was Portland cement. The Al_2O_3 nanoparticles had an average particle size of 15nm and were added in the following dosages of 0, 0.5, 1.0, 1.5, 2.0%bwoc. Two batches were created for curing times of 7, 28, 90 days, where the first batch was cured in water (denoted W in table 2.8) and the second in saturated limewater (denoted LW).

Sample designation	Nano-Al_2O_3 particle (%)	Compressive strength (MPa)		
		7 days	28 days	90 days
C0-W (control)	0	27.3	36.8	42.3
N1-W	0.5	30.4	41.1	44.1
N2-W	1.0	31.7	42.3	46.1
N3-W	1.5	31.9	42.8	45.3
N4-W	2.0	27.5	37.7	42.6
C0-LW (control)	0	27.0	35.4	39.8
N1-LW	0.5	31.1	43.5	44.0
N2-LW	1.0	33.3	46.2	46.7
N3-LW	1.5	36.7	48.1	49.0
N4-LW	2.0	39.1	51.0	51.3

Table 2.8 Compressive strength results from Nazari and Riahi (2011) [25]

Table 2.8 exhibits that all specimens which included Al_2O_3 nanoparticles had superior compressive strengths when compared with the reference specimens. Interestingly, the samples cured in saturated limewater seemingly provided greater UCS results for every curing age compared to the samples cured in water. In most cases, peak compressive strength was achieved at 2.0%bwoc for limewater cured and 1.0%bwoc for water cured samples.

Moreover, it was found that the samples containing Al_2O_3 nanoparticles experienced a decreased initial and final setting time, which peaked at the highest dosage of nano-Al_2O_3 for both cases, 2%bwoc, as witnessed in figure 2.11. Samples cured in saturated limewater contributed to the largest reduction in setting time. This suggests that nano-Al_2O_3 might accelerate the initial and final setting time when included as an additive. On the contrary the study found that the workability decreased for specimens with nano-Al_2O_3. Workability very simplified describes how easy it is to work with the concrete after it is synthesized, and poor workability is considered as adverse [26]. Finally, conduction calorimetry test, thermogravimetric and x-ray diffraction results all suggested in their own way that the addition of nano-Al_2O_3 showed potential benefits regarding physical and mechanical properties. One of the discoveries was that specimens which included Al_2O_3 nanoparticles seemed to form hydration products more rapidly. Finally, it was also discovered the pore structure was improved for specimens with added Al_2O_3 nanoparticles [25].

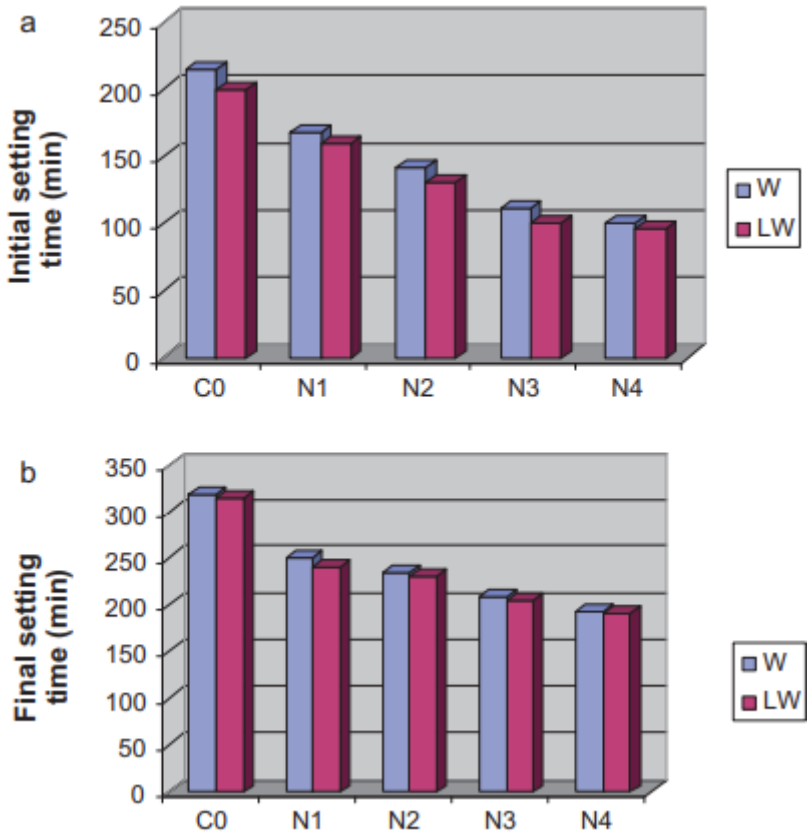

Figure 2.11 Initial and final setting time from Nazari and Riahi (2011) [25].

In a study conducted by Vipulanandan et al. (2018) [27] they added Al_2O_3 nanoparticles to H-class cement in order to evaluate the impact on electrical resistivity and compressive strength. They used a constant water to cement ratio of 0.38 and the added nano-Al_2O_3 concentrations were 0, 0.5 and 1.0%bwoc. In addition, curing ages were 1 day and 28 days. It was shown that specimens which contained Al_2O_3 nanoparticles had significantly higher compressive strengths when compared to the reference samples, depicted in figure 2.12. The highest dosage of 1,0%bwoc nano-Al_2O_3 also demonstrated the best compressive strength results. Additionally, modulus of elasticity also increases similarly to compressive strength, with 1.0%bwoc yielding the best results. Finally, the initial electrical resistivity was found to increase by 10% and 30% for 0.5%bwoc and 1.0%bwoc respectively [27].

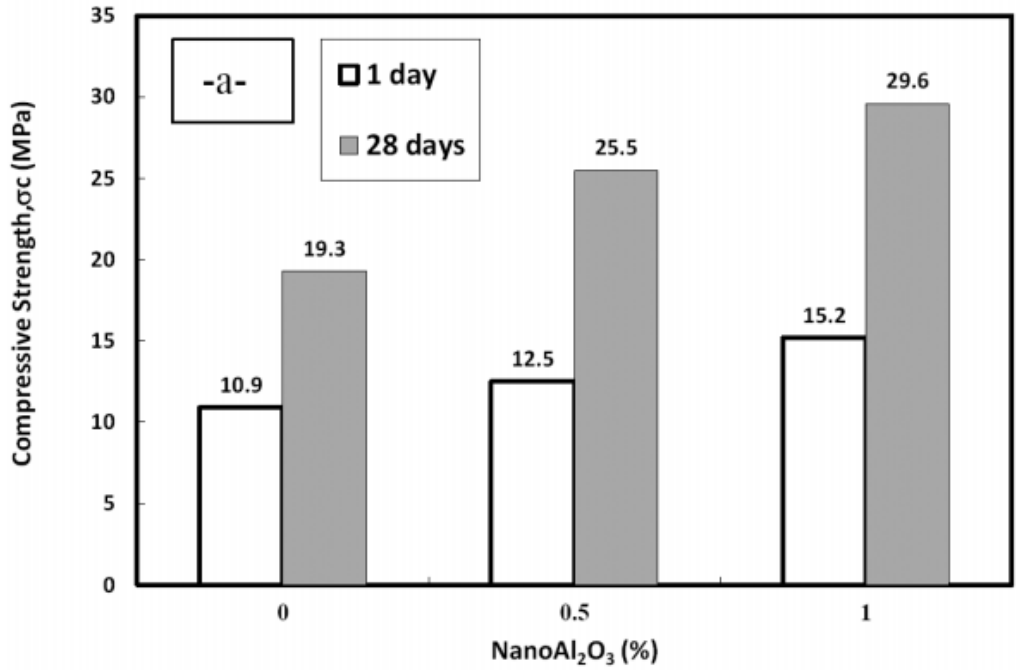

Figure 2.12 Compressive strength results from Vipulanandan et al. (2018) [27].

Another study that utilized nano-Al_2O_3 particles in cement mortar was done by Muzenski et al. (2019) [28]. They conducted various experiments on the test specimens to measure the performance of Al_2O_3 nanoparticles, especially in terms of mechanical properties. The tests included heat development during hydration, chemical shrinkage, compressive strength and SEM imaging.

The study utilized H-class cement in every batch. Three batches were created, the first had varying dosages of Al_2O_3 nanoparticles ranging from 0, 0.1, 0.25, 0.5%bwoc and 1%bwoc Silica fume (SF) kept constant. While the second batch kept nano-Al_2O_3 constant at 0.25%bwoc and varied metakaolin (MK) and SF with dosages 1, 5, 10%bwoc, thus no samples had both metakaolin and silica fumes together, only one or the other. The third batch added Al_2O_3 nanoparticles in a dosage of 0.25%bwoc along with silica fumes in a dosage of 1%bwoc for some samples and only Al_2O_3 for others. The latter batch was measuring heat development during hydration and chemical shrinkage and was cured for 7 days before testing commenced.

Another interesting factor to note is that the Al_2O_3 nanoparticles was not originally dispersed, so in the study they dispersed it for both 1 and 3 hours to see if this would have any impact in the results. Compressive strength was tested at the curing ages of 1, 28 and 90 days.

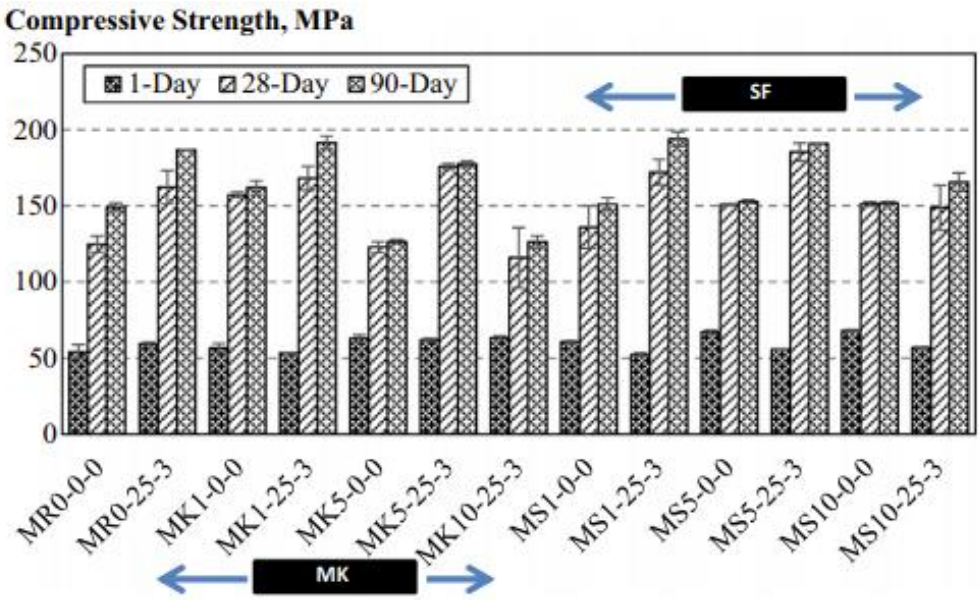

Figure 2.13 Compressive results from the batch with varying nano-Al_2O_3 concentration while keeping SF constant. [28]

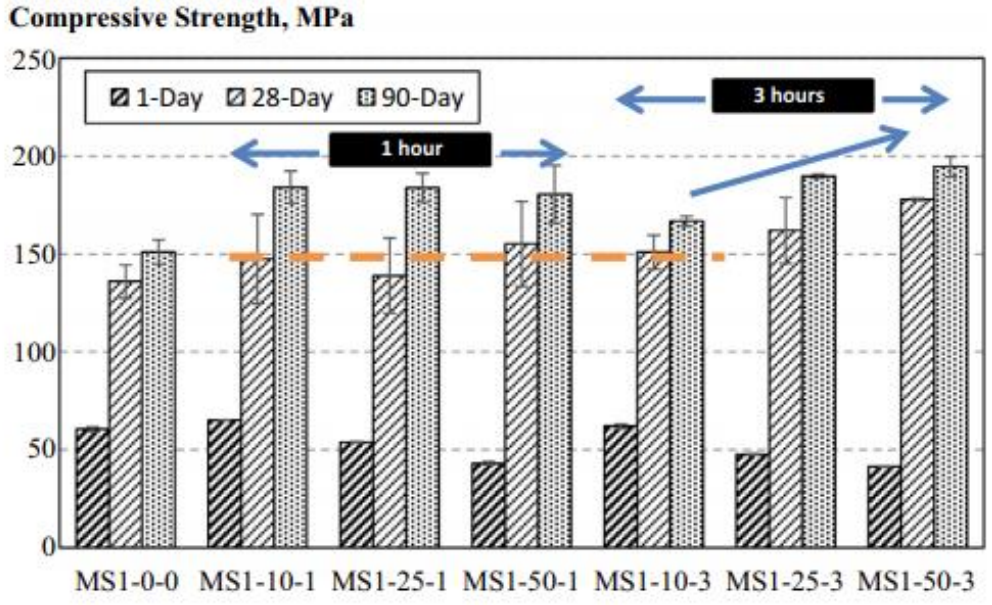

Figure 2.14 Compressive results from batch with nano- Al_2O_3 constant while varying MK and SF [28]

Figure 2.13 and 2.14 exhibit that the compressive strength results are somewhat varied. The majority of samples had improved compressive strength compared to the reference value. Notably, the samples only cured for 3 days seemingly has worst compressive results out of the three curing ages when compared to the reference sample. Also, 90 days curing age had the largest compressive strength percentage increase of the curing ages. Which indicates that the effect of nano-Al_2O_3 might be optimal for longer curing periods where the hydration process is more complete. Additionally, in the batch which kept nano-Al_2O_3 constant while varying MK and SF, the samples which included SF performed slightly better. The results also suggest that

the addition of SF or MK improves the compressive strength. For samples where dispersion times were different, it was found that longer dispersion time would result in less agglomeration of the Al_2O_3 nanoparticles, thus 3 hours dispersion time was preferred. Although, after 90-day curing, dispersion times appear to be less of an impact on the result than other curing periods. However, the opposite can be seen for the 28 days results, where 3 hours of dispersion provided superior compressive strengths. Additionally, study also found that longer dispersion times could aid in more stable dispersion [28].

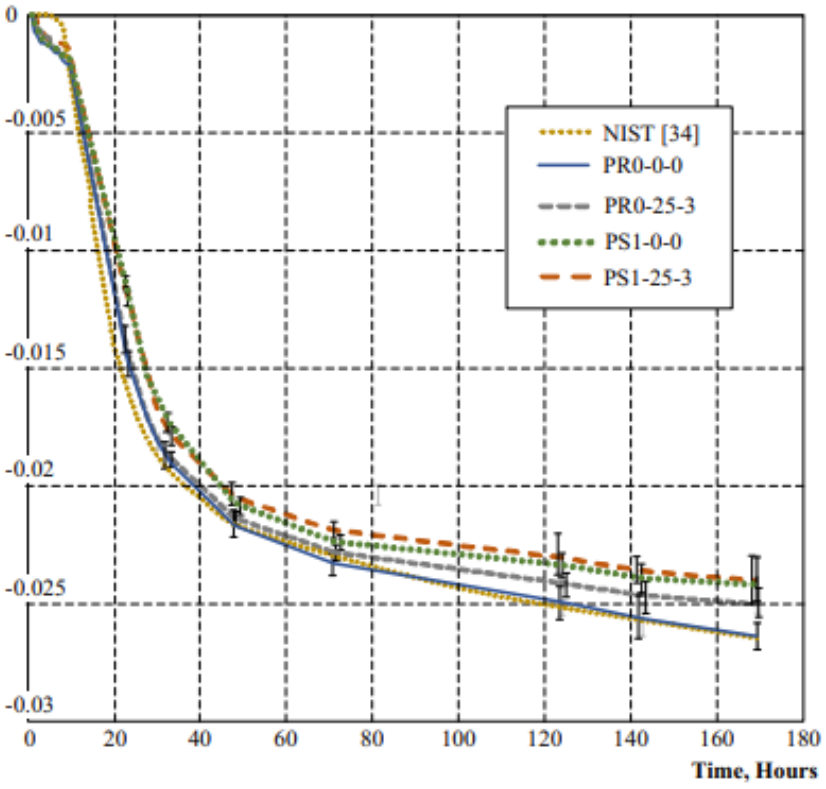

Figure 2.15 Chemical shrinkage data with respect to time (mL/g) from Muzenski et al. (2019) [28].

Finally, the batch created to examine chemical shrinkage found that samples with added nano alumina (PR0-25-3, PS1-25-3) had diminished chemical shrinkage when compared with their respective reference samples (PR0-0-0, PS1-0-0). Largest reduction in shrinkage was observed to be 34,1% compared to reference sample. It is also seen that regardless of the addition of silica fume (denoted by PS1) the Al_2O_3 nanoparticles contributed to a reduced chemical shrinkage. As for the heat of hydration results, dispersion times were insignificant, and sample with added Al_2O_3 nanoparticles had a slightly lower peak temperature. The study also concluded that the addition of Al_2O_3 nanoparticles could attribute to a reinforcing effect on the C-S-H gel [28].

2.3.2.3 MWCNT as an additive for cementing applications

Khan et al. (2016) [29] conducted a study where they added multi walled carbon nanotubes (MWCNT) in various concentrations to a well cement system and examined the mechanical properties when the cement had been cured in high pressure and high temperature (HPHT) conditions. The MWCNT used in the study had an OD of 10-20nm and the dosages they used was 0.1, 0.25 and 0.5%bwoc. This was mixed with G-class cement and regular HPHT additives, such as an anti-foaming agent, retarder and fluid loss agent among more. One of the two batches created was cured in a HPHT machine with 290°F and 3000 psi for 24 hours. Subsequently, they were crushed in order to obtain the compressive strength.

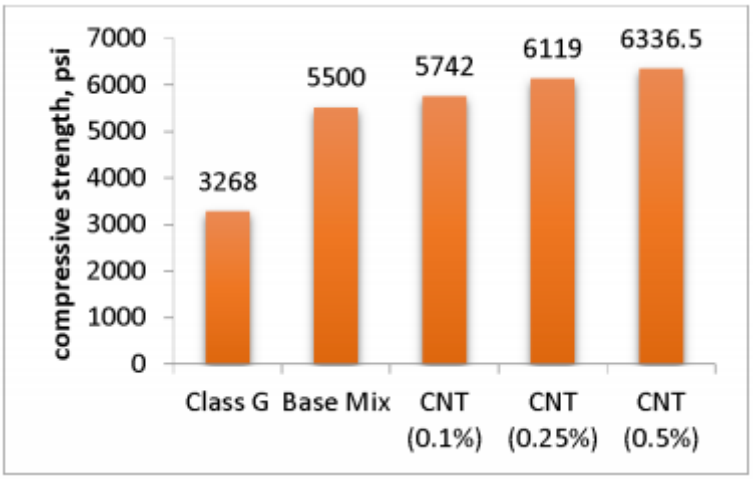

Figure 2.16 Compressive strength by crushing from Khan et al. (2016) [29].

The results from 24 hour curing in a HPHT machine and being crushed displayed that the sample which had 0.5%bwoc had the highest compressive strength, as seen in figure 2.16. This equated to a 15% increase compared to the reference (base mix). The compressive strength is steadily climbing from neat G-class cement to base mix with 0.5%bwoc of MWCNT. This of course raises the question if and for how long this trend would have continued if even higher concentrations of MWCNT were added.

Furthermore, the study also utilized an Ultra-sonic cement analyser (UCA) test to determine the compressive strength of samples cured in the same HPHT conditions for 48 hours. One of the benefits of a UCA test is that it provides the evolution of compressive strength up to the final curing age of 48 hours. From the results, depicted in figure 2.17, the sample with 0.1%bwoc yielded the best results in terms of compressive strength, which is conflicting with the results from the crushing method above in figure 2.16. However, it is important to note that

all samples with added MWCNT were superior compared to the reference value, strongly suggesting that MWCNT additives improve compressive strength

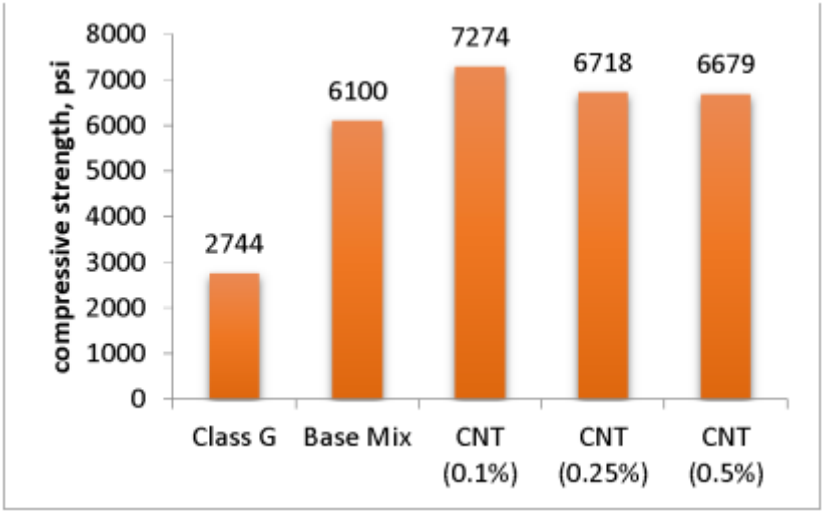

Figure 2.17 Compressive strength after 48 hours using UCA method [29]

Time (HH:MM)	Control Mix	0.1% CNT	0.25% CNT	0.5% CNT
12:00	2344	2953	2691	2785
18:00	4965	5949	5584	5386
24:00	5781	6893	6270	6149
48:00	6214	7274	6718	6679

Table 2.9 Compressive strength development by UCA testing [29]

Compressive Strength (Psi)	Control Mix	0.1% CNT	0.25% CNT	0.5% CNT
	Time (HH:MM)			
50	03:33	03:33	03:34	03:45
500	04:00	03:57	04:14	04:21
2000	09:28	05:41	08:13	07:01

Table 2.10 Time to gain 50, 500 and 2000 psi compressive strength [29]

Table 2.9 depicts the compressive strength development, in terms of the evolution of compressive strength, the sample with 0.1%bwoc gains compressive strength marginally quicker than the other specimens. This is also supported by the measurement of time from 50 psi to 500 psi (table 2.10). Furthermore, 0.1%bwoc used 24 minutes, base mix used 27 minutes, 0.25%bwoc used 30 minutes and 0.5%bwoc utilized 31 minutes for the transition from 50 to 500 psi. Suggesting that higher concentrations of MWCNT takes more time to hydrate

completely. Finally, SEM micrographs displayed that samples with MWCNT were more densely packed as the MWCNT contributed to filling the cement matrix, thus reducing porosity in the cement matrix and improving it [29].

In a study carried out by Lu et al. (2019) [30] they examined the effects of MWCNT on mechanical properties and microstructure on G-class cement. A large quantity of various tests was done to investigate the effects of MWCNT. Firstly, they made four different MWCNT suspensions using different dispersing agents, which they compared to one another to find the most optimal dispersing agent with respect to stability. This choice was made based on the centrifugal time required to stratify the suspension of MWCNT, and the dispersing agent that took the longest to reach delamination was chosen.

Subsequently, they used G-class cement with a water-to-cement ratio of 0.44 for all samples, with varying dosages including 0.00, 0.025, 0.05, 0.10, 0.25, 0.5, 1.0, 2.0wt% dispersed in the elected best dispersing agent. Then they mixed the slurries, poured them into separate curing moulds. After which they were demoulded after 24 hours and left to cure in water at standard conditions until the curing age of 28 days were reached.

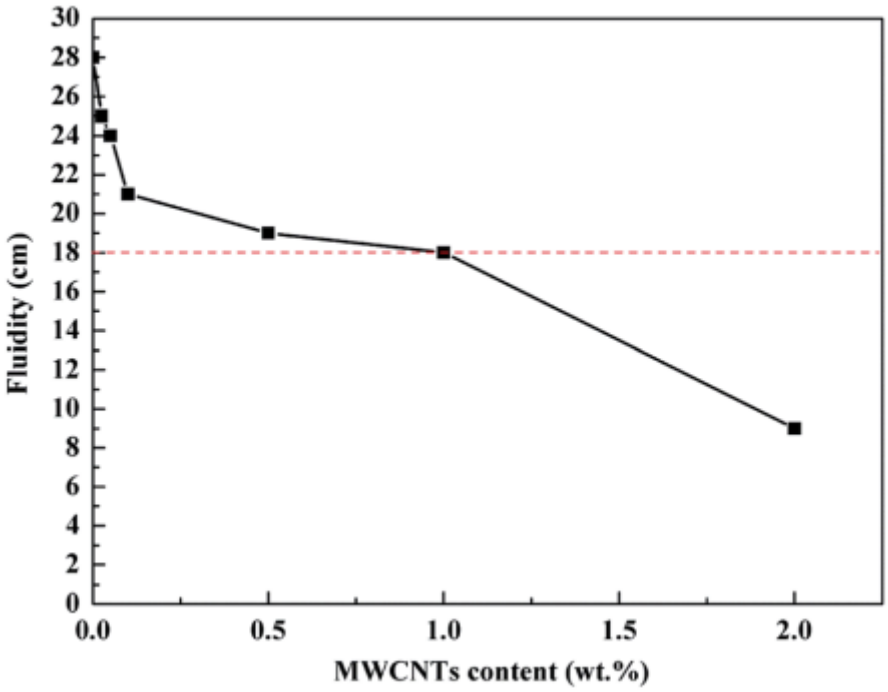

Figure 2.18 Fluidity of cement slurry from Lu et al. (2019) [30]

MWCNT content (wt%)	Shear stress values	*n*	*K* (Pa s)
0.00	96/75/61/47/25/20	0.43	2.70
0.05	65/51/36/20/8/2	0.85	0.13
0.25	70/36/26/16/5/3	0.74	0.18
0.50	104/65/54/31/20/10	0.67	0.50
1.0	140/100/72/49/17/13	0.65	0.89
2.0	160/121/103/64/19/13	0.58	1.66

Table 2.11 Rheological testing of cement slurries with MWCNT additives from Lu et al. (2019) [30].

Rheological testing of the cement slurries reveals that the slurries display shear - thinning effects, seen in table 2.11. Beneficial properties were achieved between 0.05 to 1.0wt% of MWCNT. With 2.0wt% of MWCNT the rheological properties are affected negatively as agglomeration of MWCNT had a tendency of occurring. The fluidity measurements of the slurries also confirmed this, as fluidity of slurry greatly decreased from 1.0 to 2.0wt%, seen in figure 2.18. Dosages less than 1,0wt% displayed favourable results. If the fluidity is poor, this can cause issues when pumping of the cement slurry downhole. According to this study, it needs to be approximately above 18 cm to avoid creating issues under pumping operations, as depicted by the stipulated line in figure 2.18 [30].

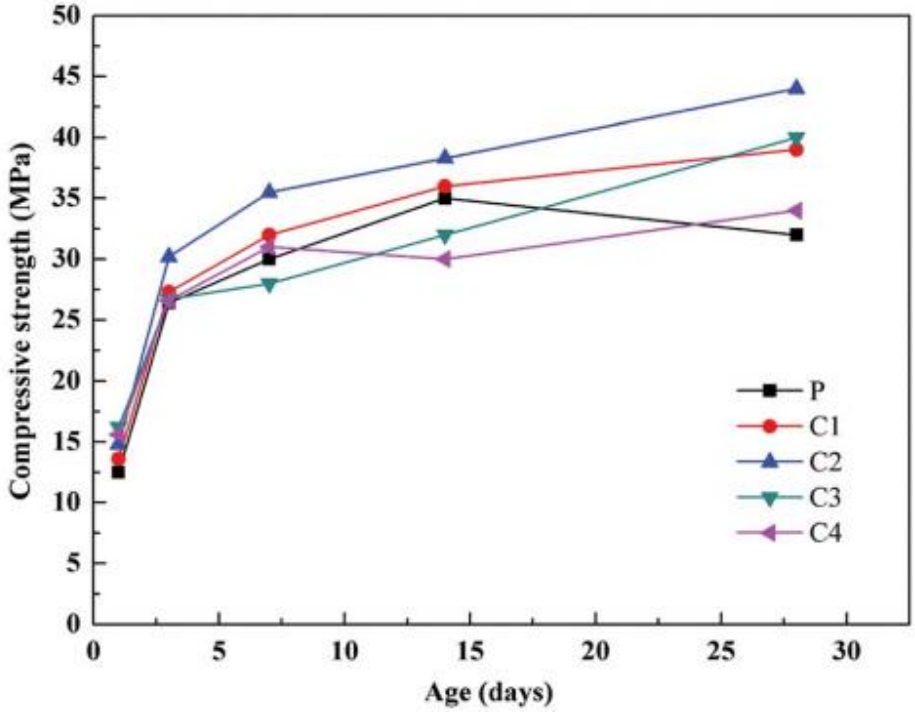

Figure 2.19 Compressive test evolution from 0-30 days of curing [30]

Sample	MWCNT content (wt%)	Compressive strength (1 day, MPa)	Compressive strength (3 days, MPa)
P	0.00	12.5	26.4
C1	0.025	13.6	27.3
C2	0.05	14.8	30.2
C3	0.10	16.2	26.7
C4	0.50	15.6	26.6

Table 2.12 Compressive strength after 1 and 3 days of curing [30]

Mechanical results acquired in this study exhibit that MWCNT in the optimal dosages provides compressive strength improvements, as seen in figure 2.19 and table 2.12. The specimen with 0.05wt% (C2) had a compressive strength increases of 18,40% after 1 day and 14,39% after day 3. This sample seems to be the most beneficial from the batch, as it gains significant compressive strength from day 1 to day 3 and improves linearly afterwards until 28 days, always being the sample with the highest compressive strength. In addition, C2 and C1 demonstrated a 37,50% and 21,88% compressive strength increase when compared to reference after 28 days of curing. Furthermore, at 7 and 14 days, the reference sample P is better than the specimens with 0.1%bwoc and 0.5%bwoc of MWCNT. However, they both improve over reference sample from 14 days to 28 days. This suggest that larger quantities of MWCNT particles may require more hydration time to acquire good compressive strength. Compressive strength benefits from MWCNT becomes more evident when the specimens have cured for longer, as the reference is the weakest of all tested specimens.

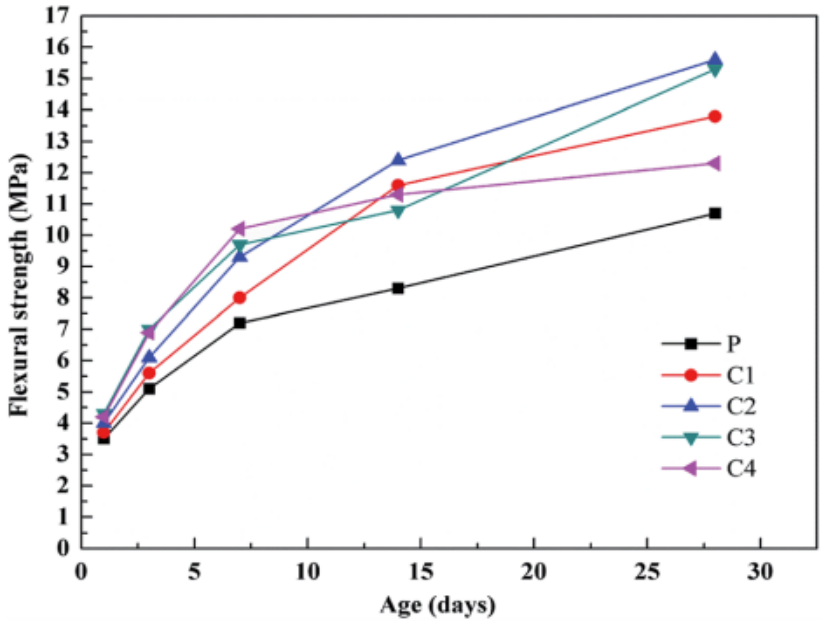

Figure 2.20 Flexural strength of samples in the study from Lu et al. (2019) [30]

Furthermore, the study also found that the flexural strength of the samples was enhanced significantly. C2, the specimen with 0.05wt%, had a 45,79% flexural strength increase after 28 days compared to the reference sample, seen in figure 2.20. In fact, all specimens which included MWCNT had superior flexural strength compared to the reference cement. Moreover, as sample C2 was regarded as the best specimen, elastic modulus was measured, and the results showed a reduction of 19,07% under uniaxial stress compared to the reference sample. This is a great feature, to increase compressive strength while also decreasing the stiffness of the plug. Finally, SEM micrographs and X-ray diffraction (XRD) analysis also suggest that MWCNT improves the microstructure of cement [30].

In 2018 a study executed by Naqi et al. (2018) [31] used MWCNT on cement to examine the effect on strength development and shrinkage. More specifically, they tested the specimens for compressive strength, autogenous shrinkage and internal relative humidity. Their experimental portion utilized type I OPC, with SF and superplasticizers additives. The concentrations of these ingredients were kept constant while adding different dosages of MWCNT. The added MWCNT concentrations were 0, 0.01, 0.02, 0.03, 0.05, 0.10, 0.20, 0.30%bwob. Additionally, the MWCNT were dispersed using very fine particles of silica fumes. Water-binder (w/b) ratio was kept constant at 0.2.

After the slurries had been properly synthesized, they were poured into moulds, and left for 24 hours. Subsequently, after 24 hours the samples were demoulded. The specimens were tested after 1 day, 3 days and 7 days curing in water saturated with $Ca(OH)_2$. Figure 2.21 shows the compressive test results. It is observed that the best increase in performance for all curing ages occurred in the specimen with 0.01%bwob. This specimen had 4,4% increase at 1 day, 9,7% at day 3 and 12,4% at day 7. All the samples with a MWCNT concentration of 0.01, 0.02 and 0.03%bwob had greater compressive strength results compared to the reference value. Samples with higher than 0.03%bwob of MWCNT experienced adverse effects as seen in figure 2.21.

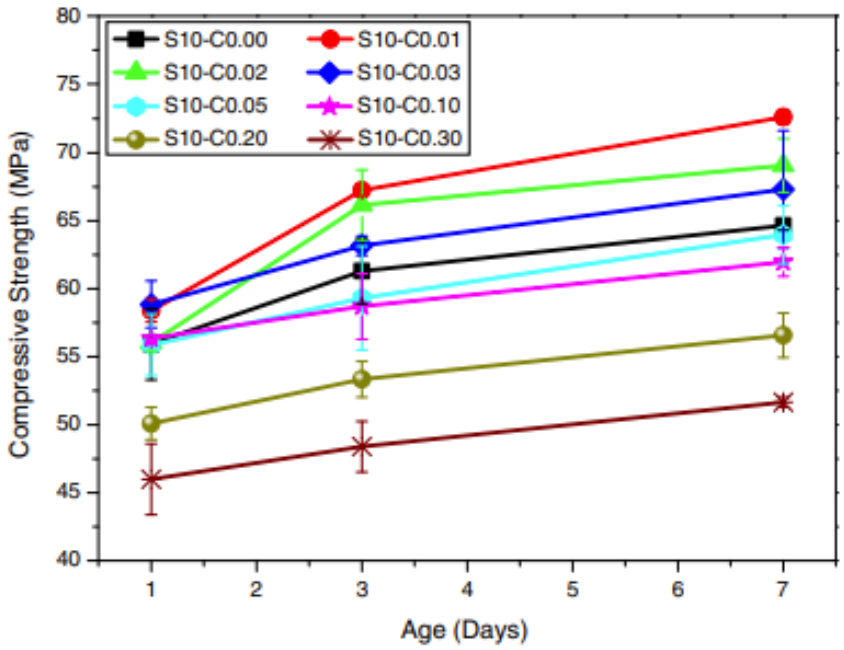

Figure 2.21 Compressive test results from Naqi et al. (2018) [31].

The autogenous shrinkage test result also found that the specimens with 0.01%bwob and 0.02%bwob experience the least amount of autogenous shrinkage, thus providing favourable results. Again, the higher concentrations of added MWCNT were unfavourable compared to the reference sample. This was consistent with the results acquired from the internal relative humidity measurements as well, where 0.01 and 0.02%bwob performed best, and the higher amounts displayed adverse effects.

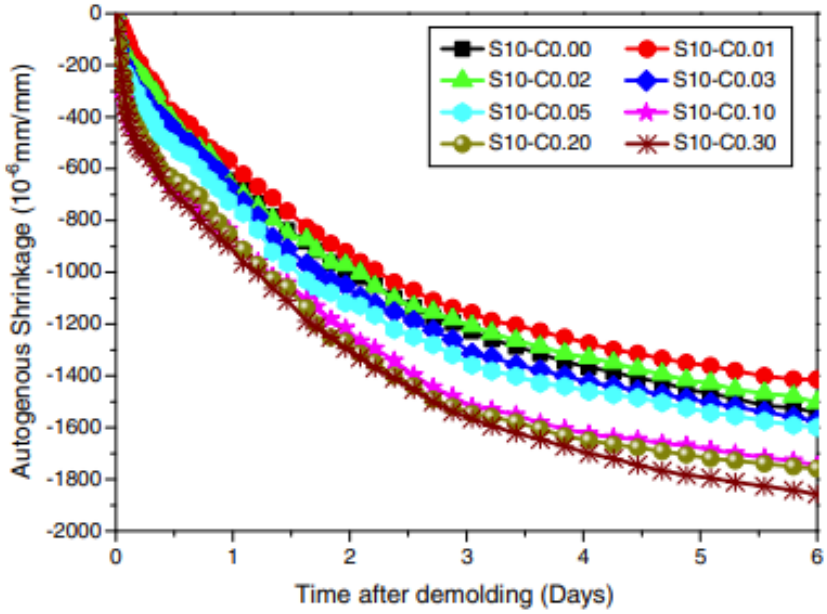

Figure 2.22 Autogenous shrinkage from Naqi et al. (2018) [31]

Conclusively, the study found that the optimum concentrations of MWCNT additives were 0.01%bwob and 0.02%bwob for the best possible results. SF was found to be a good addition as they helped break up agglomeration of MWCNT. The study also concluded that MWCNT dosages above 0.03%bwob displayed adverse effects, likely due to the larger dosages of MWCNT causing agglomeration of the particles, thus the finer pores could not be filled [31].

From this literature review of nano-SiO_2, nano-Al_2O_3 and MWCNT as additives for cement applications, it is observed that the inclusion of these nanoparticle has demonstrated significant improvements to various properties in cement samples. Particularly, mechanical properties seem to display rampant improvements, likely due to the effect nanoparticles has on the C-S-H gel and microstructure of cement. Other properties have also been ameliorated such as shrinkage, setting times, fluid loss etc. On the contrary, adverse effects has also been recorded, frequently for specimens utilizing large quantities of MWCNT, but not exclusive to MWCNT usage. A balance of nanoparticle dosages has to be struck in order to reap its full benefits. More studies will aid in our comprehension of nanoparticles and how to best utilize them before they can be used in commercial operations.

2.3.3 Fly ash as an additive for cementing applications

Fly ash contains cementitious abilities in presence of moisture, as previously established, thus usage as additive might possess enhancing abilities in cement and concrete mixtures. Generally, if fly ash is used in concrete mixtures it displays some clear advantages and disadvantages. Advantages entail decreased water demand for the mixture, workability improvements and heat reduction during the exothermic hydration process. When the concrete is cured, fly ash has been found to increase ultimate strength and reduce permeability when compared to cement only. In addition, usage of fly ash in concrete may reduce the amount of Portland cement required for concrete as fly ash acts as a partial replacement for the cement. This is environmentally friendly, due fly ash being a biproduct and existing in abundance, in fact only about 10% of the annual manufactured fly ash is used in concrete [32], [33]. By using fly ash as replacement for Portland cement, one could reduce the environmental footprint of manufacturing Portland cement to a certain degree, by manufacturing less.

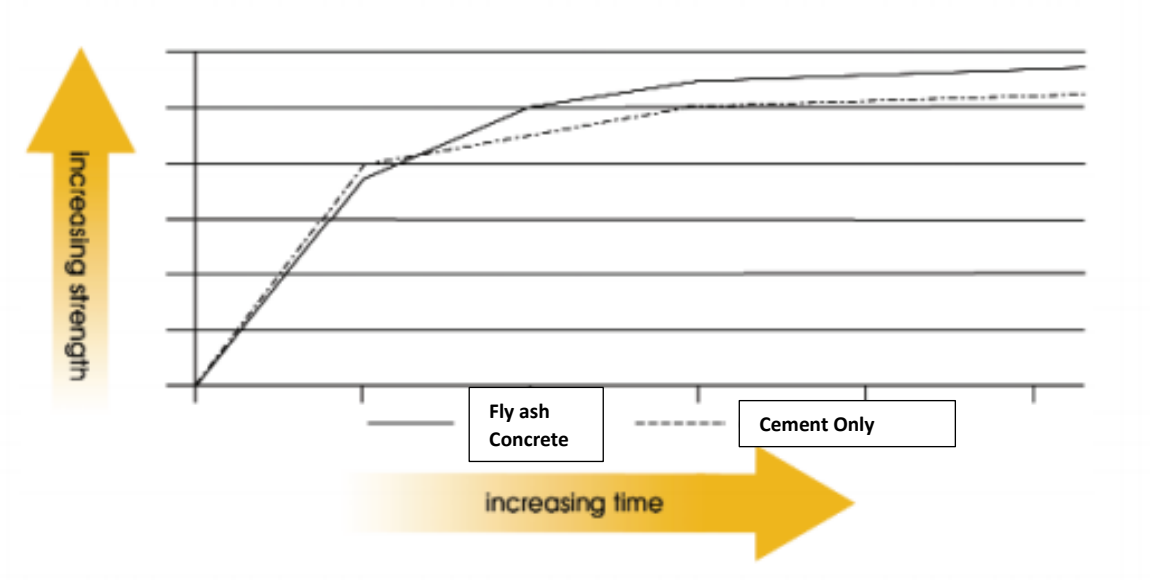

Figure 2.23 Displaying that fly ash can increase strength over time [33].

Usage of fly ash in concrete also has its disadvantages. Setting time has been found to be decreased with usage of fly ash, especially in colder environments, with temperatures below 4,4°C. In fact, fly ash mixtures might be avoided in these temperatures. This is due to fly ash mixtures having a slower hydration rate compared to regular concrete mixes. Furthermore, this results in slower early strength when fly ash is used. Additionally, fly ash mixtures are also more sensitive to moist curing environments, which can have adverse effects on the permeability of the mixture [32].

A study conducted by Kaplan et al. (2018) [34] investigated the effects of replacing Portland cement with fly ash in a cement mixture along with strength enhancers and grinding aids. Fly ash replaced Portland cement in concentrations ranging from 0%, 5%, 20% and 35wt%. Other additives utilized in the concrete study were grinding aid additives, early and final strength enhancers, and 40% mineral additive. The plugs featured varying fly ash content along with one of the previously mentioned additives. Reference specimens without any additives were also created.

Their results showed that fly ash content directly impacted Blaine fineness, which is a parameter that measures particle size/fineness of the cement in cm^2/g, surface area per unit of mass. This parameter affects hydration rate and water requirements and is important for slurry rheology and pumpability [11]. Figure 2.24 displays there is a significant increase in Blaine's fineness as fly ash content increases. Generally, an increase in Blaine fineness is considered as favourable as it is considered that it increases hydration rate and possibly compressive strength.

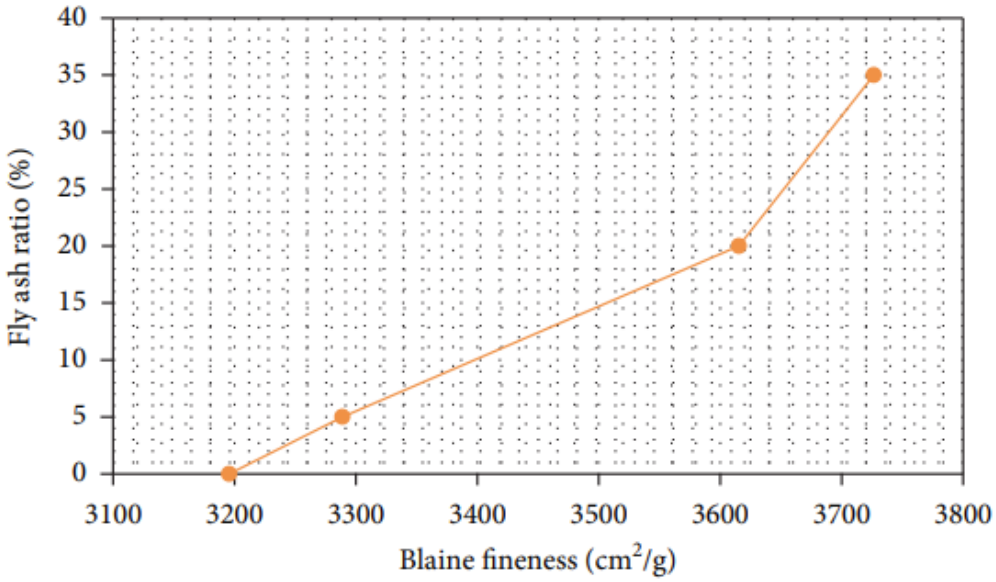

Figure 2.24 Fly ash ratio(%) vs Blaine fineness from Kaplan et al. (2018) [34].

However, the hydration rate was negatively impacted as depicted in figure 2.25. Fly ash content directly contributed to slower initial and final setting times along. Ultimately, delayed setting times are considered as an adverse effect, as they contribute to poor early strength. Also, higher contents of FA correlated to higher water demand [34].

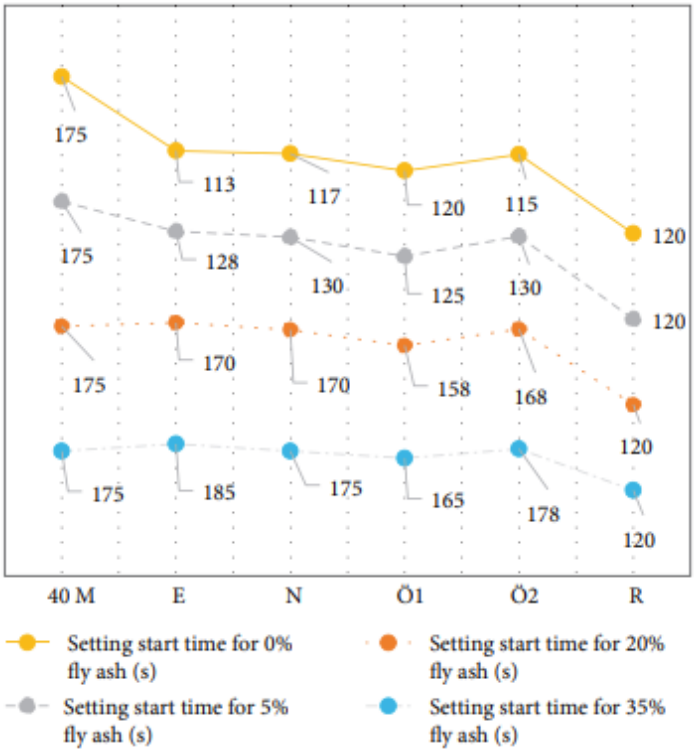

Figure 2.25 Setting time for various concentrations of FA [34].

To clarify the diagrams, 40M, E, N Ö1, Ö2 in the diagrams refers to the other additives used along with the FA content. Ö1 and Ö2 are the grinding aids, whereas E and N are strength enhancers, and 40M is cement with 40% mineral additive. R is the reference specimen, with no additives.

The study found that the compressive strength after 2 and 7 days the fly ash content largely reduced the early compressive strength for almost all concentrations. Exceptions being 5% and 20% with usage of strength enhancers (E, N). The compressive strength after 7 days is depicted in figure 2.26. The study concluded that fly ash additives were for the most part unsatisfactory for early strength after curing ages of 2 and 7 days. Again, believably due to the hydration rate being slower with fly ash.

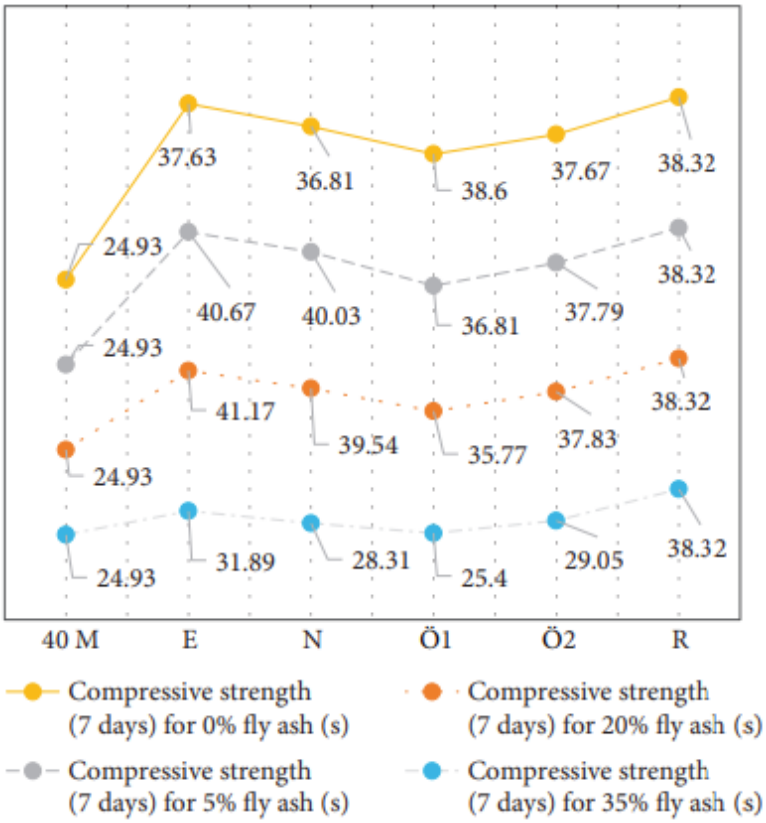

Figure 2.26 Compressive strength after 7 days of curing [34]

On the contrary, after 28 days curing, displayed in figure 2.27, the compressive strength was improved for all dosages of fly ash. From the 7 to 28 day curing age, the specimen with 20wt% had a compressive strength increase of 20.7%, thus regarded as the best specimen of the study. Conclusively, fly ash was found to inhabit adverse effects on early strength, but final strength was improved compared to reference [34].

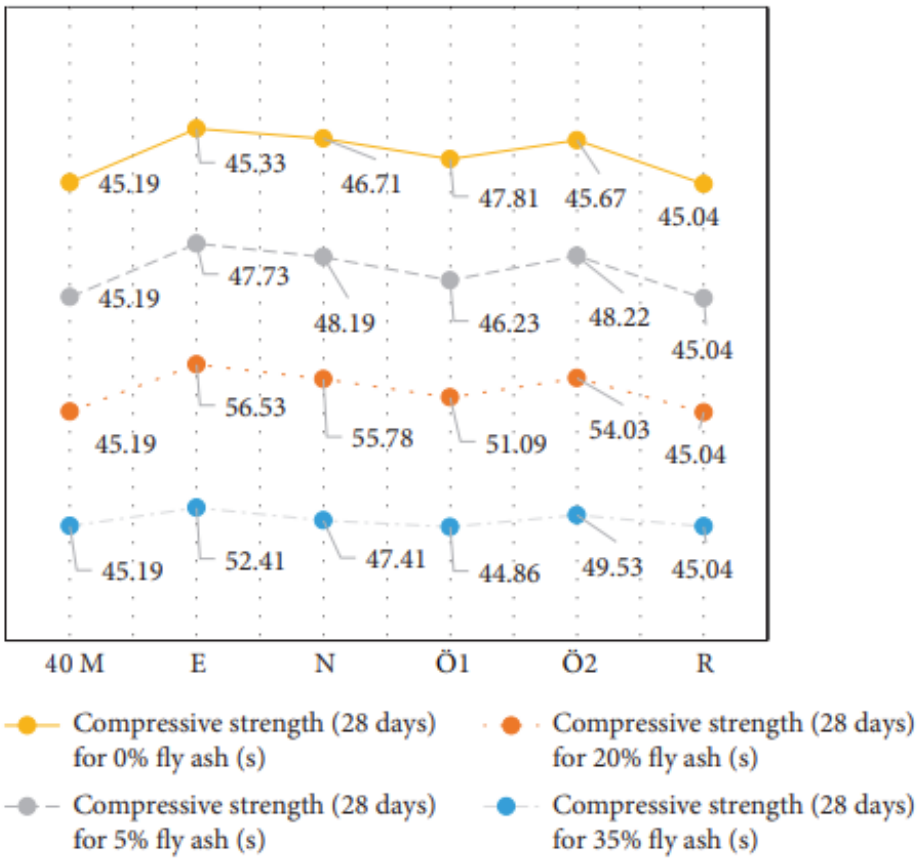

Figure 2.27 Compressive strength after 28 days [34]

The results of the study conducted by Kaplan et al. [34] matches overall pretty good with the literature review from Bremseth (2009) [32]. It shows that early strength is affected with the use of fly ash as additive, but that over extended curing periods fly ash additives prove themselves useful for compressive strength gain even though they effect hydration time negatively. Substituting Portland cement with a portion of fly ash could prove to be a viable strategy, which would be more environmentally friendly in the long run. The vast amounts of energy used for grinding and manufacturing cement annually is staggering. According to Jankovic et al. (2004) [35], the electrical energy required for 1 ton of cement is 110kW, and when current annual cement production is at 4,1 billion tons/year, from figure 2.28 [36], that is a lot of energy spent creating cement annually. That corresponds to 451 Terawatt (TW) annually for producing cement, which is substantial. If energy expenditure from manufacturing cement can potentially be reduced by using some fly ash instead of cement, this could have a tremendous impact, thus helping the environment.

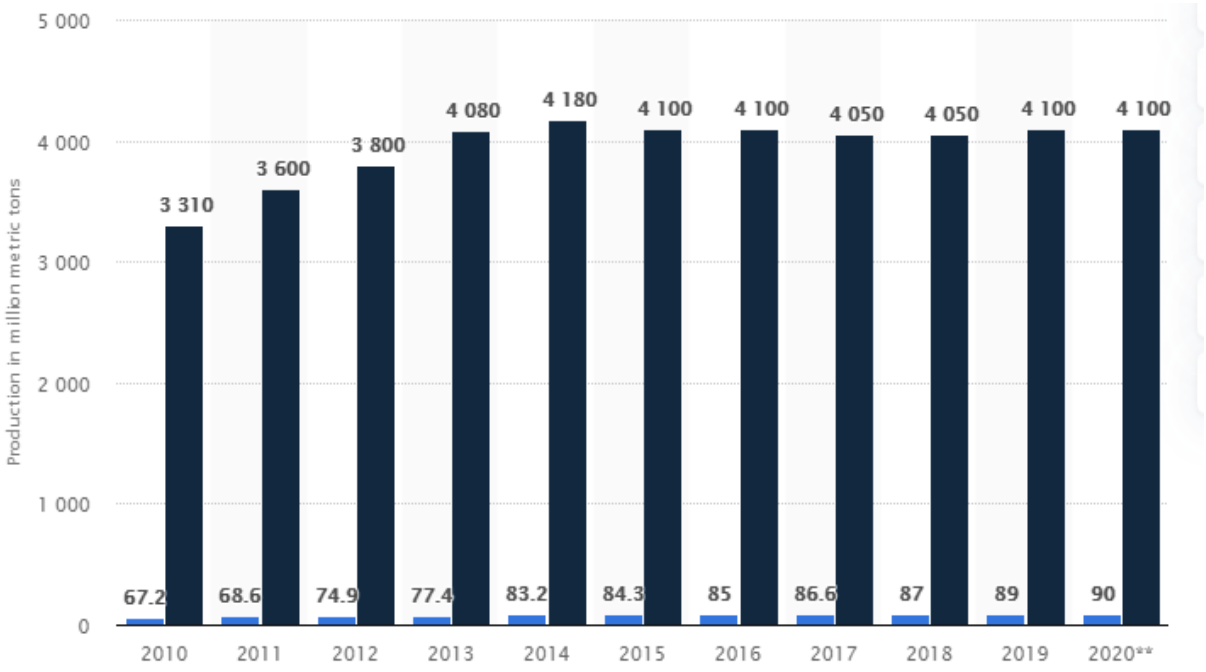

Figure 2.28 Annual cement production in million metric tons. Light blue colour is the cement production in USA. [36]

From this literature review, we have seen that both nanoparticles and fly ash as additives carry a legit potential to be beneficial in the future, and only research could help nourish this potential. Which is what this thesis aims to aid with, to further our understanding of how these additives might work for cementing applications.

2.3.4 Summary of literature review

This subsection includes a brief summary of relevant results from the literature review. It contains the bare minimum, only the results of **nano-SiO_2, nano-Al_2O_3, MWCNT** and **FA** with respect to **cementing applications**. Which entails, that if a study includes other additives, to the ones mentioned above, their results will not be in the table. Additionally, tables, figures and potential nuances are lost in this summarized table, so it is advised to read the full section above. For more information about dosages, other additives, curing ages etc. please read the full literature review.

Study title, Author [Reference] and DOI	Methodology	Key findings
"*Use of Nanomaterials in Cementing Applications*" Patil and Deshpande (2012) [20] DOI: 10.2118/155607-MS	Tested parameter: Mechanical strength Fluid loss Additive: micron-SiO_2 nano-SiO_2	Relevant findings(nano-SiO_2): • Nano-SiO_2 improved compressive strength, especially early strength. • Reduced fluid loss • Exhibited synergistic behaviour as it could be used in conjunction with other additives.
"A study on mechanical and pressure-sensitive properties" Li et al. (2003) [21] DOI: https://doi.org/10.1016/j.cemconres.2003.08.025	Tested parameters: Mechanical Strength Tested Additive: nano-SiO_2 nano-Fe_2O_3	Relevant findings(nano-SiO_2): • Improved compressive strength for all curing ages. • Improved flexural strength
"Mechanical, rheological, durability and microstructural properties of high performance self-compacting concrete containing SiO_2 micro and nanoparticles" Jalal et al. (2011) [22] DOI: https://doi.org/10.1016/j.matdes.2011.08.037	Tested parameters: Mechanical strength Rheology Durability Microstructure Additive: micron-SiO_2 nano-SiO_2	Relevant findings (nano-SiO_2): • Improved compressive strength for all curing ages. • Improved splitting tensile strength for majority of curing ages • Reduced water absorption • Enhanced microstructure

"*Effect of nanosilica on characterization of Portland cement composite"* Shih et al. (2006) [23] DOI: 10.1016/j.msea.2006.03.010	Tested parameters: Mechanical strength Microstructure Additive: nano-SiO_2	Relevant findings (nano-SiO_2): • Improved compressive strength for all curing ages. • Enhanced microstructure
"Effects of Nanosilica on Compressive Strength and Durability Properties of Concrete with Different Water to Binder Ratios" Isfahani et al. (2016) [24] DOI: 10.1155/2016/8453567	Tested parameters: Mechanical strength Durability Additive: nano-SiO_2	Relevant findings (nano-SiO_2): • Improved compressive strengths for w/b ratio of 0.65 and 0.55 after 7 and 28 days of curing • Reduced compressive strength with w/b ratio of 0.5 after 7 and 28 days of curing • w/b ratio has significant effect on compressive results
"*Improvement compressive strength of concrete in different curing media by Al_2O_3 nanoparticles*" Nazari and Riahi (2011) [25] DOI: 10.1016/j.msea.2010.09.098	Tested parameters: Mechanical strength Thermal properties Additive: nano-Al_2O_3	Relevant findings (nano-Al_2O_3): • Improved compressive strength for all curing ages. • Quicker final and initial settling time • Workability decreased. • Enhanced microstructure

"*Smart Cement Performance Enhancement with Nano-Al_2O_3 for Real Time Monitoring Applications Using Vipulanandan Models*" Vipulanandan et al. (2018) [27] DOI: https://doi.org/10.4043/28880-MS	Tested parameters: Mechanical strength Electrical resistivity Additive: nano-Al_2O_3	Relevant findings (nano-Al_2O_3): • Improved compressive strength for all curing ages. • Initial Electrical resistivity increased.
"*Ultra-high strength cement-based composites designed with aluminium oxide nano-fibres*" Muzenski et al. (2019) [28] DOI: https://doi.org/10.1016/j.conbuildmat.2019.05.175	Tested parameters: Mechanical strength Chemical shrinkage Additive: nano-Al_2O_3	Relevant findings (nano-Al_2O_3): • Improved compressive strength for the majority of curing ages. • Reduces chemical shrinkage
"*MWCNT for Enhancing Mechanical Properties of Oil Well Cement for HPHT Applications*" Khan et al. (2016) [29] DOI: https://doi.org/10.2118/178175-MS	Tested parameters: Mechanical strength in HPHT Additive: MWCNT	Relevant findings (MWNCT): • Improved compressive strength for all curing ages. • Improved strength development
"*The mechanical properties, microstructures and mechanism of carbon nanotube-reinforced oil well cement-based nanocomposites*" Lu et al. (2019) [30] DOI: 10.1039/c9ra04723a	Tested parameters: Mechanical properties Microstructure Rheology Additive: MWCNT	Relevant findings (MWNCT): • Fluidity of slurry was reduced. • Rheology was improved up until high concentrations of MWCNT, where adverse effects occurred. • Lowest dosages of MWCNT improved early strength • All specimens with MWCNT improved final strength

		• Compressive strength and rheology were highly influenced by dosages of MWNCT. • Flexural strength was improved for all curing ages. • Enhanced microstructure
"*Effect of multi-walled carbon nanotubes (MWCNTs) on the strength development of cementitious materials*" Naqi et al. (2018) [31] DOI: 10. 1016/j.jmrt.2018.09.006	Tested parameters: Mechanical strength Autogenous Shrinkage Additive: MWCNT	Relevant findings (MWNCT): • Improved compressive strength for lower dosages of MWCNT, adverse effects at higher concentrations. • Autogenous shrinkage improved for lower dosages, adverse effects for higher dosages. • Success of MWCNT was highly influenced by dosage.
"*The Optimization of Calcareous Fly Ash-Added Cement Containing Grinding Aids and Strength-Improving Additives*" Kaplan et al. (2018) [34] DOI: 10.1155/2018/8917059	Tested parameters: Mechanical strength Blaine's fineness Additive: FA	Relevant findings(FA): • Blaine's fineness increased with FA content. • Worse hydration rate – Slower initial and final setting time • Increase in water demand • Compressive early strength was significantly reduced. • Final compressive strength was improved

3 Experimental Program

The following chapter will delve into what materials was used, the experimental design and overall relevant information about the experimental portion of this thesis. All the materials and instruments used to conduct the experiments was provided by the University of Stavanger.

3.1 Materials

This section will focus on materials used to conduct the experimental program.

3.1.1 Cement

The cement used in the experimental program was an MSR/HSR API G-class Portland cement provided by Norcem located in Lilleaker, Norway.

3.1.2 Water

To synthesize the cement slurries, regular water from the faucet at the laboratory was used as this is assumed to be of the quality required to create the slurries.

3.1.3 SiO_2 nanoparticles

The nano silica employed in the experimental program was a colloidal mixture of 50 wt% silica suspended in H_2O. It was provided by Sigma Aldrich Norway. No specifications were found about actual size of the nanoparticles. pH of the dispersion was 9,0 and it had a density of 1,4g/ml in 25^oC [37]. The colour of the particles was translucent/white.

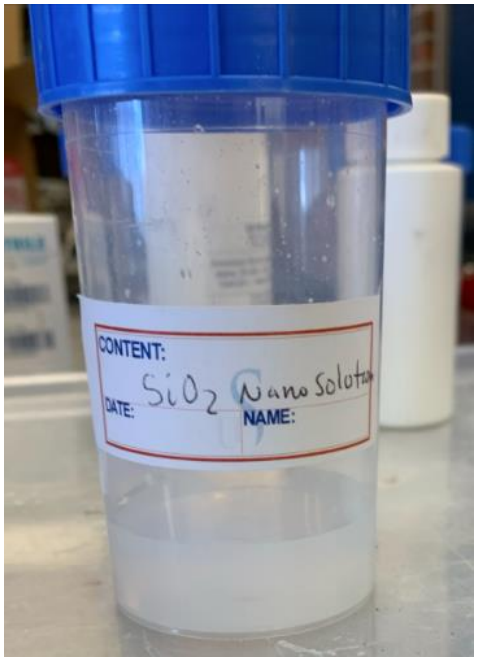

Figure 3.1 Nano-SiO_2 aqueous solution

3.1.4 Al_2O_3 nanoparticles

The Al_2O_3 originated from US Research Nanomaterials Inc in Houston, Texas. According to the label on bottle and their US Research Nanomaterial website, the particles size is around 30 nm and has purity of 99,99%. The structure is Alpha. Furthermore, the particles are dispersed in water with approximately 20%wt and a pH ranging from 6-8 [38]. Colour of the particles was white.

Figure 3.2 Nano-Al_2O_3 used in this thesis

3.1.5 MWCNT

Multi walled carbon nanotube (MWCNT) was also acquired from US Research Nanomaterials Inc, located in Houston, Texas. The particles have an ID of 5-10nm and an OD of 20-30 nm. Additionally, MWCNT is dispersed in water with a purity of >95wt%. Density of the dispersion is 2,1g/cm^3 [39]. Colour of the particles were black/dark.

Figure 3.3 MWCNT used in this thesis

3.1.6 Fly Ash

The fly ash used in this thesis was provided by Norcem in Lilleaker, Norway. By API classification the fly ash is Class F, as it holds negligible cementitious abilities on its own, but will develop it in presence of moisture [12]. It has a specific gravity of 2,3 g/cm^3. The colour of the fly ash was a light brown.

Figure 3.4 Fly Ash used utilized in this thesis

3.1.7 Cement mould

The mould used for curing of the specimens was a plastic cylinder, with height and diameter of 69mm and 34mm, respectively. After the plugs had reached their curing age, the plastic mould was gently cut, in order to retrieve the plug without compromising the samples. Cutting the plastic mould was done to prevent the requirement of using lubrication oil in order to retrieve the plug from their moulds.

Figure 3.5 Cement mould and its red cork

3.2 Test Matrices

The following section will provide information about the designed test matrices and test batches. Ingredients, procedure, and reasoning behind the matrices will be elaborated upon in the following subsections.

3.2.1 Experimental design

A total of five test matrices (TM) were designed. Each TM has three test batches (TB), which were cured for either 3 days, 7 days or 28 days. The arrangement of TMs and their respective TBs for the entire thesis is presented in table 3.1

	Test Batches	Curing age
Test Matrix 1	TB 1	3 days
	TB 2	7 days
	TB 3	28 days
Test Matrix 2	TB 4	3 days
	TB 5	7 days
	TB 6	28 days
Test Matrix 3	TB 7	3 days
	TB 8	7 days
	TB 9	28 days
Test Matrix 4	TB 10	3 days
	TB 11	7 days
	TB 12	28 days
Test Matrix 5	TB 13	3 days
	TB 14	7 days
	TB 15	28 days

Table 3.1 Test matrices in the experimental works of the thesis

- **Test Matrix 1**: Examined the effects of SiO_2 nanoparticles on 0.44 WCR neat G-class cement with curing ages of 3, 7 and 28 days.
- **Test Matrix 2**: Investigated the effects of a binary nanoparticle blend (SiO_2 and Al_2O_3 nanoparticles) on 0.44 WCR neat G-class cement with curing ages of 3, 7 and 28 days.
- **Test Matrix 3**: Studied the effects of a ternary nanoparticle blend (nano-SiO_2, nano-Al_2O_3 and MWCNT) on 0.44 WCR neat G-class cement with curing ages of 3, 7 and 28 days.
- **Test Matrix 4**: Investigated the effects of fly ash on 0.44 WCR neat G-class cement with curing ages of 3, 7 and 28 days.
- **Test Matrix 5**: Examined the effects of fly ash in conjunction with SiO_2 nanoparticles on 0.44 WCR neat G-class cement with curing ages of 3, 7 and 28 days.

3.2.2 Constants

Some variables are held constant for all conducted experiments in order to maintain some sort of consistency and prohibit excessive changes to the factors present in the designed test matrices. This translated to all test batches having some common denominators. Every batch uses G – Class cement based on the API classification table 2.2 presented in section 2.1.2

Additionally, the WCR is always 0.44 as this is a common and realistic ratio for wellbore cementing. Each batch had ten specimens created. Of the ten samples, two were reference samples, followed by two plugs for every concentration of additives. Luckily, covid-19 restrictions did not greatly affect access to the laboratories, thus allowing all samples to be tested on their planned day, which was either day 3, 7 or 28.

Test Matrices summarized					
Test Matrix #	**Additive(s)**	**Curing ages (days)**	**Cement Class**	**WCR**	**Total Plugs Created**
1	SiO_2	3,7,28	G	0.44	40
2	SiO_2 + Al_2O_3	3,7,28	G	0.44	40
3	SiO_2 + Al_2O_3 + MWCNT	3,7,28	G	0.44	30
4	FA	3,7,28	G	0.44	30
5	FA + SiO_2	3,7,28	G	0.44	30

Table 3.2 Test matrices summarized

3.2.3 Slurry synthesis procedure for experimental works

For **batches 1-9,** the procedure to synthesize the cement plugs was to measure 227,2 ± 0.05 g of dry G-class cement with 100g liquid which results in a WCR ratio of 0.44. The liquid mix was water with the sum of added nanoparticles as:

Equation 3.1

$$\left(100g\ H_2O - \sum_{i=1}^{n} y_n\right) = x\ g\ H_2O$$

$$x\ g\ of\ H_2O + \sum_{i=1}^{n} y_n = 100g\ liquid$$

$$\text{Where, } \sum_{i=1}^{n} y_n = y_1\ g\ of\ NP_1 + y_2\ g\ of\ NP_2 \ldots + y_n\ g\ of\ NP_n$$

Where, x is the unknown amount of H_2O required to get a total of 100g of liquid for synthesizing the slurries, to ensure WCR of 0.44. n is number of unique nanoparticles present in the system, y is the number of grams of the unique nanoparticle present in the system and NP is an abbreviation for nanoparticle.

All required cement, water and nanoparticle measurements were taken for the entire batch before any slurries were mixed. This minimized the time between the creation of the different plugs, thus ensuring that some specimens had not cured for unnecessarily long periods of time before the next set of specimens were created.

Furthermore, 227,2 ± 0.05 g dry cement was put in a mixing container, and then 100 g ± 0.005g liquid mixture consisting of water and desired nanoparticles would be added in the same container. The cement powder and liquid was stirred until a smooth mixture before being poured into the cement moulds. In order to prevent air bubbles from manifesting in the cement plug while pouring the slurry, the mould was continuously and gently tapped against a flat surface. Trapped air could potentially harm the cured cement plug. After the slurry was poured into the mould, the cork which belonged to the mould were put lightly on top. Note that the cork was not screwed on with force, as this could force air down in the slurry and damage the structural integrity of the specimen.

When all the subsequent cement plugs were created, they were left to cure in room temperature and atmospheric pressure for either 3,7 or 28 days. After their respective curing period, the cork was removed, and each sample was smoothened on top such that it would have a flat surface. This would prevent any point loading when they would later be crushed. Point loading can significantly diminish the compressive load of the sample, so the top had to be undeniably flat, which was controlled with a spirit level. Length, weight, and sonic velocity of each specimen was measured and finally they were all crushed to find their UCS. All batches were tested on their final curing day, the 3^{rd}, 7^{th} or 28^{th} day.

For **batches 3, 6, 9, 12, 15** which is the batches that had a curing age of 28 days. These have in common that the last 24 hours of their curing was done submerged in water. Before the specimens were submerged in water, they were removed from their mould and weighted. Subsequently, after spending 24 hours submerged in water, the weight could be measured again, and water absorption (%) was calculated from this.

Moreover, **test matrix 4 and 5** (TB 10 through TB 15), utilized fly ash as an additive, which is a dry ingredient. If fly ash was present, the amount added was then subtracted from the cement, in order to maintain a WCR of 0.44. Additionally, the fly ash was mixed properly with the cement powder, to ensure a homogenous mix between the dry ingredients, before any liquid was added to create the slurry.

3.2.4 Decision tree for test matrix 1,2 and 3

Figure 3.6 shows the decision tree for the first three test matrices. At first the research started with a single nanoparticle. Based on the best perceived SiO_2 concentration, a binary nanoparticle blend was designed to investigate if there is synergy between the particles.

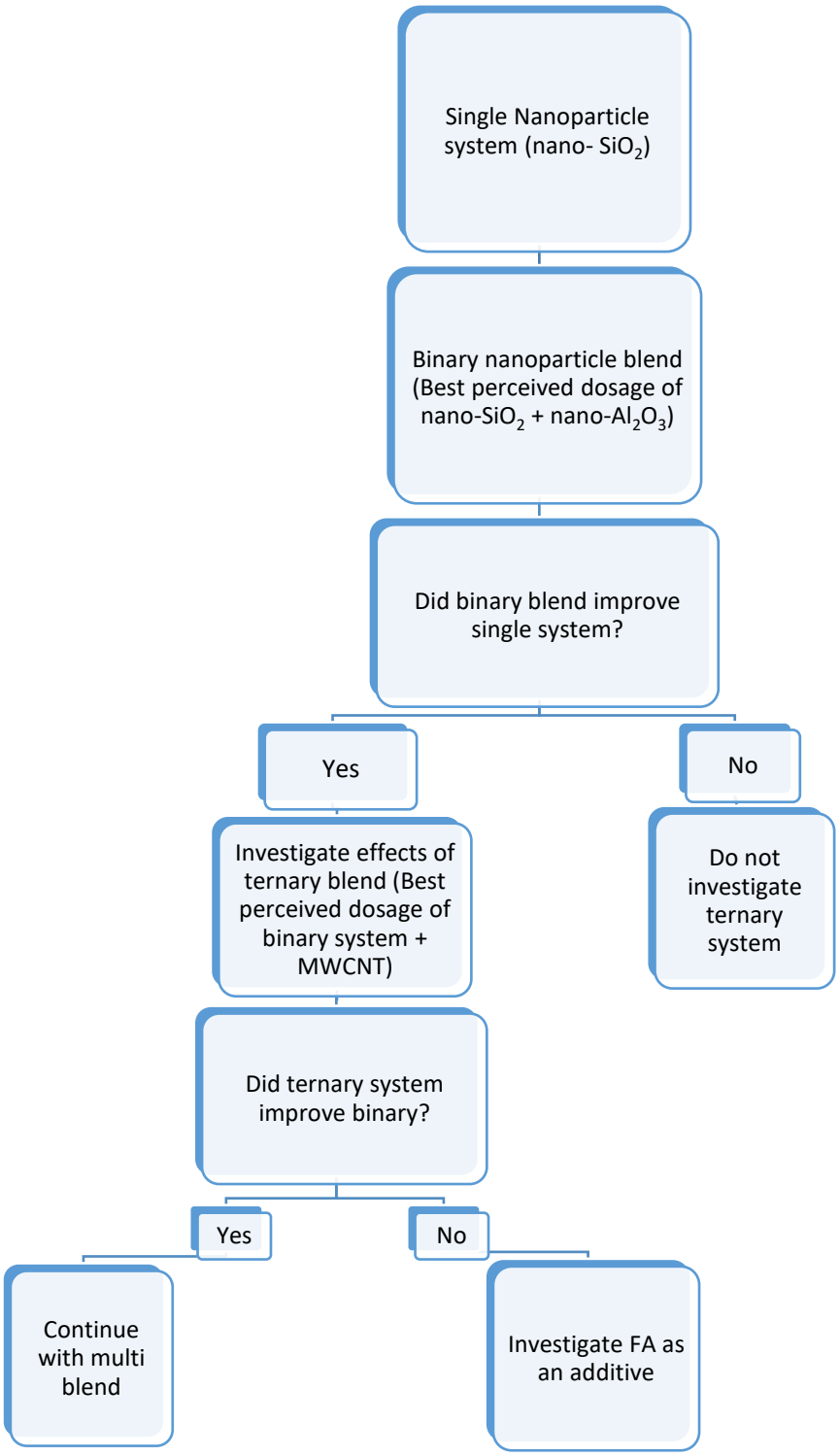

Figure 3.6 Decision tree for test matrix 1,2 and 3

3.2.5 Test Matrix 1

As shown in table 3.3, test batch 1, 2 and 3 all make up test matrix 1. The matrix was designed to study the effects of nano-SiO_2 on 0.44 WCR G-class cement.

	Test Batches	Curing age
Test Matrix 1	TB 1	3 days
	TB 2	7 days
	TB 3	28 days

Table 3.3 Test matrix 1 structure

Furthermore, the compositions of the cement slurries tested in TM 1 are depicted in table 3.4. The additives are identical for the three test batches, and the only factor differentiating the batches from each other is the curing age which is valid for other test matrices as well.

	Test Matrix 1 Composition		
Plug	**Cement (g)**	**Water (g)**	**Nano-SiO_2 (g) (aq)**
1	227,2	100	0
2	227,2	100	0
3	227,2	99,65	0.35
4	227,2	99,65	0.35
5	227,2	99,45	0.55
6	227,2	99,45	0.55
7	227,2	99,25	0.75
8	227,2	99,25	0.75
9	227,2	99	1
10	227,2	99	1

Table 3.4 Composition of test matrix 1

The synthesis of the slurries for each batch are according to the procedure described in section 3.2.3. Furthermore, SiO_2 nanoparticles were added in dosages ranging from 0.35g, 0.55g, 0.75g, and 1,0g. Ten cement plugs were created for each batch, which resulted in two plugs per concentration of nano-SiO_2 and two reference specimens in each test batch. Additionally, TB 3 was retested, hence why table 3.2 shows that this matrix has 40 created plugs instead of 30 like the majority of matrices. There was nothing wrong with the first iteration of TB 3, but to ensure the results were accurate it was retested. More information will be found in section (4.2.1).

3.2.6 Test Matrix 2

Test matrix 2 consisted of test batch 4, 5 and 6 and utilized a binary blend of Al_2O_3 and SiO_2 nanoparticles to investigate if this hybrid mixture would exhibit positive synergy and improve upon the SiO_2 nanoparticle system designed in test matrix 1. Table 3.5 depicts the matrix structure.

	Test Batches	**Curing age**
Test Matrix 2	TB 4	3 days
	TB 5	7 days
	TB 6	28 days

Table 3.5 Test matrix 2 structure

The best perceived nano-SiO_2 concentration from test matrix 1, with respect to UCS, was kept constant, while nano-Al_2O_3 was added in increasing dosages. In other words, the batch kept 0.55g nano - SiO_2 as a constant, in conjunction with adding 0.25g, 0.5g, 0.75g ,1,0g of nano-Al_2O_3. Ten samples were created for each batch, two of which were pure cement plugs used as reference, and then two per nano-Al_2O_3 concentration. The synthesis of the slurries for each batch are according to the procedure described in section 3.2.3. Composition of the designed slurries can be seen in table 3.6.

	Test Matrix 2 composition			
Plug	**Cement (g)**	**Water (g)**	**Nano-SiO_2 (g) (aq)**	**Nano- Al_2O_3 (g) (aq)**
1	227,2	100	0	0
2	227,2	100	0	0
3	227,2	99,2	0.55	0.25
4	227,2	99,2	0.55	0.25
5	227,2	98,95	0.55	0.5
6	227,2	98,95	0.55	0.5
7	227,2	98,7	0.55	0.75
8	227,2	98,7	0.55	0.75
9	227,2	98,45	0.55	1
10	227,2	98,45	0.55	1

Table 3.6 Composition of test matrix 2

Unfortunately, as a result of human error while gathering deformation data during compressive strength testing, the deformation data was not properly recorded for TB 4. This is required to plot the stress-strain curve of the samples, which then used to calculate resilience and Young's modulus, which is explained in more detail in section 3.3.1. Ultimately, this accumulated in a recreation of the batch to record the missing deformation data, which is why TM 2 also has 40 plugs created instead of 30 (table 3.2). However, by figuring out what errors was made, this was avoided for the subsequent batches.

3.2.6 Test Matrix 3

Test matrix 3 consisted of test batch 7, 8 and 9. With reference to the decision tree in section 3.2.4, the binary nanoparticle blend outperformed the single nanoparticle system, thus prompting the investigation of a ternary nanoparticle blend consisting of nano-SiO_2, nano-Al_2O_3 and MWCNT. This matrix utilized the best perceived binary blend dosage, again based upon UCS results. Table 3.7 details the structure of test matrix 3.

	Test Batches	**Curing age**
Test Matrix 3	TB 7	3 days
	TB 8	7 days
	TB 9	28 days

Table 3.7 Test matrix 3 structure

Furthermore, 0.55 g of nano-SiO_2 along with 0.25 g of nano-Al_2O_3 was kept constant while increasing MWCNT dosages from 0.25g, 0.5g, 0.75g and 1,0 grams. Ten samples were created for each batch, two of which were pure cement plugs used as reference, and then two per MWCNT concentration. Again, as with the other matrices, the only factor differentiating the batches from each other was the curing ages. The synthesis of the slurries for each batch are according to the procedure described in section 3.2.3. Table 3.8 exhibit the composition of test matrix 3.

	Test Matrix 3 composition				
Plug	**Cement (g)**	**Water (g)**	**Nano-SiO_2 (g) (aq)**	**Nano- Al_2O_3 (g) (aq)**	**MWCNT (g) (aq)**
1	227,2	100	0	0	0
2	227,2	100	0	0	0
3	227,2	98,95	0.55	0.25	0.25
4	227,2	98,95	0.55	0.25	0.25
5	227,2	98,7	0.55	0.25	0.5
6	227,2	98,7	0.55	0.25	0.5
7	227,2	98,45	0.55	0.25	0.75
8	227,2	98,45	0.55	0.25	0.75
9	227,2	98,2	0.55	0.25	1
10	227,2	98,2	0.55	0.25	1

Table 3.8 Composition of test matrix 3

3.2.7 Test Matrix 4

Test matrix 4 completely abandons any nanoparticles and studies the effect of fly ash as cement additive, to investigate if fly ash has any merit as a standalone additive. Test batch 10, 11 and 12 make up test matrix 4. It studies the effect of fly ash as an additive to 0.44 WCR G-class cement for the curing age of 3, 7 and 28 days. Table 3.9 exhibit the structure of the matrix

	Test Batches	**Curing age**
Test Matrix 4	TB 10	3 days
	TB 11	7 days
	TB 12	28 days

Table 3.9 Test matrix 4 structure

FA was added in dosages ranging from 2,5g, 5g, 7,5g and 10g. Ten samples were created for each batch, two of which were pure cement plugs used as reference, and then two per concentration of fly ash. The creation procedure was nearly identical to the previous matrices except from the fact that fly ash is a dry additive, so it was mixed with cement until a homogenous mix before adding any liquid. Otherwise, the procedure is identical as the one described in section 3.2.3. The amount of added fly ash was also subtracted from the amount of cement in order to maintain WCR of 0.44. As with the other matrices, the only differentiation between batches is their curing age. All constituents of the designed matrix are presented in table 3.10.

	Test Matrix 4 Composition		
Plug	**Cement (g)**	**Water (g)**	**FA (g)**
1	227,2	100	0
2	227,2	100	0
3	224,7	100	2,5
4	224,7	100	2,5
5	222,2	100	5
6	222,2	100	5
7	219,7	100	7,5
8	219,7	100	7,5
9	217,2	100	10
10	217,2	100	10

Table 3.10 Composition of test matrix 4

3.2.8 Test Matrix 5

Test matrix 5 examines the effect of varying dosages of fly ash in combination with a constant concentration nano-SiO_2 on 0.44 WCR G-class cement. This was conducted to see if the nanoparticle and fly ash blend would yield any increase in performance. SiO_2 nanoparticles were chosen because they showed great early strength and it was of interest to examine if SiO_2 nanoparticles could aid the early strength development when used in conjunction with fly ash as studies in the literature review found poor early strength from FA usage. The structure of test matrix 5 are presented in table 3.11.

	Test Batches	**Curing age**
Test Matrix 5	TB 13	3 days
	TB 14	7 days
	TB 15	28 days

Table 3.11 Test Matrix 5 structure

The nano-SiO_2 concentration was kept constant at 0.55g while fly ash was added in dosages ranging from 2.5g, 5g, 7.5g and 10g. Ten samples were created for each batch, two of which were pure cement plugs used as reference, and then two per dosage of fly ash. The creation procedure was identical to the procedure from test matrix 4, subtracting the amount of fly ash added from the cement, to ensure WCR of 0.44 and mixing the dry additives together before

adding any liquid. Curing age was the only difference between the batches in test matrix 5. Table 3.12 demonstrates the contents of this batch.

	Test Matrix 5 Composition			
Plug	**Cement (g)**	**Water (g)**	**FA (g)**	**Nano-SiO_2 (g) (aq)**
1	227,2	100	0	0
2	227,2	100	0	0
3	224,7	99,45	2,5	0.55
4	224,7	99,45	2,5	0.55
5	222,2	99,45	5	0.55
6	222,2	99,45	5	0.55
7	219,7	99,45	7,5	0.55
8	219,7	99,45	7,5	0.55
9	217,2	99,45	10	0.55
10	217,2	99,45	10	0.55

Table 3.12 Composition for test matrix 5

3.3 Characterization methods

The experimental portion of this thesis can be summarized as follows in the diagram below

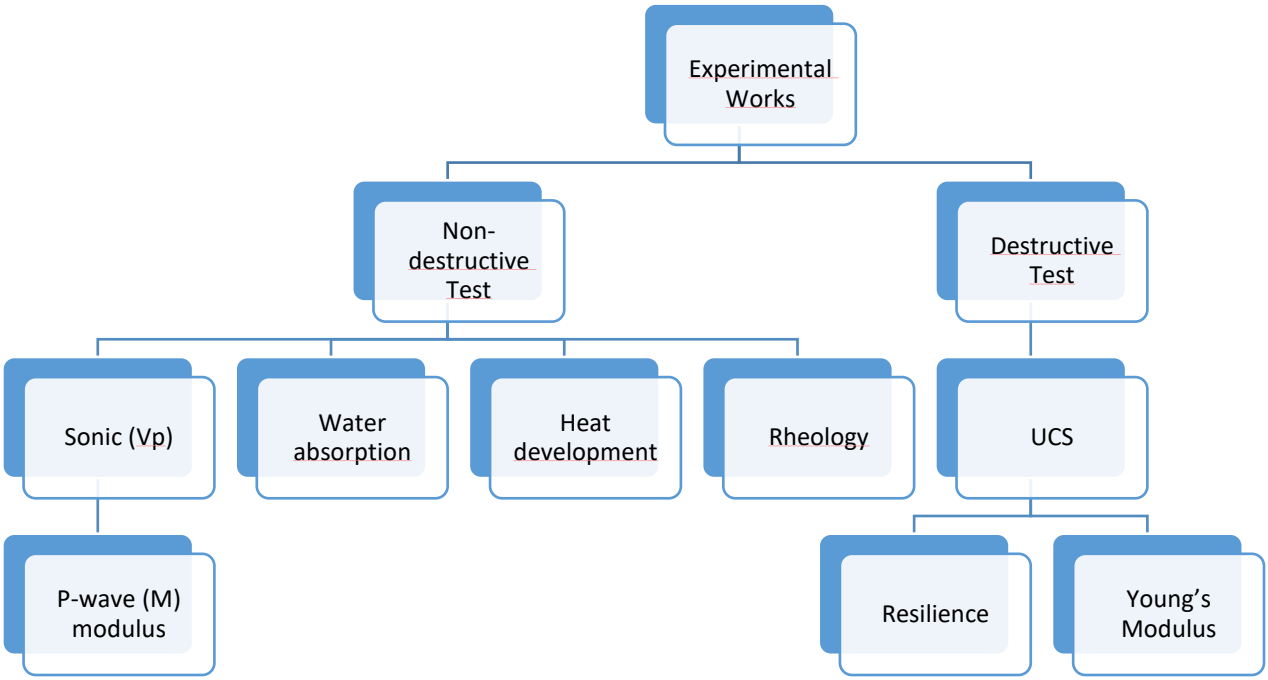

Figure 3.7 Experimental portion of the thesis

3.3.1 Destructive testing - Uniaxial Compressive Strength (UCS)

This section will inform about the destructive portion of the experiments. As the name implies, this is where the plug is put under mechanical load until failure. The outputs from a destructive test are max mechanical load and the specimen deformation data. This can be used to calculate elastic, mechanical and energy absorption capacity properties of the specimens.

3.3.1.1 Destructive measurement procedure

The apparatus used to crush all cement plugs was a modified hydraulic hand operated press. This press had a load cell installed, which allowed deformation data to be recorded as well as guaranteed accuracy of the output data. A computer to the right side of the press collected all load- and deformation measurements via a data acquisition (DAQ) software. All test batches were tested with this hydraulic shop press.

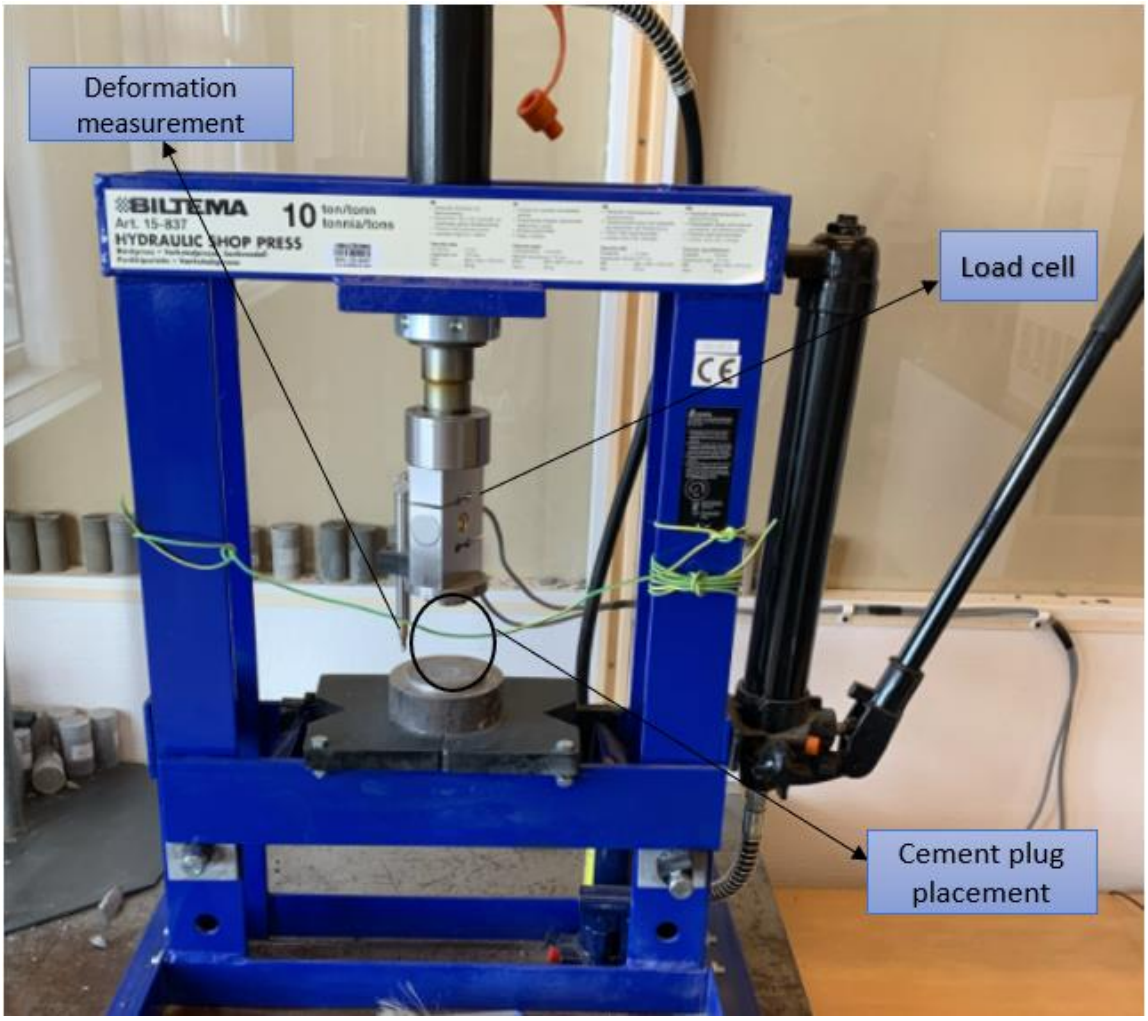

Figure 3.8 Modified shop press

Before any testing could commence, the plug had to be flat on both sides to prevent any point loading. After this was ensured with a spirit level, the samples were placed in the middle, beneath the load cell. Subsequently, the load cell was lowered to just above the cement plug. Before lowering the load cell further, some small metal plates were placed under deformation pin until the tip of the pin touched the metal plates, ensuring deformation data would be properly recorded. Finally, a plastic protective cover was placed in front of the cement plug, for protection of cement splinters, and thus the manual loading of the cement plug could commence until mechanical failure was reached. The speed while loading was kept as consistent as possible. Failure was observed visually, in addition to the software clearly showing the load difference after failure had been reached. Last step was to export the several thousand cells of data from the DAQ software to an excel spreadsheet to conduct further calculations.

3.3.1.2 UCS

The uniaxial axial compressive strength (UCS) is the maximum load carrying capacity of the plug during the uniaxial compressive test as shown in Figure 3.9. The UCS is determined from the maximum per cross-sectional load as [40]:

Equation 3.2

$$\sigma = \frac{F_{max}}{A}$$

Where σ denotes stress (MPa), F_{max} is max load (N) and A is the cross-sectional area of the cement plug (mm^2)

3.3.1.3 Young's Modulus

Young's modulus is an elastic modulus and measures the stiffness of a solid material. The Young's modulus is calculated from the linear elastic part of the stress- strain curve shown in Figure 3.9 as [41]:

Equation 3.3

$$E = \frac{\Delta\sigma}{\Delta\varepsilon}$$

Where E is Young's modulus (MPa), $\Delta\sigma$ is change in uniaxial stress (MPa) and $\Delta\varepsilon$ is change in strain (dimensionless). Conveniently, Young's modulus is also the gradient of stress strain curve before the yield point. Using an equation for a straight line

Equation 3.4

$$y = mx + b$$

For a stress-strain graph, as m denotes the gradient or slope of a straight line, it is also in this case Young's modulus [42]. This means that for the specimen used as example in figure 3.9 on next page has a Young's modulus of 4,72 GPa.

3.3.1.4 Resilience

Resilience is amount of energy a given material can absorb while being deformed, still remaining within the elastic region, meaning the material possesses the ability to release this energy upon unloading. Essentially, it is the maximum amount of energy a material can absorb before experiencing permanent changes to the material. In terms of a stress-strain curve, this is the area from zero until the elastic limit is reached [43]. After the elastic limit is reached, permanent deformation occurs, otherwise known as the plastic region.

Resilience can be calculated with [41]

Equation 3.5

$$R = \frac{\sigma_y^2}{2E} = \frac{\sigma_y \cdot \varepsilon_y}{2}$$

Where σ_y denotes stress (Pa) at yield point, ε_y strain (dimensionless) at yield point, E is Young's modulus and R is resilience (J/m^3). This formula was rarely used in this thesis but was utilized for some cases where the deformation data started to record slow due to human error, meaning that estimating the area under the curve would be more inaccurate.

Another method to find resilience is based on the area under the stress strain, which was used for the vast majority of samples in this thesis. As shown in Figure 3.9, the resilience is estimated from the area under the curve as follows:

Equation 3.6

$$R = \left| \sum \frac{\left(\varepsilon_{(i+1)} - \varepsilon_{(i)}\right) \cdot \left(\sigma_{(i+1)} + \sigma_{(i)}\right)}{2} \right|$$

Where ε is strain (dimensionless) and σ is stress (Pa).

Figure 3.9 depicts a visual representation of the determination of resilience (R), UCS and Young's Modulus (E) from the stress-strain graph of the actual specimens.

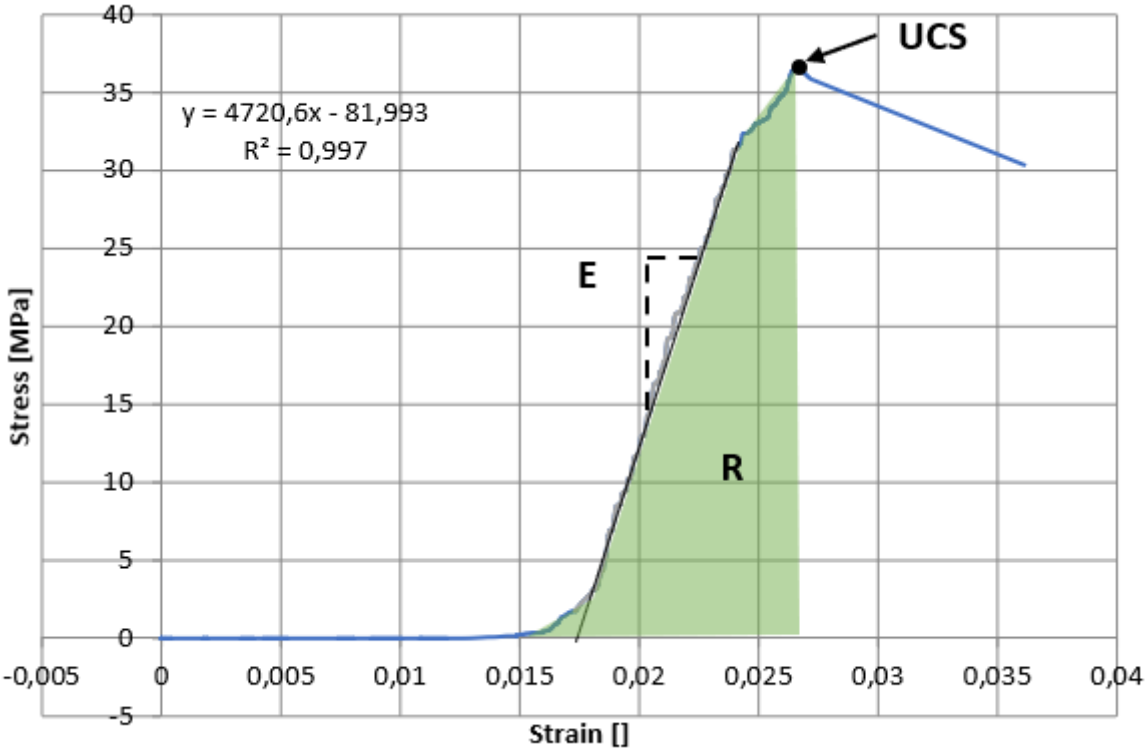

Figure 3.9 UCS, Young's modulus and resilience

3.3.2 Non-destructive testing

This subsection presents the procedure and parameter determination of the non-destructive testing done on the cement specimens.

3.3.2.1 Ultrasonic velocity measurement

Ultrasonic velocity is measured by placing the plug in between an emitter and a receiver. The emitter transmits an ultrasonic pulse, and the receiver records the time it takes to propagate through the length of the cement plug. This information can give indications about how well the cement sample has cured, if there is trapped air in the specimen or if there are significant cracks or other deformities.

Figure 3.10 shows the CNS Farnell Pundit-7. It has a tube with an emitter and receiver on opposite sides, with a hydraulic switch to ensure that the sensors are in contact with the specimen placed between them. Before measuring the ultrasonic velocity, the apparatus had to

be calibrated. This is done with a homogenous plug with a known travel time of 25,2 μs, which is used to calibrate the apparatus.

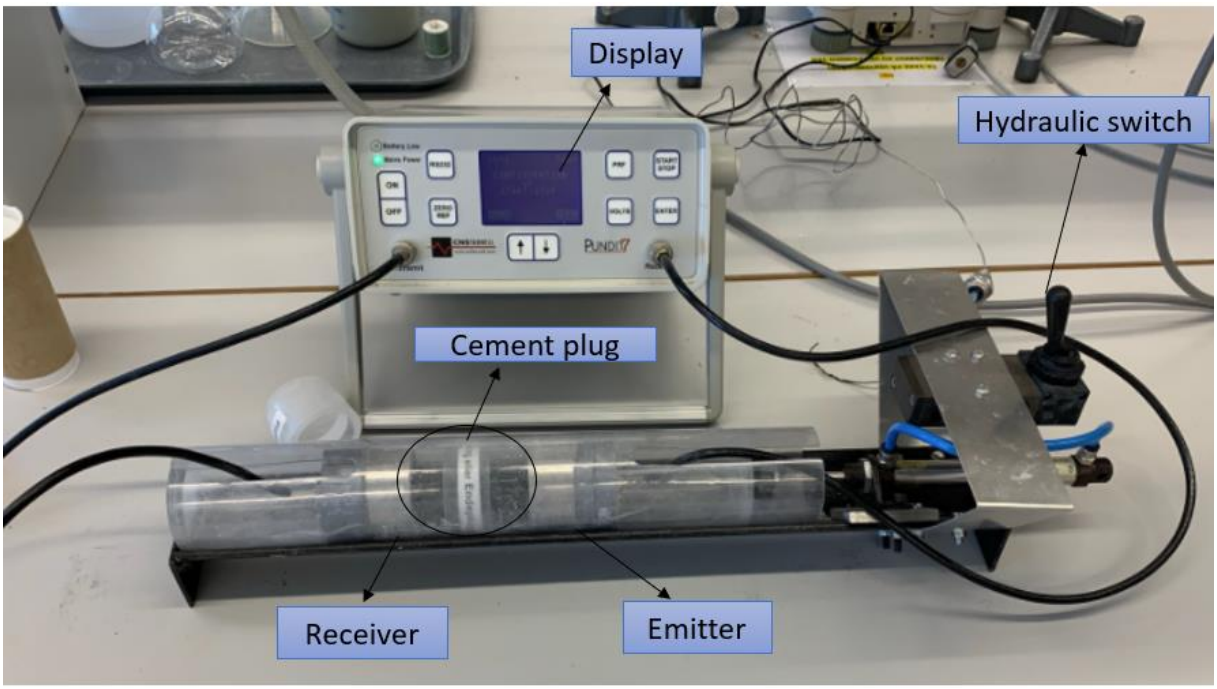

Figure 3.10 CNS Farnell Pundit-7 used to measure ultrasonic velocity

When the calibration was completed, the testing of cement plugs could commence. The cement plugs were placed in the tube. Afterwards, the hydraulic switch would be flicked, and the cement specimen would be firmly placed between the emitter and receiver. Finally, the pulse would be transmitted, and the display would display the travel time. Another important factor to note, was that each cement plug was placed in the same direction within the tube for consistency. The bottom of the sample always placed in contact with the emitter, and top with the receiver.

Velocity of sound

The velocity of sound for a plug is calculated as

Equation 3.7

$$V_p = \frac{L}{t}$$

Where, Vp is compressional wave velocity (m/s), L is the length of the plug (m) and t is the sound travel time (ms)

3.3.2.2 P-wave-modulus (M-modulus)

P-wave modulus (M - modulus) is one the elastic moduli, which are utilized to characterize isotropic homogenous materials. More specifically, p-wave-modulus is defined as a measurement of the ratio of axial stress to axial strain in a uniaxial stress strain state [44]

Equation 3.8

$$M = \frac{\sigma_{zz}}{\varepsilon_{zz}}, \qquad \varepsilon_{xx} = \varepsilon_{yy} = \varepsilon_{xy} = \varepsilon_{xz} = \varepsilon_{yz} = 0$$

Where M is the p wave-modulus, σ_{zz} is axial stress and ε_{zz} is axial strain where there is only strain in one direction, specifically the longitudinal direction [44]. Due to this reason P-wave modulus is also referred to as constrained modulus in some cases, as strain is constrained to only occurring in the longitudinal plane [45]. M-modulus can also be described by using shear modulus (G) and bulk modulus (K), which are two other elastic moduli, by the following relationship

Equation 3.9

$$M = K + \frac{4G}{3}$$

Where G is shear modulus (GPa), K is bulk modulus (GPa) of the material. Finally, M is P-wave-modulus (GPa).

Furthermore, P-wave modulus can also be expressed as velocity of a P-wave and the density of the medium it travels through

Equation 3.10

$$v_p^2 \cdot \rho = K + \frac{4G}{3}$$

The P-wave-modulus is ultimately given as:

Equation 3.11

$$M = \frac{v_p^2 \cdot \rho}{10^9}$$

Where M is P-wave-modulus (GPa), ρ is the density of the medium (cement plug in this case) (kg/m^3), and v_p denotes compressional wave velocity (m/s), which is calculated as eq. 3.7.

3.3.2.3 Water Absorption

Water absorption was tested for specimens which had cured for 28 days. With water absorption data, information is acquired about the microstructure of the cement sample. An increased water absorption in a specimen is generally considered as unfavourable as it strengthens the belief of a compromised cement matrix, with increased pore spaces or other defects which would allow for more water to be absorbed. Ultimately, in a wellbore scenario, this could possibly cause problems with fluid leakages over time, meaning the cement integrity could be negatively impacted. From the literature review, it is believed that nanoparticles have the ability to act as fillers in the cement matrix, thus improving it [22], which should lead to reduced water absorption.

The procedure for measuring water absorption was simple, after the cement plugs had cured for approximately 27 days, they were demoulded, and their dry weight was measured. Subsequently, they were submerged in 24 hours in ordinary water. After 24 hours had passed, they were properly dried, and the weight was measured once again. Water absorption was calculated by the use of the following formula:

Equation 3.12

$$\Delta M = \frac{M_w - M_d}{M_d} \cdot 100$$

Where M_w (g) is the weight of the specimen after 24 hours of submersion in water, M_d (g) is the dry weight before being submerged and ΔM (%) is the percentage change in mass.

3.3.2.4 Rheology measurement and model

Rheology describes the flow and deformation of fluids. The knowledge of the rheological parameters for drilling fluids and cement is very important for the determination of well circulation - and pump pressure to ensure that no problems arise during pumping of the fluids/slurries into the well [4].

Rheology procedure

The apparatus used for rheological testing was an O-Fite 8-Speed viscometer, depicted in figure 3.11. Cement slurries were mixed to a smooth mixture, before being poured in the measurement cup. Subsequently, viscometer responses of the slurry were measured at 300, 200, 100, 60, 30, 6,3 RPM. Notably, 600 RPM was not tested as this is not a relevant measurement for cement slurries.

Figure 3.11 Rheometer used for the testing

Rheology model

There are several models which describe the rheology of a material. However, this thesis will utilize the Casson rheological model as it is commonly used to describe the rheology of cement slurry. It is a two parameter model read as [4]:

Equation 3.13

$$\tau^{0.5} = \tau_c^{0.5} + \mu_c^{0.5} \cdot \gamma^{0.5}\,, \qquad for\ \tau < \tau_C$$

$$\gamma = 0.\ for\ \tau \geq \tau_C$$

Where, τ is shear stress ($lb_f/100ft^2$), τ_c denotes Casson yield stress ($lb_f/100ft^2$), μ_c is Casson plastic viscosity ($lb_f/100ft^2$) and γ is shear rate (sec^{-1}).

To clarify, viscosity is simply defined as a measurement of resistance to flow for a material. And yield stress is defined as the minimum amount of stress required to make a material flow

[46]. Both these parameters are important to have information about in order to pump the cement slurry downhole.

3.3.2.5 Heat development

When cement comes in contact with water, hydration occurs, which is an exothermic reaction. An exothermic reaction releases heat, and during the hydration of cement, the heat released can be of interest. Usually, the heat liberated is of no concern when concrete/cement is used for construction purposes, as it dissipates without causing any major harm. However, concrete/cement can crack due to excessively high temperature increases during the hydration process. This is because if a rapid and/or nonuniform cooling occurs, it will cause harmful stresses on the cement, and it may crack either during the process of cooling to temperature of the surrounding environment or after being cooled [47].

Furthermore, when cement is used in wells, this heat released can be a cause of concern. Predominately because the casing is relatively sensitive to thermal loads and can as a result expand. As we witnessed in figure 1.1, the primary cement job is to seal the space between annulus and the casing, meaning that if the heat released during curing of the cement is substantial enough, it can cause expansion of the casing. As a result, it is important to gain information about the heat development during hydration.

For the heat development test, the best results based on the UCS value are selected from each text matrices and compared with the neat G-class cement. The slurry composition was scaled up with a factor of two, to ensure proper contact between sensors and the synthesized slurries. Subsequently, the slurries were poured into plastic bags, where temperature sensors were placed in contact with them. These loggers were calibrated using a software called Easy Log. The data was also retrieved from this software after the experiment. After the slurries had been poured into plastic bags and the sensors had placed in contact, they were put into 10x10x10 cm Styrofoam compartments, where the cement would be insulated (Figure 3.13). Lastly, the Styrofoam lid was placed on top of the compartments to ensure full insulation. Figure 3.12 shows the temperature sensor, and figure 3.13 shows when the sensor has been submerged in the cement slurry and placed in thermal insulator compartment.

Figure 3.12 Logger used to gather temperature development

Figure 3.13 Complete set-up for measuring heat development

3.3.3 Empirical UCS model

The uniaxial compressive load is the maximum compressive strength that a right-cylindrical specimen can endure before failure [48]. It is a common loading scenario of cement and concrete when used for industrial purposes, which is why it is an important measurement. One major inconvenience with measuring UCS is that the sample has to be destroyed. Essentially, reaching failure by maximum compressive stress in order to accurately measure the peak compressive strength. It would be convenient to have a model which could measure the UCS of right-cylindrical specimen accurately, without destructive testing.

Horsrud (2001) [49] developed an empirical correlation equation that relates UCS with compressional wave velocity based on shale rocks extracted from the North Sea [49]. The model reads:

Equation 3.14

$$UCS = 0.77 \cdot {V_p}^{2,93}$$

Where, UCS denotes uniaxial compressive strength (MPa) and V_p is the compressional wave velocity through the material (km/s).

Even though, the Horsrud model was developed from shale, in this thesis the model will be tested on cement data and will compared with the empirical model developed in this thesis.

4 Results and Discussion

This section presents all the results gathered in the experimental works of the thesis, which includes destructive (UCS, Young's modulus and resilience) and non-destructive (p-wave-modulus, water absorption, heat of hydration and rheology) testing. Appendix A will present bar graphs for all results, while Appendix B will contain the load vs deformation profiles for the samples.

4.1 General information

The subsequent sections will present the results in diagrams which combines the data from each curing age (test batch) into one diagram. Y-axis is the performance achieved in the tested parameter, while x-axis is the additive concentration in grams. Furthermore, the colour scheme is always the same, with the blue curve exhibiting the 3 days results, orange curve showing the 7 days results and red curve displaying 28 days results. Furthermore, the values closest to each point is the actual value recorded.

If the diagrams presented in the results section are unclear or cluttered as sometimes the curves entwine, bar diagrams for each tested parameter are available in appendix A, where they follow the same style as the water absorption diagram in the results. Here, the values should be clear.

For the absolute majority of results the values presented are the average of two plugs. However, there are instances where it is based on 3-4 if a batch was recreated. This is valid for TB 3 and TB 4. Additionally, in some rare cases the results are also based on one plug, as some cement plugs were compromised and damaged.

Also, the reference values are the average reference value of across all test batches, with the same curing age. For instance, this means that all the 3 days reference values across all designed matrices have been collected and the average reference has been calculated and is displayed in the diagrams. This is done to get as accurate reference value (control value) as possible.

4.2 Test Matrix 1 (Effect of nano-SiO_2)

This section will be dedicated to test matrix 1, which is the effect of nano-SiO_2 on 0.44 WCR neat G-class cement for curing ages of 3,7 and 28 days. Just to reiterate, this batch used nano-SiO_2 as standalone additive in dosages from 0.35, 0.55, 0.75, 1,0grams.

4.2.1 Effect of nano-SiO_2 on UCS

UCS is of interest because the higher the value is, the stronger the cement is, meaning that it can withstand greater loads in the demanding well environment, by the likes of higher pressures and harsher conditions. Figure 4.1 displays the UCS results for test matrix 1. It can be observed

that the UCS results are very dosages dependent and fluctuates non-linearly. After curing for 3 and 7 days, nano-SiO_2 exhibits mostly improvements over the reference value, with some very promising peak compressive strengths, although poor results are also observed for some dosages.

After 3 days of curing, the plugs with 0.35g and 1.0g of nano-SiO_2 had a compressive strength of 17,88 MPa and 15,13 MPa, respectively. Which corresponds to a 23,27% improvement for 0,35g and 4,29% improvement for 1,0g of SiO_2. However, the plugs with 0.55g and 0.75g of nano-SiO_2, had average values of 14,61 MPa and 13,80 MPa, resulting in a small increase of 0.74% in UCS for 0.55g, whereas 0.75g caused a decrease of 4,86% in UCS.

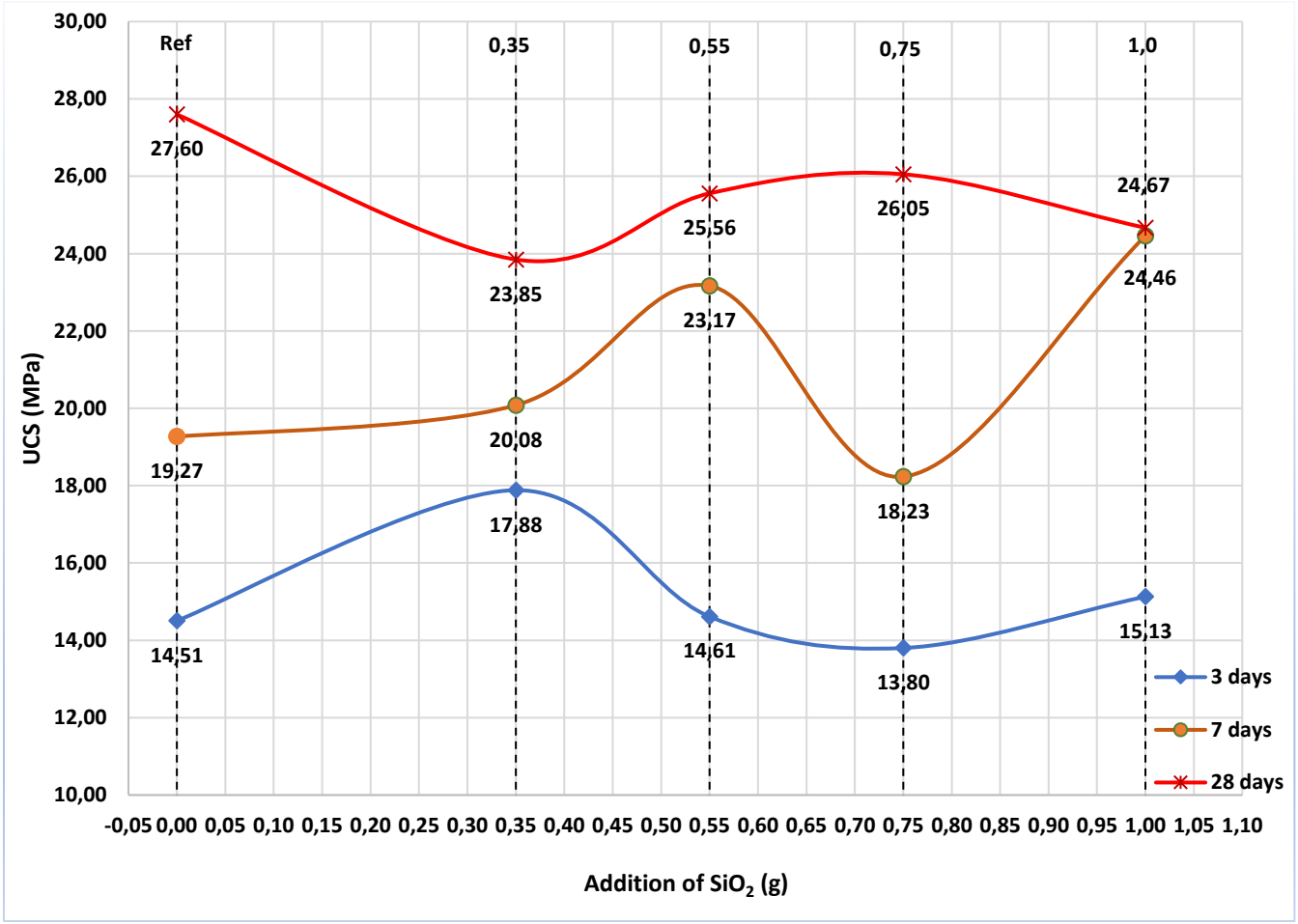

Figure 4.1 UCS for test matrix 1

After 7 days of curing, the highest compressive strength is the dosage with 1,0g of SiO_2 followed up by 0.55g of SiO_2 with 24,46 MPa and 23,17 MPa, respectively. When compared with the reference value cured for 7 days, an 26,95% increase for 1,0g SiO_2 and 20.24% increase for 0.55g SiO_2 was obtained. Furthermore, the specimen with 0.35g SiO_2 experienced an 4,22%

increase in UCS whereas 0.75g of SiO_2 similarly to the results after 3 days, still provides the worst results, with a 5,36% reduction.

The higher early UCS results are believably due to the accelerated formation of C-S-H gel, which is fuelled by a rapid consumption of crystalline $Ca(OH)_2$. The reactivity of nano-SiO_2 is thought to impact the liberation of $Ca(OH)_2$, thus directly supplying the accelerated formation of C-S-H gel [22]. This is because it is speculated that the creation of the first stage of C-S-H gel is largely determined by amount of free $Ca(OH)_2$, hence why more liberated $Ca(OH)_2$ causes faster hydration times and better early compressive strength. [4]. Furthermore, it is also believed that due to the miniscule size of nano-SiO_2, it could act as a filler in the cement matrix, blocking and filling pores, ultimately resulting in a more refined microstructure [22].

The compressive strength after 28 days, all experienced adverse results. In terms of compressive strength, the two best dosages were 0.75g and 0.55g of SiO_2, as they demonstrated 26,05MPa and 25,56MPa, respectively. This ultimately resulted in a compressive strength loss of 5,61% and 7,40%, compared to the reference value. It is also observed that UCS results fluctuates less between the different dosages of nano-SiO_2, than the 3 days and 7 days results.

One issue with these compressive results is that they are they contradicts the majority of the results from the literature review. The study conducted by Shih et al. (2006) [23] found that nano-SiO_2 increased compressive strength for every wt%, when compared with the control value, as depicted by figure 2.8. Of course, the experiments are not identical, as they had WCR of 0.55 opposed to 0.44, and used ASTM Type I C150 cement opposed to G-class cement. In addition, Li et al. (2003) [21] also found that nano-SiO_2 improved compressive strength after 28 days, when used as an additive in cement mortar, this can be seen in table 2.4. Again, this test was done on cement mortar, with other additives present and not on neat G-class cement. Finally, the study conducted by Jalal et al. (2011) [22] found that nano-SiO_2 gave significant improvements in compressive strength in high performance self-compacting concrete (HPSCC) after 28 days, seen in table 2.6.

However, the study conducted by Isfahani et al. (2016) [24] where they added SiO_2 nanoparticles to concrete with different w/b ratios, found that for the w/b ratio of 0.5 provided adverse compressive strength results after 28 days of curing, depicted in figure 2.10. It is also evident from the study that w/b ratio significantly affected the ability of the added SiO_2 nanoparticles to increase the compressive strength. This might suggest that 0.44 WCR, used in

this thesis is not conducive to achieve superior UCS values after extended curing periods when only using SiO_2 nanoparticles.

Additionally, the SiO_2 nanoparticles used were dispersed in water, and the chemical additive used to stabilize the dispersion is not provided by the manufacturer. Therefore, it could be possible that the chemical additive meant to stabilize the dispersion, might chemically interact and degrade compressive strength over time. Resulting in poor UCS after 28 days compared to the average reference values of neat G-class cement. This might also be the cause for the discrepancies between the majority of results documented in the literature study (section 2.3.2.1) and the findings of this thesis. Unfortunately, the SEM (Scan Electron Microscope) was out of order during the duration of this thesis, therefore it was hard to investigate further.

To be clear, TB 3 was recreated and retested, and the results were very similar, both iterations exhibited a slight decrease in compressive strength compared to the reference values, and red curve presented in figure 4.1 is the average of both iterations. Conclusively, SiO_2 nanoparticles caused impairments after 28 days with my experimental conditions.

4.2.2 Effect of nano-SiO_2 on Young's modulus

Young's Modulus is a measurement which can be applied to describe the stiffness of a material. A high Young's modulus corresponds to a stiffer material, whereas a low value corresponds to a less stiff material. Generally, a high UCS and low E-modulus is considered to be favourable. In a wellbore situation, a cement plug with high UCS and low E-modulus would be able to deform under greater loads without suffering permanent damage while still enduring the loads. Usually, Young's modulus is correlated with UCS, and as the UCS increases, so does Young's modulus. Figure 4.2 displays the E-modulus results for test matrix 1.

After 3 days, the majority of dosages in this batch provided an increase in E-modulus, with the exception of 0.55g of SiO_2. Noteworthy, the sample with worst compressive strength also had the highest E-modulus, as 0.75g of nano-SiO_2 decreased UCS and increased E-modulus, which is the opposite of the ideal. In essence, it has the worst strength and most stiff behaviour of the plugs in the batch.

After 7 days, the concentrations that demonstrated an increase in UCS, also exhibited an increase in Young's modulus after 7 days of curing, which correlates to more stiff behaviour. The two highest E-modulus values belongs to 0.35g and 1,0g SiO_2, which increased the E-modulus of neat cement with 103,52% and 69,96%, respectively. Obviously, this is disadvantageous. As a result the 0,55g of SiO_2 might be the most beneficial dosage after 7 days

due providing a UCS improvement of 20,24% with an 30,88% increase in E-modulus whereas, 1,0g of SiO_2 displayed a slightly higher UCS improvement of 26,95%, but also increasing E-modulus by 69,96%. Simply because both UCS results were great, but 1,0g SiO_2 has far higher increase in Young's modulus.

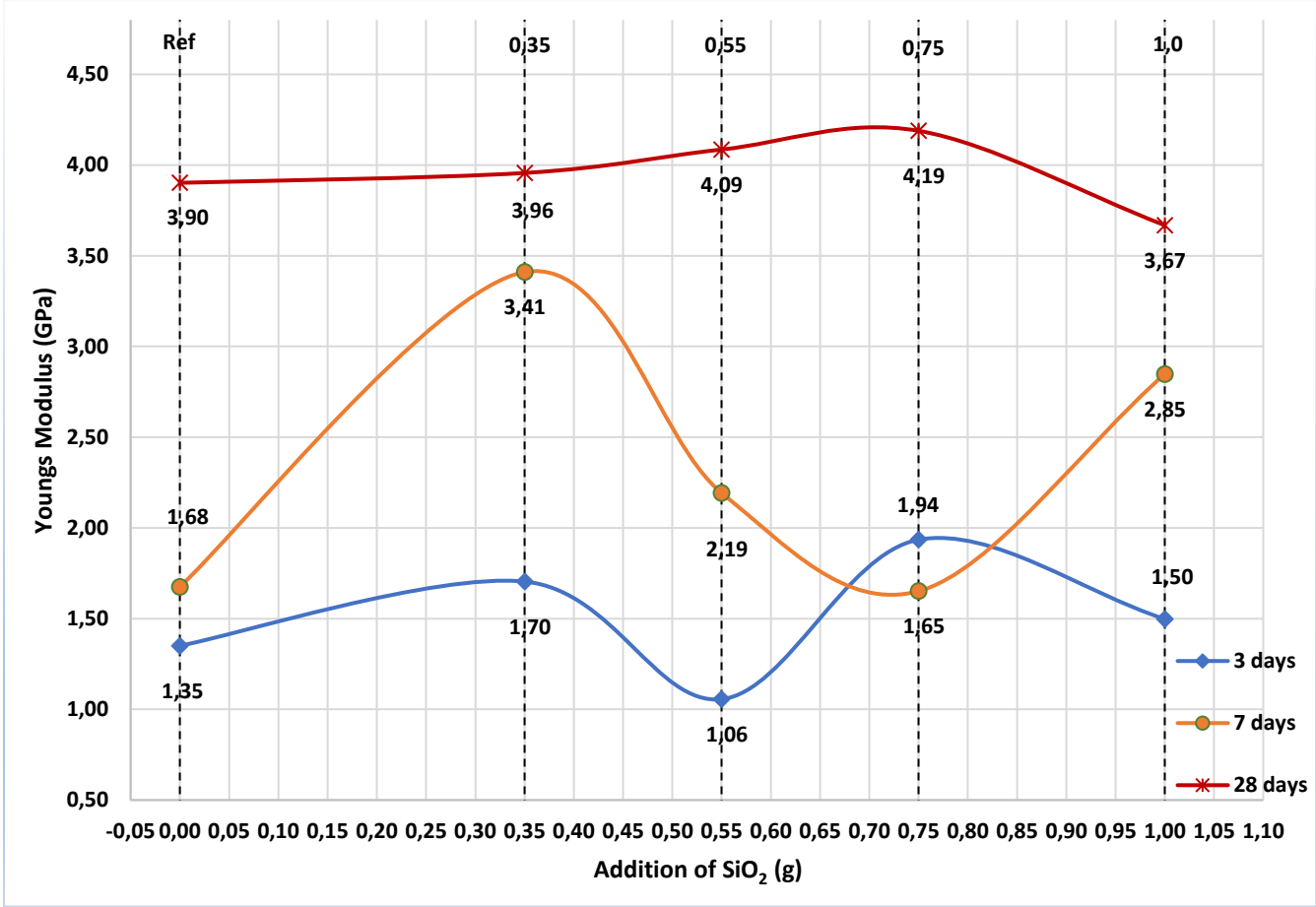

Figure 4.2 Young's modulus for TM 1

E-modulus after 28 days, shows that E-modulus was slightly increased for the three lowest dosages of SiO_2, whereas 1,0g decreased E-modulus. It is observed that the fluctuation in E-modulus results for the different SiO_2 dosages within the batch is minor compared to the curves of the 3 and 7 days results. Nevertheless, a reduction in UCS and increase in E-modulus is unfavourable results. Conclusively, E-modulus increases with curing age, as the cement undergoes a more complete hydration and gains higher compressive strengths.

4.2.3 Effect of nano-SiO_2 on resilience

Resilience is a measurement of how much energy a material can absorb before the maximum stress is reached. This was predominantly calculated by finding the area under the stress-strain graph of each plug, eq. 3.6. or in some rare instances it was also calculated with eq. 3.5 (section 3.3.1.4). The resilience of a material is dependent on the ratio between max compressive

strength (UCS) and E-modulus. It is sought after to have the highest resilience value possible, certainly higher than the reference value. The resilience results are presented in figure 4.3.

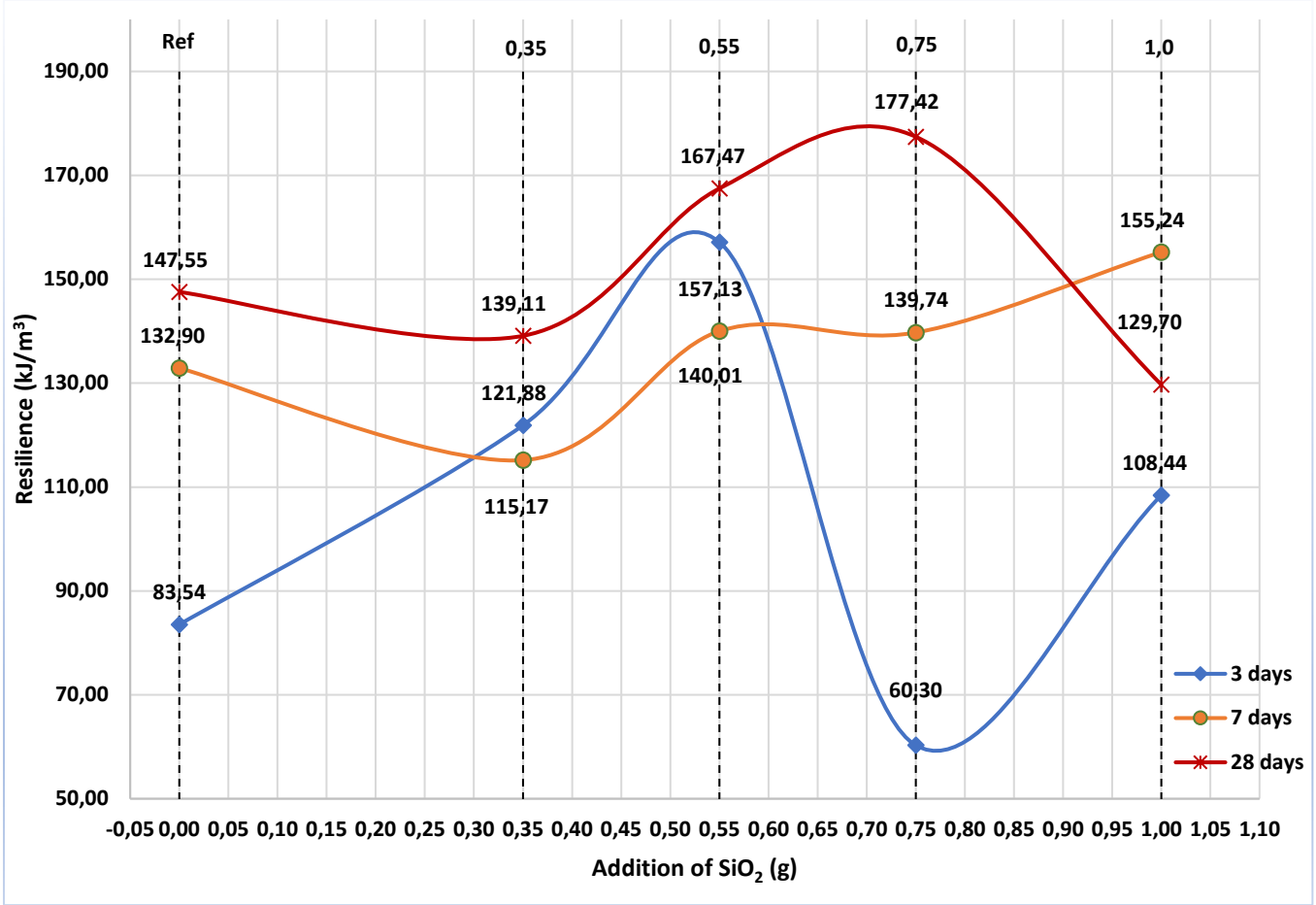

Figure 4.3 Resilience of TM 1

After 3 days of curing, resilience is up for 3 out of 4 specimens, which is auspicious. On the contrary, there is a strong reduction in resilience for the plugs with 0.75g of nano-SiO_2. This is due to the weak compressive strength and very high E-modulus (as can be seen in figure 4.1 and 4.2), causing the plugs to be a lot less resilient. Additionally, the low E-modulus of 0.55g concentration of nano-SiO_2 is also the reason why its resilience is very high. Additionally, 0,35g of SiO_2 exhibited highly beneficial resilience augmentation of 45,90% compared to neat cement.

As for the results after 7 days of curing, all specimens improved the resilience of the reference sample except for the 0.35g concentration. Moreover, 1,0g of nano-SiO_2 demonstrated an improvement of 22,20% compared to the reference sample, whereas 0,55g only increased resilience by 5,35% despite having a significantly lower E-modulus value. Finally, the 0.35g concentration displayed a reduction of 9,34% compared to the control value. Again, similarly to the 3 days results, a high E-modulus is often detrimental for resilience. For instance, 0.35g

of nano-SiO_2 exhibited E-modulus increase of 103,52% which is likely the reason for the 9,34% reduction in resilience.

For the red 28 days curve, 0.55g and 0.75g of SiO_2 shows an increase of 13,50% and 20,25%, respectively. While 0.25g and 1.0g underperformed in terms of resilience, with reductions of 5,72% and 12,10%, respectively. An improvement in resilience for 0.55g and 0.75g after poor UCS and Young's modulus results is unexpected, and a redeemable quality for the batch.

4.2.4 Effect of nano-SiO_2 on M-modulus

M-modulus for this matrix is presented in figure 4.4. A high M-modulus values corresponds to a low ultrasonic travel time, which suggests that the medium the pulse travels through is adequately dense. A dense medium further indicates that the microstructure is in good shape, with no significant cracks or pore spaces. For this reason, a high M-modulus is often believed to a have a correlation with high UCS values, as it suggests a more refined microstructure.

Both the M-modulus and the UCS are functions of the velocity of sound in the plugs. However, in this matrix, we can observe the inverse relation of the UCS with the M-modulus. For example, 0.35g and 0.75g of SiO_2 in TB 3 (28 days), has significantly higher M-modulus than the reference value, while also having reduced UCS. For both TB 1 and TB 2, 0.75g of SiO_2 was the only specimen which exhibited adverse UCS results, and it still has by far the highest M-modulus after both 3 and 7 days of curing. Furthermore, the best performing concentration of TB 2, 1,0g of nano-SiO_2 also has low M-modulus despite demonstrating a 26,95% UCS augmentation. After 3 days, all specimens had an improved M-modulus regardless of their compressive strength whereas after 7 days the majority had a reduced M-modulus.

Reasonably, if any dosages are differing massively from the rest of the batch with worse M-modulus, it could indicate inadequacies with the inner structure of the cement plug. There is a fluctuant trend for the different dosages after 3 and 7 days are present in figure 4.4. As TB 1 and TB 2 have been fluctuating significantly for every tested parameter, there are likely no major outliers present in terms of M-modulus, which indicates that all cement plugs tested had adequate inner structure. It also observed that generally, M-modulus increases with extended curing periods, as the cement plugs become denser and more hydrated, thus providing better mechanical properties.

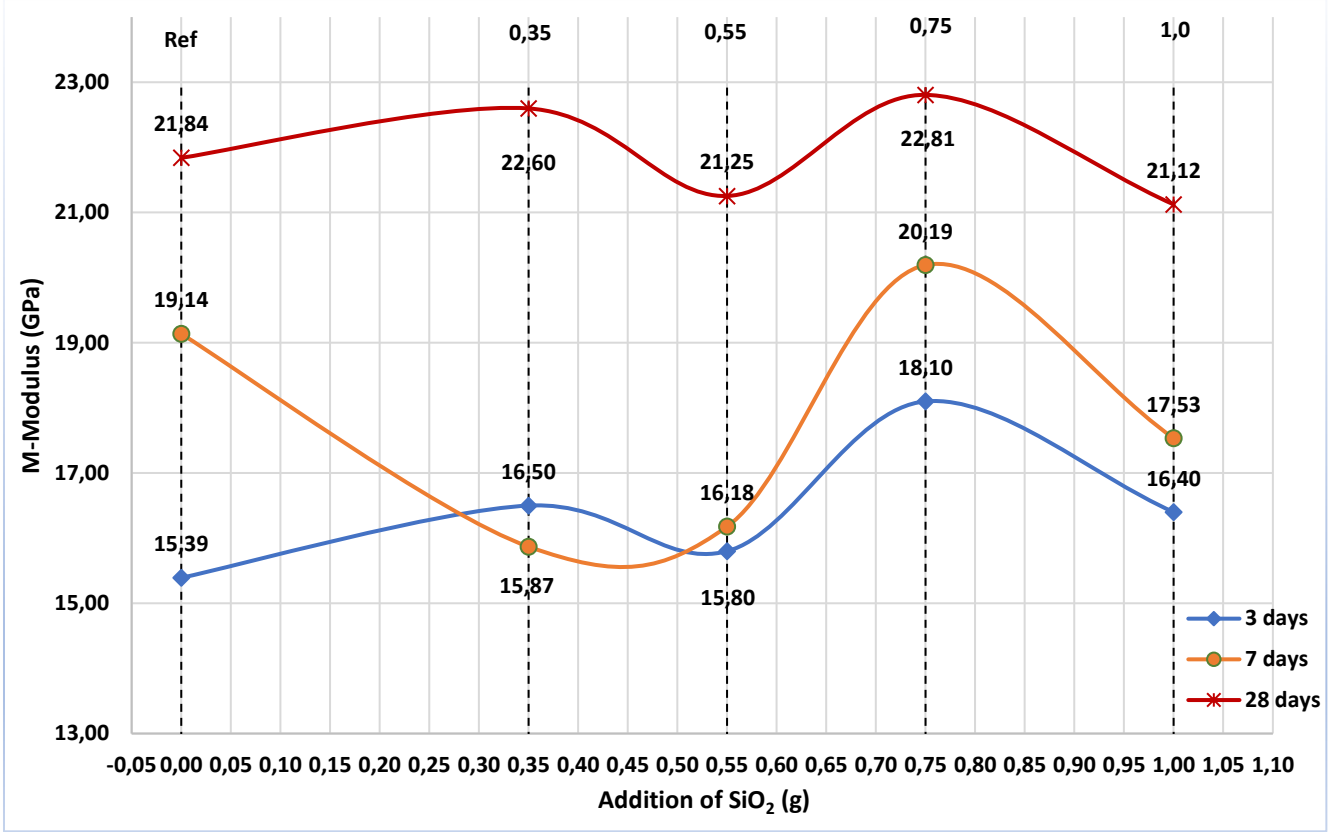

Figure 4.4 M-modulus for TM 1

4.2.5 Effect of nano-SiO_2 on water absorption

Mass absorption was tested by submerging the cement samples in 24 hours of water and measuring the weight after 24 hours in order to find the amount of water absorbed into the cement plugs, see section 3.3.2.3 for more information. Figure 4.5 displays that all dosages of SiO_2 considerably increased water absorption compared to the average reference value (Avg ref). The largest increase was 42.92% and 40.88%, by 0.25g and 0.55g, respectively. Generally, a higher water absorption suggests that the microstructure within the plugs could have larger pore spaces and/or cracks, resulting in compromised inner structure. This would of course mean, that nanoparticles have not filled or blocked any significant pore spaces within the plugs. With the context of the weak UCS results after 28 days, this could likely be the case. However, it could also indicate that the nano-SiO_2 has contributed to reducing cement shrinkage during the hydration process, which would mean that the samples with nano-SiO_2 have a larger bulk volume, thus allowing for more water absorption.

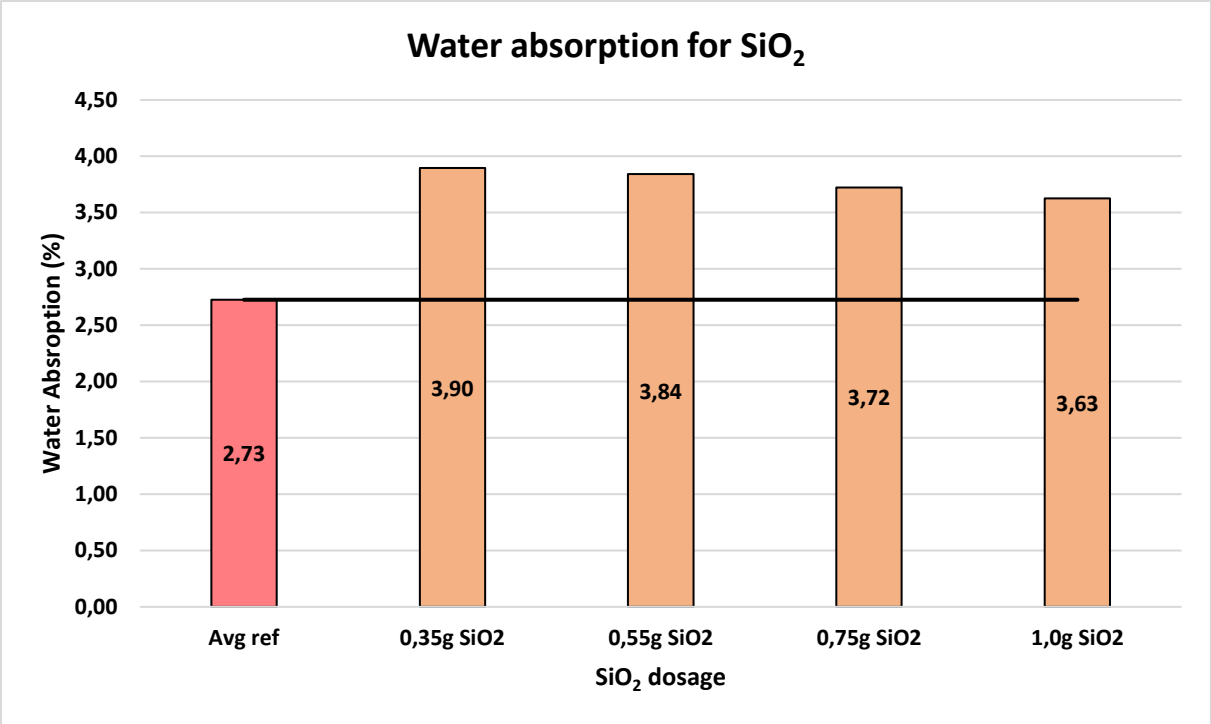

Figure 4.5 Water absorption for TM 1

4.3 Test Matrix 2 (Effect of binary blend)

Based on the results from the literature review, it is easy to imagine that a binary blend of nano-SiO_2 and nano-Al_2O_3 could yield magnificent results, as both constituents alone are promising. This matrix will exhibit the results achieved from a binary nanoparticle blend. As mentioned previously, it used a constant dosage of 0.55g of nano-SiO_2 in combination with dosages of 0.25, 0.5, 0.75 and 1,0grams of nano-Al_2O_3.

4.3.1 Effect of the binary blend on UCS

Compressive strength results are displayed in figure 4.6. This time the x-axis measures the amount of Al_2O_3 instead of SiO_2. This is of course because 0.55g of SiO_2 is kept constant for every cement plug except the reference plugs. Immediately, there is far less fluctuations in figure 4.6 opposed to figure 4.1.

The compressive strength results after 3 days for the binary nanoparticle blend provides almost equal strength. It is observed that 0.5g, 0.75g and 1,0g all show minor compressive strength improvements of 5,45%, 4,45% and 3,70%, respectively. The lowest concentration of 0.25g of Al_2O_3 gave a UCS reduction of 2,72%. Even though, 15,30MPa (peak for binary) is a long way from the promising 17,88MPa (peak for SiO_2, figure 4.1), the results are more consistent across the varying dosages for the binary blend. The consistency is reassuring, in the sense that the incredible high 17,88MPa provided by the SiO_2 might have been an outlier, whereas there

seems to be no outliers present in the binary system thus far. The trend of the UCS results seems to be that after 0.5g Al_2O_3, there is a minor decline in compressive strength performance.

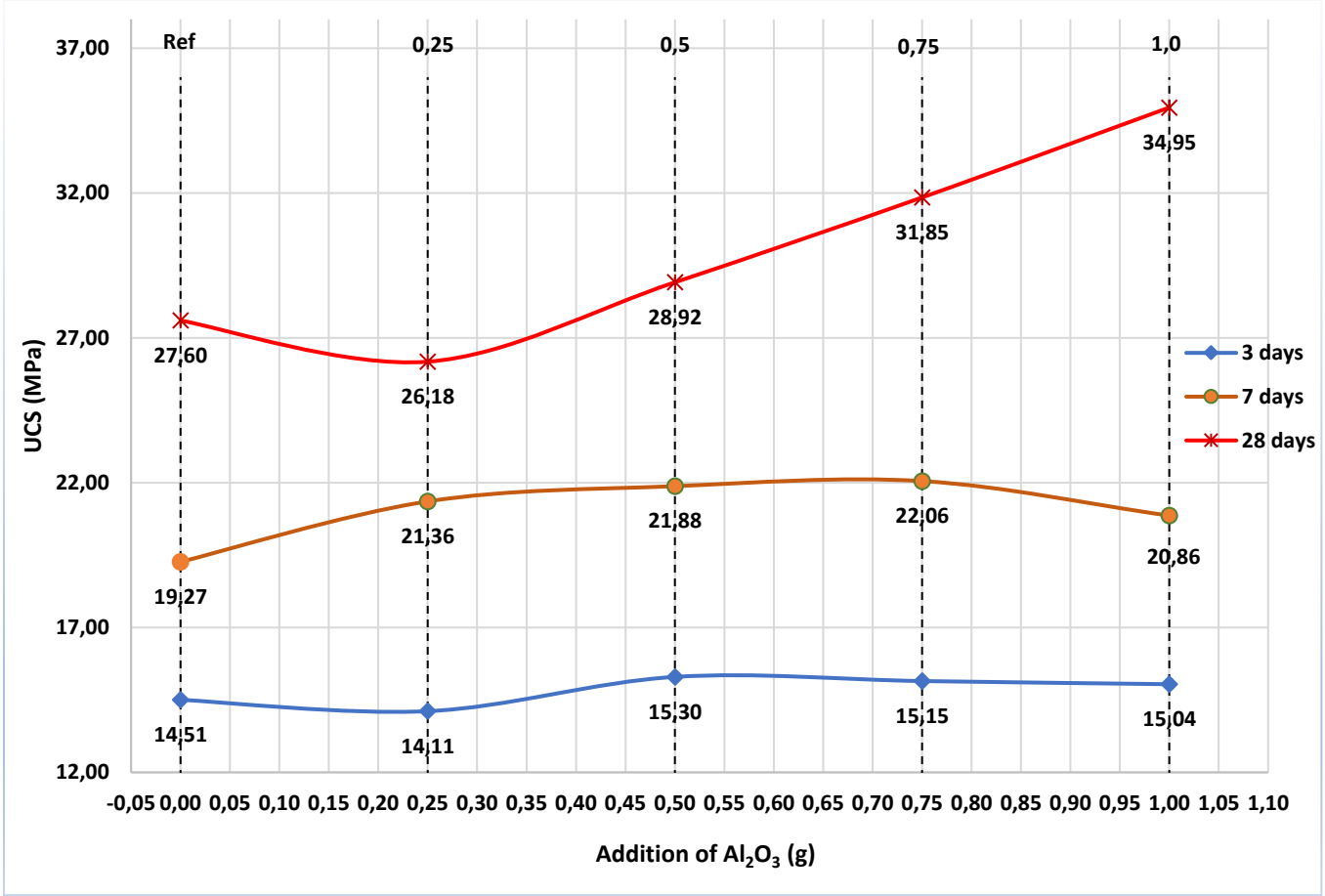

Figure 4.6 UCS for TM 2

After 7 days, the binary blend gave superior compressive strength increases for every dosage tested. Furthermore, the results are similar in terms of the improvements, with 0.75g marginally giving highest UCS increase. In fact, 22,06 MPa, 21,88MPa and 21,36MPa compressive strength translates to a 14,48%, 13,57% and 10,84% augmentation in UCS, respectively. Whereas the highest dosage of 1.0g Al_2O_3 gave a UCS increase of 8,29%.

When compared to TB 2 (7 days SiO_2), these results are more balanced across the batch, albeit there is a lower peak performance compared to the results from SiO_2 alone. Additionally, the binary blend does not display any adverse effects on UCS after 7 days, which SiO_2 nanoparticles did demonstrate as 0,75g provided a UCS reduction of 4,86%

For the 28 days results, 1.0g and 0.75g Al_2O_3 are the best performers in terms of UCS and provides an incredible 34,95MPa and 31,85 MPa. This correlates to a 26,64% and 15,39% improvement compared to the reference value. In fact, an average compressive strength of

34,95MPa was the highest recorded value of all specimens tested in this thesis. The lowest dosage gave adverse effects, as it reduced UCS with 5,14%. Whereas 0.5g of Al_2O_3 exhibited an average UCS of 28,92 MPa, which resulted in a 4,78% increase in compressive strength.

Furthermore, there seems to be almost a symmetry in the UCS increase as the dosages rise. Each increase in Al_2O_3 nanoparticle dosage, achieved a strength increase of roughly 3 MPa, resulting in a satisfying rising trend of higher dosages yielding higher compressive strength. However, this trend is incompatible and opposite with the trend observed after 3 and 7 days of curing. The rising trend raises the question of how an even higher dosage of the binary blend would have performed after 28 days, as diminishing returns are not observed in figure 4.6.

A possible explanation why the binary nanoparticle blend seemingly has so profound and consistent results is likely due to nano-SiO_2 and nano-Al_2O_3 having synergistic abilities. The superior results achieved in the study by Muzenski et al. (2019) was believably due to Al_2O_3 having a reinforcing effect on the C-S-H gel [28]. Maybe, nano-SiO_2 might act as an accelerator to the C-S-H gel, whereas maybe nano-Al_2O_3 plays a different role, affecting some other parameter in the complex hydration process, i.e., a reinforcement effect of the C-S-H gel. Furthermore, in tandem they might possess a superior ability to fill the cement matrix, due to there being two separate nanoparticles present compared to only one. This could result in a stronger and more refined cement matrix, thus creating a beneficial result for a wider array of dosages. All in all, binary nanoparticle blend offers the best UCS results among the other test matrices.

4.3.2 Effect of the binary blend on Young's modulus

Figure 4.7 exhibits the E-modulus results for test matrix 2. After 3 days of curing, it is observed that the E-modulus results are somewhat consistent, as they do not significantly deviate from each other. The 0.5g and 1,0g samples provides higher E-modulus, with a 9,87% and 2,17% increase, respectively. While the specimens with 0.25g and 0.75g provides small decreases of 2,5% and 7,05%. Normally, E-modulus is expected to be higher when the corresponding UCS is high, which is seemingly the case here apart from of 0.75g. Ultimately, the fluctuations between the dosages are relatively minor, so it likely would not have a profound effect in real applications.

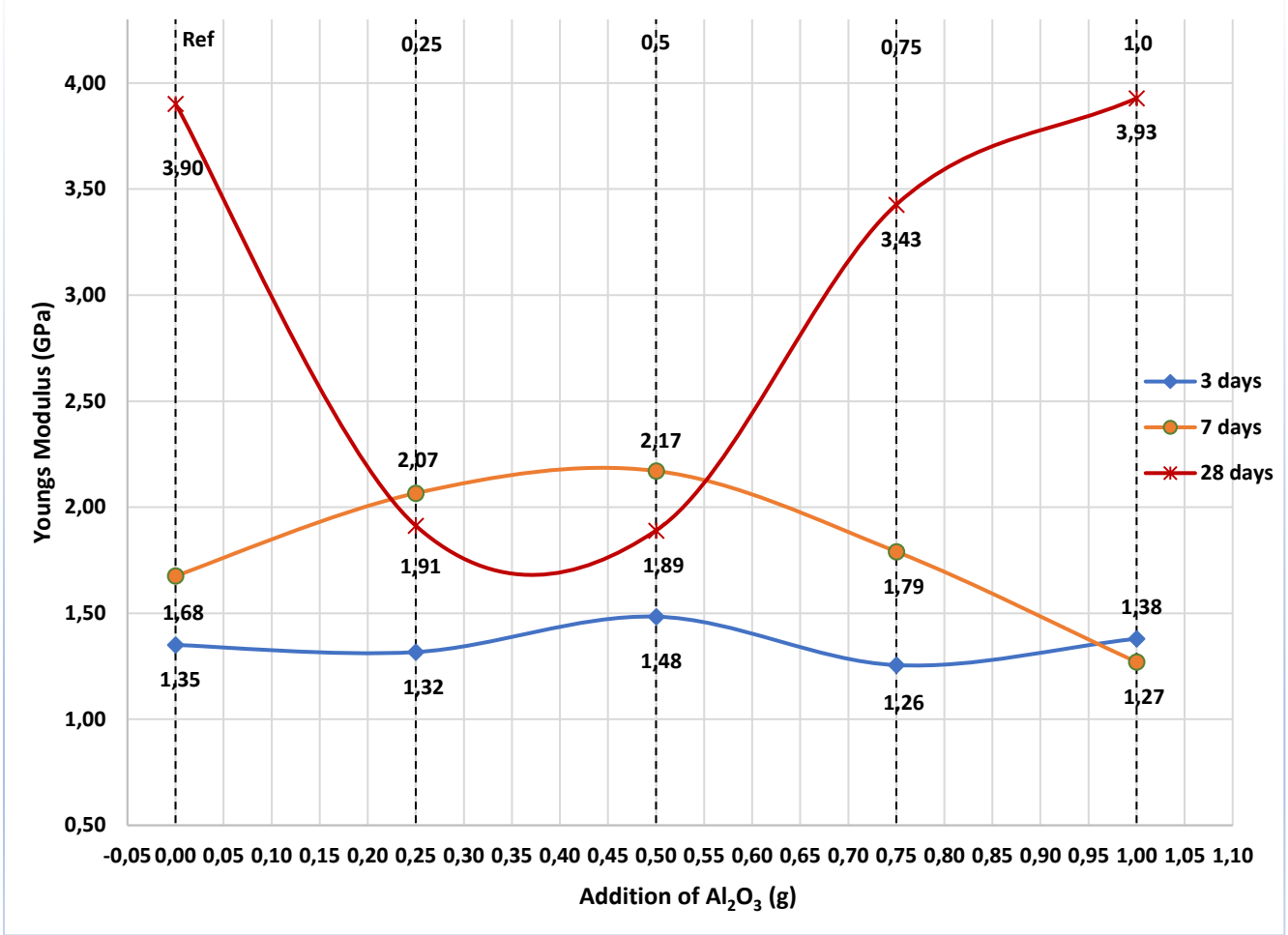

Figure 4.7 E-modulus for TM 2

After 7 days of curing, all specimens except the highest dosage of 1,0g Al_2O_3 displays an increase in Young's modulus, which means that they have more stiff behaviour. Compared to the reference sample, 0.25g and 0.5g of Al_2O_3 increased E-modulus by 23,59% and 29,55%, respectively. In addition, 0.75g of Al_2O_3 also increased E-modulus by 6,85%, whereas 1,0g caused a reduction of 24,21%. On the other hand, the 0,75g and 1,0g concentrations has shown 14,48% and 8,29% improvements in compressive strength, respectively, without significantly increasing the stiffness of the cement.

Finally, after 28 days of curing, the majority of plugs show a decrease in Young's modulus. It is observed that all dosages apart from the highest dosage demonstrates a reduction in Young's modulus. Notably 0,75g of Al_2O_3 provided UCS improvement of 15,39% while also decreasing Young's Modulus with 12,18%. Even 1,0g Al_2O_3 which enhanced compressive strength by 26,64%, exhibited only a small 0.67% increase in E-modulus, which sounds like a great trade-off for the minuscule effect on stiffness. All evidence points toward the E-modulus of 0.25g and 0.5g being anomalies, as they are so significantly low compared to the most of the other 28

days plugs. Nevertheless, the UCS increases witnessed in figure 4.6 coupled with the E-modulus results presented in figure 4.7, are very promising.

4.3.3 Effect of the binary blend on resilience

Figure 4.8 shows the resilience results for the binary blend. Typically, a trend that is often observed is that the high compressive strength leads to high E-modulus, which in combination can cause a reduction in resilience depending on the ratio between the UCS and E-modulus. After 3 days, in figure 4.7 and figure 4.8, this trend is present. Evident by the highest E-modulus of 1,48GPa resulting in the lowest resilience of 63,86kJ/m^3, which is a decrease of 23,56% compared to neat cement. Similarly, the lowest E-modulus of 1,26GPa also exhibits the highest resilience of 89,85kJ/m^3, thus the most resilient cement plugs had 0.75g of Al_2O_3, which translated to a 7,55% resilience improvement. Both these dosages had comparable UCS values, with only 0,15MPa differentiating them, but 0,5g of Al_2O_3 also caused stiffer behaviour, seen in figure 4.7.

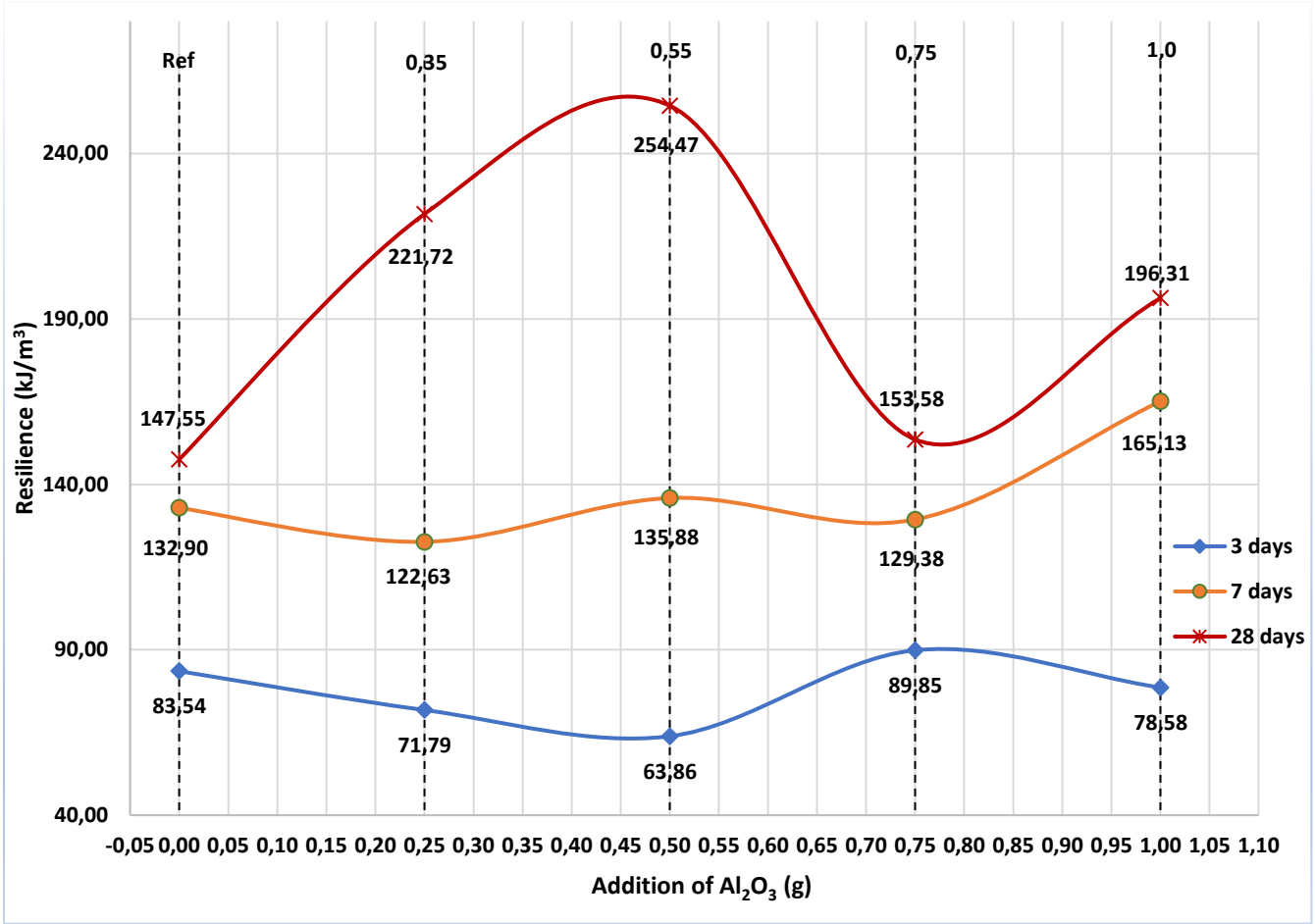

Figure 4.8 Resilience for test matrix 2

After 7 days, 0.5g and 1,0g experienced an improvement in terms of resilience. These dosages have also increased the compressive strength of the neat cement significantly. Even though, 0.5g of Al_2O_3 had the highest E-modulus of 2,17GPa, which is 23,29% higher than the reference, it still experienced a slight resilience increase of 2,24%. The most resilient dosage was 1,0g of Al_2O_3, with an increase of 24,95% compared to the reference sample.

As for resilience after 28 days, 0.25g and 0.5g of nano-Al_2O_3, expectedly inflated the resilience substantially, as E-modulus was significantly lower for these concentrations. This is manifested as an 50.37% and 72,46% increase in resilience, respectively. However, 0.75g and 1,0g of Al_2O_3 also improved resilience of the cement, with a 4,08% and a very favourable 33,05% increase. Even though, they had a higher E-modulus relative to the two lowest dosages, their UCS also was higher resulting in good resilience values, which is highly favourable. 1,0g of Al_2O_3 had magnificent results, with a UCS improvement of 26,64%, small E-modulus increase of 0,67% and finally, a resilience enhancement of 33,05%.

4.3.4 Effect of the binary blend on M-modulus

In Figure 4.9, it is observed that M-modulus increased steadily as the samples are allowed to cure longer. This is also anticipated as the microstructure becomes more refined with more complete hydration. Again, there is a discrepancy between high UCS results and high M-modulus values across this matrix. This is clear looking at the 7 and 28 days results, as almost all cement plugs had superior compressive strength, while simultaneously showing worse M-modulus values, compared to their respective reference values. This weakens the assumption that a high M-modulus is conducive to a high compressive strength. However, as the M-modulus values barely fluctuates within the test batches, this signifies the presence of adequate microstructure within the tested cement plugs.

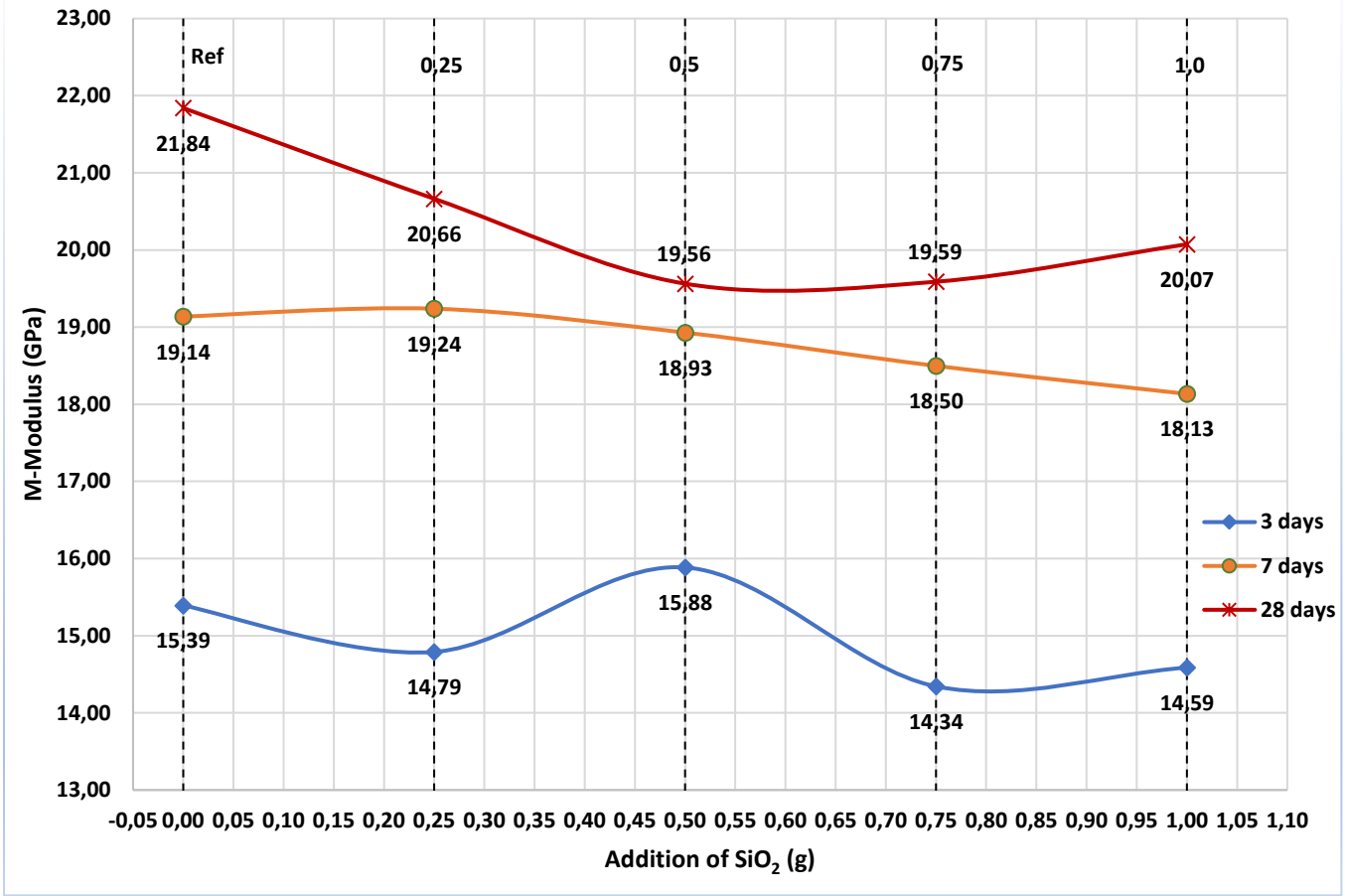

Figure 4.9 M-modulus for TM 2

4.3.5 Effect of the binary blend on water absorption

Figure 4.10 exhibits the water absorption results for this batch. The majority of dosages are around the reference value, with 0.25g and 0.75g being slightly higher, while 0.5g is somewhat lower. This indicates that these plugs had adequate microstructures within the cement plugs. However, it is observed that 1,0g has a 4,14% water absorption, which translates to a 51,82% increase, compared to neat cement. This is interesting as normally an increase in water absorption indicates bigger/more pores in the microstructure and that the binary nanoparticle blend has not filled or blocked off a significant amount of pores. Nevertheless, the impressive 26,64% augmentation in UCS contradicts that the 1,0g plugs had an abnormally porous or defect core. As mentioned previously, higher water absorption could be also caused by a reduction in cement shrinkage which occurs during hydrating, thus resulting in more bulk volume.

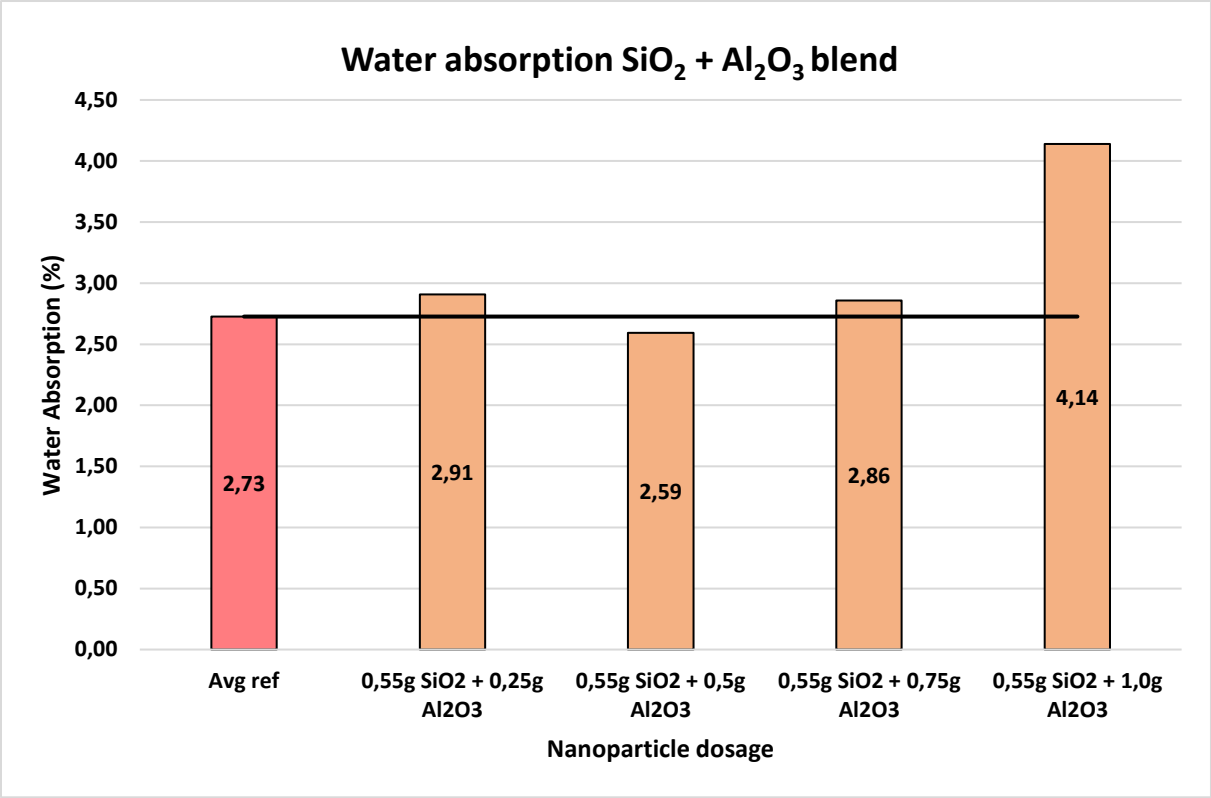

Figure 4.10 Water Absorption for TM 2

4.4 Test Matrix 3(Effect of ternary blend)

This section will exhibit the results from a ternary nanoparticle blend. It had a constant dosage of 0.55g nano-SiO_2 and 0.25g nano-Al_2O_3 in combination with varying dosages of MWCNT from 0.25g, 0.5g, 0.75g and 1,0g.

4.4.1 Effect of the ternary blend on UCS

Compressive strength results are displayed in figure 4.11. This time the x-axis measures the amount of MWCNT instead of SiO_2 or Al_2O_3 as their concentrations are kept constant for every cement plug except the reference plugs. Looking at the 3 days results from figure 4.11, it is observed that there are UCS improvements for all specimens. With 0.75g of MWCNT demonstrating the highest UCS increase of 10,26%, while 0.25g and 1,0g of MWCNT providing UCS improvements of 4,98% and 2,36%, respectively. The lowest performing dosage was 0.5g, which displayed a small UCS increase of 0.83%. As all dosages demonstrated augmented UCS values, it makes this batch satisfactory in terms of early strength.

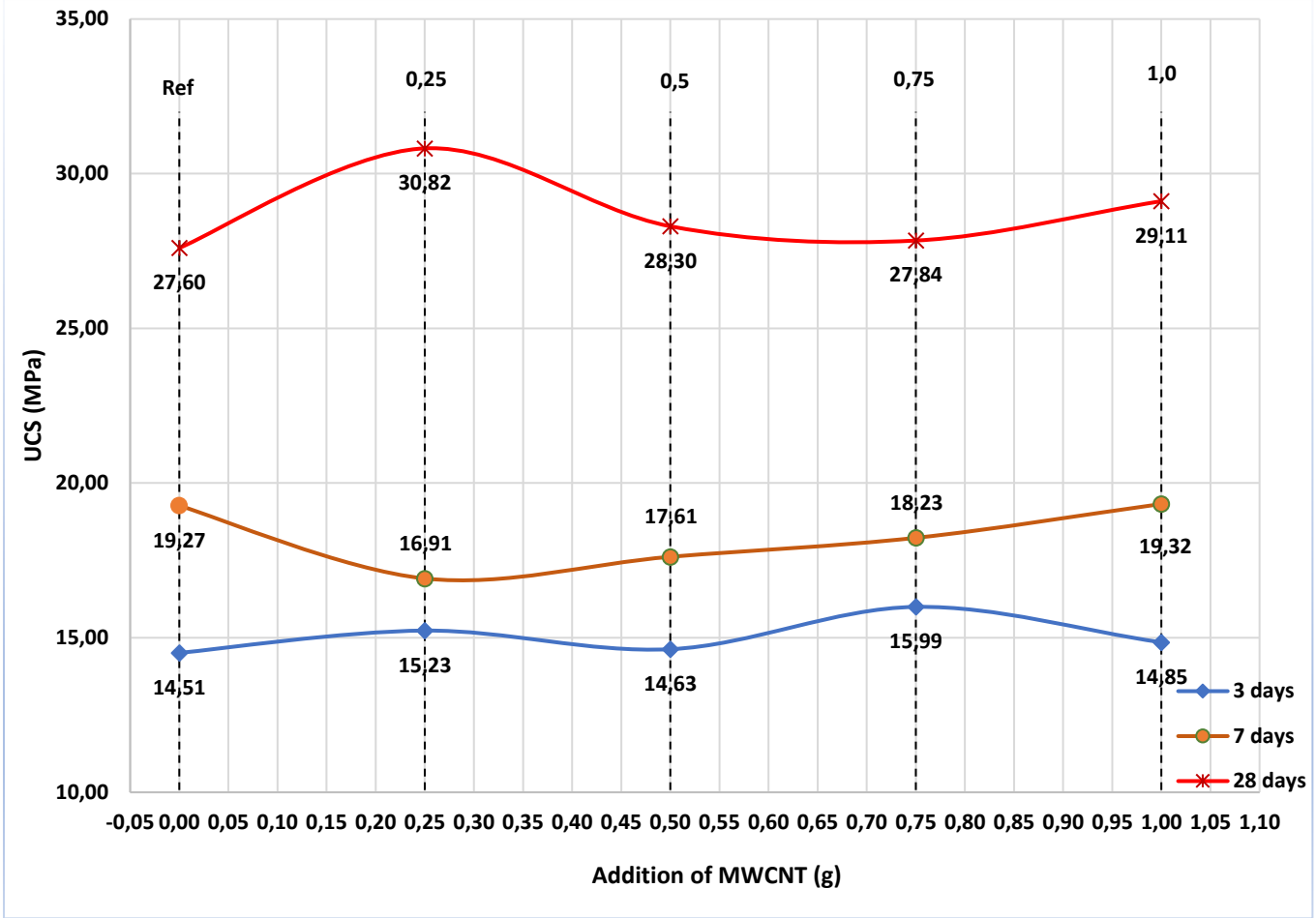

Figure 4.11 UCS results for TM 3

The peak value of nano-SiO_2 alone (TB 1) was 17,88MPa which is far better than 15,99MPa of this batch. Although this batch was slightly better after 3 days than that of the binary blend in terms of peak UCS values. Also, this was the only 3 days batch which displayed improvements for every dosage thus far.

The compressive results after 7 days are poor, as seen in figure 4.11. All specimens except 1,0g of MWCNT experienced a reduction in compressive strength. Additionally, the three lowest dosages 0.25g, 0.5g and 0.75g had a UCS reduction of 12,22%, 8,58% and 5,39%, respectively, whereas 1,0g put up a small 0.28 % UCS increase. To put things into perspective, the peak dosage of nano-SiO_2 after 3 days, had a compressive strength of 17,88MPa which is higher than the two worst performing dosages in this batch, at 16,91 MPa and 17,61 MPa. Keep in mind that this batch has cured for more than twice the number of days at the time of the results. Furthermore, this is the worst 7 days batch thus far with respect to UCS results

After 28 days of curing, the lowest dosage of the blend gave compressive strength results of 30.82 MPa, whereas the highest dosage gave 29,11MPa, which was the two best performances. This translates to an 11,67% and 5,48% increases, respectively, compared to UCS value for neat cement. Whereas the two middling dosages of 0.25g and 0.5g demonstrated an 2,54% and 0.86% UCS increase, with values as 28,30MPa and 27,84MPa. Even though, these are positive results, they are overshadowed by the great results for the binary blend after 28 days.

Another notable feature is that no dosage exhibited adverse UCS results, which is peculiar when, essentially, the 7 days UCS results were nothing but adverse results. Even the great 28 days results of the binary blend showed negative UCS results for the weakest concentration, with a UCS reduction of 5,14%.

Nonetheless, this batch has been very erratic in terms of compressive strength, going from decent 3 days results to far worse 7 days results and ending up with improved 28 days results. Again, due to the SEM apparatus being out of order during this thesis, it was impossible to investigate further, but there exists a possibility that agglomeration between the nanoparticles might occur. Based on this result alone, the viability of a ternary nanoparticle blend consisting of the same constituents is questionable at best, since it is a clear step down from the binary blend and it has poor economic viability, compared to TM 1 and TM 2.

4.4.2 Effect of the ternary blend on Young's modulus

Figure 4.12 presents E-modulus results for the ternary blend. After 3 and 7 days of curing, the E-modulus values are all reduced compared the respective control values. This is great for the 3 days results, as all specimens provided UCS improvements. The best dosage of 0,75g showed an UCS enhancement of 10,26% while reducing E-modulus by 16,82%. The largest reduction was 1,0g which displayed a 23,97% reduction in Young's Modulus. However, as all plugs cured for 7 days experienced adverse UCS results, their reduced E-modulus values are inconsequential.

After 28 days curing, the 0.5g, 0.75 and 1.0g MWNCT increase the E-modulus of the neat cement by 2.6%, 25.9% and 30.8%, respectively, whereas the 0.25g MWCNT decreased the E-modulus by 19.5%, the dosage also increased the UCS by 11.7%. This was both the largest UCS improvement and the greatest reduction in E-modulus after 28 days of curing.

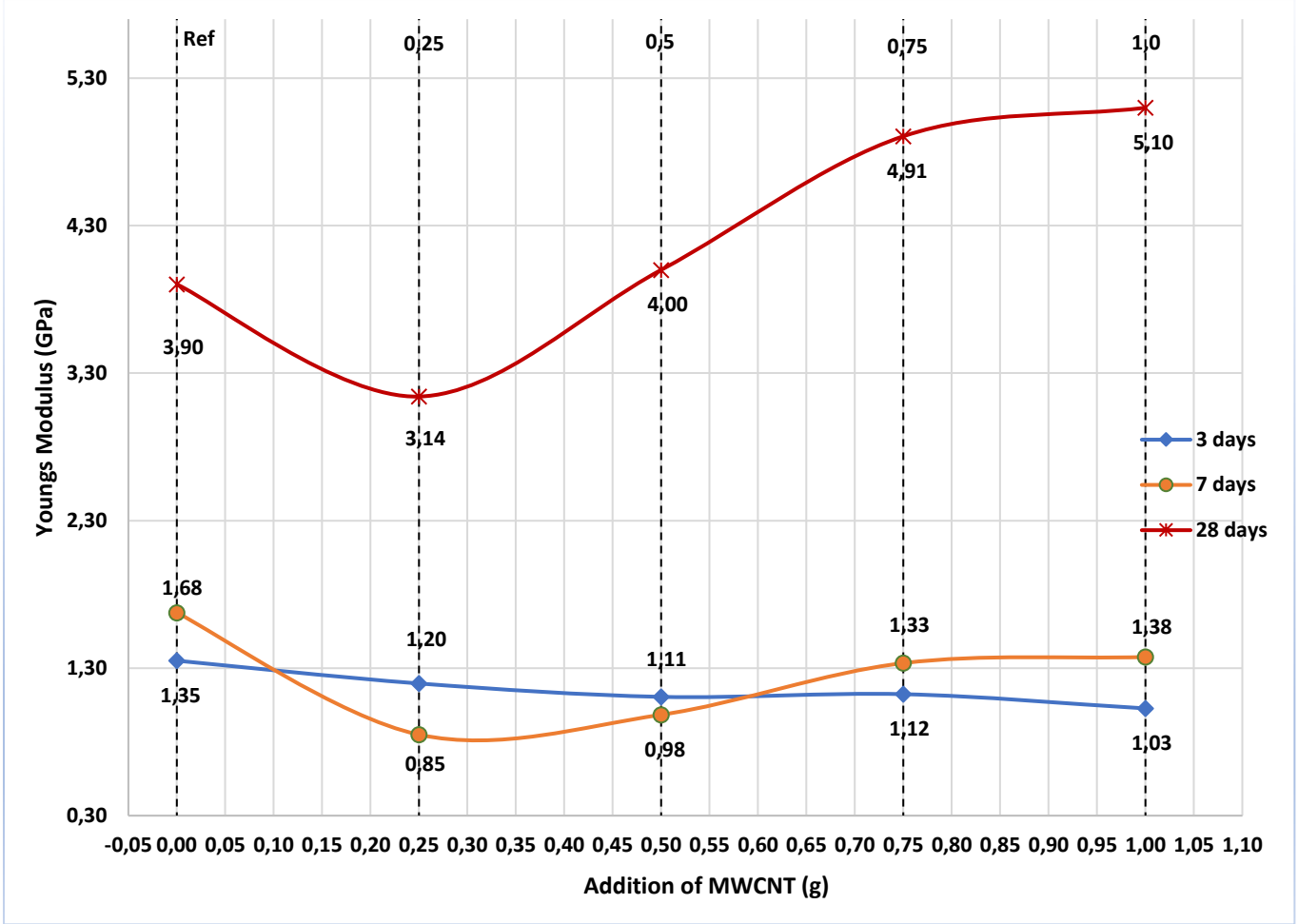

Figure 4.12 E-modulus for TM 3

4.4.3 Effect of the ternary blend on resilience

Resilience for this matrix is chaotic as the curves entwine, as can be seen in figure 4.13. For the most part the ternary blend provides higher resilience for every curing age compared to the neat cement. Resilience is improved for every dosage after 3 days of curing, as expected by good UCS and reduced E-modulus values. Notably, 0,75g of MWCNT provided a resilience increase of 58,92%, while having the best UCS and E-modulus results from the 3 days batch.

Again, the resilience values for the 7 days batch are somewhat inconsequential as they have very poor UCS values.

Furthermore, after 28 days, resilience is greater than the control value for every dosage, which is unexpected, especially for the latter dosages as the E-modulus values were notably high. For 0.75g of MWCNT, E-modulus increased with 30.68%, while also displaying an 48,43% increase in resilience, simultaneously only offering a small 0.86% UCS improvement. Interestingly, even though 0,25g of MWCNT had the highest UCS and lowest E-modulus, it still only provides a resilience increase of 14,82%. Nonetheless, the resilience increases

observed by the 3 days and 28 days batches are promising. Additionally, the 3 days and 28 days curves display similar increasing trends.

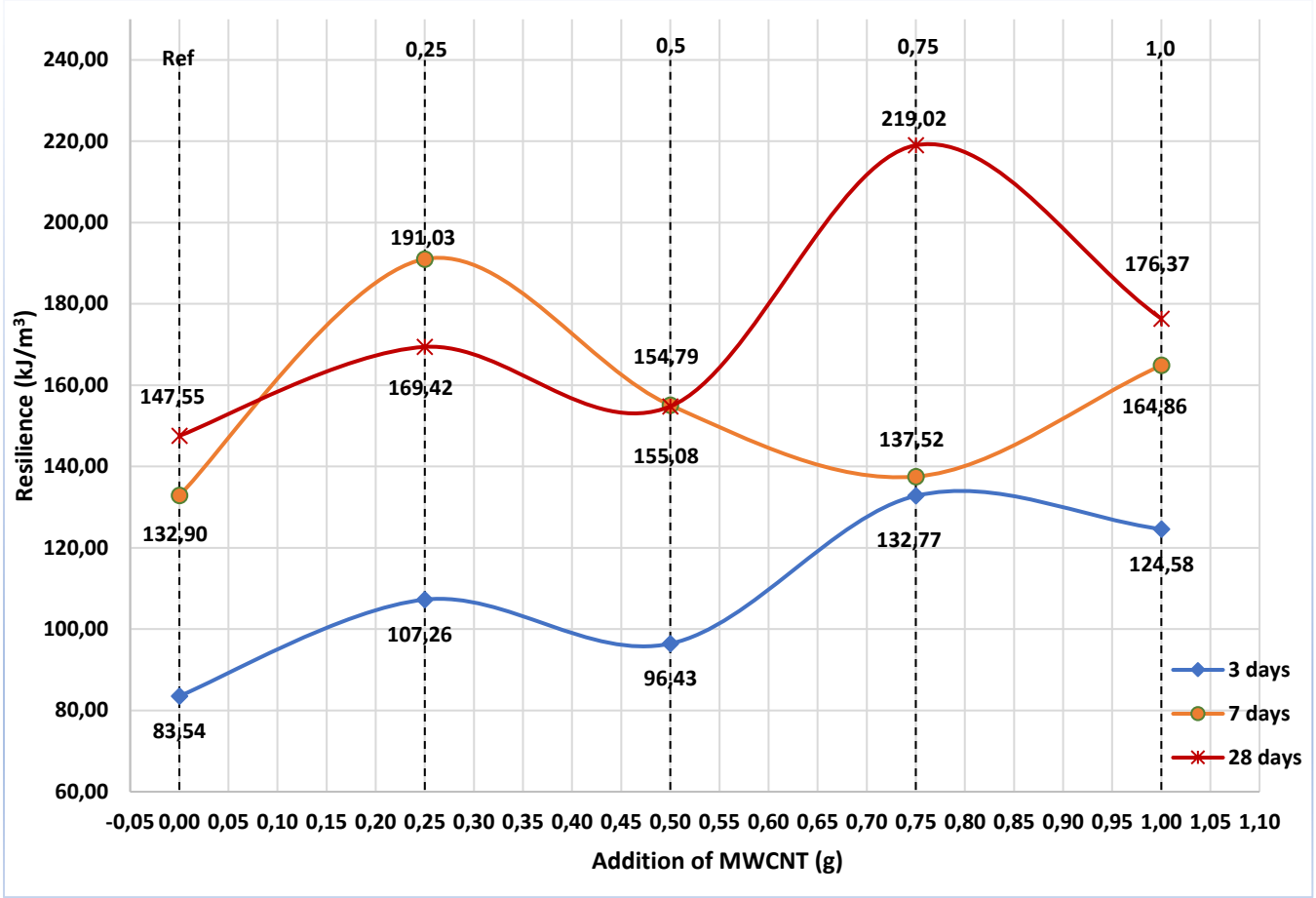

Figure 4.13 Resilience of TM 3

4.4.4 Effect of the ternary blend on M-modulus

Figure 4.14 depicts M-modulus for test matrix 3, and almost the entirety of the test matrix has either matched the respective reference values or improved upon it. Additionally, the trend of very small deviations within the individual test batches continues. In continuity with the previous matrices, extended curing periods allow for denser cement plugs even with the addition of a ternary nanoparticle blend. Interestingly, for the 7 days curve, even though it exhibited negative UCS results, it has the highest M-modulus average % increase compared to the respective control value, which again, is reflecting badly on the correlation between high M-modulus and high UCS. Nevertheless, as fluctuations between the various dosages are miniscule, it is safe to assume that the cement matrix is intact and adequate for all tested cement plugs.

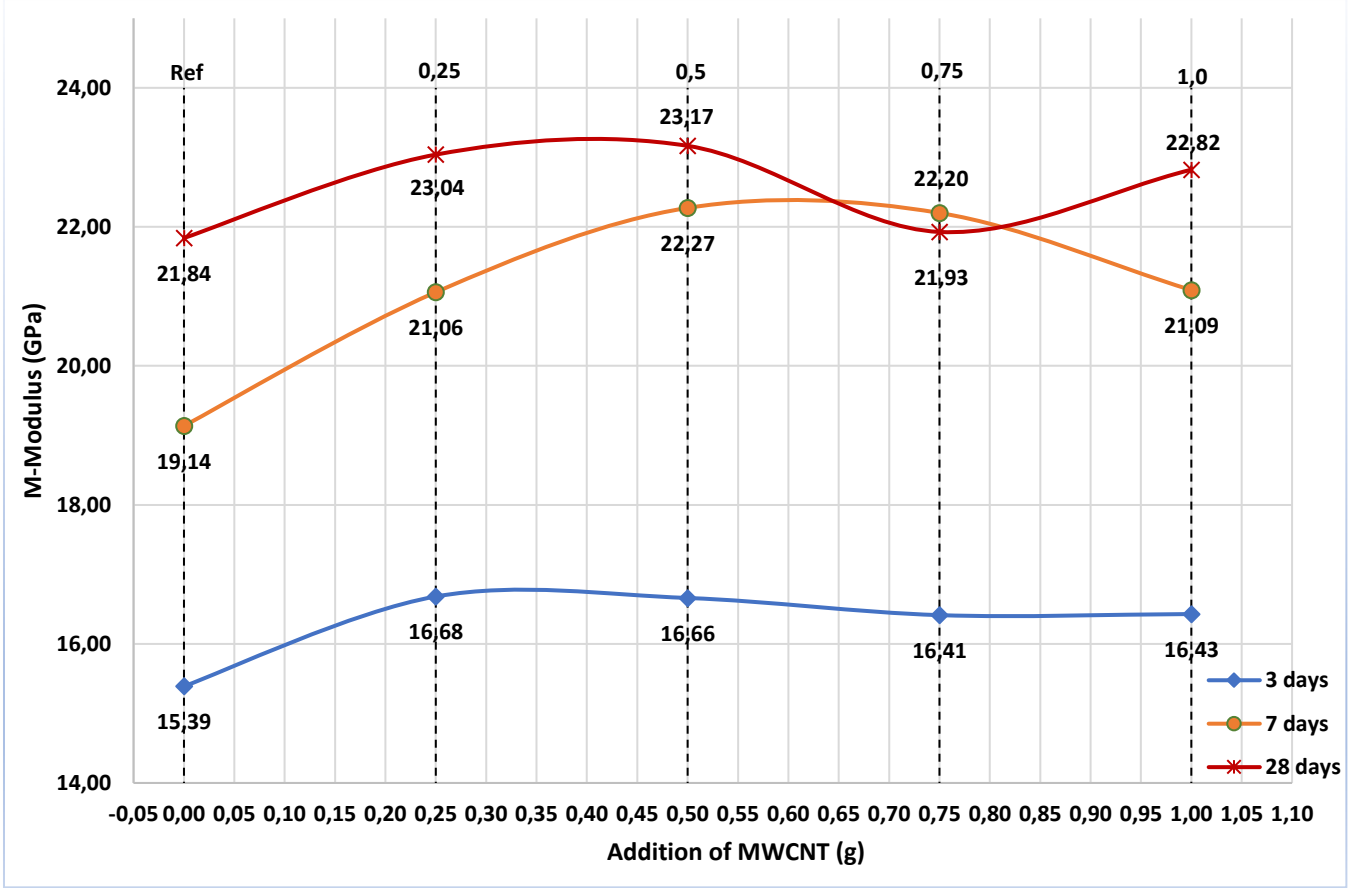

Figure 4.14 M-modulus for TM 3

4.4.5 Effect of the ternary blend on water absorption

For the first time across the 28 days batches thus far, all plugs with the ternary blend showed a reduction in water absorption, which considered as favourable. A probable reason for this could be that the ternary blend of nanoparticles has caused a refinement in the inner structure of the cement plugs, by filling of blocking pore spaces, at least to some extent. This would match the M-modulus results, in the sense that both suggests an improved cement matrix. This also weakens the belief that any significant agglomeration of the nanoparticles would have caused an inability to fill the cement matrix.

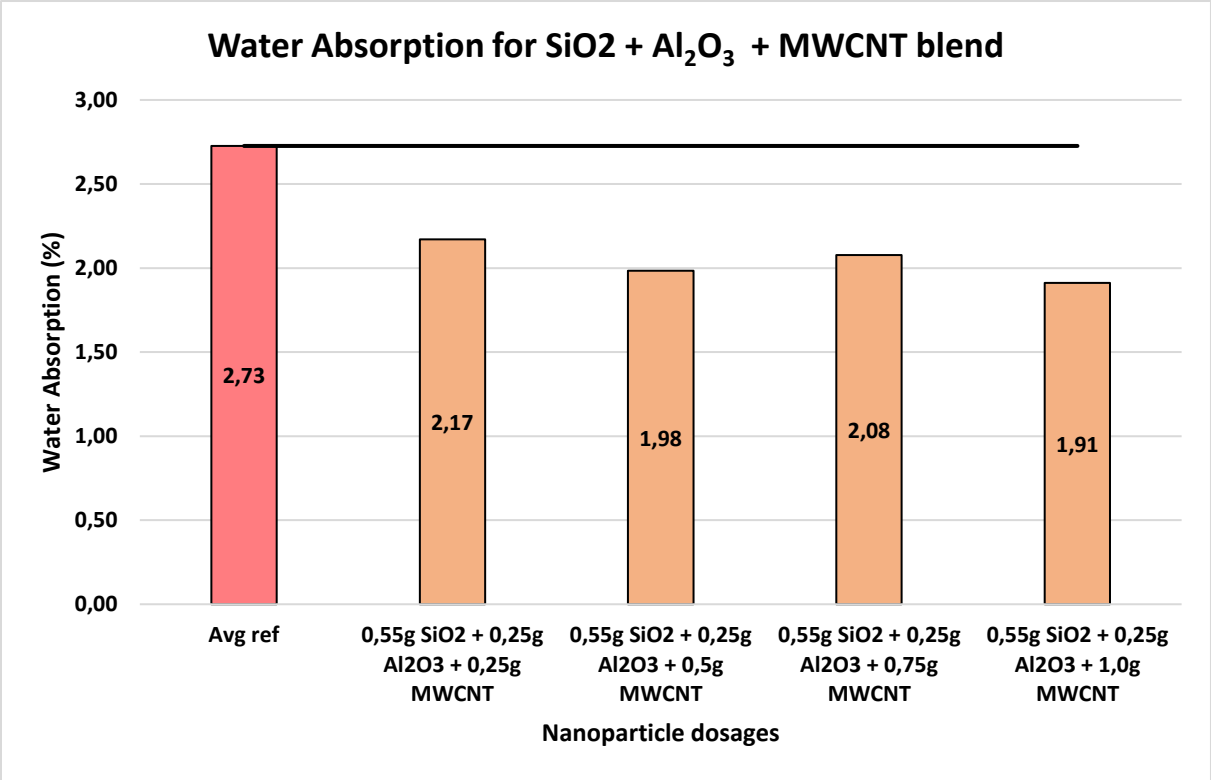

Figure 4.15 Water absorption for TM 3

4.5 Test Matrix 4 (Effect of fly ash)

This test matrix completely abandons the usage of nanoparticles, utilizes instead fly ash as a standalone additive in dosages from 2.5g, 5g, 7,5g and 10g. All graphs follow the same scheme as the previous ones have done.

4.5.1 Effect of fly ash on UCS

This time the x-axis in figure 4.16 denotes the amount of added fly ash. Note that the dosages here are tenfold compared to the nanoparticle dosages. As shown in figure 4.16, there is a notable decrease in compressive strength development after 3 days of curing for every dosage of FA. The two dosages providing the worst compressive strength, 5g and 7,5g of fly ash have a compressive strength of 9,33MPa and 9,92MPa. This translates to a UCS decrease of 36,61% and 32,65%. The best performing dosage was 2,5g, and it gave UCS value of 12,28MPa thus 16,59% reduction compared to neat cement. This is the worst 3 days batch when comparing with the other 3 days batches.

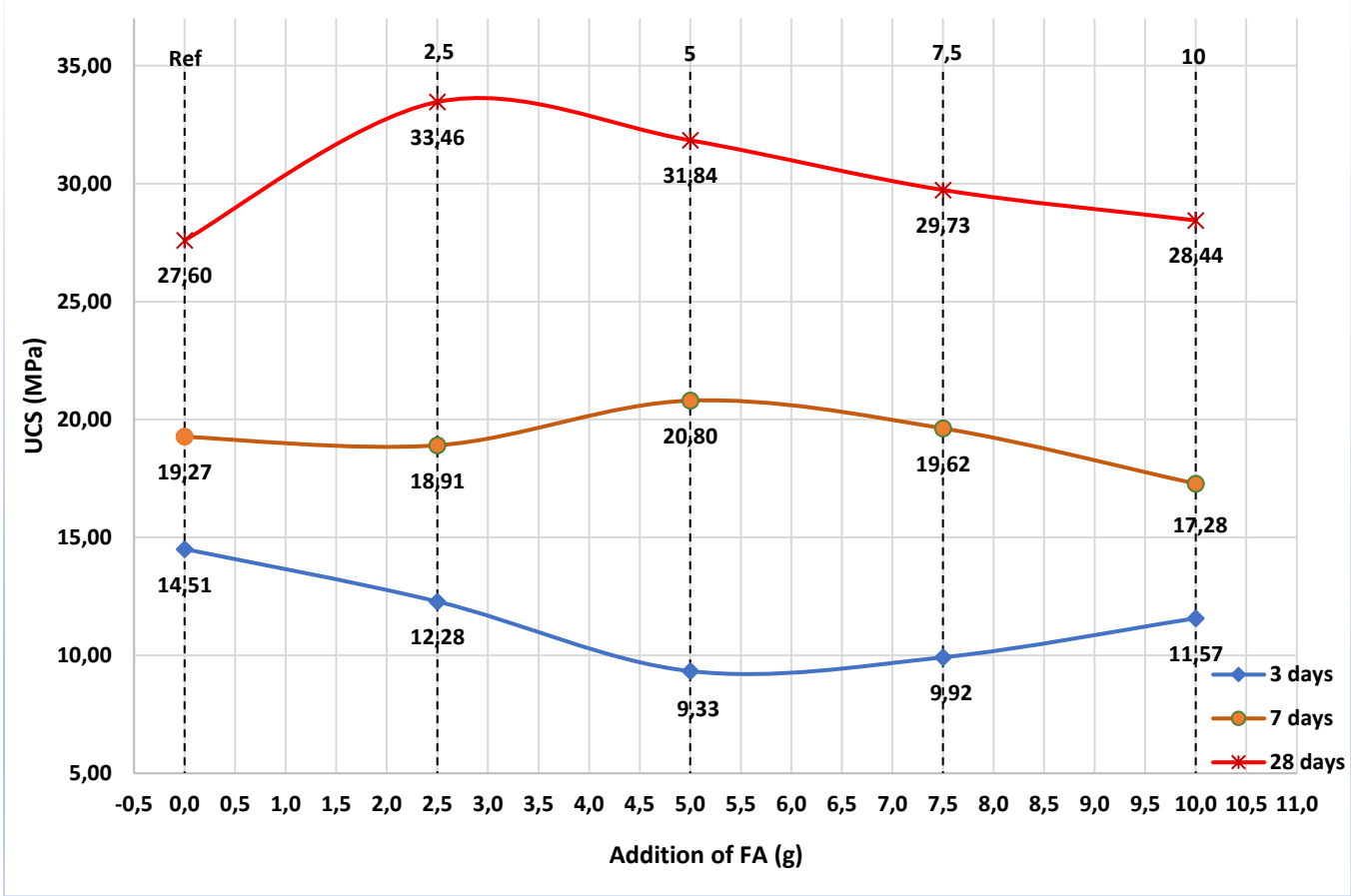

Figure 4.16 UCS for TM 4

Even though, these results are poor, they are expected as this exactly what was found in the literature review with studies from Bremseth (2009) [32] and Kaplan et al. (2018) [34]. It was found that fly ash as an additive was found to significantly decrease early compressive strength and setting time. These unfavourable effects have also been found in my results, and they are very prevalent after 3 days of curing. Figure 2.25 clearly exhibits that FA negatively impacted the setting time of the cement.

As for the 7 days results, they have progressed significantly since the 3 days compressive strength, as they compare to the reference value far better and two dosages show improvements in UCS. An increase of 7,96% and 1,86% in compressive strength was shown in the specimens with 5g and 7,5g of fly ash, with 20.80MPa and 19,62MPa, respectively. Adverse UCS was also experienced for the 2,5g and 10g fly ash samples, with the 10g fly ash yielding a UCS reduction of 10.31%. When compared to previous 7 days results from the other matrices, this batch falls in the lower end of the spectrum, being surpassed by both the single and binary systems. On the contrary, the ternary system still provided the worse UCS results after 7 days.

After 28 days, it is clear that fly ash as an additive has really improved over the extended 21 days of curing. This time all dosages of fly ash exhibited enhancements in compressive strength. Furthermore, the trend is really clear, as higher contents of fly ash diminishes UCS values. The two lowest dosages of 2,5g and 5g demonstrated an average compressive strength of 33,46MPa and 31,84MPa, respectively. Which translates to an 21,24% and 15,15% enhancement in UCS. For 7,5g and 10g of FA, the improvements are 7,73% and 3,05%, respectively.

This is magnificent results, after 28 days the results nearly match the binary 28 days batch (TB 6) and improves massively upon the 28 days results gathered from the single and ternary system (TB 3 and TB 9). This opens for an interesting discussion when considering the economic side of the equation. Nanoparticles are not considered to be cheap, with some types being more expensive than others. But seemingly, FA can perform similarly after 28 days at a fraction of the cost, which is exceptional. On the contrary, FA as additive is seemingly not viable for early strength, as the hydration rate and early strength suffered massively, whereas nanoparticles also offer UCS enhancements more rapidly.

All compressive results match the trend in figure 2.23 and study by Kaplan et al. (2018) , where fly ash was shown to give increased compressive strength after increased hydration time. An explanation for the improved results from the 3 days results, is that the negative effects of fly ash on early strength and hydration time is starting to subside after longer curing periods. Conclusively, not only do fly ash mirror what was found in the literature review, they give incredible compressive strength increase, which are comparable to the effects of nanoparticles.

4.5.2 Effect of fly ash on Young's modulus

Figure 4.17 shows the Young's modulus for the plugs. The results show that after 3 and 7 days curing the E-modulus values are less stiff with fly ash compared to neat cement. This is insignificant for the 3 days batch, as they demonstrated very poor UCS values. However, after 7 days, 5g of FA provided a 7,96% UCS improvement while also reducing E-modulus with 25,62% which is favourable. 7,5g of FA also decrease E-modulus by 13,65% while exhibiting a small UCS augmentation of 1,86%.

After 28 days, the E-modulus curve follow an identical trend as the respective UCS trend from figure 4.16. For the three lowest dosages of FA, 2,5g, 5g and 7,5g, the E-modulus values increased with 21,39% and 12,46% and 2,79% respectively. Interestingly, 10g of fly ash provided a 3,05% increase in UCS, while also lowering E-modulus with 12%.

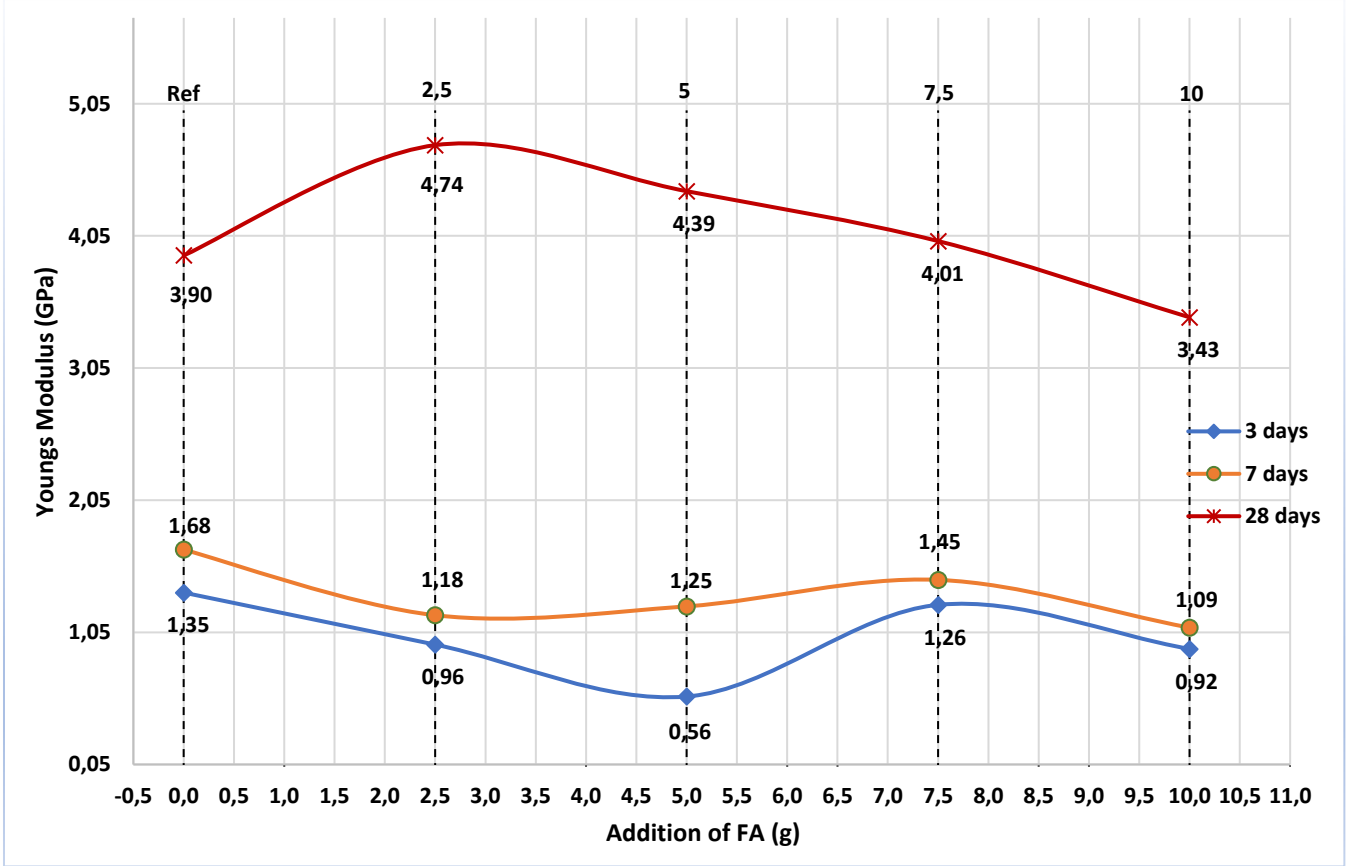

Figure 4.17 E-modulus for TM 4

4.5.3 Effect of fly ash on resilience

After 3 days of curing, the resilience is of the 3 out of 4 plugs with added FA absorb less energy than the reference, shown in figure 4.18. This is due to the slower strength development. Regarding the 7 days results all FA dosages also displayed a higher resilience than the reference samples. The highest resilience was experienced with 5g FA, and it gave a 38,88% augmentation. This dosage also had the highest compressive strength of 20.88MPa and second lowest E-modulus of 1,25GPa, and are as a result by far the best dosage after 7 days of curing. Furthermore, 7,5 of FA also provided a resilience improvement of 21,24%, while also displaying a favourable UCS increase of 1,86%.

Moreover, after 28 days, the red curve again follows the same trend as figure 4.16 and figure 4.17. All dosages had superior resilience when compared with the reference value. The 2,5g and 5g dosages of FA improved the resilience by 34,20% and 26,74% when compared to neat cement, respectively. Whereas 7,5g and 10g of fly ash increased resilience with 18,32% and 8,02%, respectively. The overall impact of FA on the neat G-class cement in general has shown positive effects in terms of the improving the UCS, E-modulus and resilience. Therefore, this matrix design is very promising.

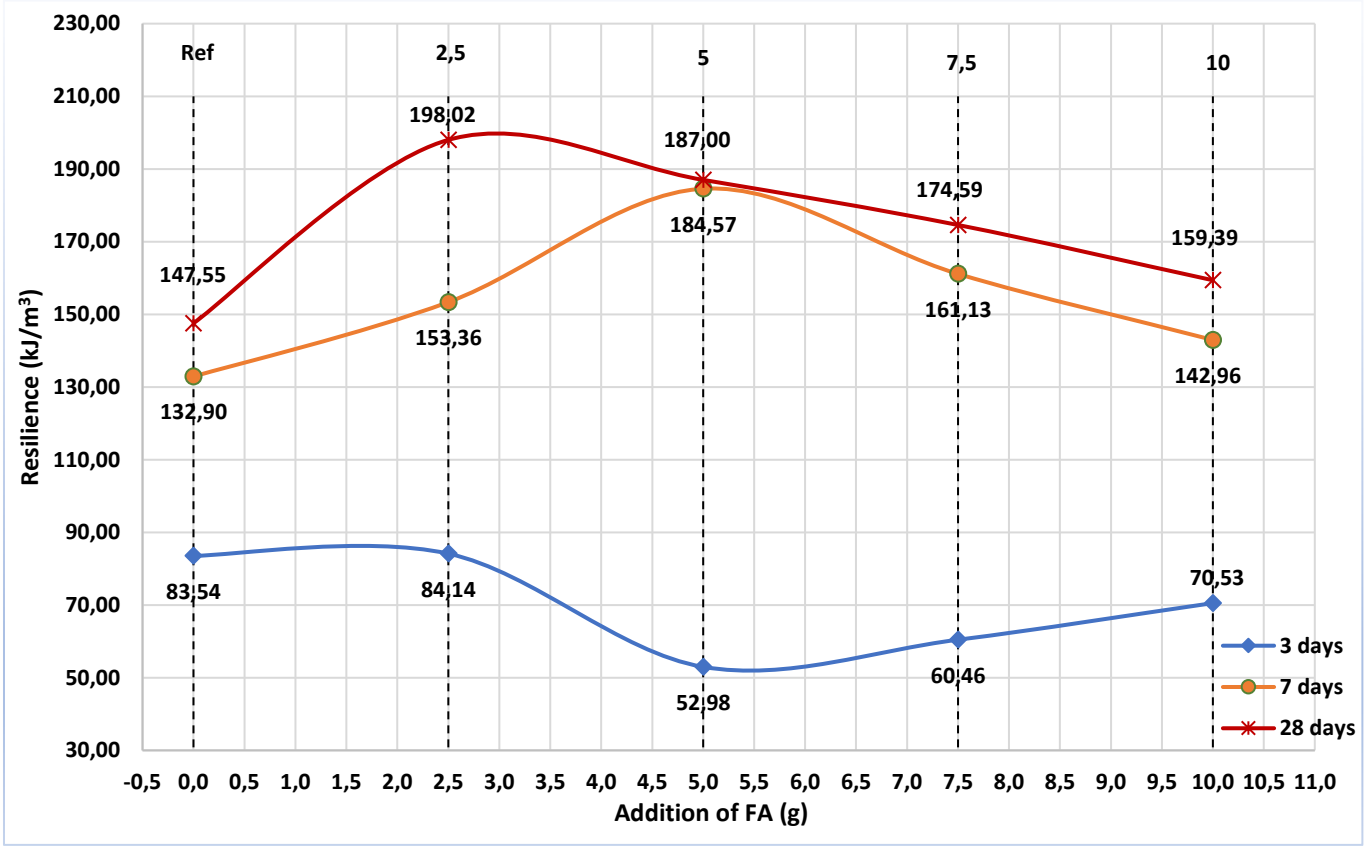

Figure 4.18 Resilience for TM 4

4.5.4 Effect of fly ash on M-modulus

M-modulus results are presented in figure 4.19. There is nothing out of the ordinary with these results when compared to the other matrices. M-modulus gradually increases with as the curing periods get longer. Similarly, to the other matrices, there is no significant fluctuations between the dosages within each respective curing age. It is observed that the M-modulus values after 3 days of curing matches the reference value despite having very poor UCS results. However, this time the 7 and 28 days curves seems to follow similar trends to their respective UCS trends, as seen in figure 4.16. The best performers after each curing age, 2,5g for 28 days and 5g for 7 days, has the largest M-modulus increase, while also providing the best UCS results as well.

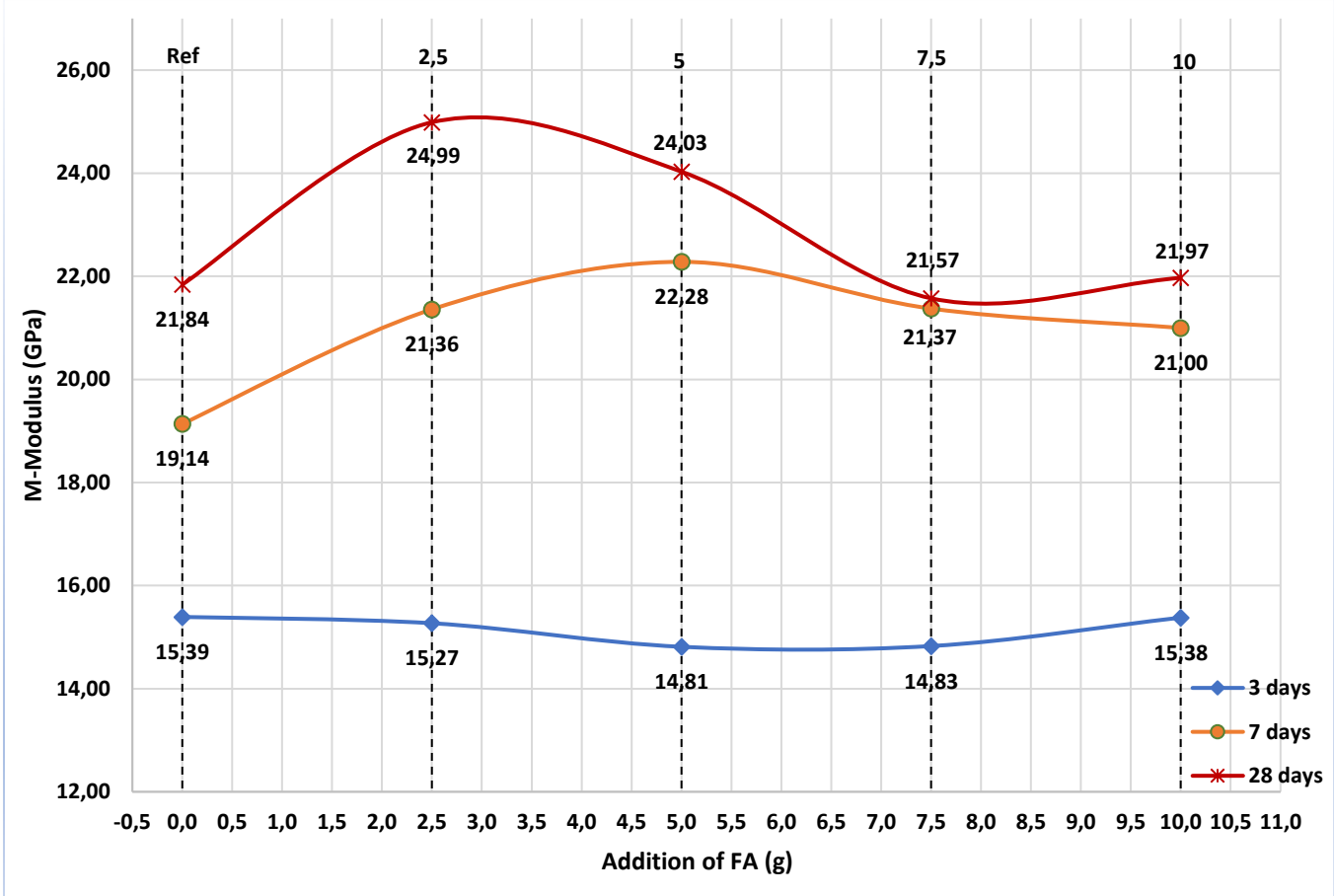

Figure 4.19 M-modulus for TM 4

4.5.5 Effect of fly ash on water absorption

Figure 4.20 shows the water absorption data for TM 4. It can be observed that all specimens expect for 10g of fly ash, absorbs less water than that of the reference value. The two best performing dosages of 2,5g and 5g also has the lowest water absorption with a 11,58% and 13,10% decrease. Whereas 10g of fly ash increases water absorption with only 0.23%. All in all, the water absorption data is favourable, and suggests a more refined cement matrix in the specimens.

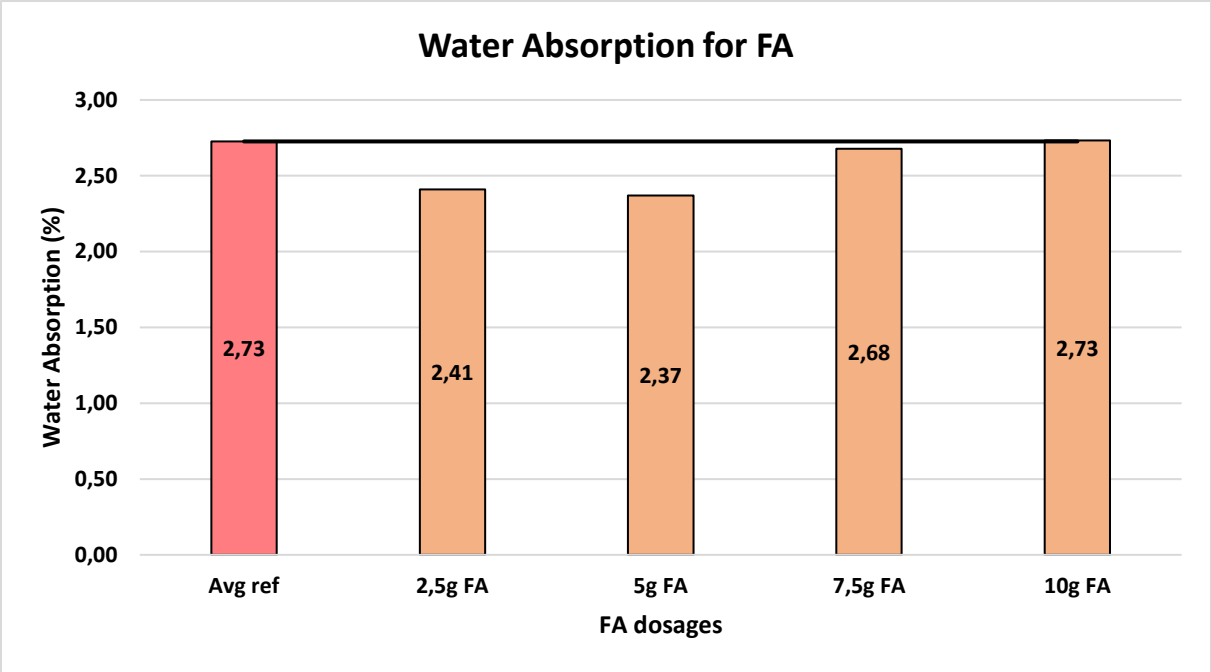

Figure 4.20 Water absorption for TM 4

4.6 Test Matrix 5 (Effect of fly ash +0.55g SiO_2 blend)

This matrix investigated the effects of a constant concentration of nano-SiO_2 in conjunction with varying concentrations of FA on 0.44WCR G-class cement. The dosages of fly ash are the same as in TM 4, which was 2,5g, 5g, 7,5g and 10g.

4.6.1 Effect of fly ash + SiO_2 blend on UCS

This time the x-axis also measures the amount of FA instead of SiO_2. This is because 0.55g of SiO_2 is kept constant for every cement plug except the reference plugs. Figure 4.21 depicts UCS for test matrix 5.

UCS after 3 days show that all FA dosages reduces the early compressive strength development. For instance, the 2,5g and 7,5g of fly ash reduces the UCS with 8,93% and 13%, respectively. Again, poor display of compressive strength, but this is expected as fly ash again is used as an additive, which as seen by TM 4 and literature review negatively impacts early strength and setting time.

When comparing this batch with the 3 days FA batch (TB 10), in figure 4.16, we actually notice that nano-SiO_2 presumably has positively affected the early strength as fly ash alone had significantly worse UCS results. Although, the compressive strength of this batch is still unsatisfactory compared to regular neat G-class cement and other matrices in this thesis, it is interesting to note that nano-SiO_2 probably has aided slightly with early compressive strength

despite being in a blend with fly ash. Nevertheless, the results are still severely weaker than the neat cement.

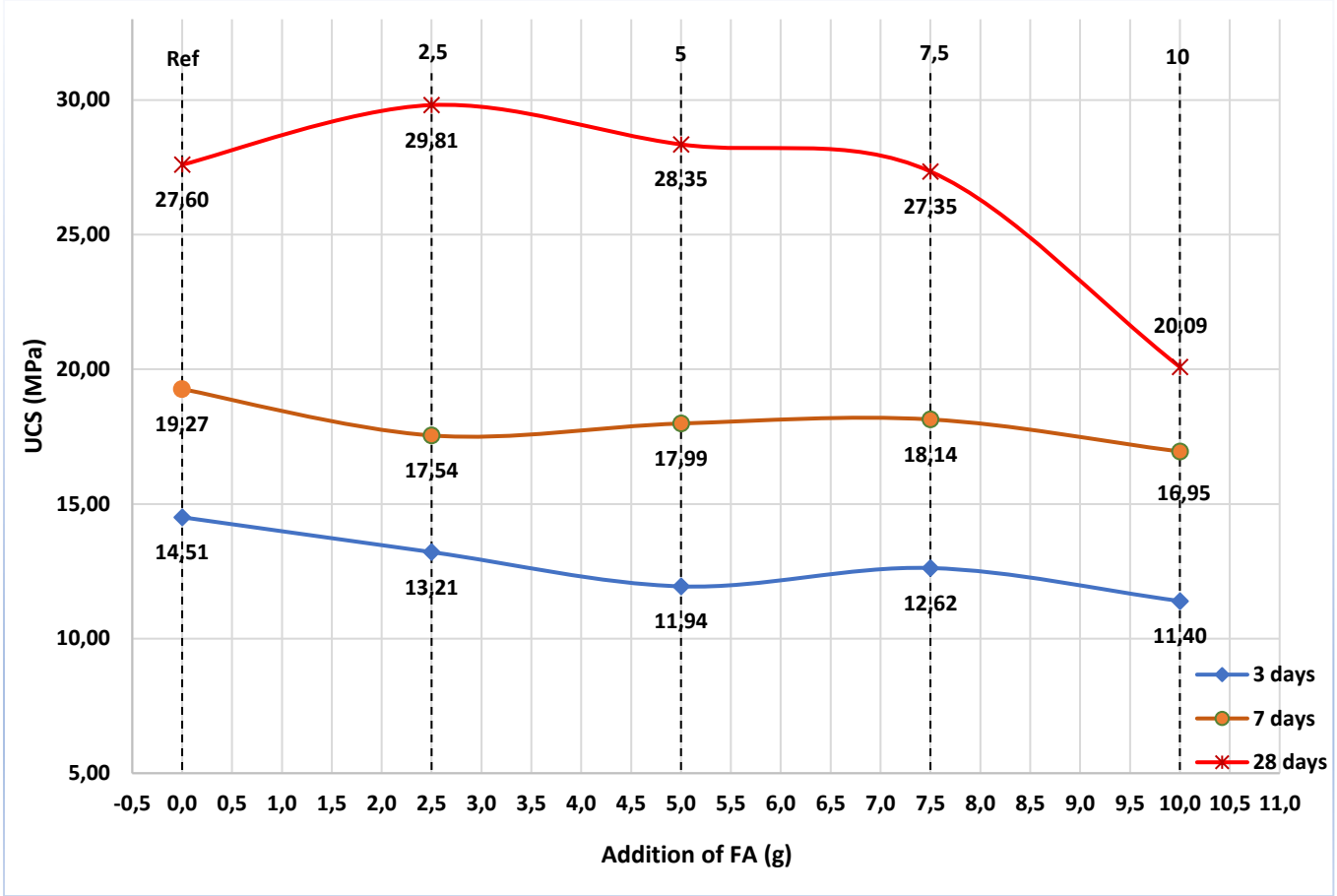

Figure 4.21 UCS for TM 5

Similarly, the 7 days curing data showed that all the FA additives in the 0.55g SiO2 system reduced the UCS of the neat cement. Even TB 8 (ternary blend after 7 days), which came extremely close to only presenting adverse results, had one dosage which provided a slight increase in UCS compared to the reference sample. As figure 4.21 shows that the two highest performing dosages was 5g and 7,5g of FA reduced the UCS by 6,64% and 5,85%, respectively. This means that fly ash alone gives a better effect than that of FA + SiO_2 does after 7 days, as TB 11 was significantly better than this batch. Also, nano-SiO_2 as a standalone additive was better after 7 days of curing.

Moreover, in figure 4.21, after 28 days of curing, it is observed that the 2,5g and 5g of FA blended with SiO_2 increase the UCS by 8,02% and 2,73%, respectively. Furthermore, 0,75g of fly ash gives a small 0.92% increase in UCS whereas 10g of FA reduces UCS by 27,22%. Similarly, to the TM 4, it is observed that the lower dosages of FA give the best compressive strength after 28 days, this trend can be seen in both figure 4.16 and 4.21.

Again, FA performance is seemingly higher when used alone, as it gave a UCS improvement of 21,24%. Whereas, when used in combination with SiO_2 the best performance is only an 8,02% improvement. This is the second worst UCS results after 28 days of curing this entire thesis, behind nano-SiO_2 alone (TB 3). A reasonable explanation for this is likely due to some chemical and physical interactions between the nano-SiO_2 and the added fly ash might occur, which had negative impact on cement hydration. The results and the interpretation are valid for the considered 0,55g SiO_2 concentration. However, changing the SiO_2 concentration and FA, one may get different results. The seemingly negative synergy of the FA and SiO_2 is not investigated due to lack of chemical analysis equipment such as XRD, Scan electron microscope (SEM). The results however indicate further investigations.

4.6.2 Effect of fly ash + SiO_2 blend on Young's modulus

E-modulus is displayed in figure 4.22. After 3 days, the E-modulus is reduced for across all concentrations. The E-modulus reduction is inconsequential due to the poor UCS results. The poor UCS results are also the reason for the low E-modulus results.

After 7 days of curing, the E-modulus is improved for all dosages, which is unexpected and adverse. However, it is also insignificant as the UCS results were negative. In comparison, TB 11, which only utilized FA in the same dosages without nano-SiO_2, displayed better compressive strength, and a reduction in E-modulus.

After 28 days, positive results can be seen in figure 4.22, it is observed that the reference value is notably higher than the E-modulus values which included the blend of FA and SiO_2. This is favourable results, especially promising for 2,5g and 5g dosages, which both provided UCS improvements. Moreover, 2,5g gave an 8,02% UCS increase while reducing E-modulus with 19,52%, whereas 5g gave a 2,73% UCS advancement while demonstrating 33,33% reduction in E-modulus. Either way, both are beneficial results for this test matrix.

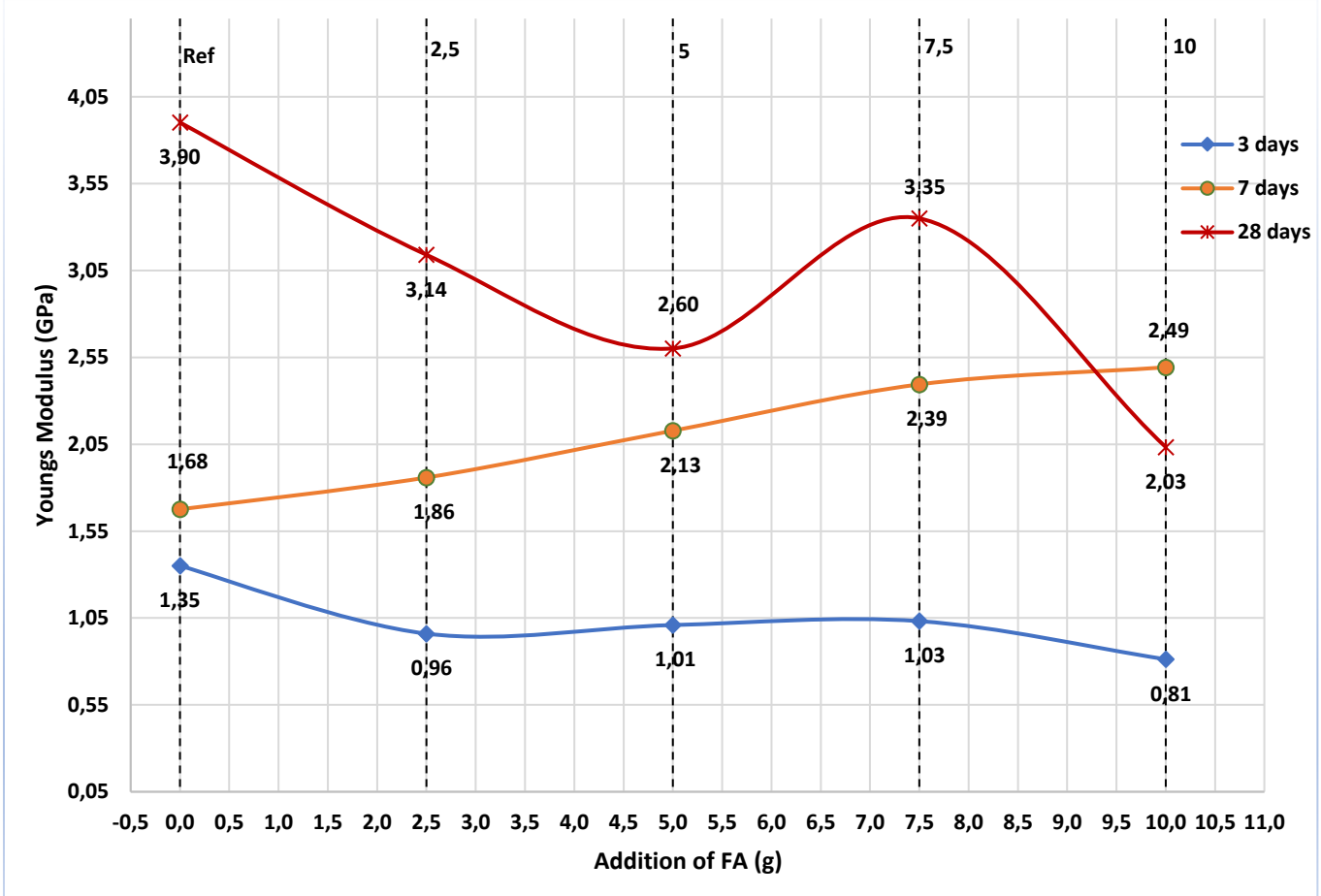

Figure 4.22 E-modulus for TM 5

4.6.3 Effect of fly ash + SiO_2 blend on resilience

By looking at the 3 days of curing in figure 4.23, it is observed that the trend varies non-linearly for the specimens which include FA. 2,5g and 7,5g of fly ash gave improves the energy absorbing capabilities of neat cement while 5g and 10g decreases it. Nevertheless, in regard to the UCS results from figure 4.21, resilience improvements are insignificant.

After 7 days the resilience shows a decreasing trend as FA concentrations increase to 7,5g. In addition, 10g of FA exhibit slightly higher resilience than 5g and 7,5g, however still below neat cement. Again, due to poor UCS results, these reductions in resilience are expected and insignificant.

After 28 days curing, it is observed that 3 out of 4 dosages exhibited improvements in resilience. This is most significant for the 2,5g dosage, as it also demonstrated an 8,03% UCS improvement, E-modulus reduction of 19,52% and an 27,74% increase in resilience. It was also improved for 10g of FA, but since it provided a 27,22% decrease in UCS, the resilience is

irrelevant. After curing 28 days, 2,5g of FA is seemingly the best performing dosage of this blend.

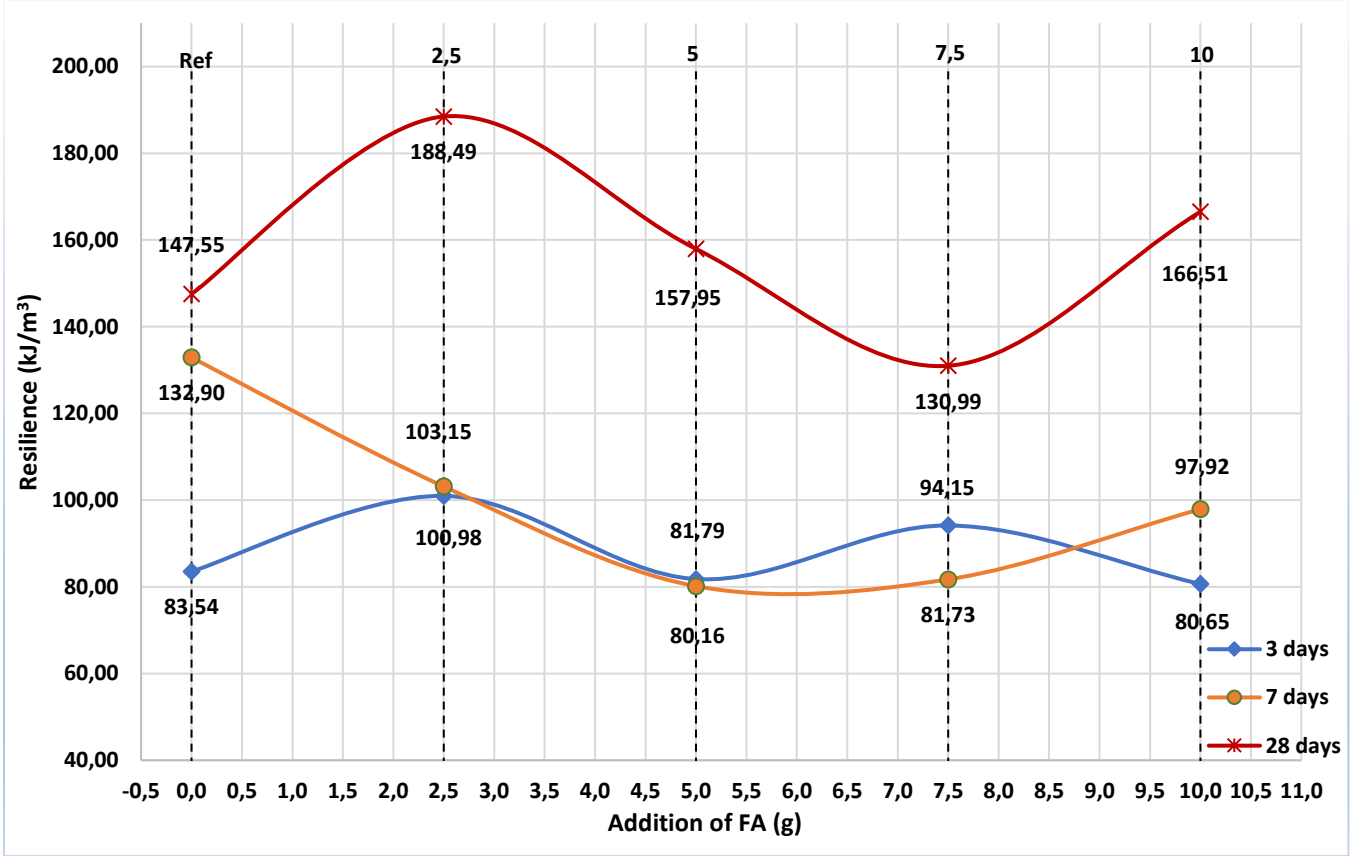

Figure 4.23 Resilience for TM 5

4.6.4 Effect of fly ash + SiO_2 blend on M-modulus

Figure 4.24 presents M-modulus for TM 5. Results show that FA + SiO_2 blending did not show any impact on the M-modulus after 3 days of curing. After 7 days curing, the M-modulus consistently decreases as the concentration increases. This matches with the UCS results from figure 4.21, as they were all below the reference value.

After 28 days, the M-modulus values are significantly higher than the neat cement. It might suggest an additional refinement in the cement matrix compared to the reference samples, however the UCS results suggests otherwise. Even though, 2,5g and 5g of fly ash gave UCS improvement and M-modulus augmentation. The opposite occurred for 7,5g and 10g, where they gave significant reductions in UCS while still providing significant M-modulus improvements.

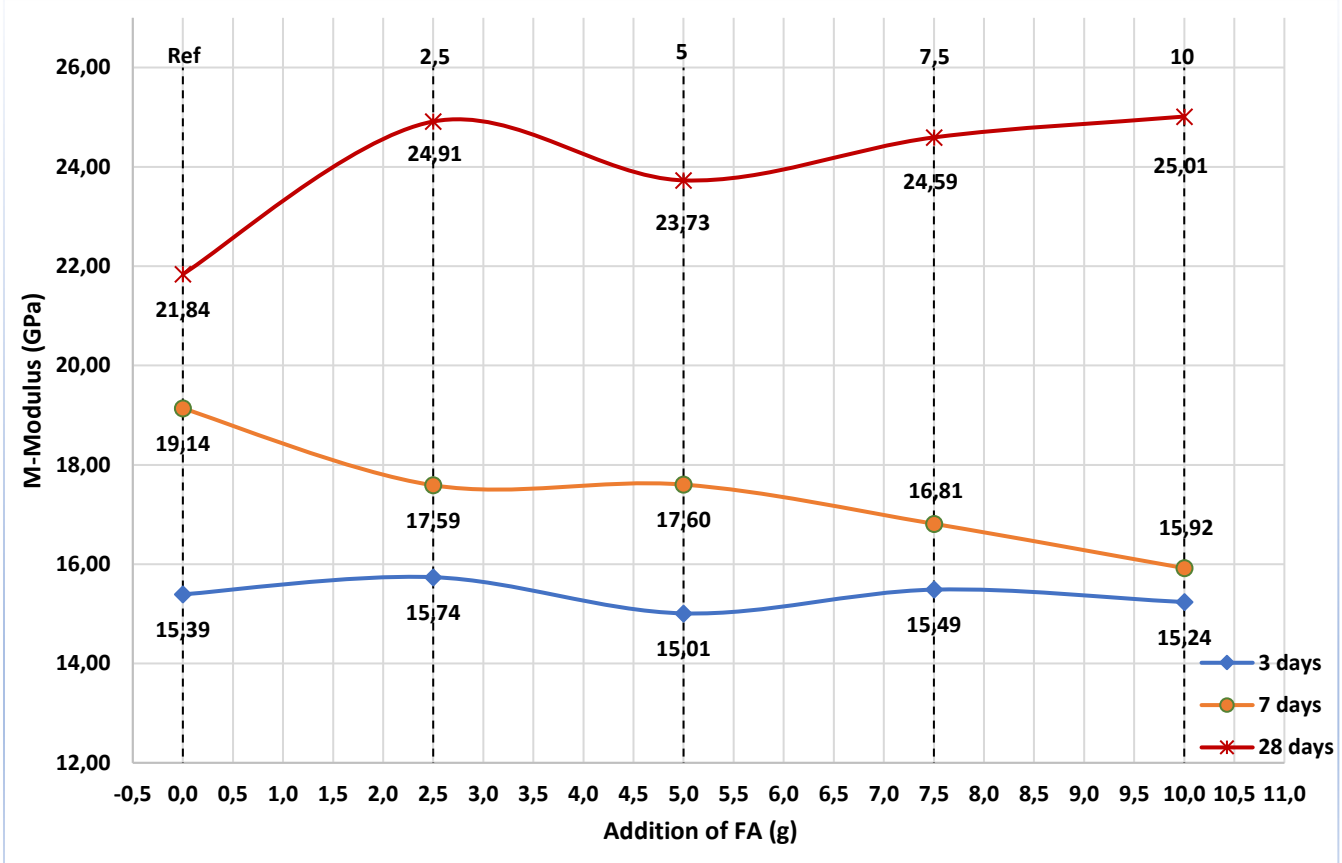

Figure 4.24 M-modulus for TM 5

4.6.5 Effect of fly ash + SiO_2 blend on water absorption

Water absorption data is presented in figure 4.25. It is observed that this time, all dosages of the blend increase water absorption compared to the reference value. This could be caused by SiO_2 in the blend, as FA alone provided reduction in water absorption, as seen in figure 4.20 while nano-SiO_2 provided only higher water absorption when it was included, depicted in figure 4.5. Again, it is preferred to have a reduction in water absorption, as it indirectly describes how good the internal structure that inhibit the possible fluid flows into the cement plug.

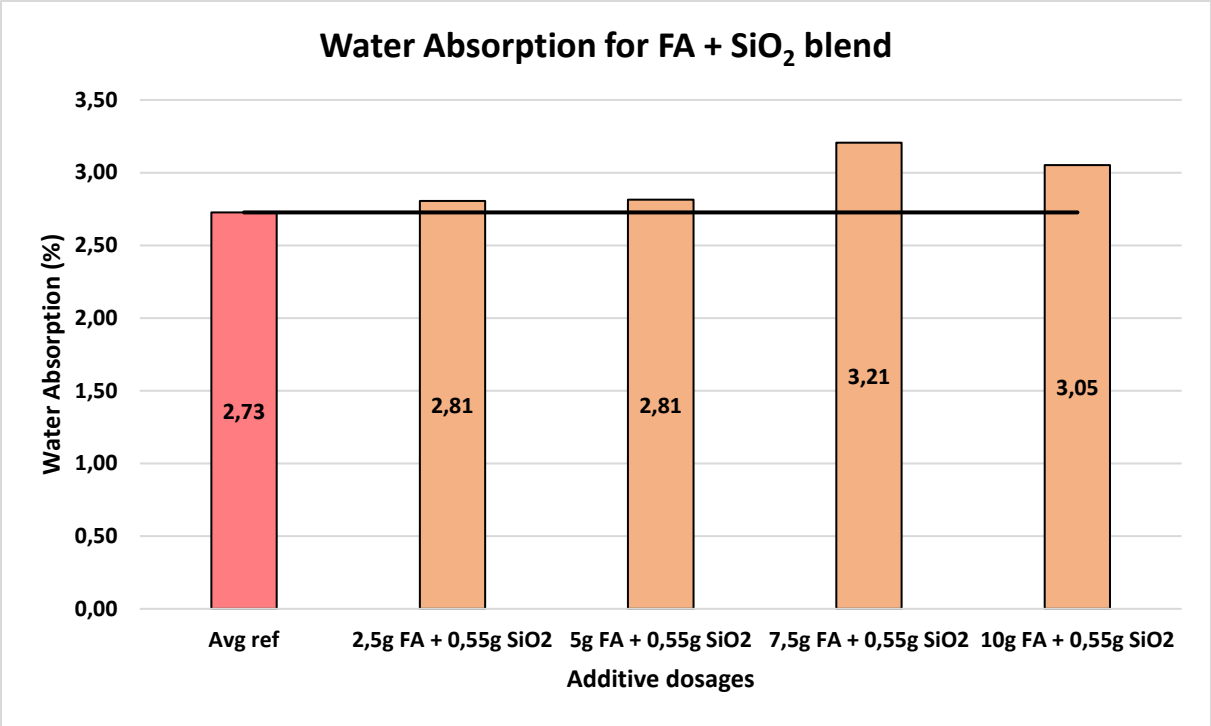

Figure 4.25 Water absorption for TM 5

4.7 Further characterization of the best systems

This section will investigate further on the best system from the previous test matrices. The selection is based on the 28 days UCS performances from the experimental works. Furthermore, the ternary system will not be present as it likely not economically viable and got overshadowed by other test matrices. The selected dosages are:

- Reference (neat G-class cement)
- 0.75g SiO_2 from TM 1
- 0.55g SiO_2 + 1,0 Al_2O_3 from TM 2
- 2,5g of FA from TM 3
- 2,5g of FA + 0.55g SiO_2 TM 4

4.7.1 Rheology

In the petroleum industry, there is a lot of fluid transport present, therefore rheology is paramount. This provides pivotal information about flow and deformation for flowing materials. The primary cement job during the well construction phase is important to get right the first attempt, and rheological properties will aid in designing and executing this properly. By knowing the rheological properties of a cement slurry, it will help determine the pump pressure and rate required to pump the cement slurry downhole. Furthermore, rheology is useful

for determining frictional pressure in wellbore when pumping cement downhole and it helps to optimize placement of the cement slurry [4].

Figure 4.26 presents the shear stress of tested cement slurries. Seemingly when nanoparticles are added to neat G-class cement, it improves the shear stress of the slurry for every shear rate. While the opposite can be said when FA is used as additive alone, as it reduces shear stress, seen by the orange curve. Interestingly, when FA + SiO_2 is used, SiO_2 seemingly mitigates the reducing effects of FA on shear stress.

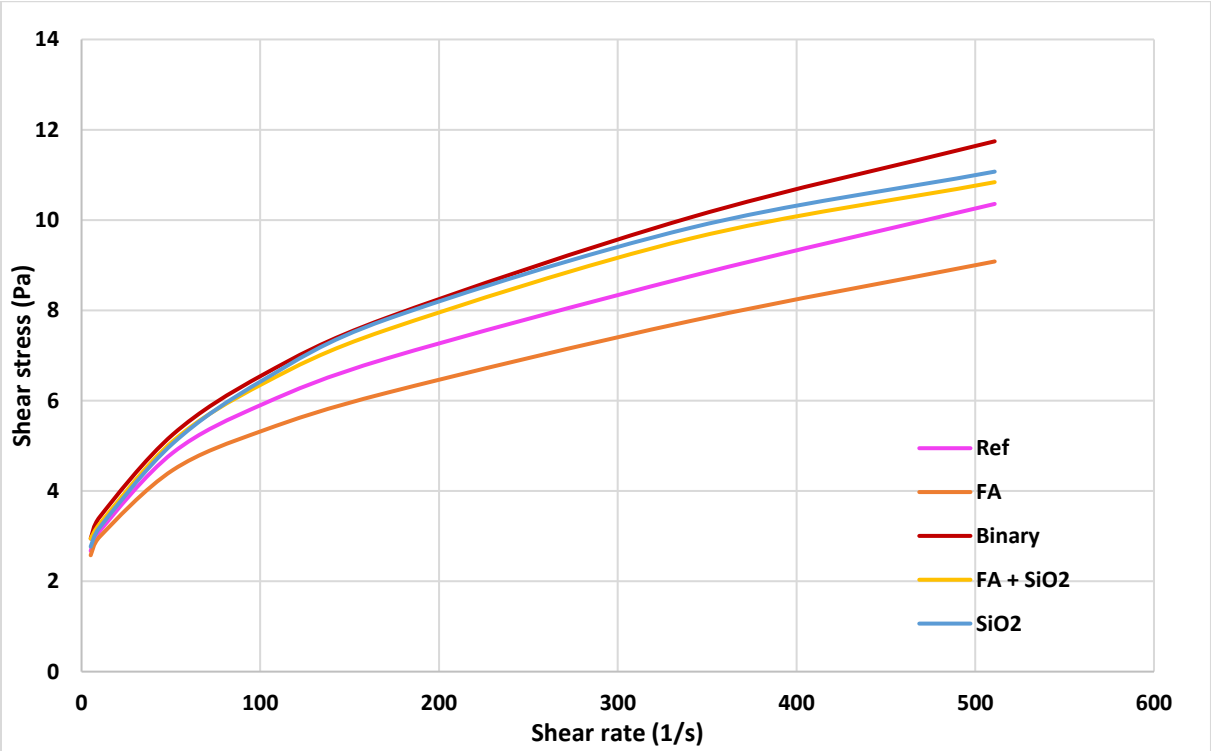

Figure 4.26 Shear stress of the tested cement slurries

Furthermore, figure 4.27 display the Casson yield stress of the slurries, it is observed that all slurries improve the yield stress compared to the reference sample. In practice this means that the slurries with higher yield stress will require more force to flow. This means that in order to pump slurries with nanoparticles and/or FA , a higher pump pressure is required to adequately pump the slurry downhole.

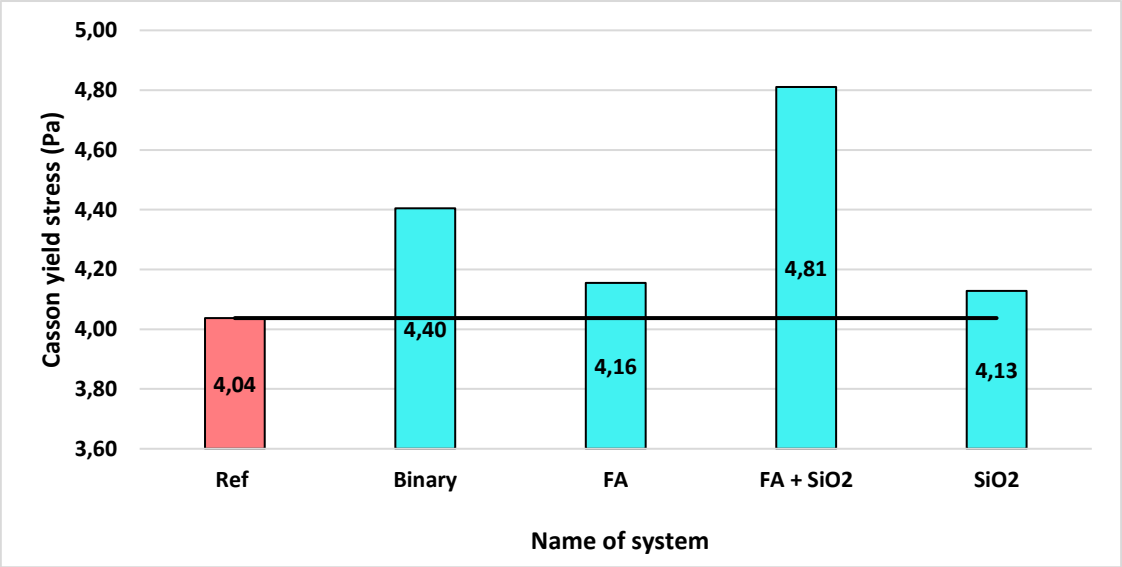

Figure 4.27 Casson yield stress

Also, Casson PV (plastic viscosity) is displayed in the figure 4.28. Similar to figure 4.26, slurries with nanoparticles experienced higher PV than the reference slurry, whereas when FA is alone, there is a significant reduction is PV. A high PV means that the fluid in question is more resistant to flow, thus creating more friction when flowing. This also translates into requiring more pump pressure in order to flow adequately. A potential benefit to the thicker cement is that it possesses the ability to carry solids and clean out any residual particles after usage of washers and spacers. Opposite is the case for the standalone FA slurry, it will create significantly less friction and require less pump pressure to pump downhole.

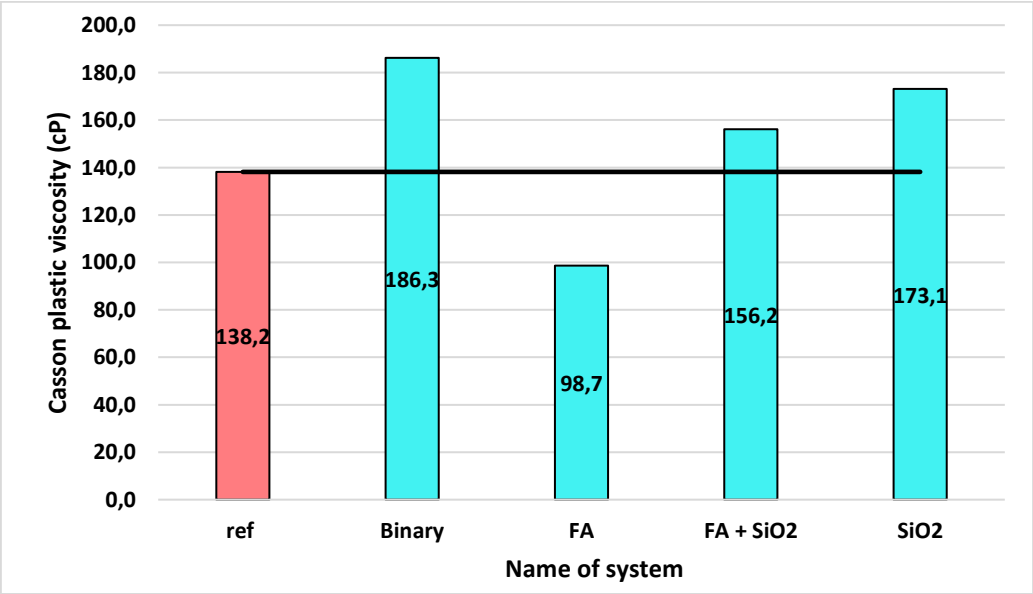

Figure 4.28 Casson PV

It is worth noting that these rheological parameters alone cannot tell us whether or not a cement slurry is adequate for a specific well operation. In order to achieve a full picture, well simulations need to be conducted using the rheological parameters measured above, in order find out all the intricacies. This was not done in this thesis.

4.7.2 Heat development

As mentioned in section 3.3.2.5, when cement comes in contact with water, an exothermic reaction ensues, thus releasing heat during the reaction. Temperature loggers were placed in contact with the cement slurry for 8540 minutes (142,3 hours) during the hydration process and gathering temperature input every 30 seconds.

Figure 4.29 depicts the temperature profiles, it is observed that all the slurries behave very similarly in terms of their temperature profile. Figure 2.2 show that the hydration stage presented in the figure below is the induction period, acceleration, deacceleration and diffusion period. This is because the preinduction period is very succinct, only lasting couple of minutes, thus the set-up time for the logging equipment surpassed this short period.

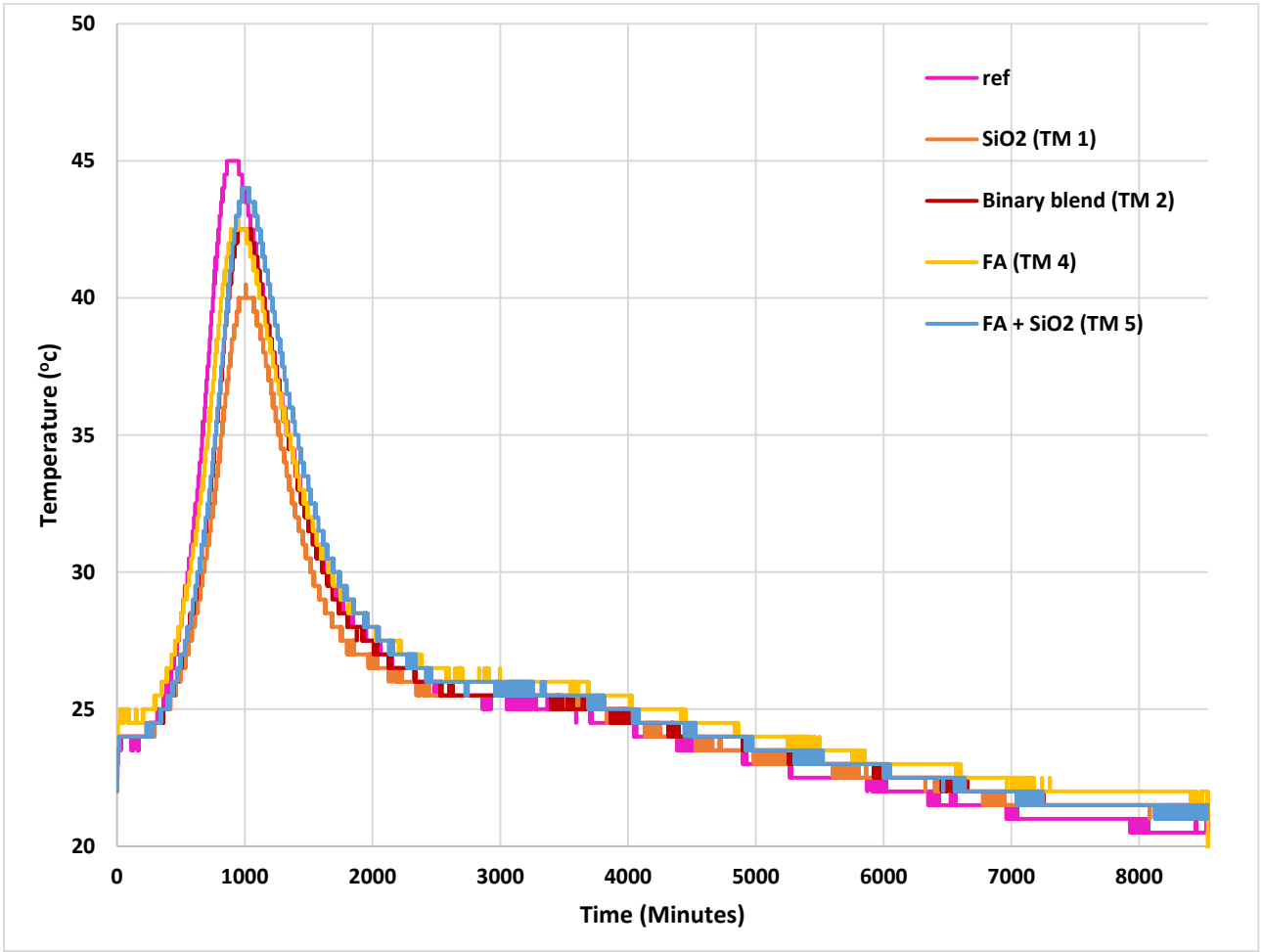

Figure 4.29 Heat profiles for various slurries

Furthermore, it is observed that the reference slurry seems to start its acceleration phase slightly earlier than the slurries with additives, however it also reaches the highest peak temperature of the tested slurries with 45°C, as can be seen in figure 4.30. The lowest temperature was seen from SiO_2 (TM 1) at 40.5°C. There is really no impactful difference between the slurries, as their temperature profiles are very similar, and only a 4,5°C deviation in peak temperatures for every tested slurry. With that being said, none of the slurries tested are likely to be the root of any heat related issues, like the ones mentioned in section 3.3.2.5.

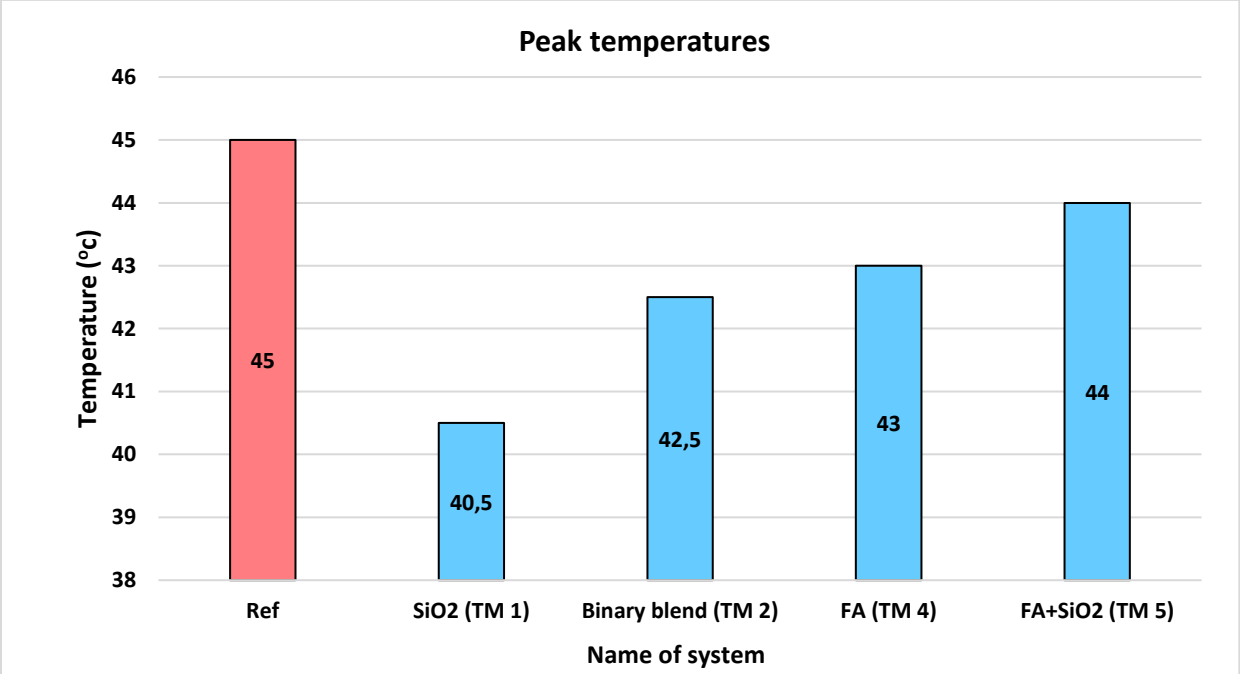

Figure 4.30 Peak temperatures of the various systems

4.8 Uncertainties

This section will focus on uncertainties with the experimental portion of this thesis.

Slurry synthesis*:* All the slurries were prepared using the same procedure and were hand mixed. However, during mixing, it was observed that the slurries contain some air bubbles, which could affect the compressive strength of the plug. This is why the slurries were continuously tapped gently into a flat surface when pouring the cement. It is uncertain if all the air bubbles were removed during the tapping. Furthermore, it is also uncertain if the cement powder was completely dissolved during the mixing. There may have been some small clustering in some samples.

Plug preparation: Plug preparation was also done identical from batch to batch. However, despite this effort, on some rare occasions there were defective plugs, with structural defects, often manifesting as either cracks, big pores or trapped air in the specimens, causing them to

tolerate significantly lower compressive downforce. One example of this can be seen in Appendix D.

Additionally, all tested plugs had to be levelled on the top, to make sure they were completely even. This was done using sandpaper. Although the flatness was tested with a spirit level for every plug, there exists a possibility that some plugs were not flattened enough, which could result in a minor point load, where the loading distribution is uneven and result in lower compressive strengths.

Human error: All testing and creation procedures were conducted by humans. And as unfortunate as it might be, we are subject to making mistakes from time to time, so there is always a possibility of human error affecting the experiments. A known mistake that was made in this thesis, was that the deformation measurement was not properly set up for the first iteration of TB 4, causing the deformation data to either start slowly or not at all in some rare instances.

Quantity of experiments: In order to obtain the most accurate results possible, it is important to test multiple times to ensure that results are consistent. Due to time constraints, two plugs were created per dosage of additive. This was to use the average value of the two plugs as the final results. Ideally, more samples should have been created to ensure as accurate results as possible. In addition, some plugs were defective or human error was done measuring deformation, leading to some results being reported being a single result instead of the average of two. Although this was rare, one should strive to create more specimens if time and economic situation allows for it.

5 Empirical Modelling

Section 3.3.3 introduced Horsrud's model for UCS estimation, using a relationship between UCS and compressional wave velocity instead of conducting destructive testing. The model was based on shale and will therefore be analysed using cement results from this thesis in the subsequent section. This will be done to determine the accuracy of the model for cement.

5.1 Analysis of Horsrud's model

The data used to analyse the accuracy of Horsrud's model is one batch from each curing age. A varying range of data has been chosen to analyse, meaning some results are considered as either poor, mediocre or favourable. The calculated UCS will be plotted against the actual UCS obtained from destructive testing.

- 3 days FA from TM 4 (TB 10) – poor
- 7 days Al_2O_3 and SiO_2 blend from TM 2 (TB 5) – favourable
- 28 days FA mixed with SiO_2 from TM 5 (TB 15) - mediocre

Figure 5.1 shows actual UCS vs Horsrud's model for TB 10 (FA after 3 days), it is observed that for this batch, the Horsrud model clearly overestimates the measured UCS values.

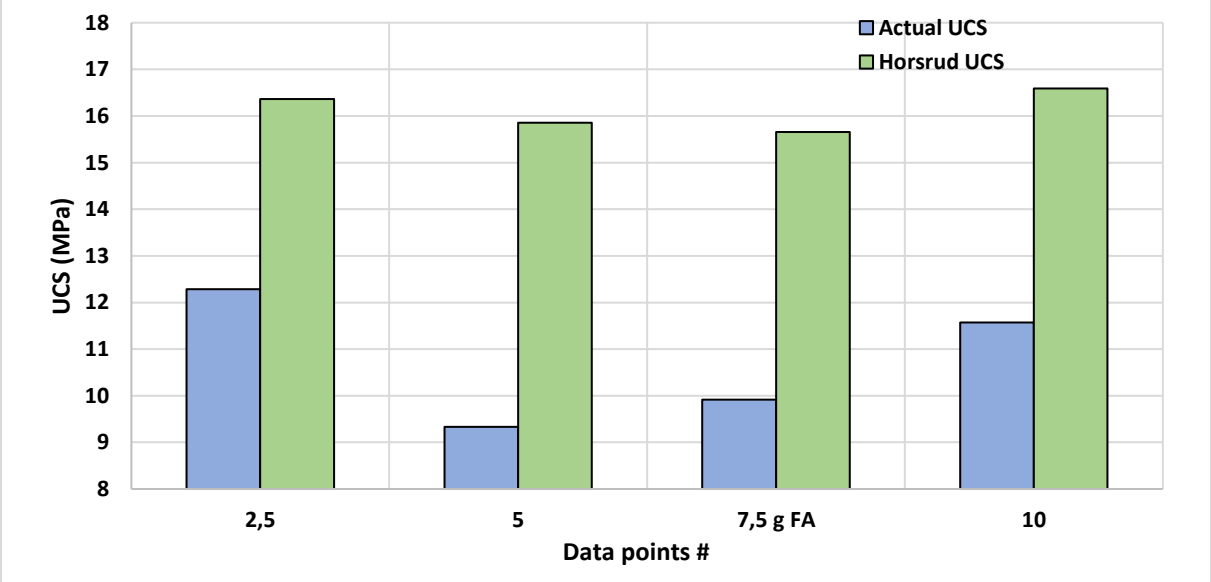

Figure 5.1 Horsrud's model vs actual UCS for TB 10

Furthermore, the 7 days UCS data from TB 5 (binary blend after 7 days) is plotted vs UCS estimates from using the Horsrud model in figure 5.2. The Horsrud model is far more accurate for this batch than the previous batch, figure 5.1. This might be due to these results being favourable, thus they fit with the overestimating tendency of the Horsrud model.

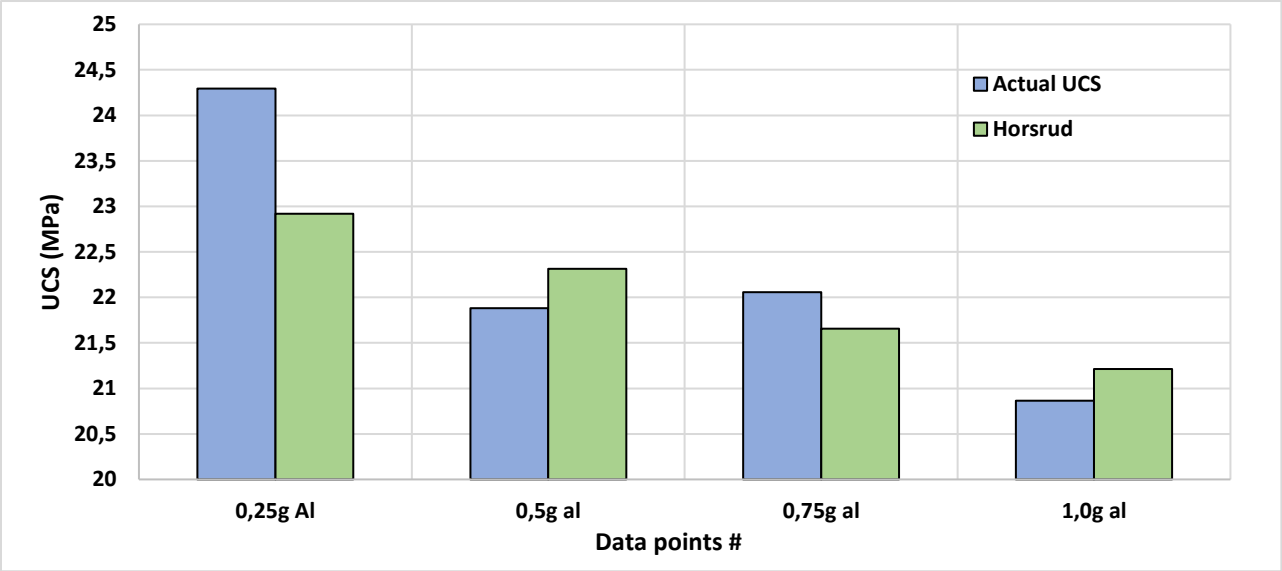

Figure 5.2 Horsrud's model vs actual UCS for TB 5

Finally, figure 5.3 shows data from TB 15 (FA + SiO_2 after 28 days) vs Horsrud estimates. Again, there is a trend of Horsrud's model overestimating the UCS compared to the actual UCS.

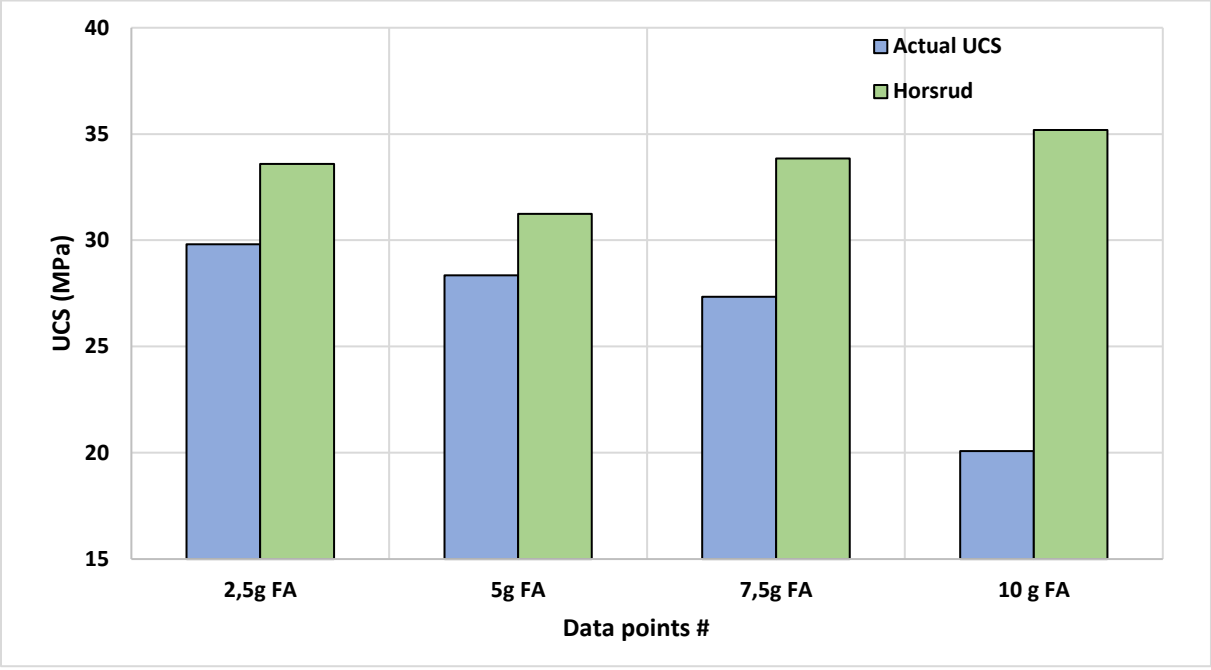

Figure 5.3 Horsrud's model vs actual UCS for TB 15

From this analysis it is observed that the Horsrud model tends to overestimate the UCS for cement plugs. This is likely due to the model being developed for shale and not cement. However, there is still a need for a more accurate model to predict UCS in cement plugs, based on the compressional wave velocity.

5.2 New model

The data acquired in the experimental portion of this thesis was utilized to create a new model in order to estimate UCS without conducting destructive testing. Like Horsrud's model, this model is based on estimating UCS from the compressional wave velocity values calculated from ultrasonic testing of the cement plugs. More information about ultrasonic testing can be found in section 3.3.2.1. Figure 5.4 exhibits the datapoints used to create the model. The y-axis depicts UCS while the x-axis is the compressional wave velocity. As the figure displays, the model can be expressed pretty accurately with the power law function as seen by R^2 value being 0.9496.

Equation 5.1

$$UCS = 0.2191 \cdot V_p^{3,9503}$$

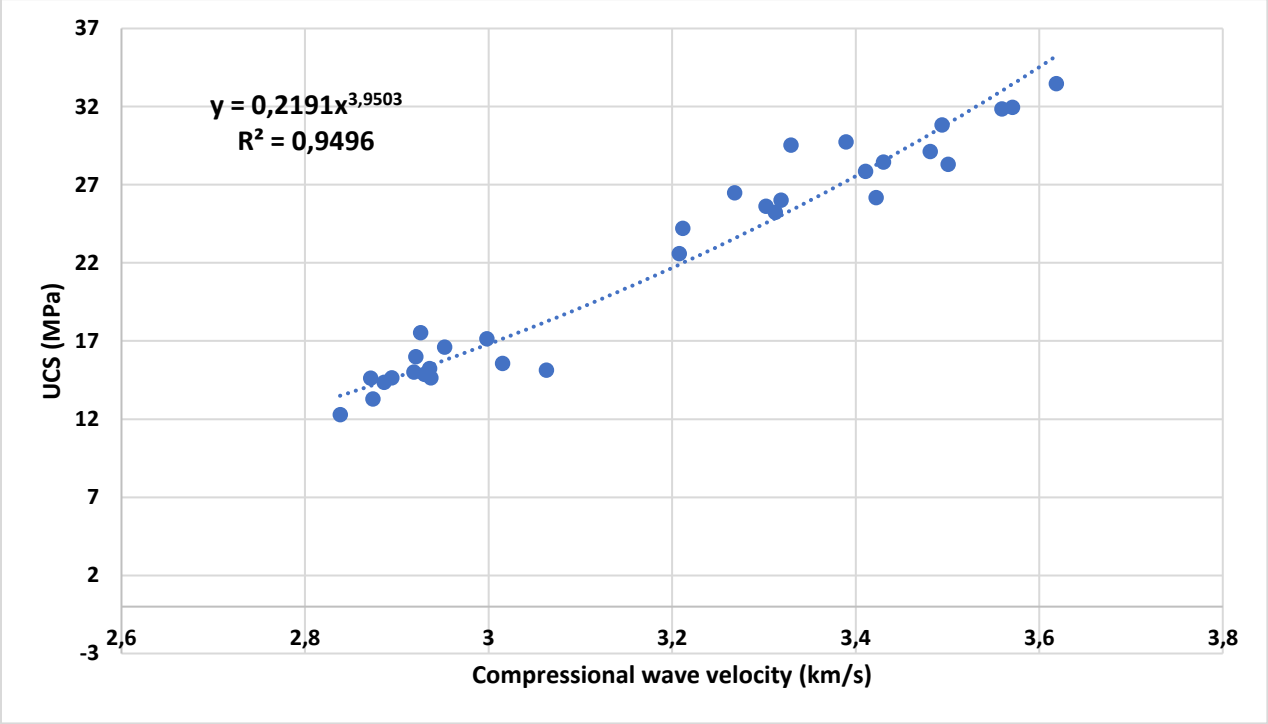

Figure 5.4 UCS vs Vp

In order to test the model from equation 5.1, data will be used from Senoor and Zakaria (2018) and Jiwar (2021). The new model and the Horsrud model will be used to estimate UCS and then plotted against the actual UCS.

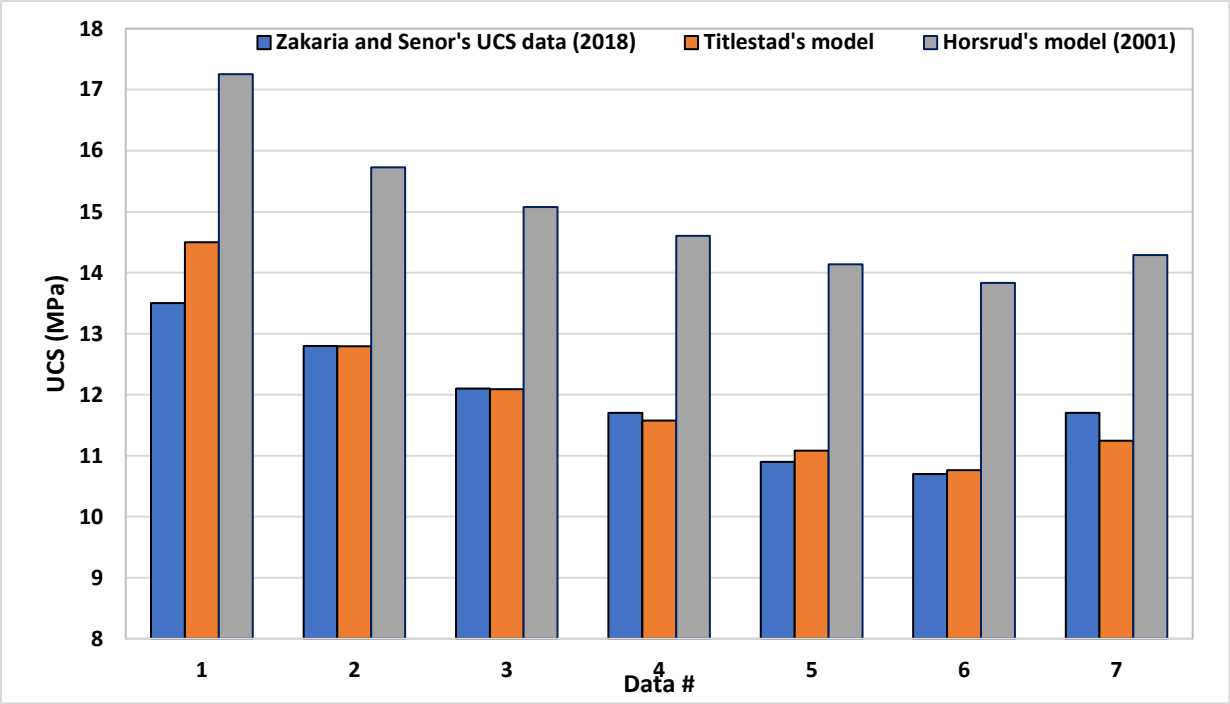

Figure 5.5 Actual UCS data from Senoor and Zakaria vs model predictions

Titlestad's model is more accurate than Horsrud's model and provides far close UCS estimates compared to the actual data, as seen in figure 5.5. Similar to figure 5.1, and 5.3, Horsrud's model tend to overestimate the UCS, which is the case again here. Figure 5.6 shows model predictions vs Jiwar actual UCS values. This time, it is observed that Horsrud's model overestimates slightly again, however the predictions are more accurate. The last data point, 4, the estimate from Horsrud is 0.33% shy of the actual UCS value.

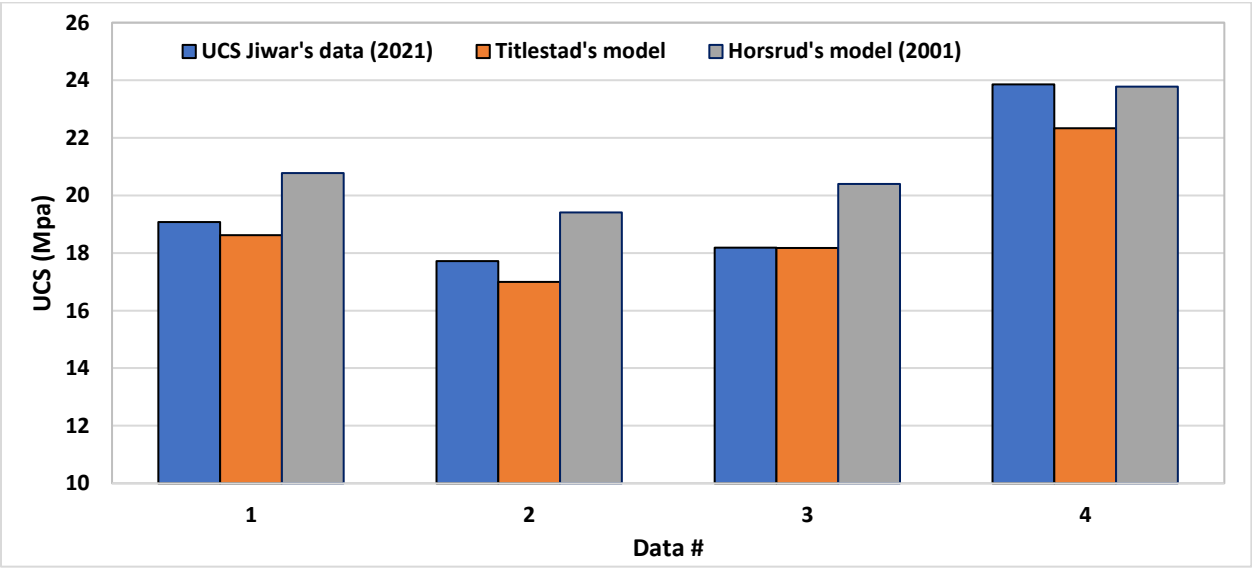

Figure 5.6 Jiwar's UCS data vs model predictions

To summarize, the new model developed based on UCS data from this thesis is more accurate than Horsrud's model. Overall, Titlestad's model matches pretty well with the actual UCS data. The reason why Horsrud's model overestimates is likely due to it being based on shale, and thus it might be best suited for sedimentary rocks.

6 Summary and conclusion

In this thesis, a total of five experimental designs were developed which investigates the impact of nanoparticles and fly ash on 0.44 WCR neat G-class cement. In this section, the experimental works are summarized based on the best UCS results obtained from the test matrices. The last column with the green shaded cells denotes UCS increase (positive) and the red shaded display UCS reductions (negative), as seen in table 6.1.

Best UCS result from each batch						
Test Matrix	**Curing time (days)**	**Additive**	**Best Concentration for UCS (g)**	**Reference neat G-class cement UCS (MPa)**	**Cement + Additive UCS (MPa)**	**UCS increase (%)**
TM 1	**3**	SiO_2	0.25	14,51	17,88	23,27
	7	SiO_2	1,00	19,27	24,46	26,95
	28	SiO_2	0.75	27,60	26,05	-5,61
TM 2	**3**	SiO_2 + Al_2O_3	0.55 + 0.75	14,51	15,30	5,45
	7	SiO_2 + Al_2O_3	0.55 + 0.75	19,27	22,06	14,48
	28	SiO_2 + Al_2O_3	0.55 + 1,0	27,60	34,95	26,64
TM 3	**3**	SiO_2 + Al_2O_3 + MWCNT	0.55 + 0.25+ 0.75	14,51	15,99	10.26
	7	SiO_2 + Al_2O_3 + MWCNT	0.55 + 0.25 + 1,0	19,27	19,32	0.28
	28	SiO_2 + Al_2O_3 + MWCNT	0.55 + 0.25 + 0.25	27,60	30.82	11,67
TM 4	**3**	FA	2,50	14,51	12,28	-15,33
	7	FA	5,00	19,27	20.80	7,96
	28	FA	2,50	27,60	33,46	21,24
TM 5	**3**	FA + SiO_2	2,5 + 0.55	14,51	13,21	-8,93
	7	FA + SiO_2	7,5 + 0.55	19,27	18,14	-5,85
	28	FA + SiO_2	2,5 + 0.55	27,60	29,81	8,02

Table 6.1 Best UCS results from every batch

From the investigations of the experimental works the following observations were made:

- The majority of test batches utilizing NPs or FA exhibited superior UCS values. Compressive strength improvements were generally highest after a curing period of 28 days, except for the nano-SiO_2 system, as shown in table 6.1 (TM 1).
- Resilience was improved frequently.
- E-modulus performance was unpredictable as there were not clear trends. Some UCS improvements caused significantly higher E-modulus, whereas some caused reduced or similar values compared to the reference cement.
- Nano-SiO_2 significantly improved early compressive strength, reaching peak UCS increase of 23,27% after 3 days and 26,95% after 7 days. This is possibly due to its accelerating effects of the C-S-H gel. As adverse results were exhibited for every dosage after 28 days, SiO_2 might be best utilized in cases where high early strength is required. The reason for the adverse UCS results after 28 days are undetermined, and due to lack of lab equipment and time it was difficult to investigate further. However, as discussed in section 4.2.1 it might be due to the WCR or chemical interaction with stabilization additive present in the aqueous solution.
- Even though NPs and FA consistently caused superior results compared to the reference values, there is a high degree of unpredictability when choosing the optimal dosages of nanoparticles and FA, as this seemingly varies heavily depending on curing age.
- The binary blend of SiO_2 and Al_2O_3, gave consistently great results for the different tested parameters. They also improved progressively as curing periods got longer, with a peak UCS of 34,95MPa after 28 days. This was an 26,64% increase over the control value. SiO_2 and Al_2O_3 performs great in tandem, which is indicating synergistic effects.
- A ternary blend of SiO_2, Al_2O_3 and MWCNT displayed satisfying results for the 3 day and 28 day batch, however to a lesser degree than the binary blend. On the contrary, the 7 day results were unsatisfactory. Furthermore, due to the amount of nanoparticles added, this test matrix is not economically viable.
- The binary and ternary blend seemingly gave more consistent UCS improvements between the various additive concentrations for each respective curing age, whereas the UCS trend for SiO_2 was more erratic, non-linear and unpredictable.

- FA as a standalone additive showed weak early strength (3 days of curing), but significantly improved after 28 days of curing, as seen in figure 4.16. Very favourable and interesting results, as the performance of FA is comparable to the results of nanoparticles after 28 days. This opens for interesting investigations into FA as an additive, as the material is cost effective and improved the performance of neat-G-class cement.
- The FA and SiO_2 blend exhibited reduced early compressive strength, compared to the reference neat G-class cement. However, the nano-SiO_2 and FA blend (TM 5) improved early strength compared to FA alone (TM 4), but it still had unsatisfactory UCS values compared to neat G-class cement. The combined effect of FA and SiO_2 provided mostly favourable results after 28 days. Of all the designed test matrices, the results from this matrix were overshadowed as they were probably the weakest out of any of the designed test matrices.
- Aside from the small early strength boost SiO_2 gave, FA seemingly performed better alone instead of in a blend with SiO_2. There is likely interference between these SiO_2 and FA.
- With respect to UCS, the preferred dosage of FA after 3 and 28 days is 2,5g. As it was found to be the best performing dosage in all instances of fly ash utilization after a curing age of 3 and 28 days, whether alone or in the blend with SiO_2.
- There is conflicting evidence for the correlation between a high M-modulus value and a high UCS value, seen throughout the results.
- The developed empirical UCS-Vp model predicted UCS relatively accurately.
- Nanoparticles improved shear stress and Casson PV, whereas FA reduced shear stress and Casson PV. All additives increased Casson yield stress compared to neat cement.
- Peak temperature development of the neat cement is higher than the slurries which included nanoparticles and FA additives by 1 - 4.5^{o}C. Moreover, the rate of temperature development of the neat cement is also slightly faster than the rest of the slurries.

The results presented in this thesis are valid for the considered test matrix compositions with the same testing and curing conditions, i.e., pressure or temperature when curing. Changing these parameters and/or the slurry compositions, one may get different results. However, based

on the considered systems, this thesis investigated and answered the research questions addressed in section 1.2. Furthermore, the results also indicated the huge potential of nanoparticles in improving the conventional neat cement properties. FA as an additive also showed promising results, which could be investigated further. The same observations are also reported in the literature review part.

7 Future work

During the experimental works of this thesis, new ideas for future work has spawned. This can either be in the form of improvements or new and interesting ideas to investigate.

Large sample size: A limitation of the experiments conducted in this thesis is clearly the sample size, as only two plugs were created per dosage of additive. Flawed and compromised specimens carry a larger impact when the sample size is small, causing more uncertainties in the results. In addition, more cement samples will reduce the impact of compromised specimens, and lead to smaller uncertainties as a result. It can give a more consistent perspective of the performance of the nanoparticles and FA. From the results of this thesis, it has been established that there is a certain degree unpredictability when choosing optimal dosages of the tested additives as they vary depending on curing age. A large sample size could help mitigate this issue, as outliers would have diminished effect and it could also be easier to spot trends.

SEM analysis: SEM imagery could be taken of the microstructure for the tested cement specimens with nanoparticle and FA additives after every curing age. This was planned for this thesis, however the SEM machine at the university was out of order. Characterization of the internal structure of the cement matrix, should be valuable information as it could help understanding the impact of the additives.

HPHT: The samples in this thesis was cured at atmospheric pressure and room temperature. It should be valuable to investigate what impact more realistic well conditions will have the cement samples with nanoparticles and FA. This would help to determine the viability of the additives in a more realistic environment.

Brazilian tensile strength testing: An investigation into what effects the tested additives would have on tensile strength could yield valuable information. Cement in a wellbore environment is subjected to stresses from every direction, which is why this also should be examined.

Further FA testing: Fly ash as a standalone additive proved to have comparable results to nanoparticles with extended curing periods, which is very interesting considering it is a biproduct and is a lot cheaper than nanoparticles. Investigations into how cement samples with fly ash would have been impacted if cured at either different pressures and temperature or submerged in water could give more information about the applicability of FA as an additive in demanding well environments.

Shrinkage testing: NORSOK D-010 requires plugging materials to be non-shrinking. Cement does shrink somewhat, however not massively. An investigation of what impact nanoparticles and FA has on shrinkage could yield valuable information, to determine the viability of these additives. Shrinkage can allow for fluid leaks in wellbores.

References

[1] NORSOK, "NORSOK D-010: Well intergrity in drilling and well operations, rev 4," Standards Norway, Lysaker, 2013.

[2] B. Vignes and B. S. Aadnøy, "Well-Integrity Issues Offshore Norway," *Presented at IADC/SPE Drilling Conference, Orlanda, Florida,* doi: 10.2118/112535-ms. 2008.

[3] S. Bachu and T. L. Watson, "Possible indicators for CO2 leakage along wells," *Presented at 8th International Conference on Greenhouse Gas Control Technologies,* p. 6, 2006.

[4] E. B. Nelsen and D. Guillot, Well Cementing, 2 ed., Sugar Land, Texas: Schlumberger, 2006.

[5] K. Feather, "Better Well Integrity," *US-Norway Technology Partnership Conference, Minimising Oil Spills and Discharge to Sea,* p. 14, 2011.

[6] D. Stokes, "Integrated milling, underreaming approach streamlines P&A operations in the North Sea," Offshore-mag.com, 2017. [Online]. Available: https://www.offshore-mag.com/drilling-completion/article/16756041/integrated-milling-underreaming-approach-streamlines-pa-operations-in-the-north-sea. [Accessed 08 01 2021].

[7] Pegasus Vertex, Inc, "Drilling Industry Glossary," Pegasus Vertex, Inc, [Online]. Available: http://www.pvisoftware.com/drilling-glossary/sustained-casing-pressure.html. [Accessed 08 03 21].

[8] BP, "Statistical Review of World Energy, 69th Edition," BP, 2020.

[9] L. Juniper and G. Schumacher, The Coal Handbook: Towards Cleaner Production: Volume 2: Coal utilisation, Philadelphia: Woodhead Publishing, 2013.

[10] A.-P. Bois, A. Garnier, F. Rodot and N. A. Jeremie Sain-Marc, "How To Prevent Loss of Zonal Isolation Through a Comprehensive Analysis of Microannulus Formation," *SPE Drilling and Completion,* vol. 26, no. 1, pp. 13 - 31 doi: https://doi.org/10.2118/124719-PA, 2011.

[11] Schlumberger, "Schlumberger Oilfield Glossary," Schlumberger, [Online]. Available: https://glossary.oilfield.slb.com/en/Terms/b/blaine_fineness.aspx. [Accessed 20 04 21].

[12] A. Bahadori, Essentials of Coating, Painting, and Lining for the Oil, Gas and Petrochemical Industries, 1 ed., Gulf Professional Publishing, 2015.

[13] K. D. Weerdt, "Geopolymers - State of the art," *COIN project report,* no. 37, p. 39, 2011.

[14] R. Bawa, S. B. Maebis, T. Flynn, C. Wei and S. Bawa, "Protecting new ideas and inventions in nanomedicine with patents," *Nanomedicine: Nanotechnology, Biology and Medicine,* vol. 1, no. 2, pp. 150-158 doi: https://doi.org/10.1016/j.nano.2005.03.009, 2005.

[15] R. Booker and E. Boyson, Nanoparticles for Dummies, Wiley Publising Inc, 2005.

[16] A. S. Ball, V. Gurtler and S. Soni, Nanotechnology, Oxford: Elsevier Science & Technology, 2019.

[17] A. Arora, "Ceramics in Nanotech Revolution," *Advanced Engineering Materials,* vol. 6, no. 4, p. 244–247. doi: 10.1002/adem.200300532 , 2004.

[18] M. T. Alsaba, M. F. Dushaishi and A. K. Abbas, "A comprehensive review of nanoparticles applications in the oil and gas industry," *Journal of Petroleum Exploration and Production Technology,* vol. 10, pp. 1389 - 1399 doi: https://doi.org/10.1007/s13202-019-00825-z, 2020.

[19] M. Khalil, B. M. Jan, C. W. Tong and M. A. Berawi, "Advanced nanomaterials in oil and gas industry: Degn, application and challenges," *Applied Energy,* vol. 191, p. 287–310. doi: 10.1016/j.apenergy.2017.01.074 , 2017.

[20] R. Patil and A. Deshpande, "Use of Nanomaterials in Cementing Applications," *Presented at SPE International Oilfield Nanotechnology Conference and Exhibition,* doi: 10.2118/155607-ms ,2012.

[21] H. Li, H.-g. Xiao and J.-p. Ou, "A study on mechanical and pressure-sensitive properties," *Cement and Concrete Research,* vol. 34, no. 3, pp. 428-435 ,doi: https://doi.org/10.1016/j.cemconres.2003.08.025, 2003.

[22] M. Jalal, E. Mansouri, M. Sharifipour and A. R. Pouladkhan, "Mechanical, rheological, durability and microstructural properties of high performance self-compacting concrete containing SiO2 micro and nanoparticles," *Materials & Design,* vol. 34, p. 389–400. doi: https://doi.org/10.1016/j.matdes.2011.08.037, 2011.

[23] J.-Y. Shih, T.-P. Chang and T.-C. Hsiao, "Effect of nanosilica on characterization of Portland cement composite," *Materials Science and Engineering,* vol. 424, no. 1-2, pp. 266- 274 DOI: 10.1016/j.msea.2006.03.010, 2006.

[24] F. T. Isfahani, E. Redaelli, F. Lollini, W. Li and L. Bertolini, "Effects of Nanosilica on Compressive Strength and Durability Properties of Concrete with Different Water to Binder Ratios," *Advances in Materials Science and Engineering,* vol. 2016, no. 2, pp. 1-16, doi: 10.1155/2016/8453567, 2016.

[25] A. Nazari and S. Riahi, "Improvement compressive strength of concrete in different curing media by Al2O3 nanoparticles," *Materials Science and Engineering,* vol. 528, no. 3, p. 1183–1191. doi: 10.1016/j.msea.2010.09.098 , 2011.

[26] Gilson Inc., "Globalgilson," Gilson, Inc, [Online]. Available: https://www.globalgilson.com/blog/what-is-workability-of-concrete. [Accessed 17 05 21].

[27] C. Vipulanandan, A. Mohammed and A. Ganpatye, "Smart Cement Performance Enhancement with NanoAl2O3 for Real Time Monitoring Applications Using Vipulanandan Models," *Presented at the Offshore Technology Conference, Houston, Texas,* doi: https://doi.org/10.4043/28880-MS , 2018.

[28] S. Muzenski, I. Flores-Vivian and K. Sobolev, "Ultra-high strength cement-based composites designed with aluminum oxide nano-fibers," *Construction and Building Materials,* vol. 220, pp. 177- 186, doi: https://doi.org/10.1016/j.conbuildmat.2019.05.175, 2019.

[29] W. Khan, M. Rahman, M. Mahmoud and P. Sarmah, "MWCNT for Enhancing Mechanical Properties of Oil Well Cement for HPHT Applications," *Presented at SPE/IADC Middle East Drilling Technology Conferance and Exhibition, Abu Dhabi, UAE,* doi: https://doi.org/10.2118/178175-MS, 2016.

[30] S. Lu, X. Wang, Z. Meng, Q. Deng, F. Peng, C. Yu, X. Hu, Y. Zhao, Y. Ke and F. Qi, "The mechanical properties, microstructures and mechanism of carbon nanotube-reinforced oil well cement-based nanocomposites," *RSC Advances,* vol. 9, no. 46, pp. 26691 - 26702, doi: https://doi.org/10.1039/C9RA04723A, 2019.

[31] A. Naqi, N. Abbas, N. Zahra and A. Hussain, "Effect of multi-walled carbon nanotubes (MWCNTs) on the strength development of cementitious materials," *Journal of Materials Research and Technology,* vol. 8, no. 1, pp. 1203 - 1211, doi: https://doi.org/10.1016/j.jmrt.2018.09.006, 2018.

[32] S. K. Bremseth, "Fly ash in concrete: A literature study of the advantages and disadvantages," *SINTEF Building and Infrastructure,* vol. COIN project report, no. 18, p. 37, 2010.

[33] Federal Highway Administration, "https://www.fhwa.dot.gov/pavement," 27 06 2017. [Online]. Available: https://www.fhwa.dot.gov/pavement/recycling/fach03.cfm. [Accessed 06 04 2021].

[34] G. Kaplan, S. A. Yildizel, S. Memis and A. U. Ozturk, "The Optimization of Calcareous Fly Ash-Added Cement Containing Grinding Aids and Strength-Improving Additives," *Advances in Civil Engineering,* vol. 2018, pp. 1-9, doi: https://doi.org/10.1155/2018/8917059, 2018.

[35] A. Jankovic, W. Valery and E. Davis, "Cement grinding optimisation.," *Minerals Engineering,* vol. 17, no. 12-12, p. 1075–1081. doi:10.1016/j.mineng.2004.06.031, 2004.

[36] Statista, "Statista," [Online]. Available: https://www.statista.com/statistics/219343/cement-production-worldwide/. [Accessed 01 05 21].

[37] Sigma Aldrich, "sigmaaldrich.com," Sigma Aldrich, [Online]. Available: https://www.sigmaaldrich.com/catalog/product/aldrich/420778?lang=en&region=NO. [Accessed 18 04 21].

[38] US Research Nanomaterials, Inc, "us-nano.com," US Research Nanomaterials, Inc, [Online]. Available: https://www.us-nano.com/inc/sdetail/623. [Accessed 18 04 21].

[39] US Research Nanomaterials, Inc, "us-nano," US Research Nanomaterials, Inc, [Online]. Available: https://www.us-nano.com/inc/sdetail/228. [Accessed 18 04 21].

[40] E. Fjær, R. Holt, A. Raaen and P. Horsrud, Petroleum Related Rock Mechanics, 2 ed., Elsevier Science, 2008.

[41] A. P. Boresi and R. J. Schmidt, Advanced Mechanics of Materials, 6 ed., Wiley, 2002.

[42] University of Washington, "depts.washington.edu," [Online]. Available: https://depts.washington.edu/matseed/mse_resources/Webpage/Biomaterials/young's_modulus.htm. [Accessed 20 04 21].

[43] F. C. Campbell, Elements of Metallurgy and Engineering Alloys, ASM International, 2008.

[44] G. Mavko, T. Mukerji and J. Dvorkin, The Rock Physics Handbook; Tools for Seismic Analysis of Porous Media, Cambridge University Press, 2010.

[45] J. M. Duncan and A. Bursey, "Soil Modulus Correlations," *Foundation Engineering in the Face of Uncertainty,* p. doi: 10.1061/9780784412763.026, 2013.

[46] Schlumberger, "Schlumberger Oilfield Glossary," Schlumberger, [Online]. Available: https://glossary.oilfield.slb.com/en/terms/y/yield_stress. [Accessed 21 04 05].

[47] Portland Cement Association, "Portland Cement, Concrete and Heat of Hydration," *Concrete Technology Today,* p. 8, 1997.

[48] Schlumberger, "Schlumberger Oilfield Glossary," Schlumberger, [Online]. Available: https://glossary.oilfield.slb.com/en/Terms/u/unconfined_compressive_strength.aspx. [Accessed 02 06 21].

[49] P. Horsrud, "Estimating Mechanical Properties of Shale From Empirical Correlations," *SPE Drilling & Completion,* vol. 16, no. 02, pp. 68–73. doi:10.2118/56017-pa , 2001.

Appendix A – Bar diagrams for the results

This appendix will present bar diagrams for each tested parameter as these were cut from the thesis to reduce the number of pages. For all the subsequent bar diagrams, the red coloured column always represents the value of the specimen without any additives, otherwise known as the reference sample. The black line that goes across horizontally in the bar diagrams, is placed at the reference point and is present to make comparisons between samples more seamless. Furthermore, the values within each individual column are the actual results of the specimens.

Test Batch 1 (3 days)

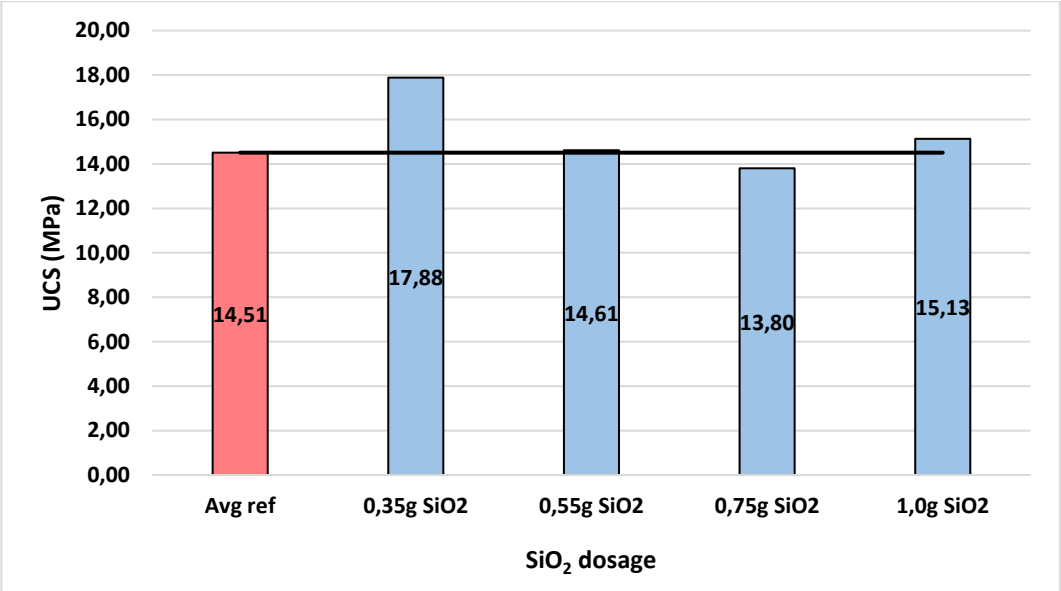

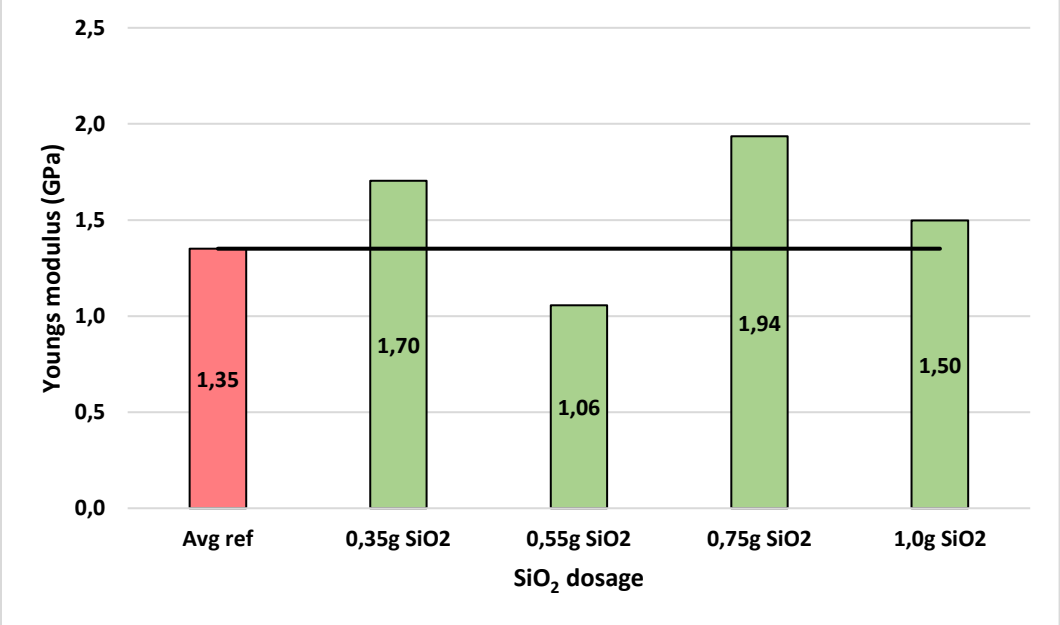

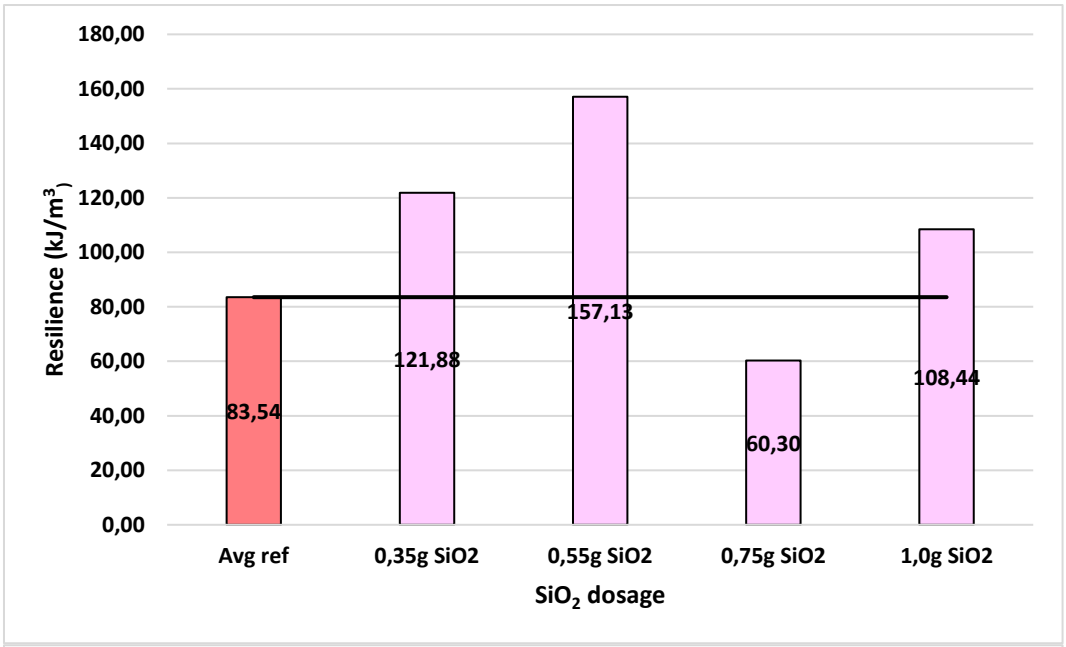

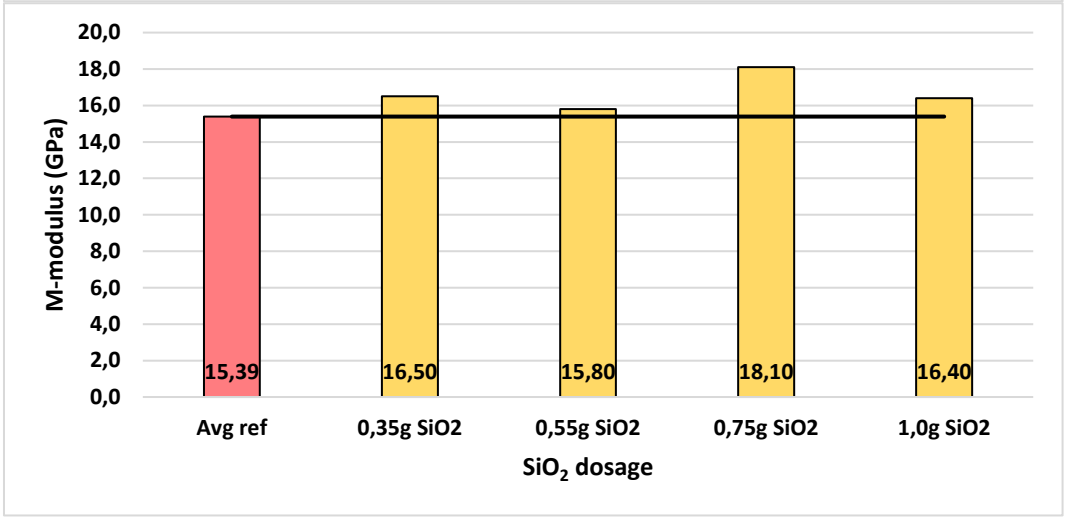

Test Batch 2 (7 days)

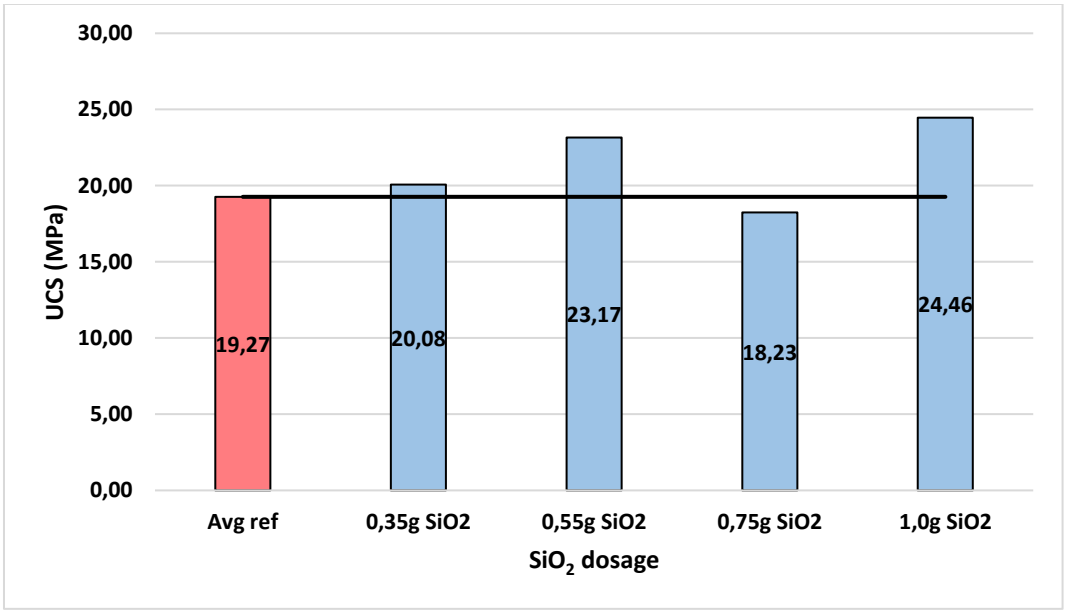

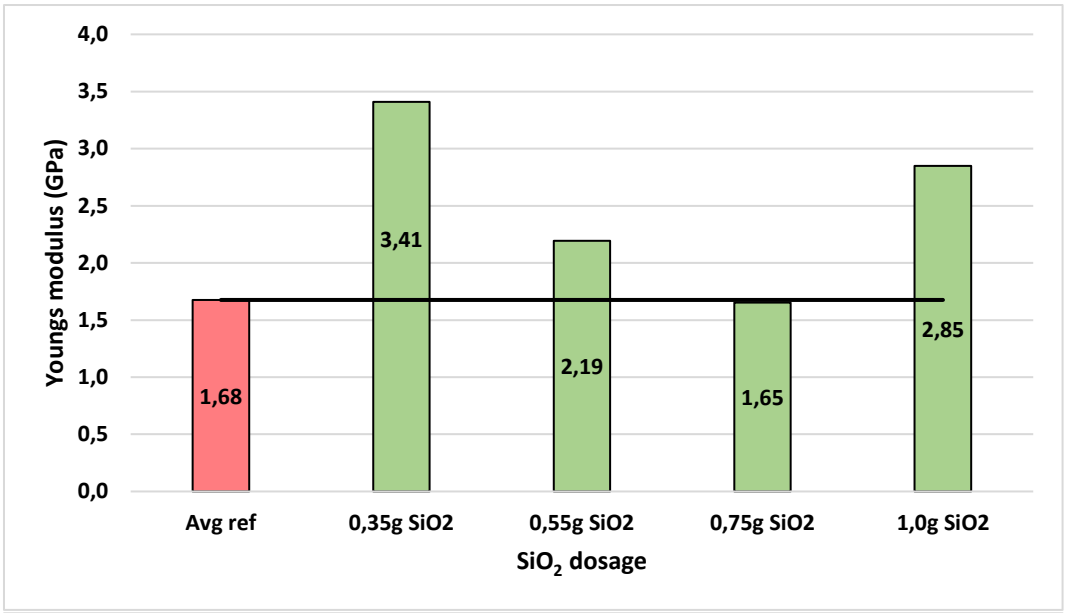
Youngs modulus (GPa)
4,0
3,5
3,0
2,5
2,0
1,5
1,0
0,5
0,0
1,68
3,41
2,19
1,65
2,85
Avg ref
0,35g SiO2
0,55g SiO2
0,75g SiO2
1,0g SiO2
SiO2 dosage

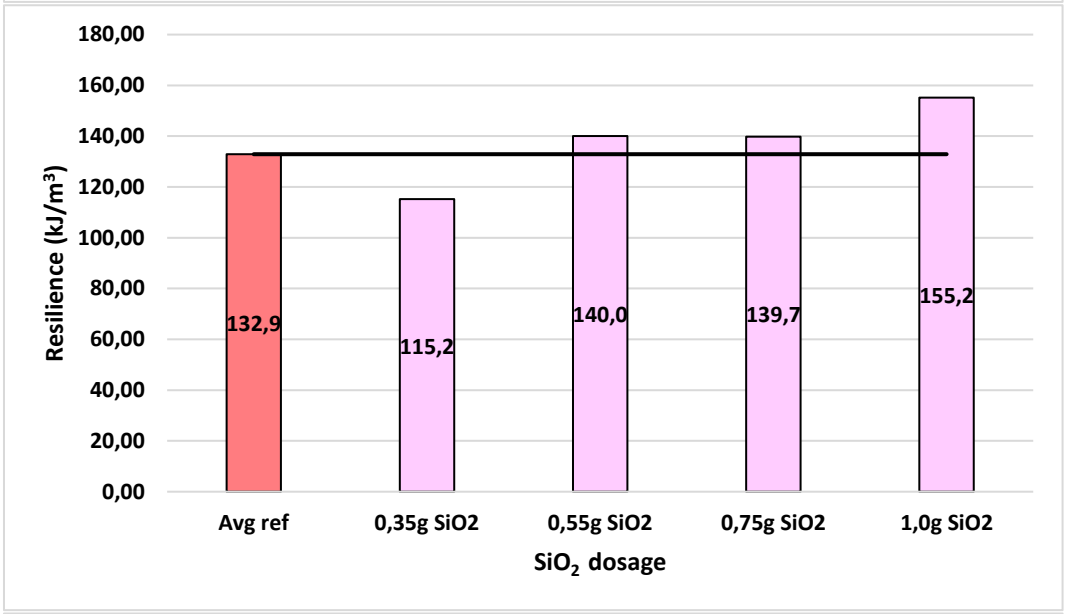
Resilience (kJ/m³)
180,00
160,00
140,00
120,00
100,00
80,00
60,00
40,00
20,00
0,00
132,9
115,2
140,0
139,7
155,2
Avg ref
0,35g SiO2
0,55g SiO2
0,75g SiO2
1,0g SiO2
SiO2 dosage

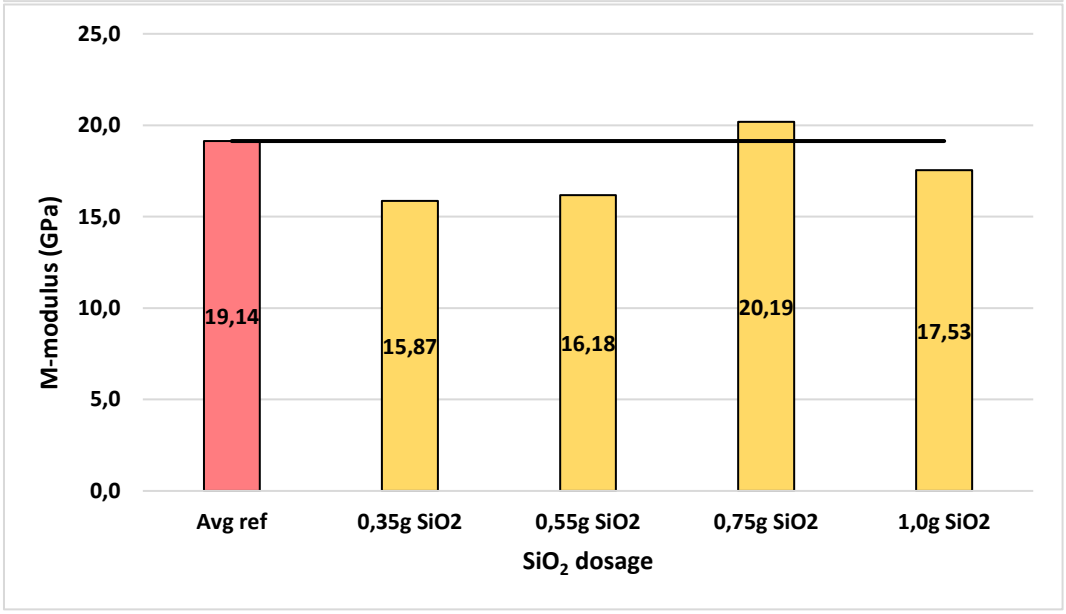
M-modulus (GPa)
25,0
20,0
15,0
10,0
5,0
0,0
19,14
15,87
16,18
20,19
17,53
Avg ref
0,35g SiO2
0,55g SiO2
0,75g SiO2
1,0g SiO2
SiO2 dosage

Test batch 3 (28 day)

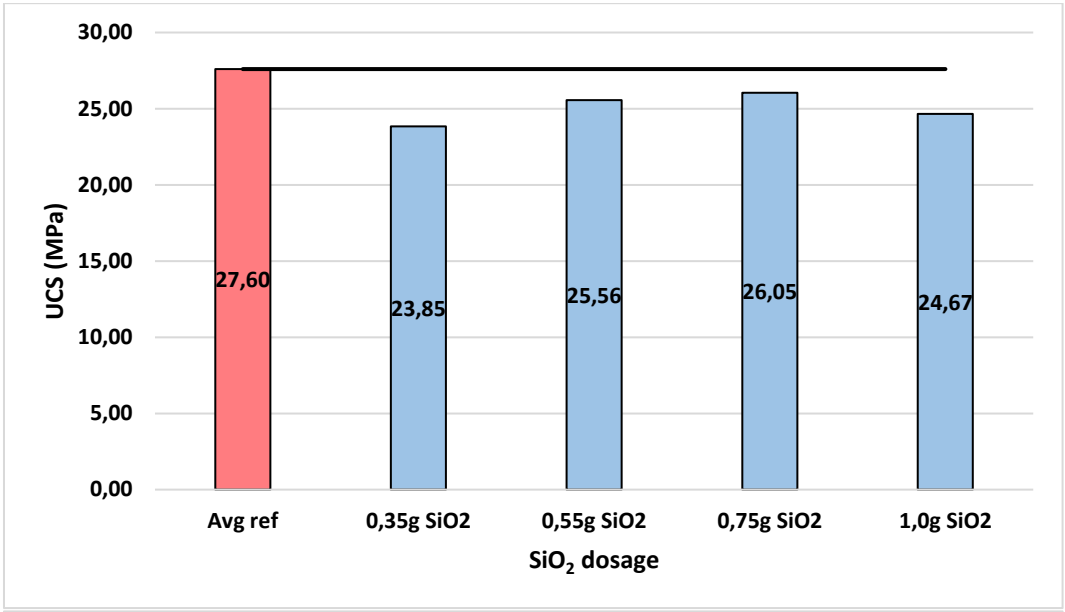

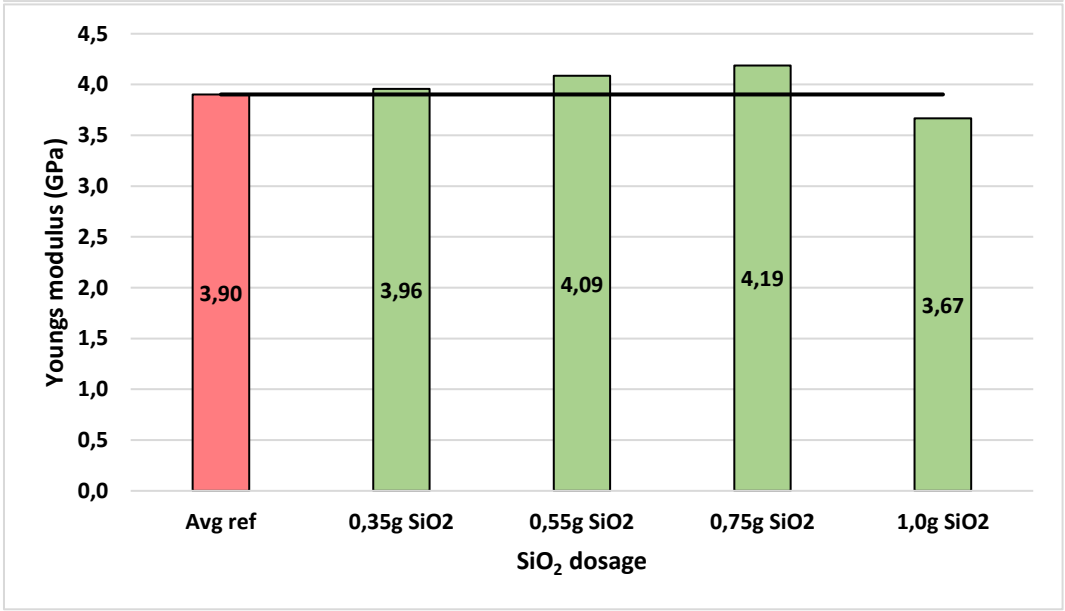

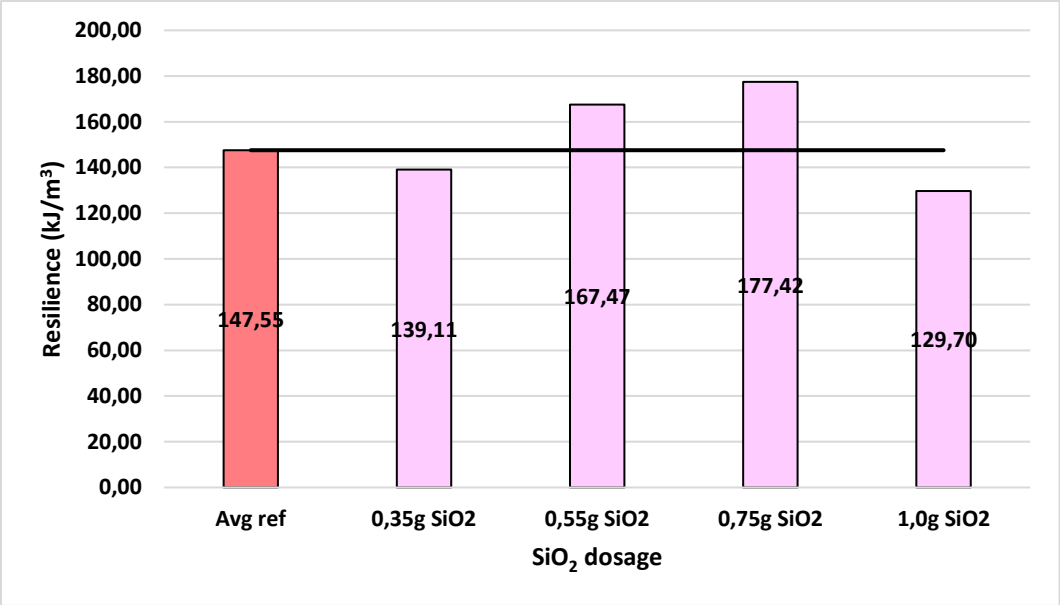

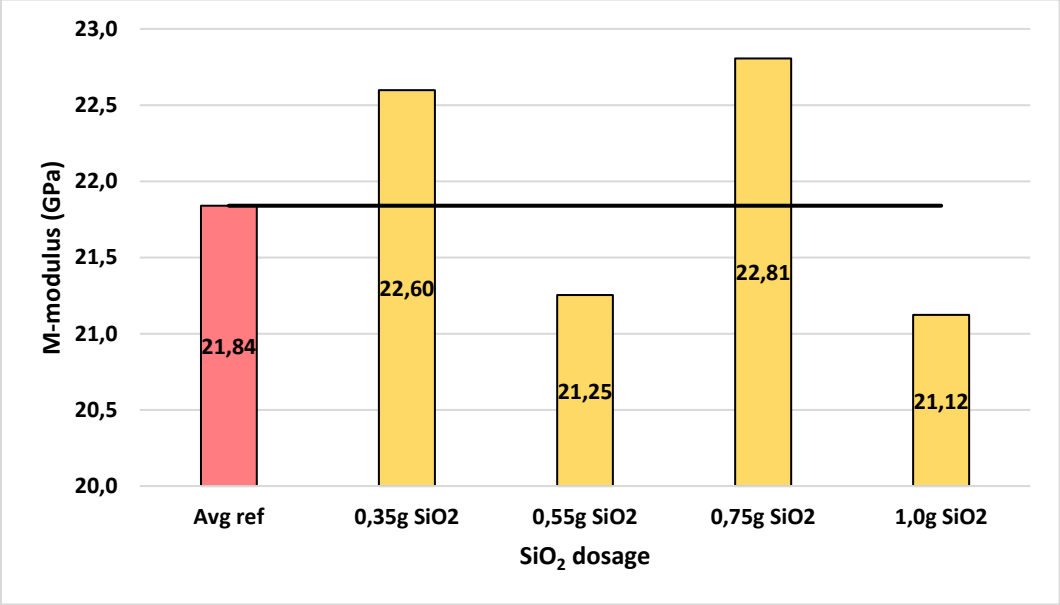

Test Batch 4 (3 day binary)

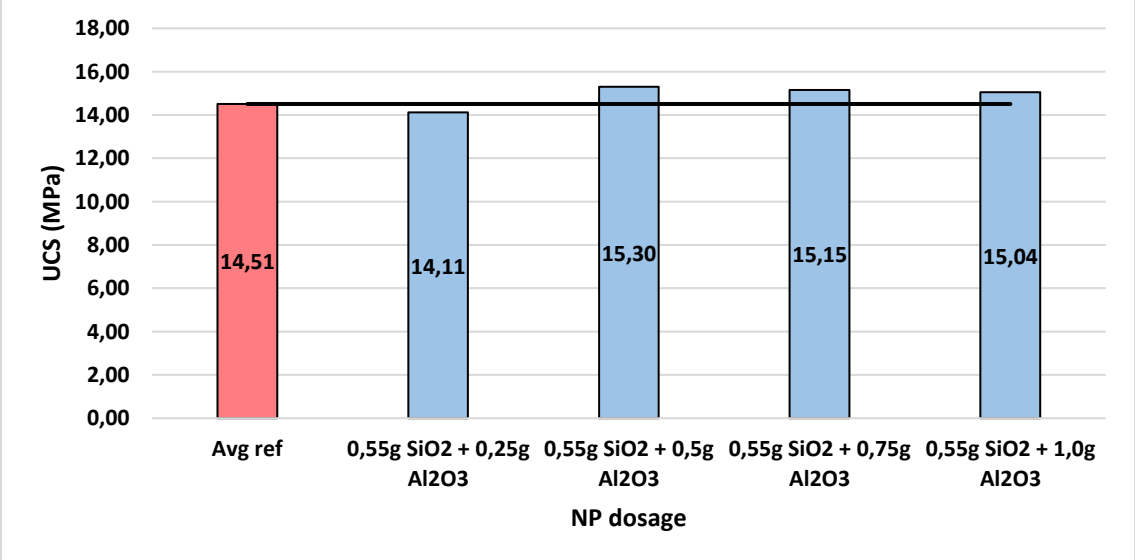

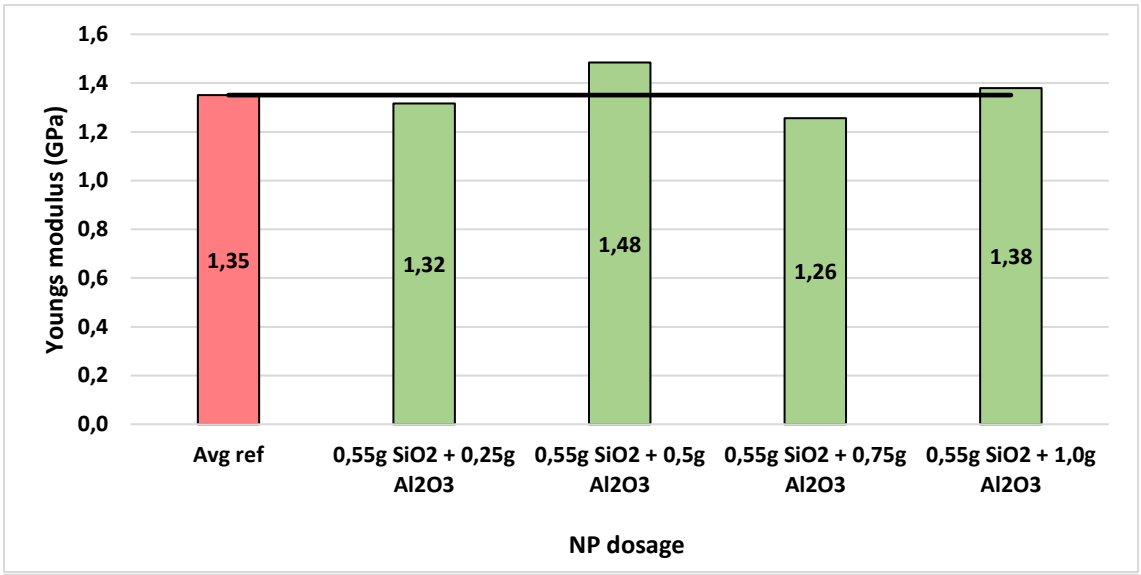
Youngs modulus (GPa)
1,6
1,4
1,2
1,0
0,8
0,6
0,4
0,2
0,0
1,35
1,32
1,48
1,26
1,38
Avg ref
0,55g SiO2 + 0,25g Al2O3
0,55g SiO2 + 0,5g Al2O3
0,55g SiO2 + 0,75g Al2O3
0,55g SiO2 + 1,0g Al2O3
NP dosage

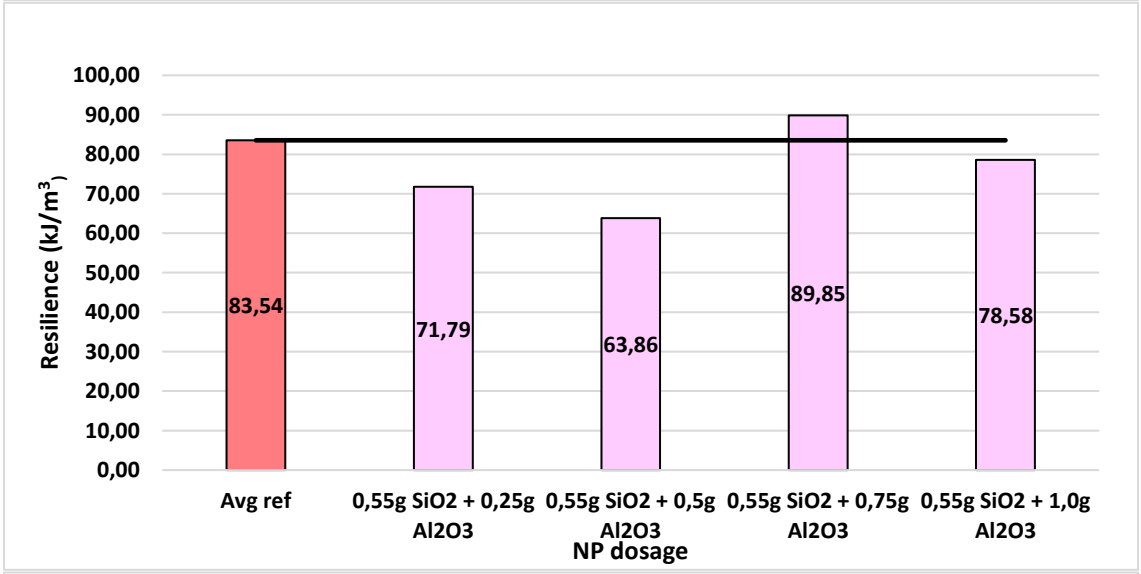
Resilience (kJ/m3)
100,00
90,00
80,00
70,00
60,00
50,00
40,00
30,00
20,00
10,00
0,00
83,54
71,79
63,86
89,85
78,58
Avg ref
0,55g SiO2 + 0,25g Al2O3
0,55g SiO2 + 0,5g Al2O3
0,55g SiO2 + 0,75g Al2O3
0,55g SiO2 + 1,0g Al2O3
NP dosage

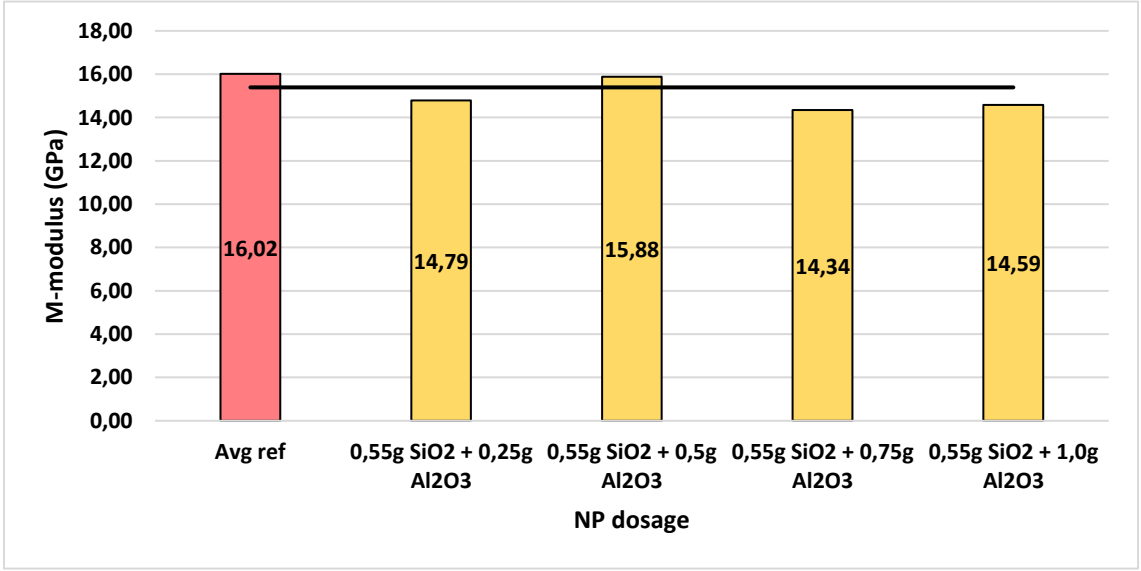
M-modulus (GPa)
18,00
16,00
14,00
12,00
10,00
8,00
6,00
4,00
2,00
0,00
16,02
14,79
15,88
14,34
14,59
Avg ref
0,55g SiO2 + 0,25g Al2O3
0,55g SiO2 + 0,5g Al2O3
0,55g SiO2 + 0,75g Al2O3
0,55g SiO2 + 1,0g Al2O3
NP dosage

Test Batch 5 (7 day binary)

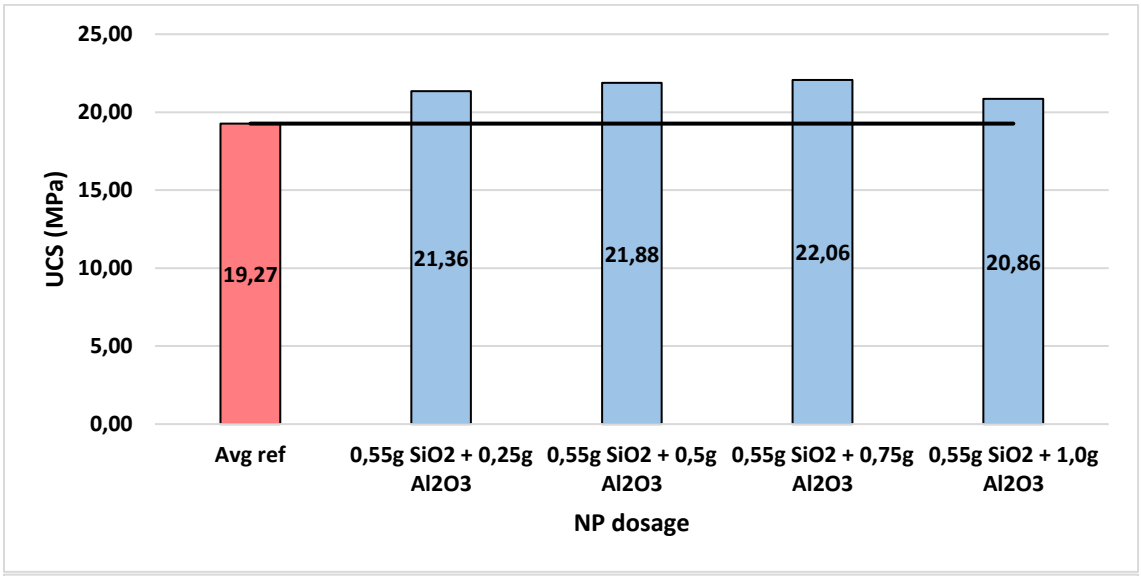

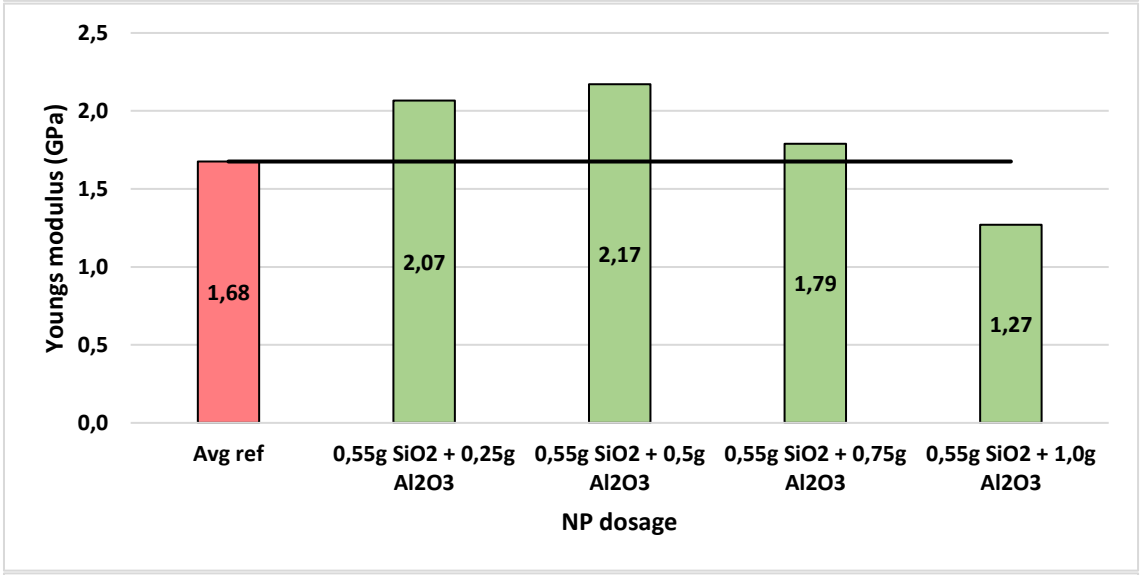

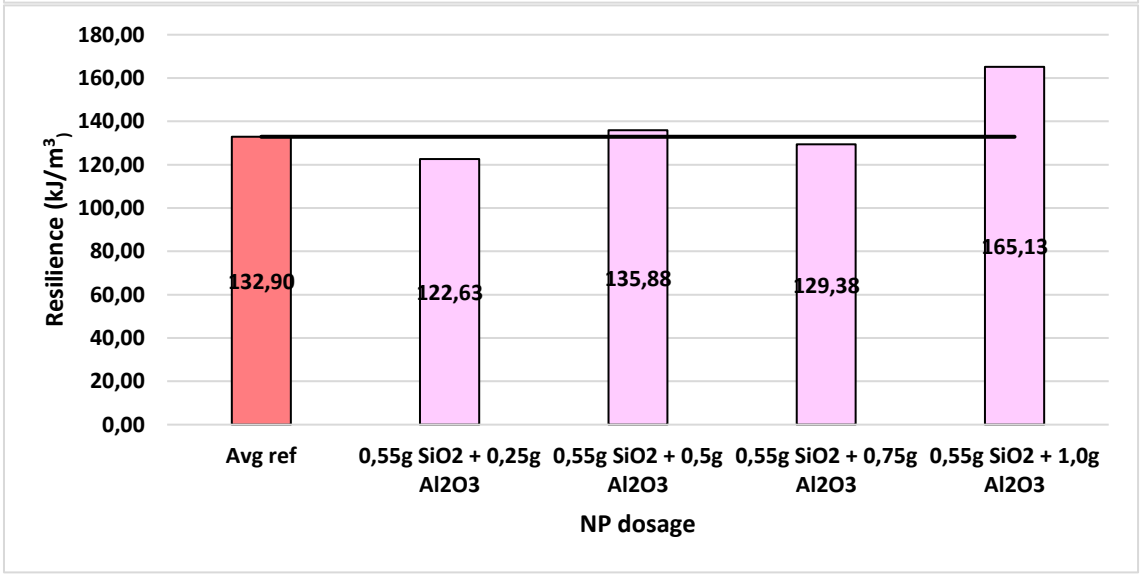

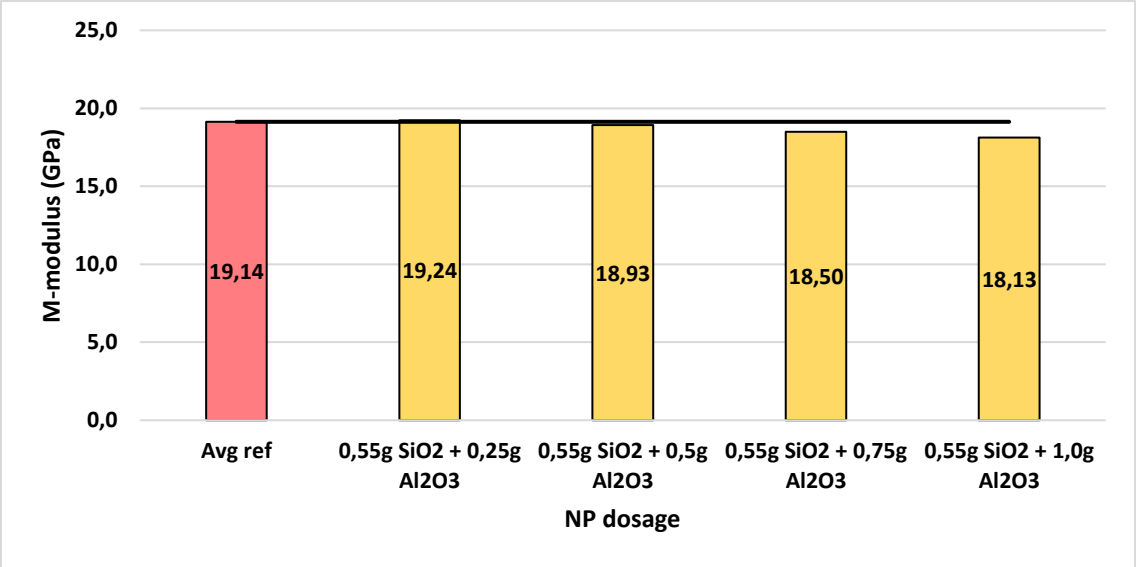

Test Batch 6 (28 day binary)

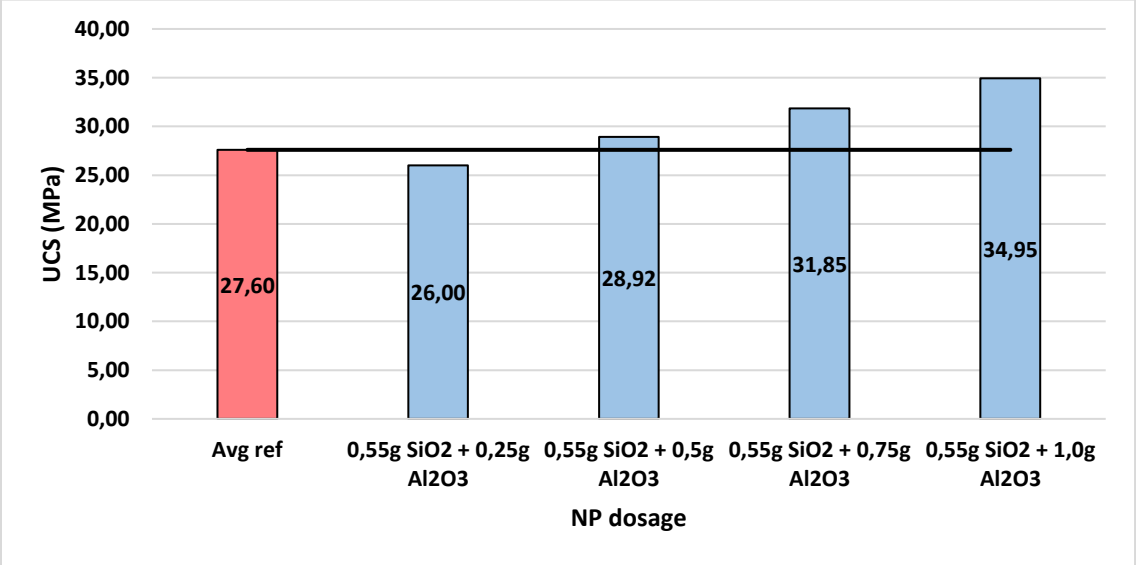

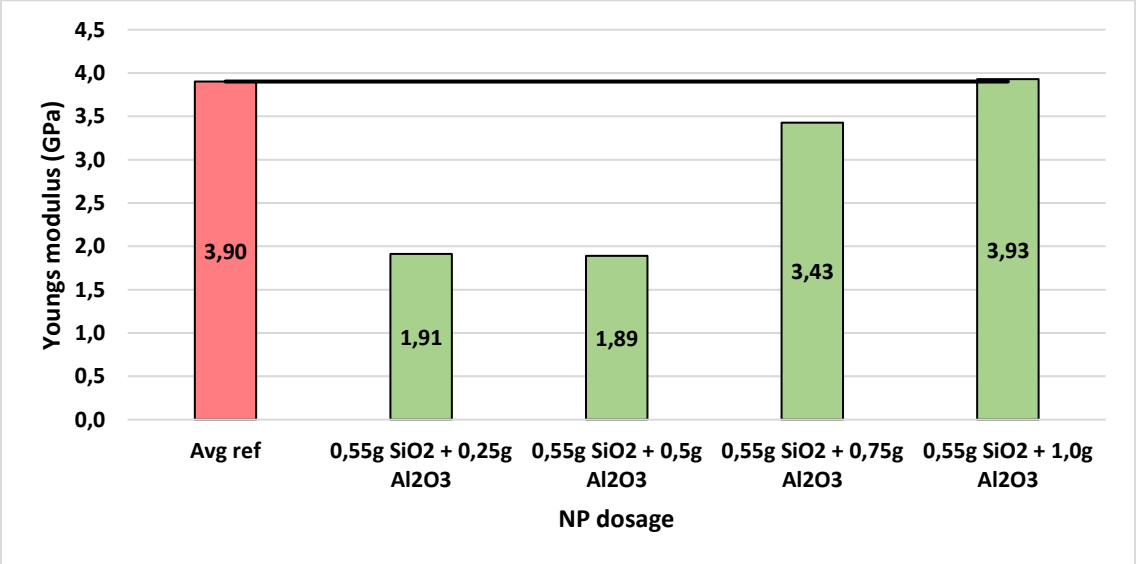

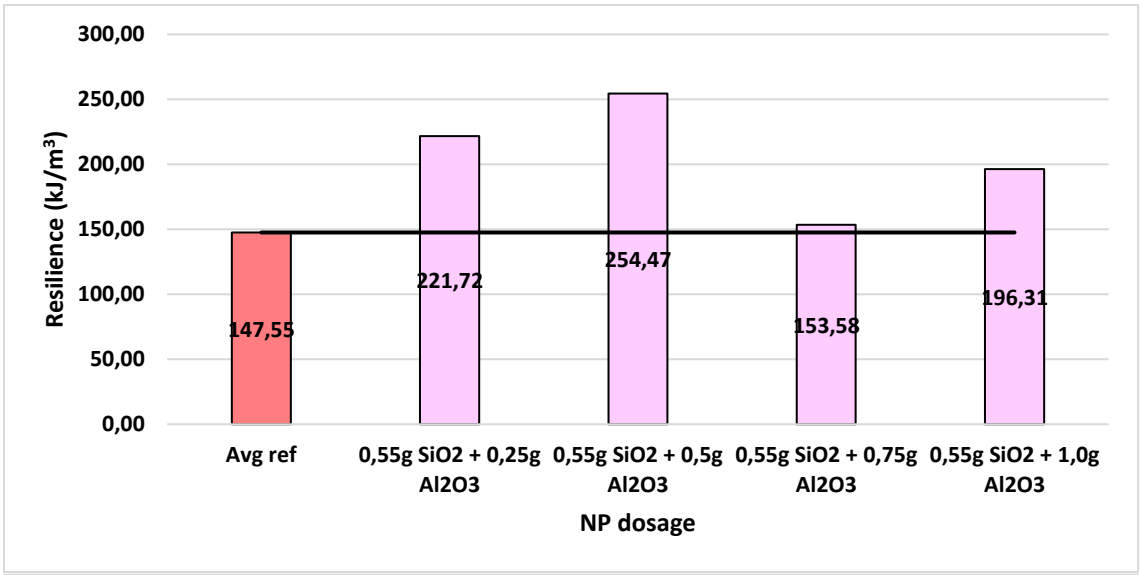

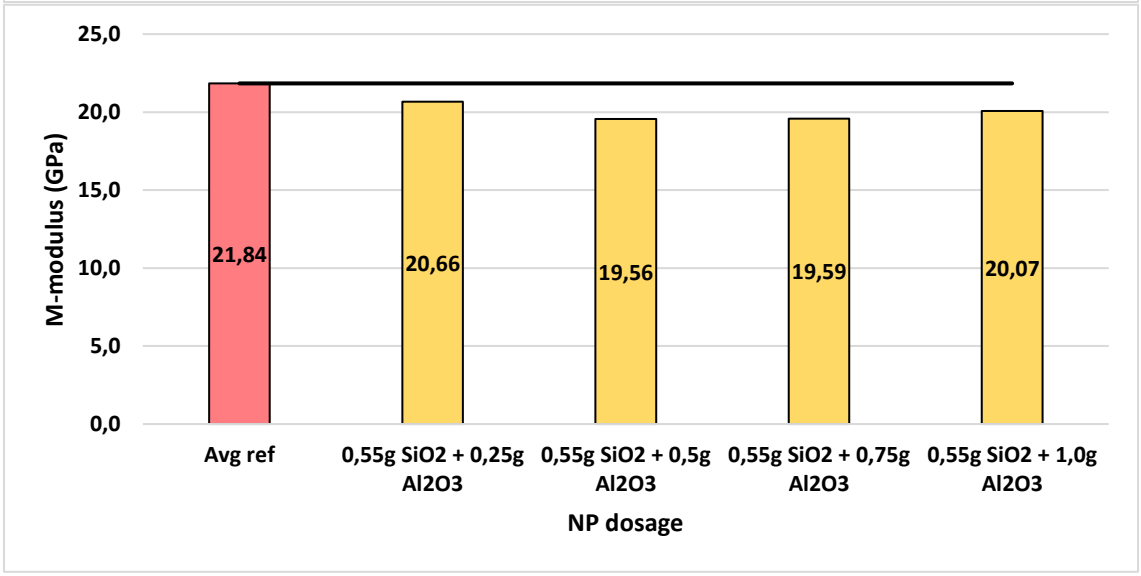

Test batch 7 (3 day ternary)

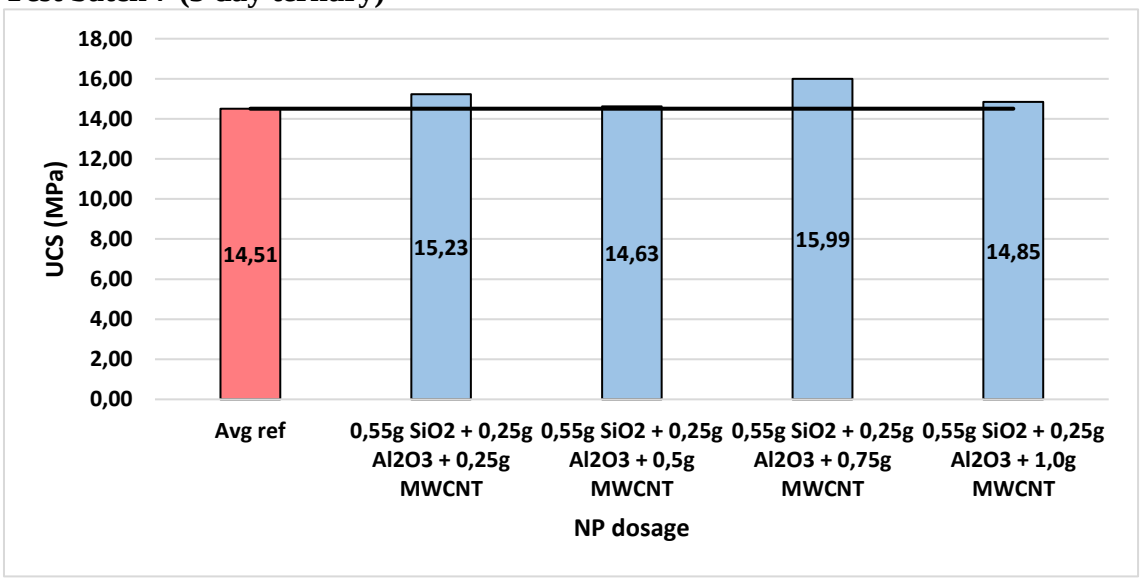

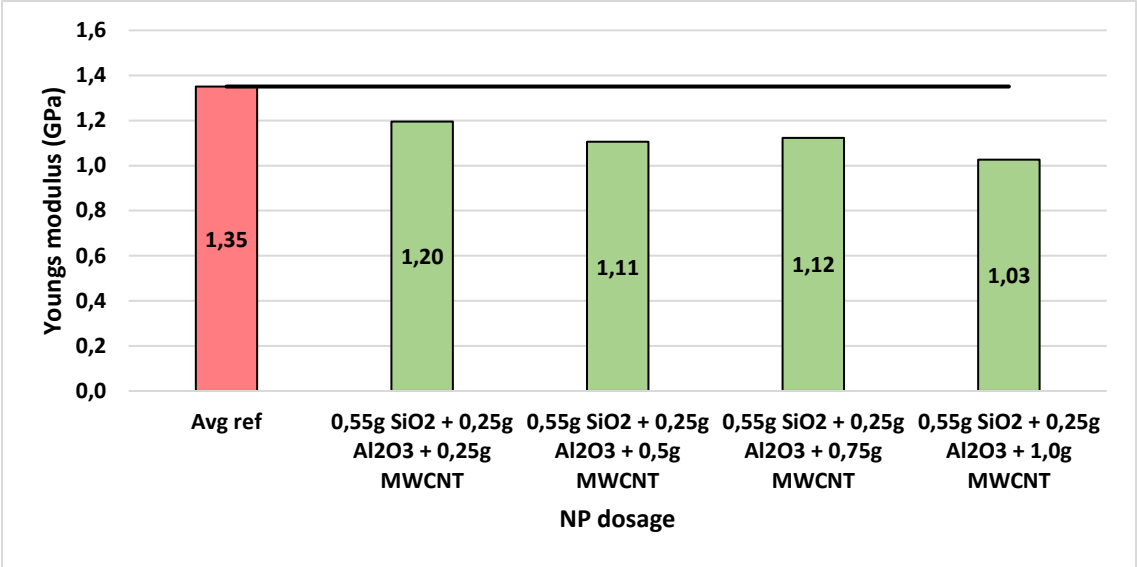
Youngs modulus (GPa)
1,6
1,4
1,2
1,0
0,8
0,6
0,4
0,2
0,0
1,35
1,20
1,11
1,12
1,03
Avg ref
0,55g SiO2 + 0,25g Al2O3 + 0,25g MWCNT
0,55g SiO2 + 0,25g Al2O3 + 0,5g MWCNT
0,55g SiO2 + 0,25g Al2O3 + 0,75g MWCNT
0,55g SiO2 + 0,25g Al2O3 + 1,0g MWCNT
NP dosage

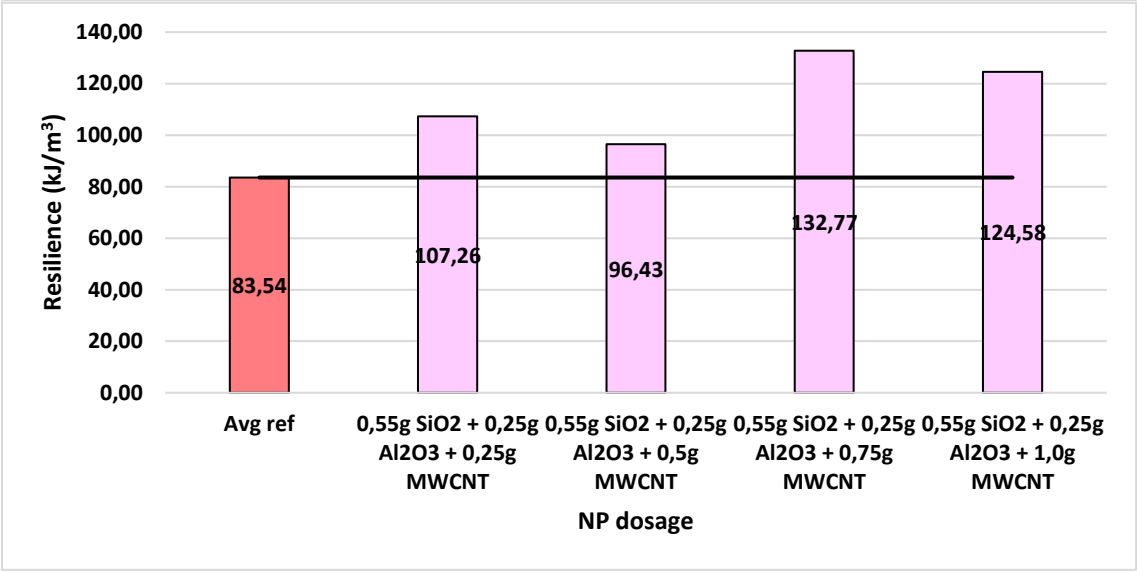
Resilience (kJ/m³)
140,00
120,00
100,00
80,00
60,00
40,00
20,00
0,00
83,54
107,26
96,43
132,77
124,58
Avg ref
0,55g SiO2 + 0,25g Al2O3 + 0,25g MWCNT
0,55g SiO2 + 0,25g Al2O3 + 0,5g MWCNT
0,55g SiO2 + 0,25g Al2O3 + 0,75g MWCNT
0,55g SiO2 + 0,25g Al2O3 + 1,0g MWCNT
NP dosage

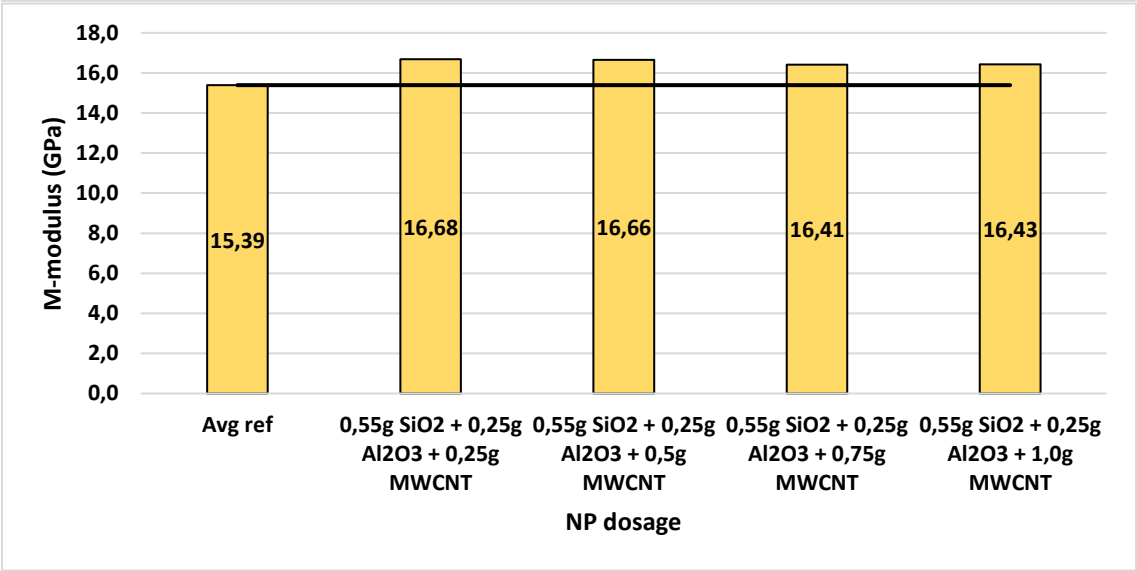
M-modulus (GPa)
18,0
16,0
14,0
12,0
10,0
8,0
6,0
4,0
2,0
0,0
15,39
16,68
16,66
16,41
16,43
Avg ref
0,55g SiO2 + 0,25g Al2O3 + 0,25g MWCNT
0,55g SiO2 + 0,25g Al2O3 + 0,5g MWCNT
0,55g SiO2 + 0,25g Al2O3 + 0,75g MWCNT
0,55g SiO2 + 0,25g Al2O3 + 1,0g MWCNT
NP dosage

Test batch 8 (7 day ternary)

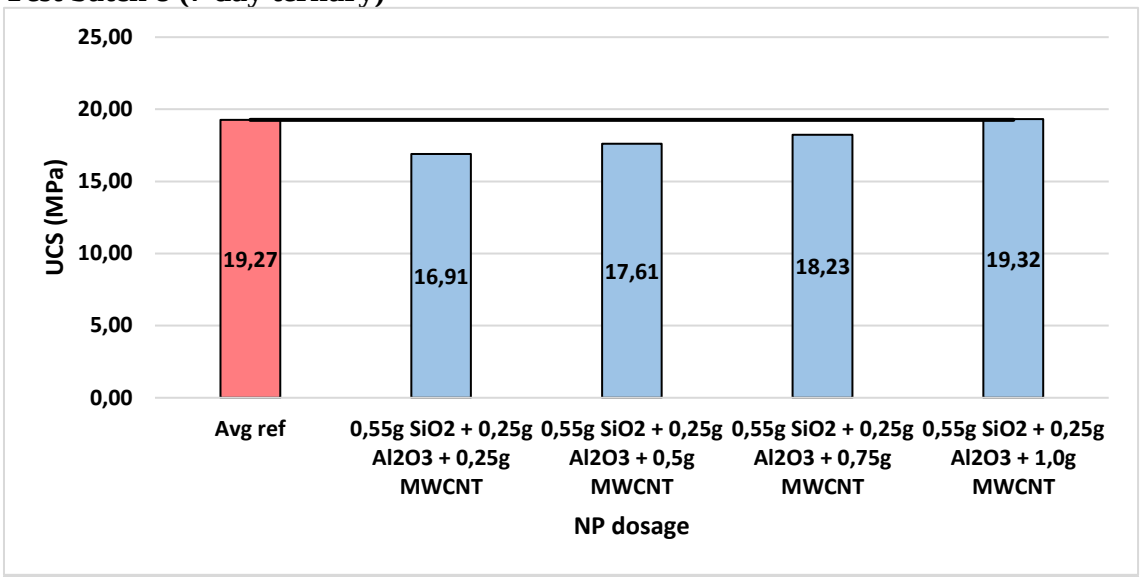

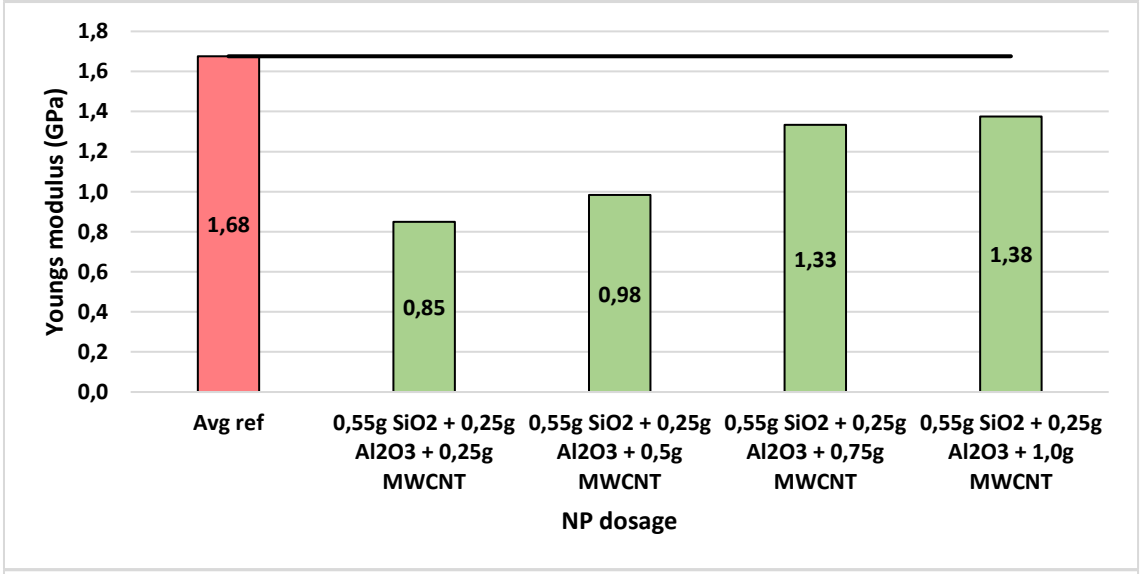

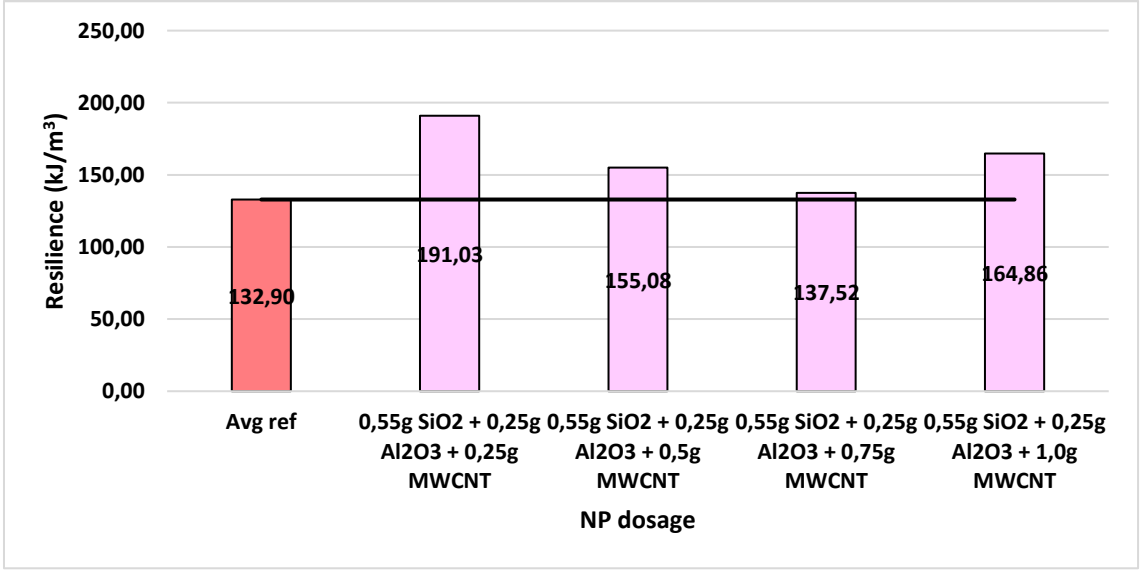

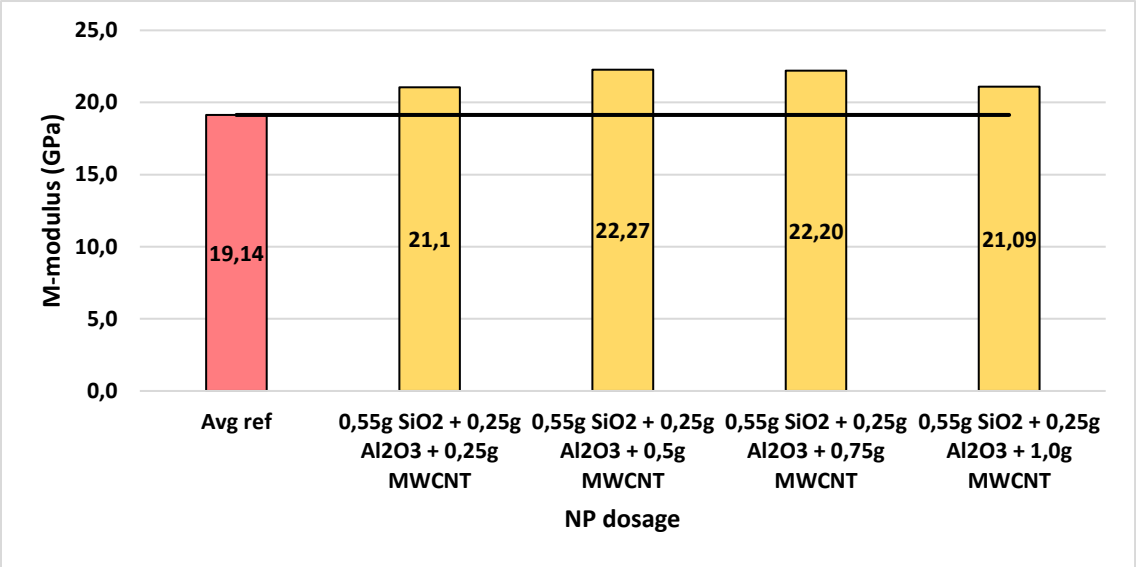

Test batch 9 (28 day ternary)

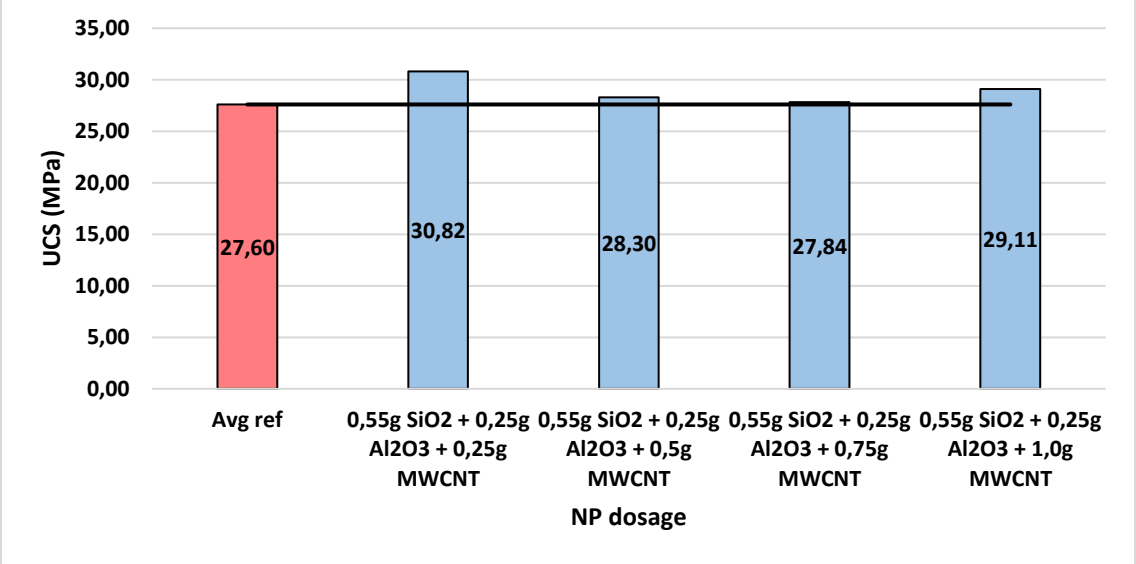

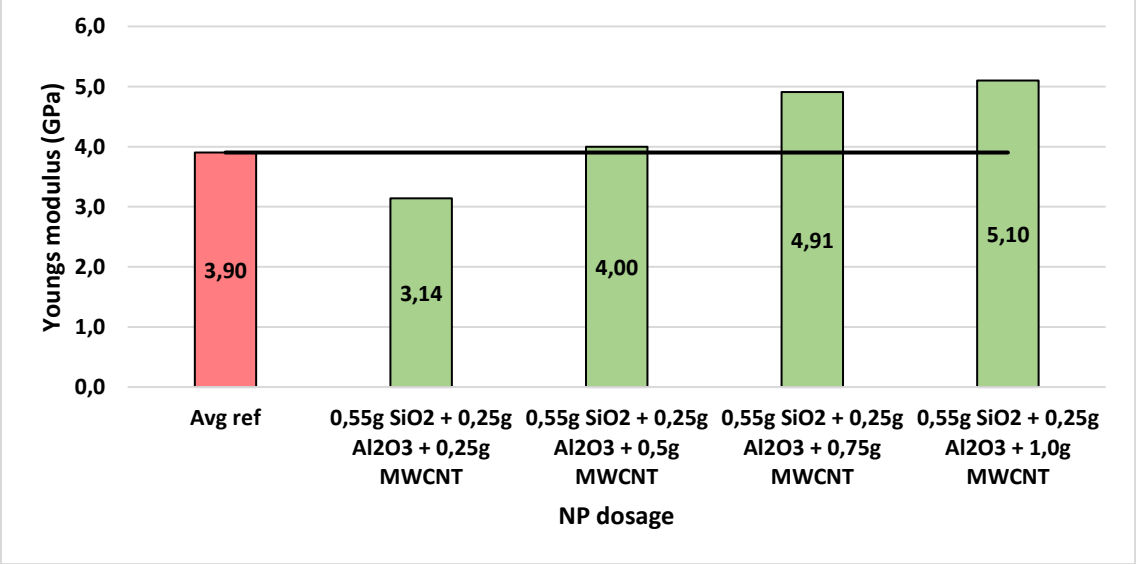

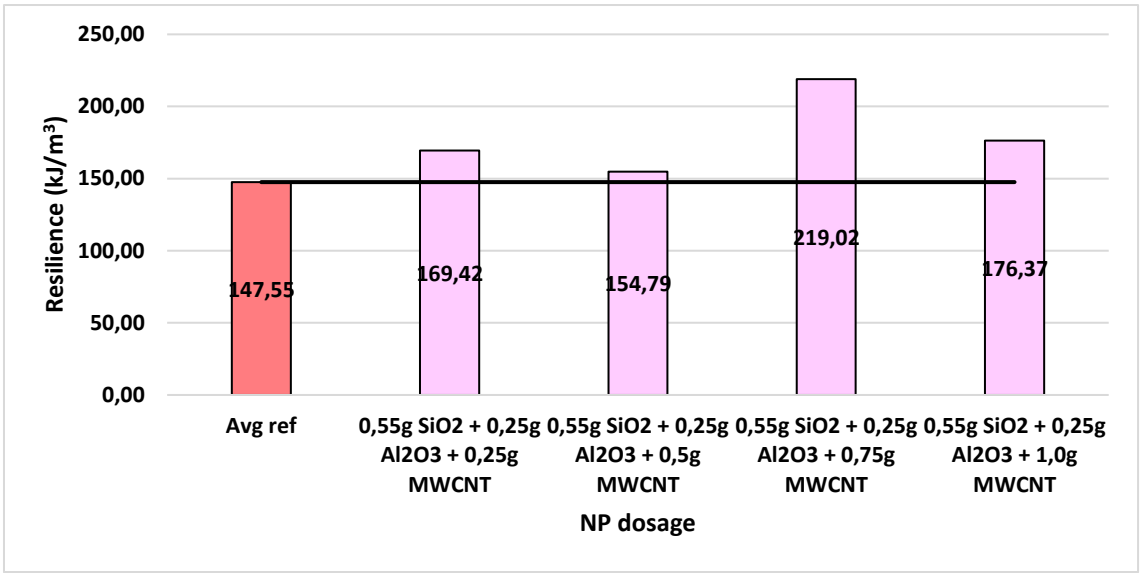

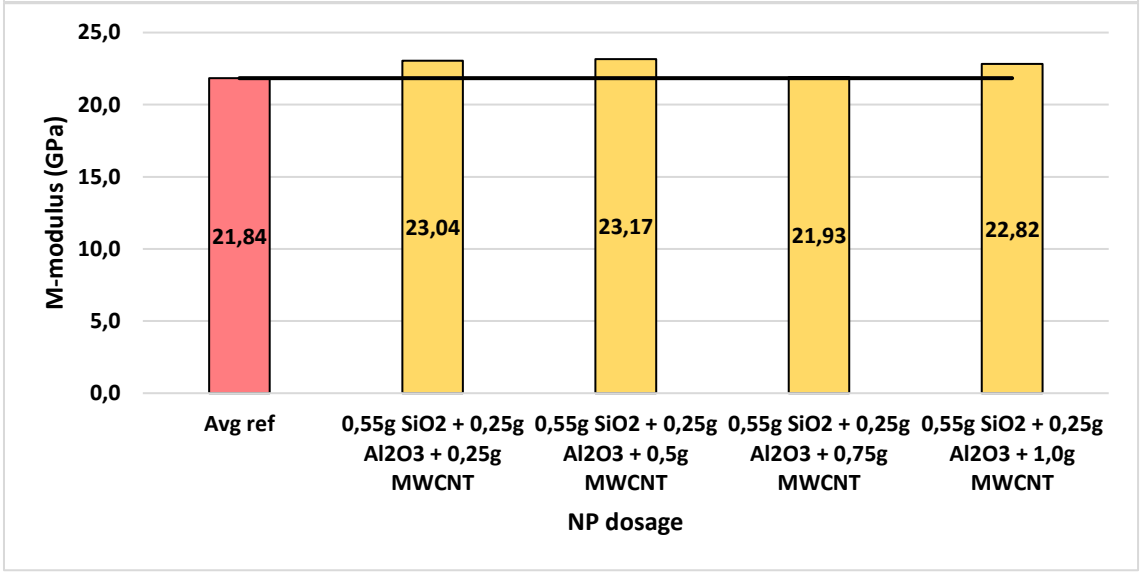

Test batch 10 (3 day FA)

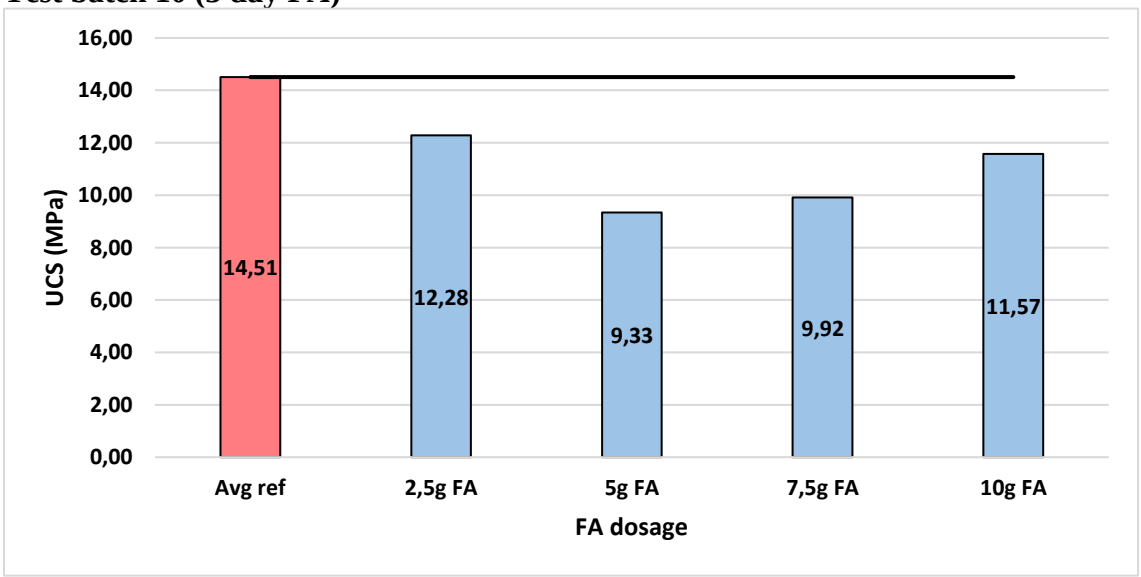

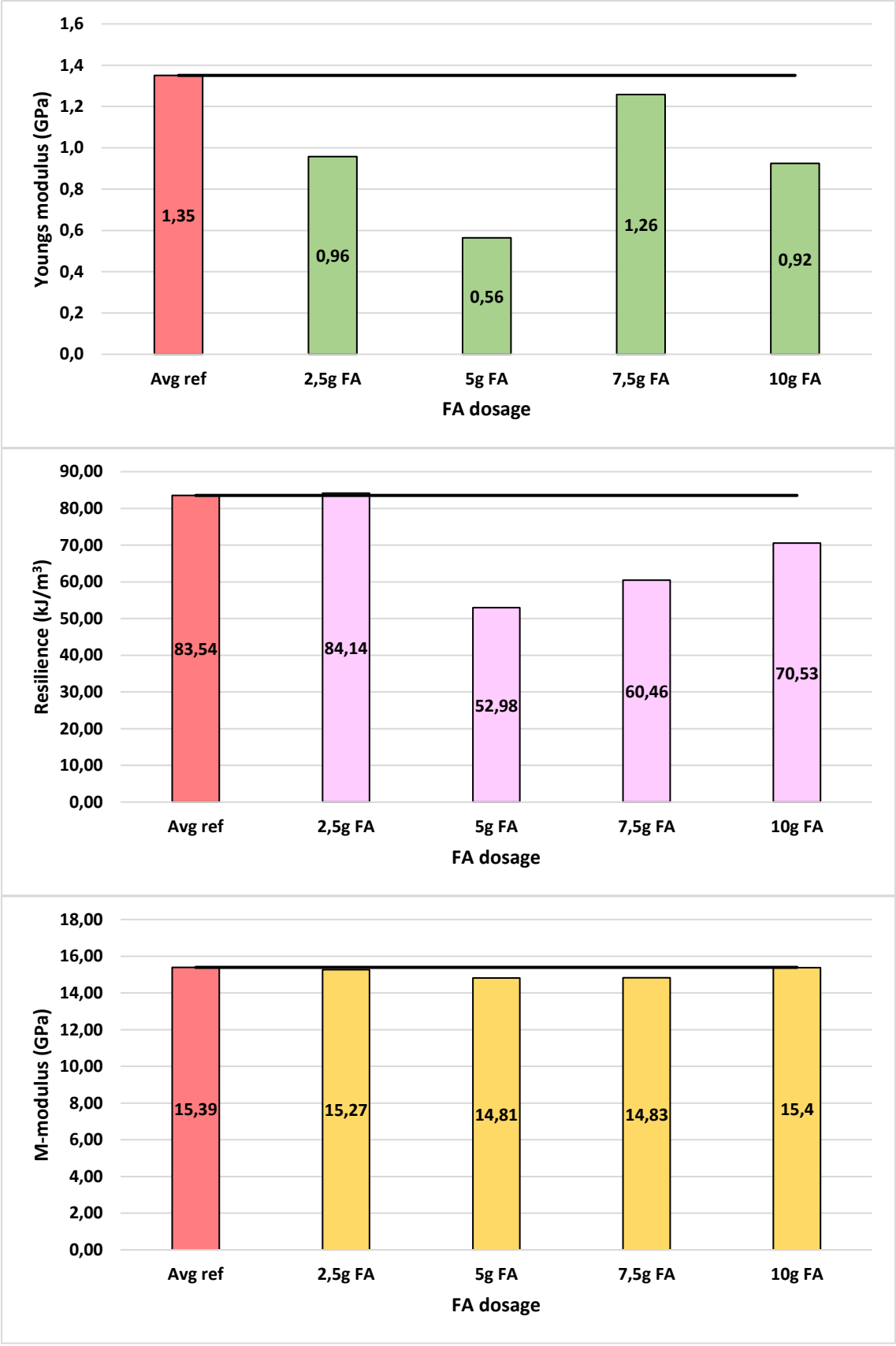
Youngs modulus (GPa)
1,6
1,4
1,2
1,0
0,8
0,6
0,4
0,2
0,0
1,35
0,96
0,56
1,26
0,92
Avg ref
2,5g FA
5g FA
7,5g FA
10g FA
FA dosage
Resilience (kJ/m³)
90,00
80,00
70,00
60,00
50,00
40,00
30,00
20,00
10,00
0,00
83,54
84,14
52,98
60,46
70,53
Avg ref
2,5g FA
5g FA
7,5g FA
10g FA
FA dosage
M-modulus (GPa)
18,00
16,00
14,00
12,00
10,00
8,00
6,00
4,00
2,00
0,00
15,39
15,27
14,81
14,83
15,4
Avg ref
2,5g FA
5g FA
7,5g FA
10g FA
FA dosage

Test batch 11 (7 day FA)

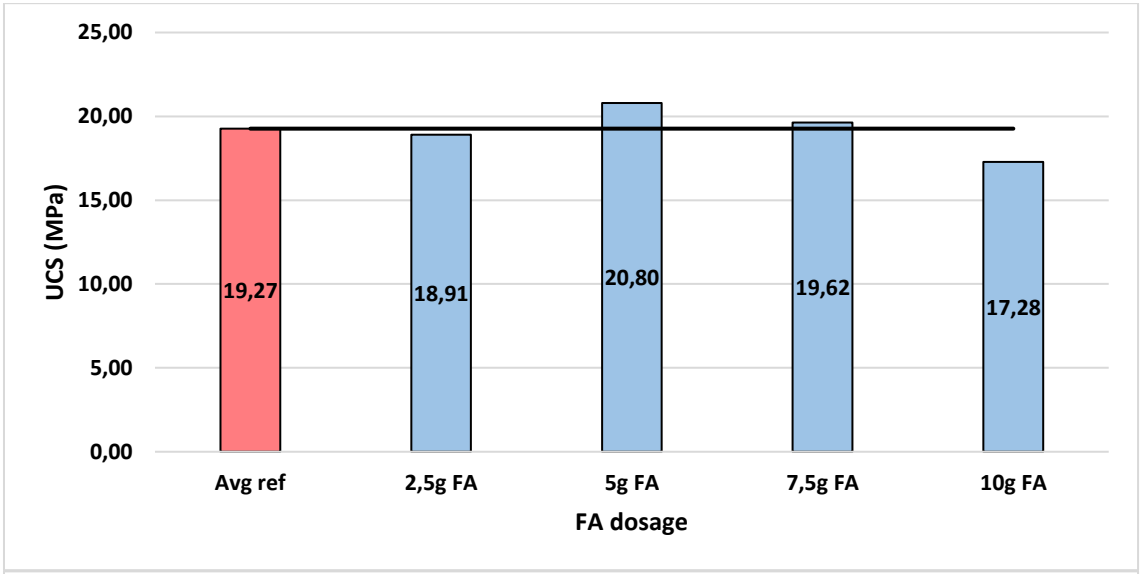

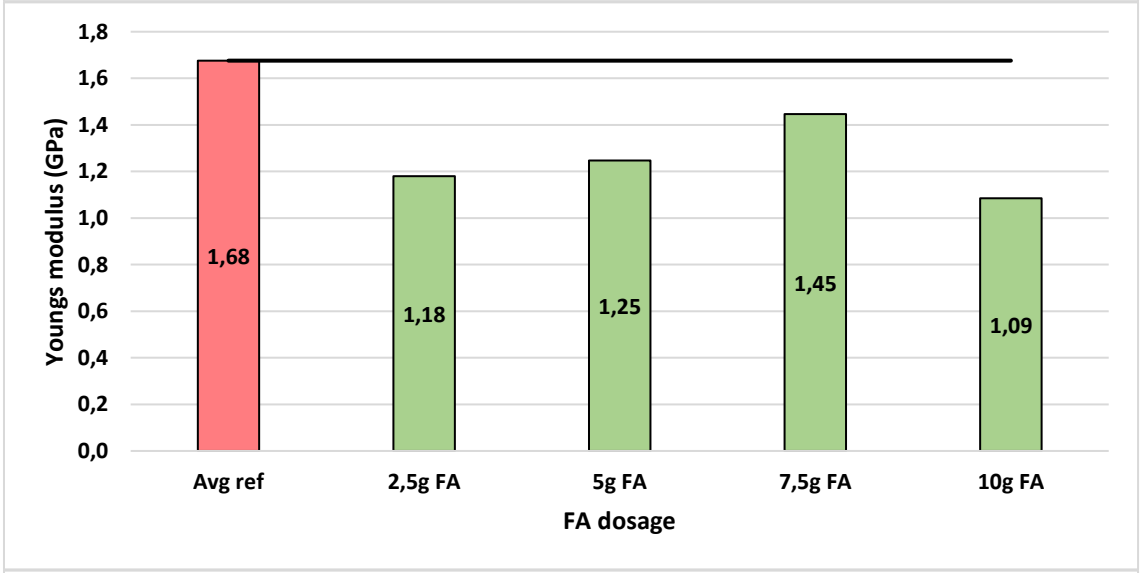

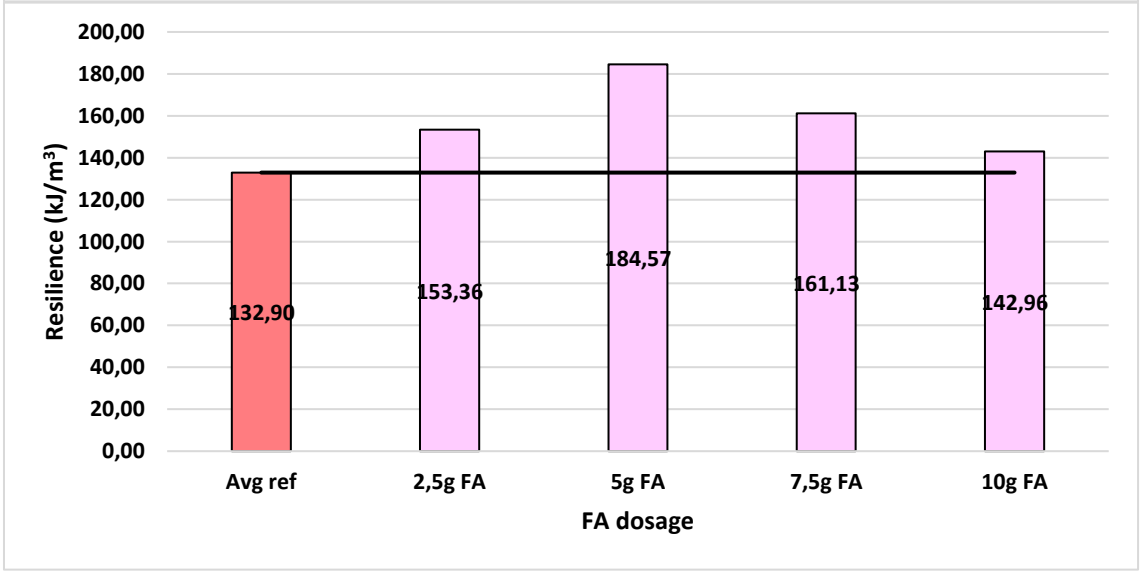

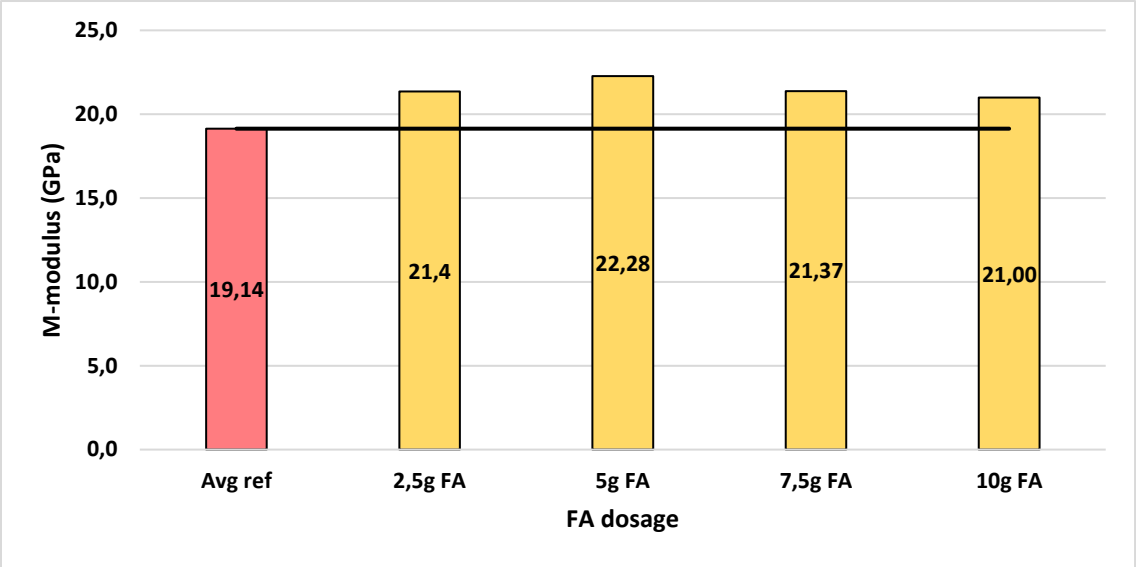

Test batch 12 (28 day FA)

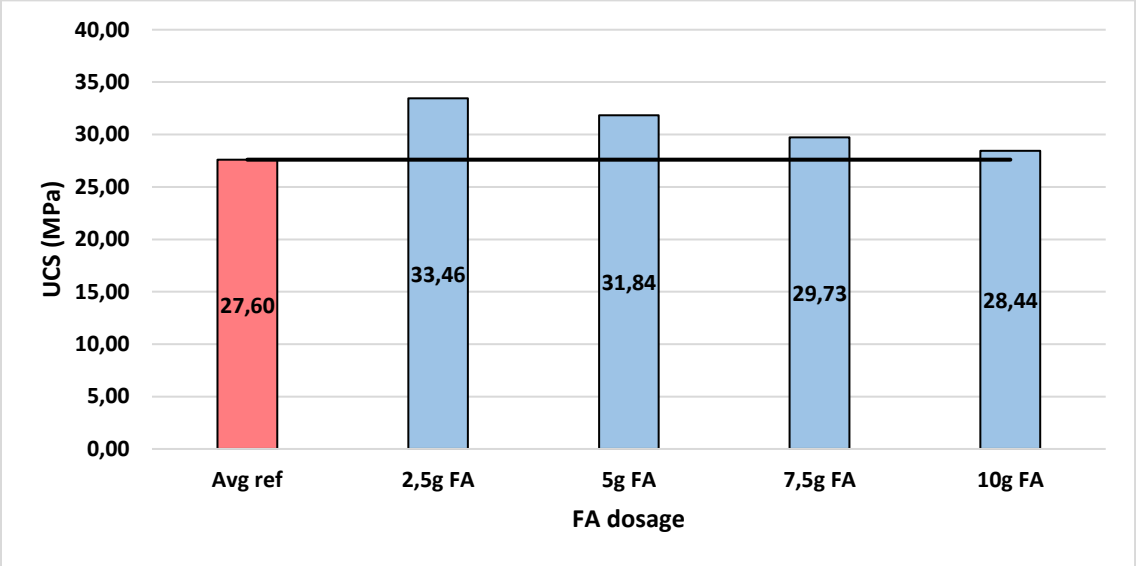

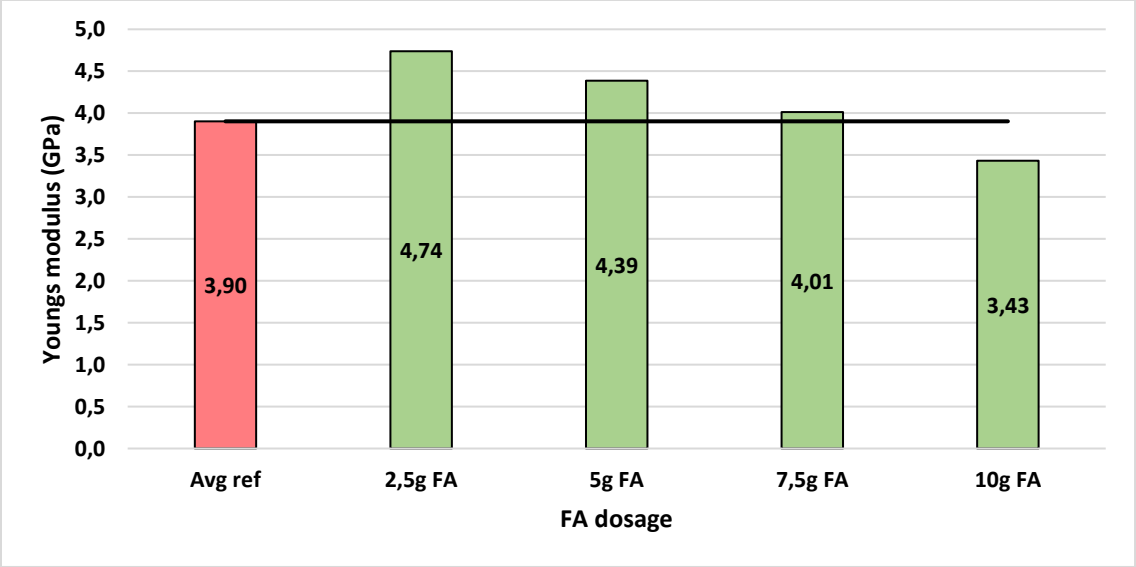

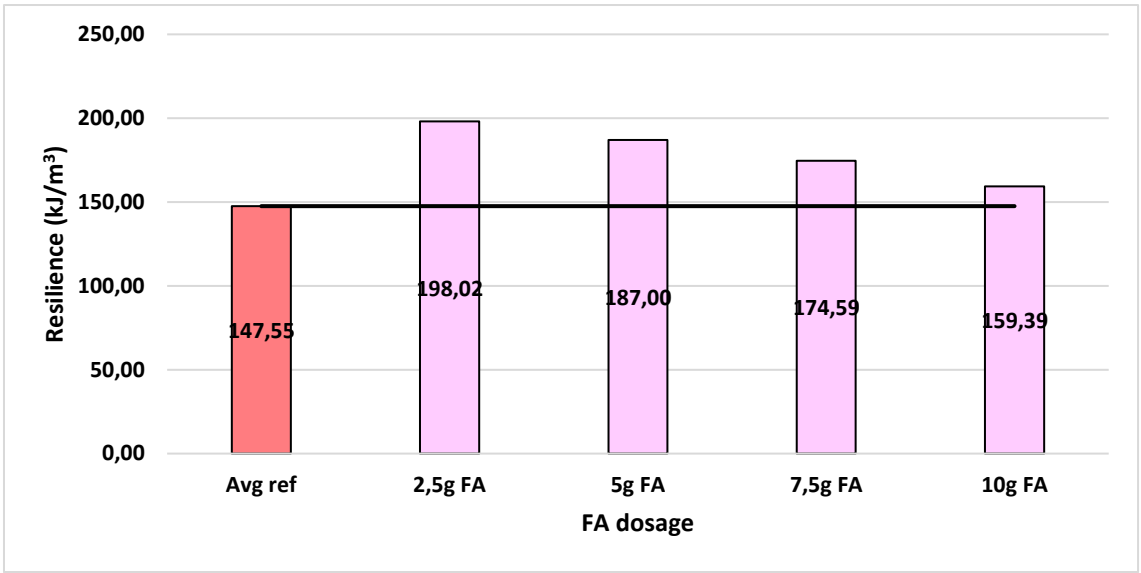

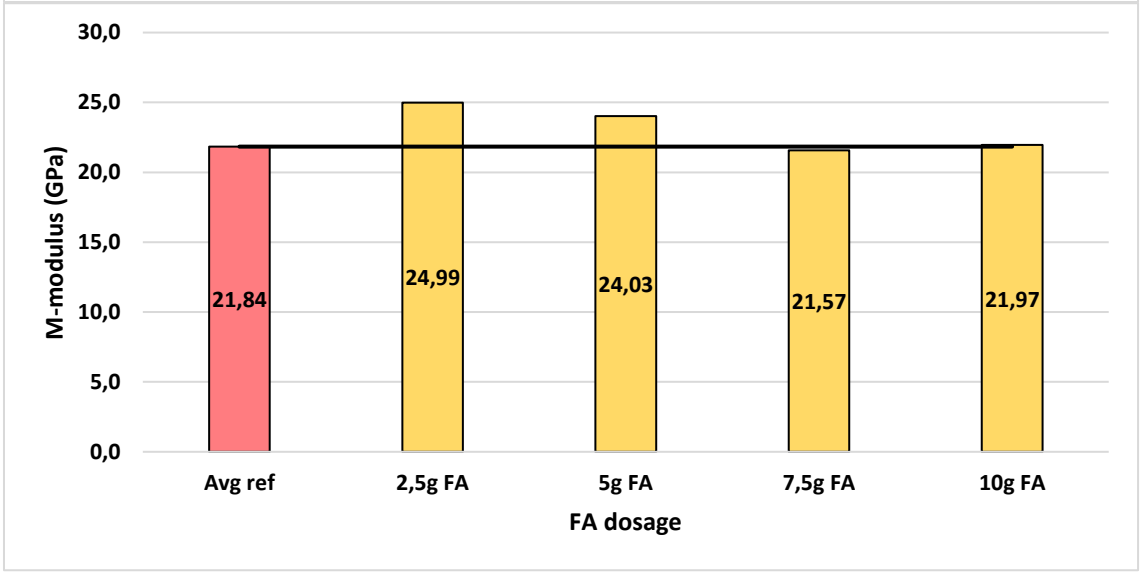

Test batch 13 (3 day FA + SiO_2)

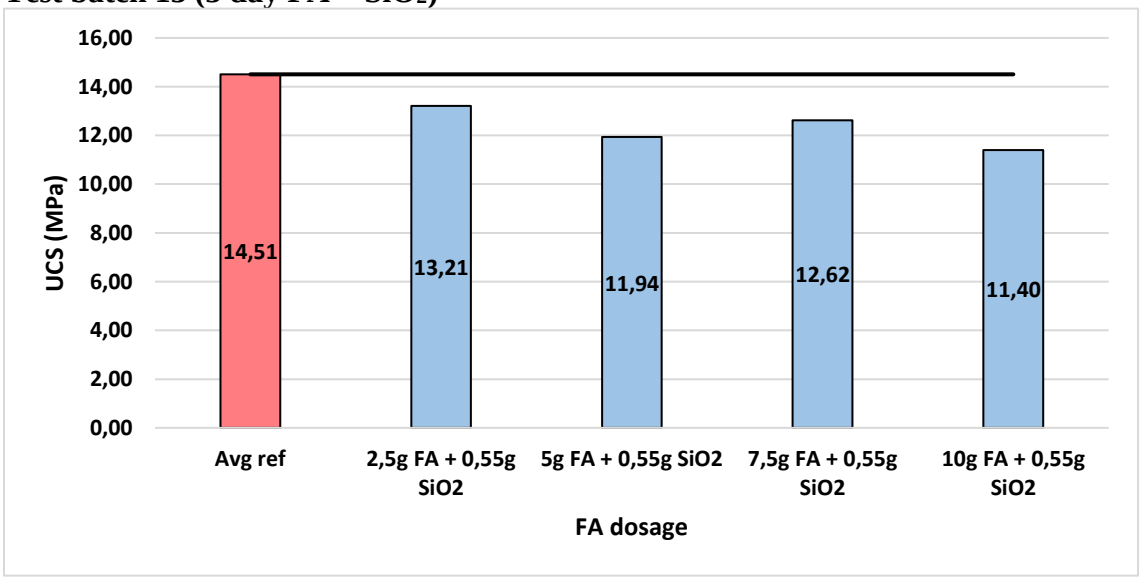

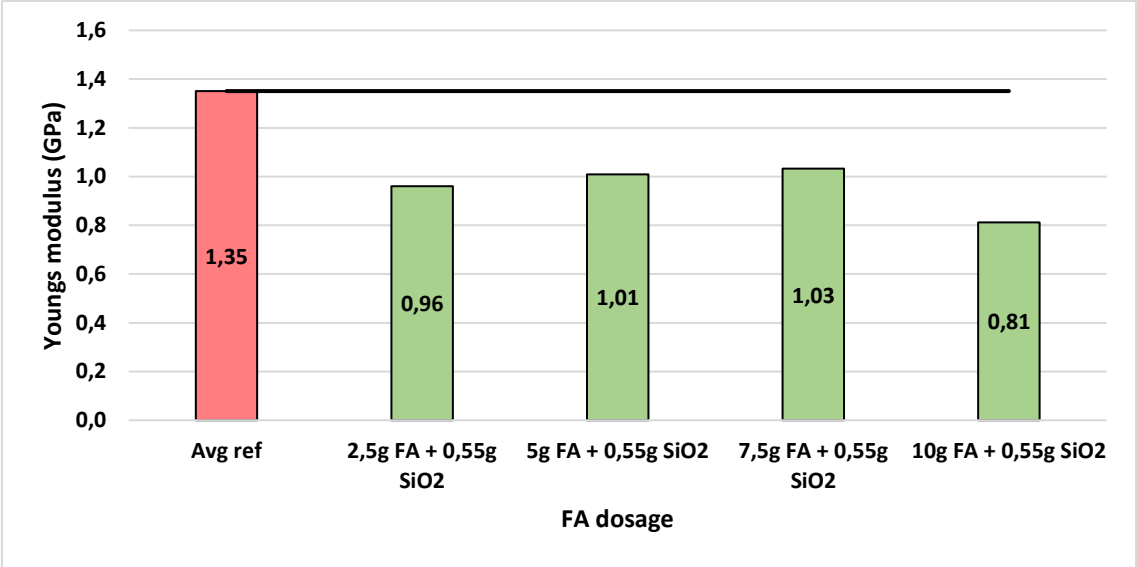
Youngs modulus (GPa)
1,6
1,4
1,2
1,0
0,8
0,6
0,4
0,2
0,0
1,35
0,96
1,01
1,03
0,81
Avg ref
2,5g FA + 0,55g SiO2
5g FA + 0,55g SiO2
7,5g FA + 0,55g SiO2
10g FA + 0,55g SiO2
FA dosage

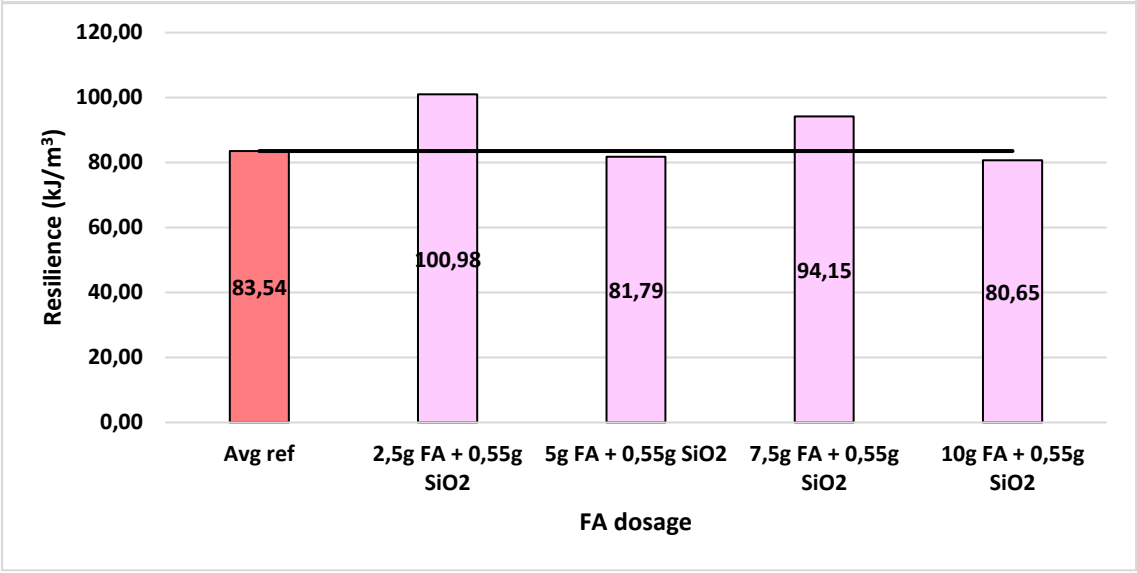
Resilience (kJ/m³)
120,00
100,00
80,00
60,00
40,00
20,00
0,00
83,54
100,98
81,79
94,15
80,65
Avg ref
2,5g FA + 0,55g SiO2
5g FA + 0,55g SiO2
7,5g FA + 0,55g SiO2
10g FA + 0,55g SiO2
FA dosage

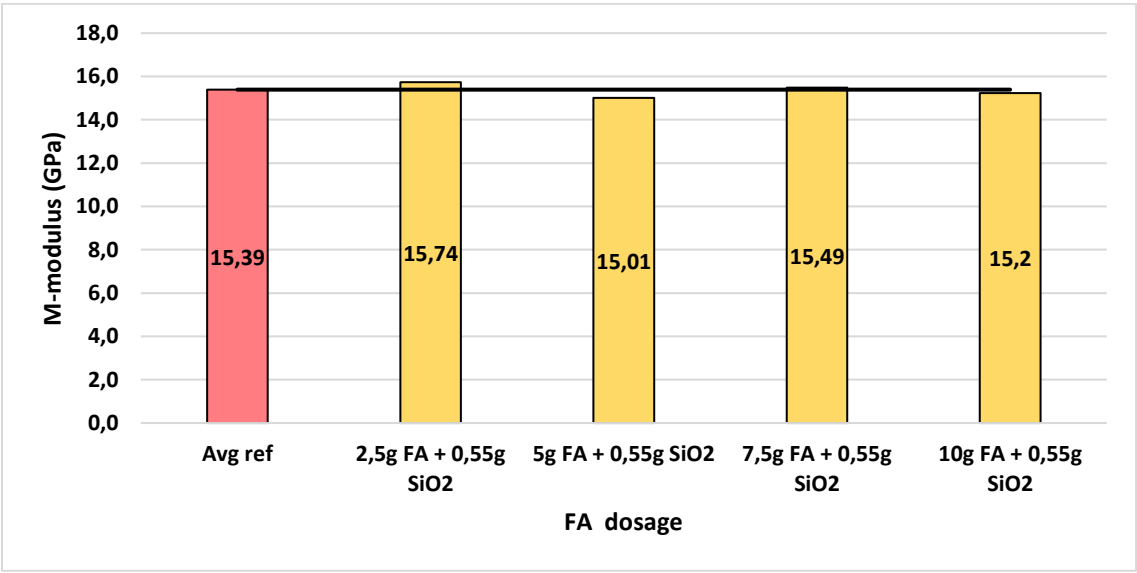
M-modulus (GPa)
18,0
16,0
14,0
12,0
10,0
8,0
6,0
4,0
2,0
0,0
15,39
15,74
15,01
15,49
15,2
Avg ref
2,5g FA + 0,55g SiO2
5g FA + 0,55g SiO2
7,5g FA + 0,55g SiO2
10g FA + 0,55g SiO2
FA dosage

Test batch 14 (7 day FA + SiO_2)

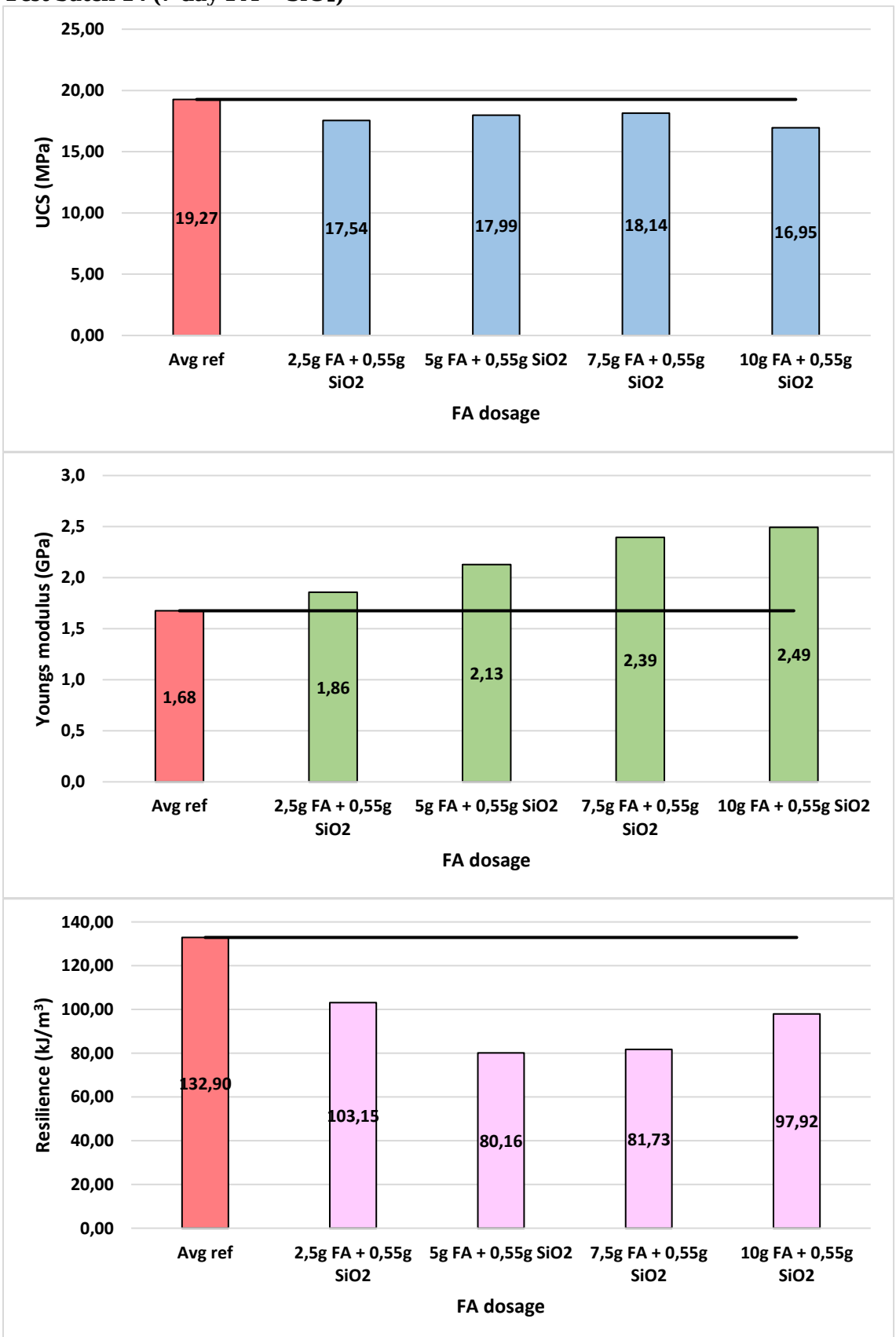

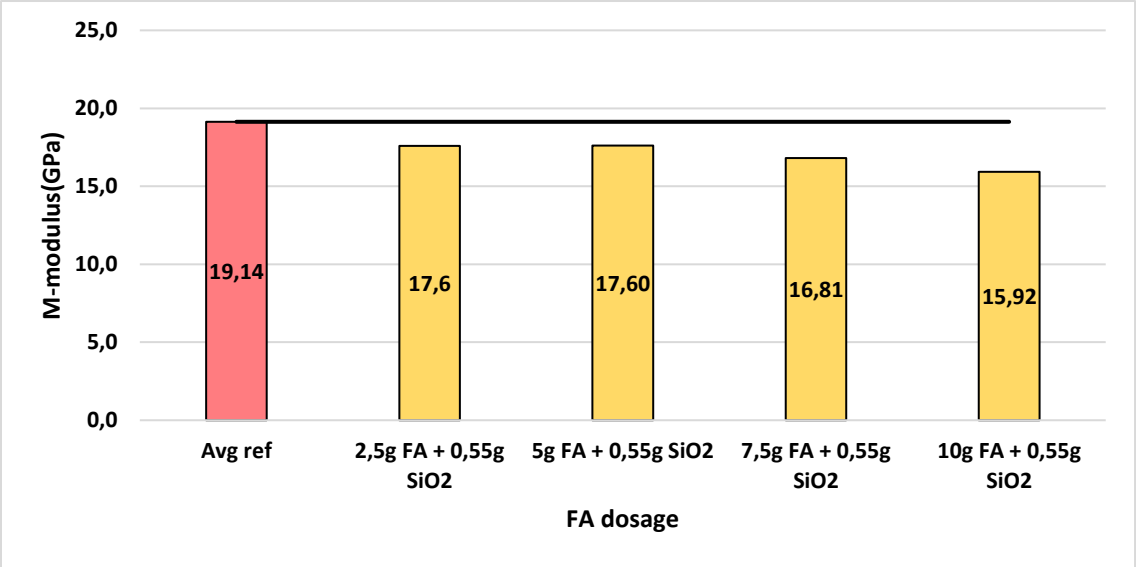

Test batch 15 (28 day FA + SiO_2)

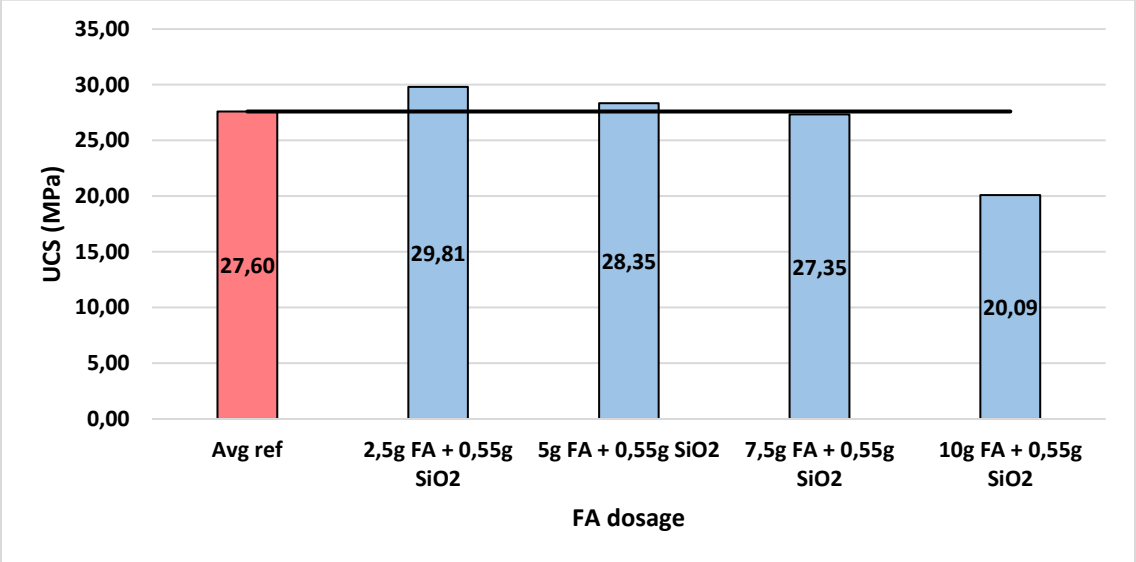

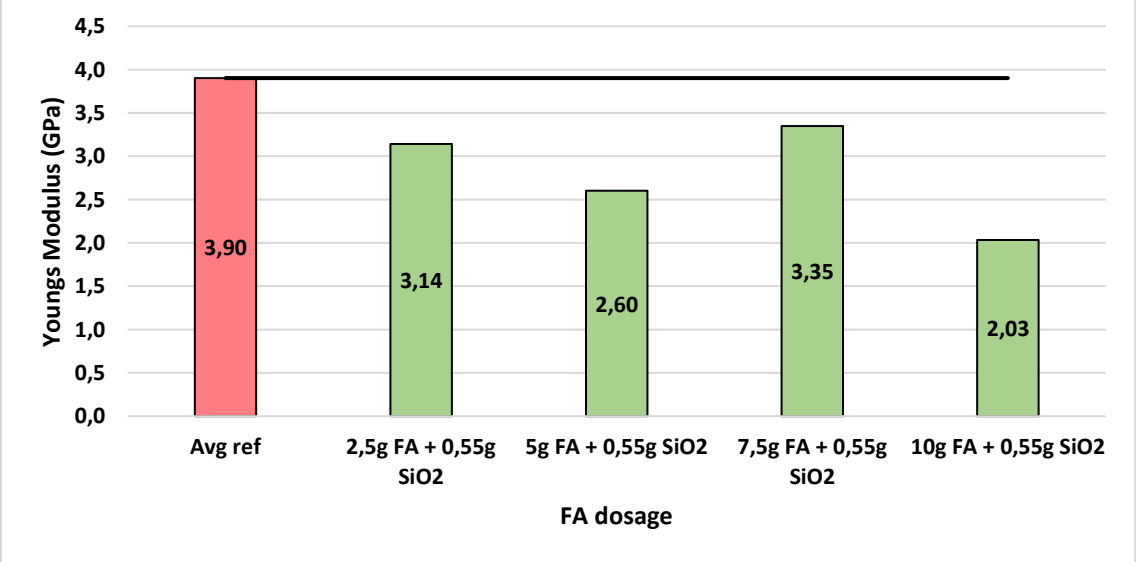

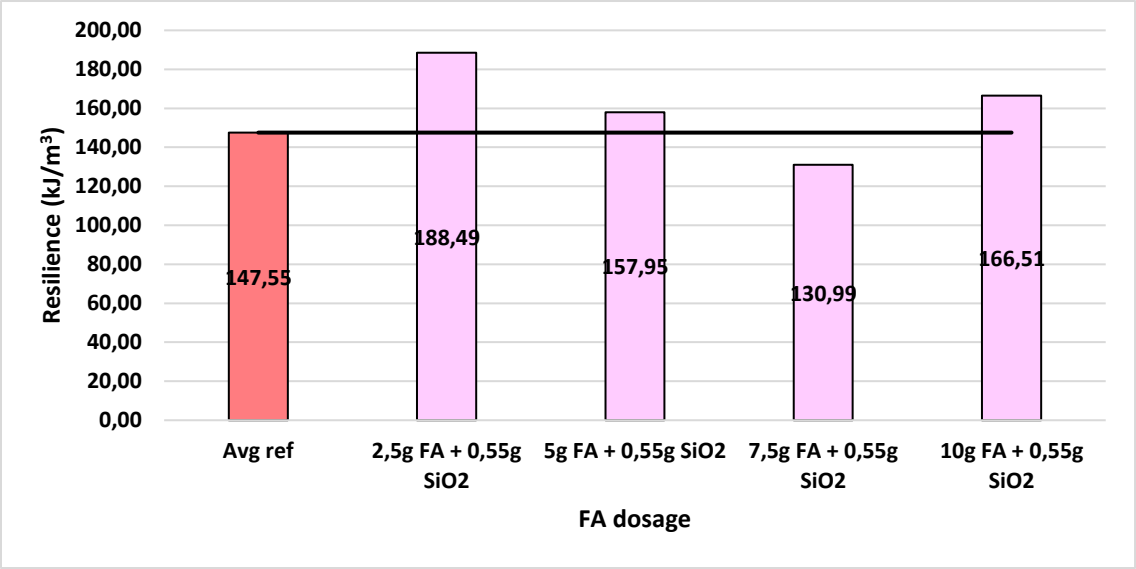
200,00
180,00
160,00
140,00
120,00
100,00
80,00
60,00
40,00
20,00
0,00
Resilience (kJ/m³)
147,55
188,49
157,95
130,99
166,51
Avg ref
2,5g FA + 0,55g SiO2
5g FA + 0,55g SiO2
7,5g FA + 0,55g SiO2
10g FA + 0,55g SiO2
FA dosage

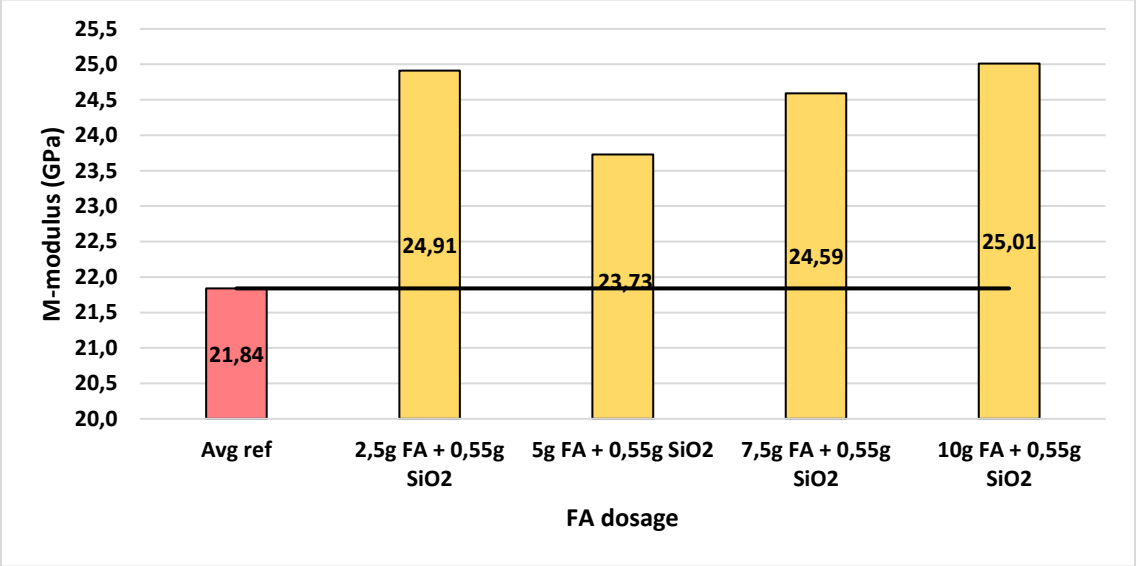
25,5
25,0
24,5
24,0
23,5
23,0
22,5
22,0
21,5
21,0
20,5
20,0
M-modulus (GPa)
21,84
24,91
23,73
24,59
25,01
Avg ref
2,5g FA + 0,55g SiO2
5g FA + 0,55g SiO2
7,5g FA + 0,55g SiO2
10g FA + 0,55g SiO2
FA dosage

Appendix B – Load vs deformation

Shows load (kN) on y- axis vs deformation (mm) on x-axis of all cement plugs. Keep in mind that if a sample is missing it is due to the specimen being defect, as this occurred from time to time. It might also be missing due to human error when measuring deformation which also unfortunately occurred a few times.

Test Batch 1 (3 day)

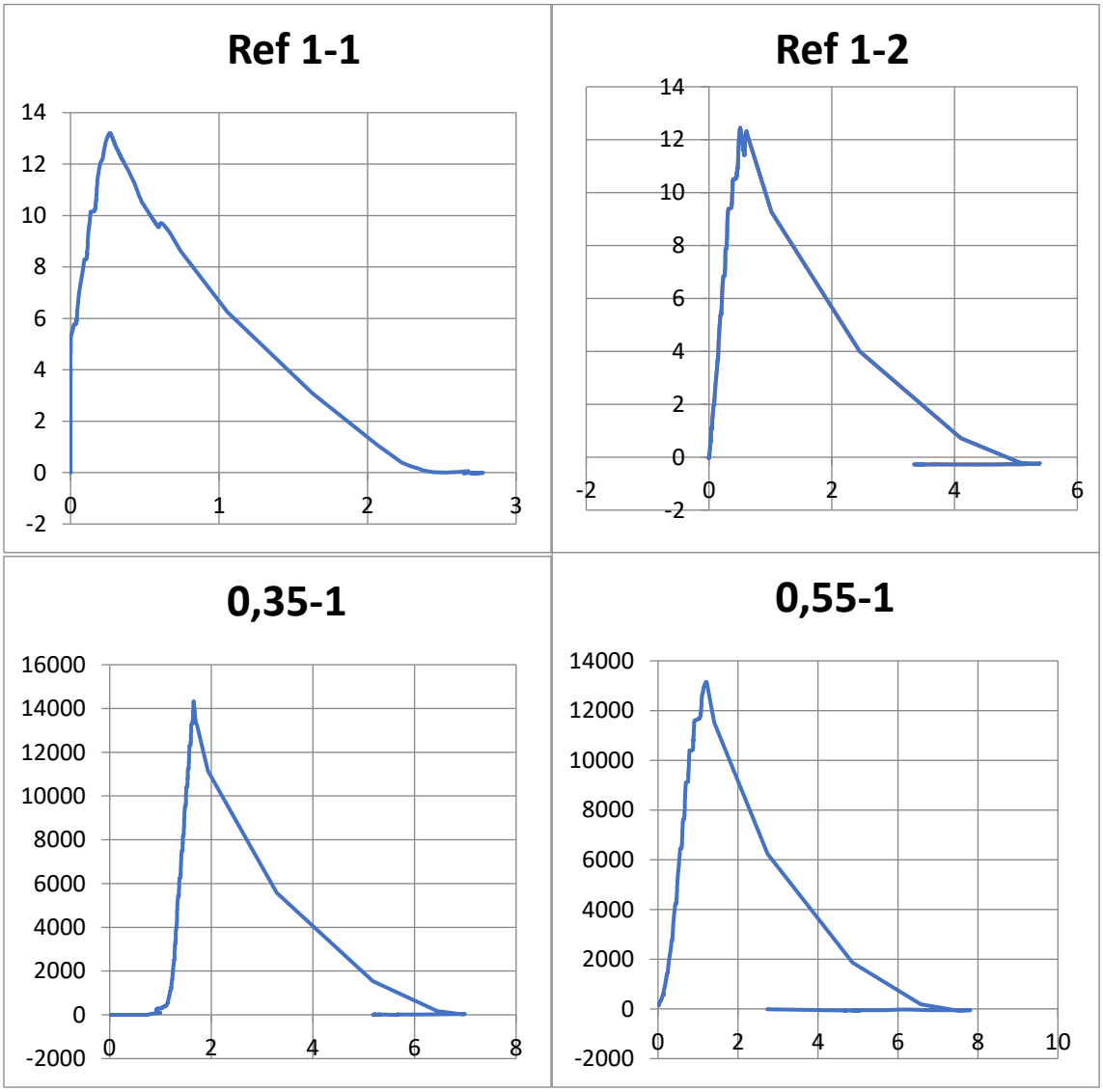

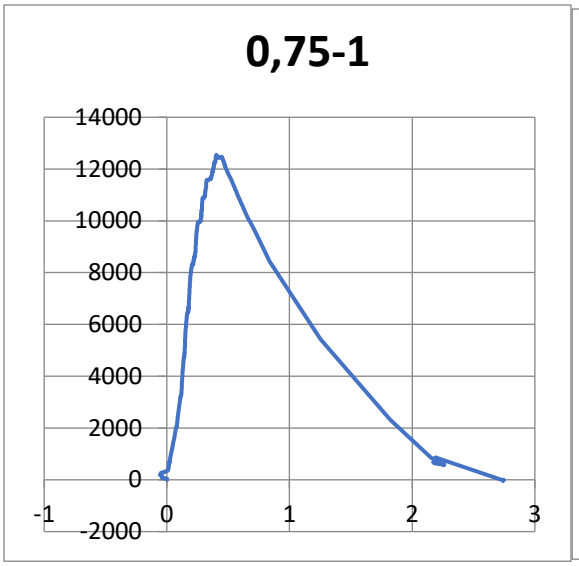
0,75-1
14000
12000
10000
8000
6000
4000
2000
0
-2000
-1
0
1
2
3

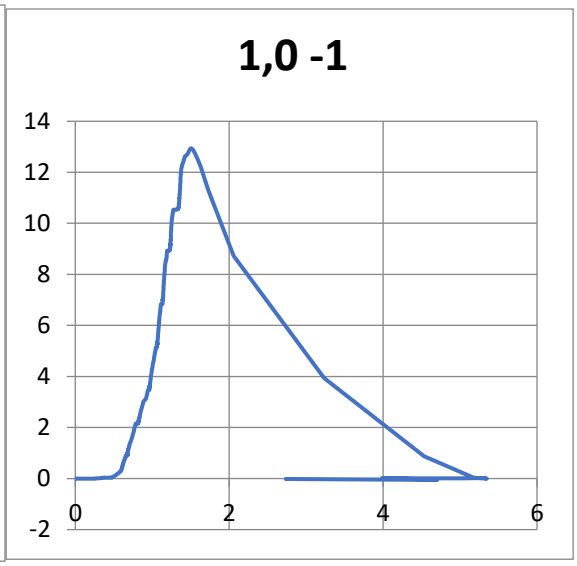
1,0 -1
14
12
10
8
6
4
2
0
-2
0
2
4
6

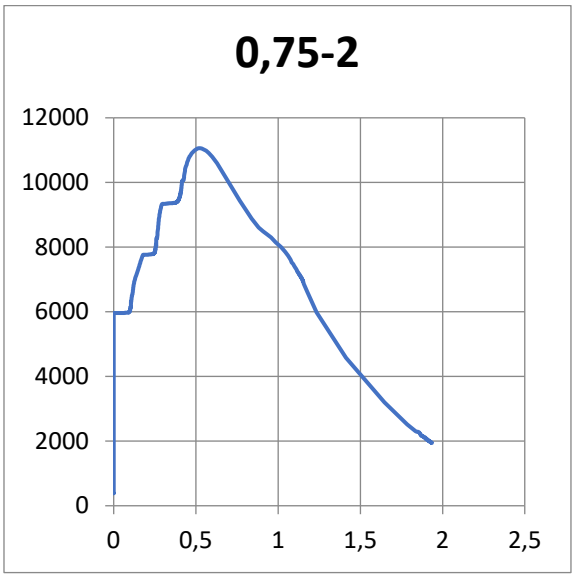
0,75-2
12000
10000
8000
6000
4000
2000
0
0
0,5
1
1,5
2
2,5

Test batch 2 (7 day)

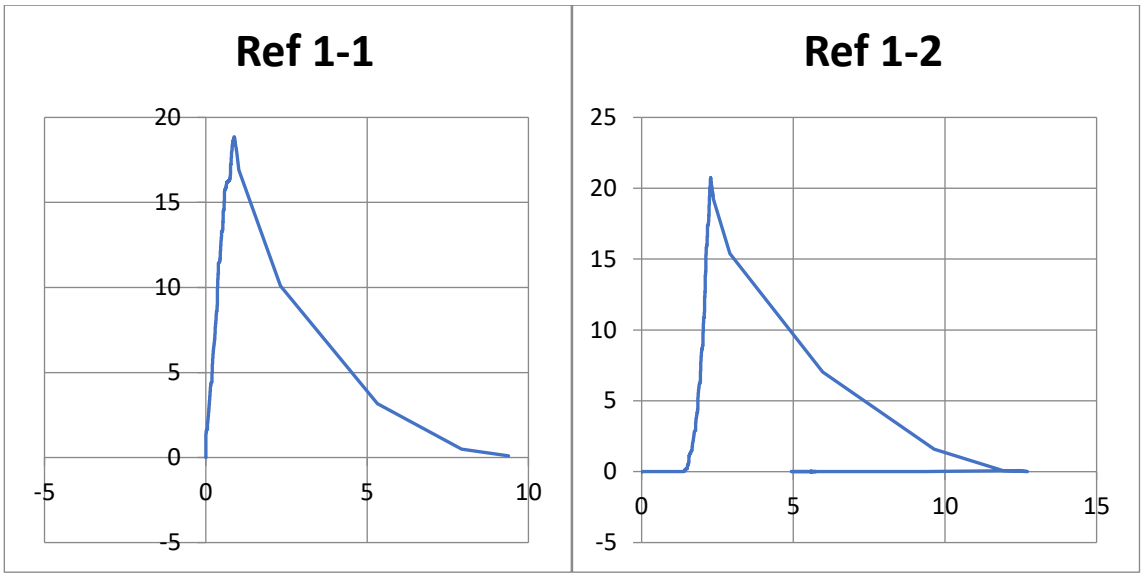

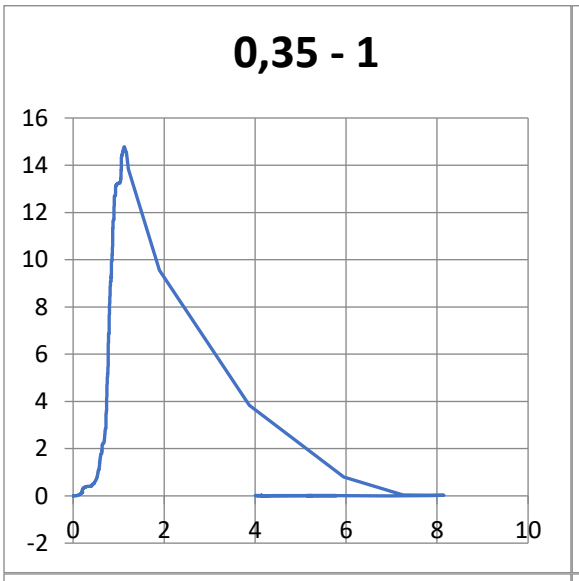

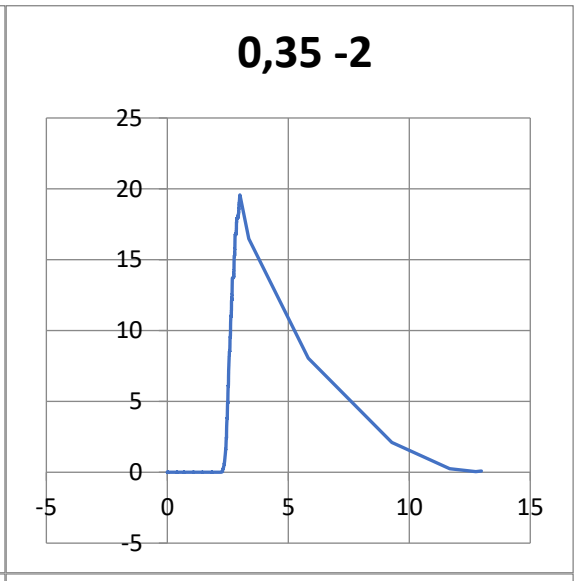

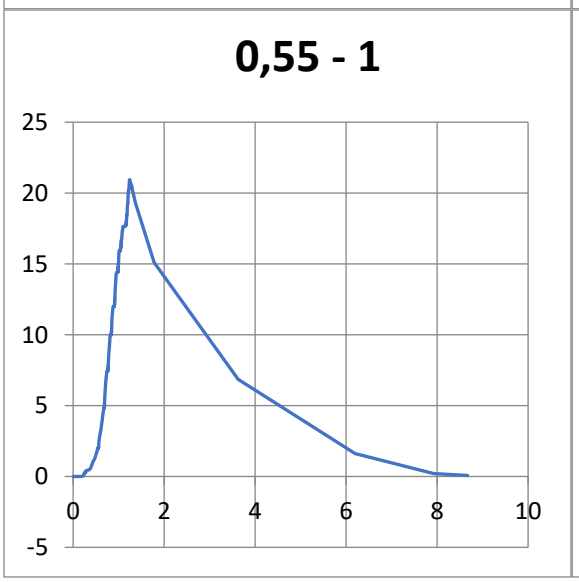

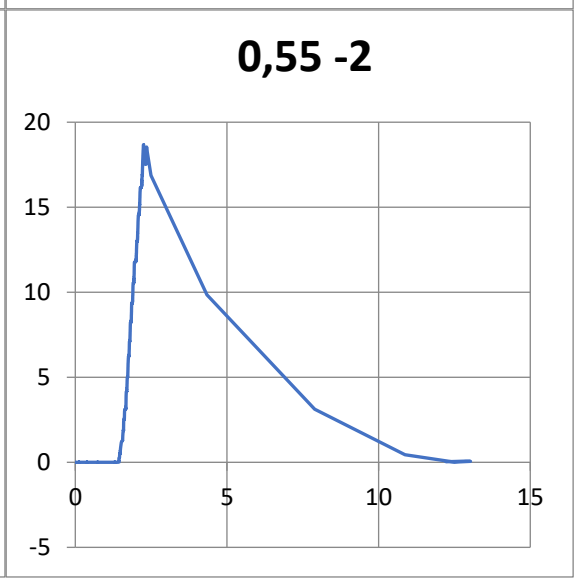

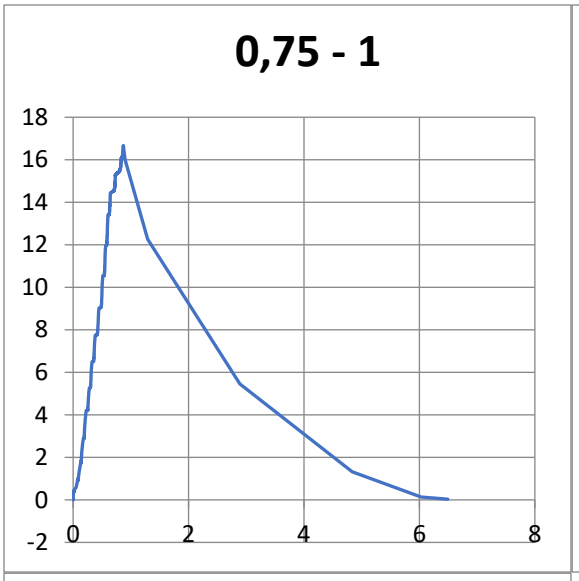
0,75 - 1
18
16
14
12
10
8
6
4
2
0
-2
0
2
4
6
8

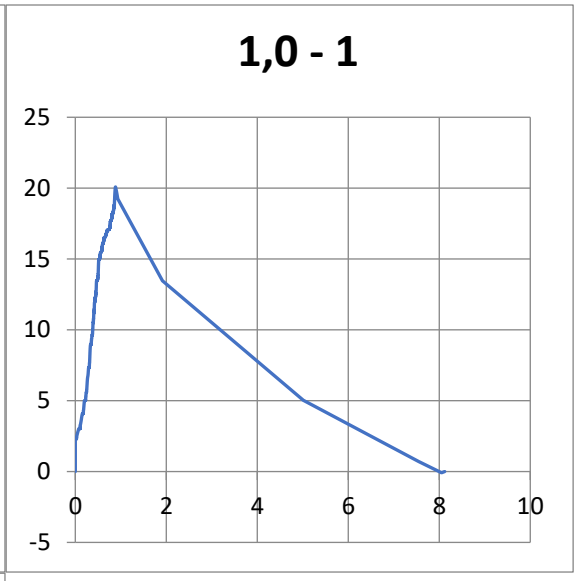
1,0 - 1
25
20
15
10
5
0
-5
0
2
4
6
8
10

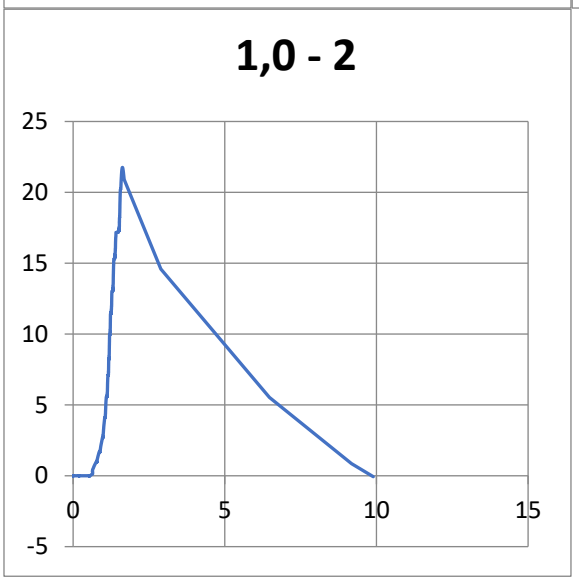
1,0 - 2
25
20
15
10
5
0
-5
0
5
10
15

Test Batch 3 (28 days)

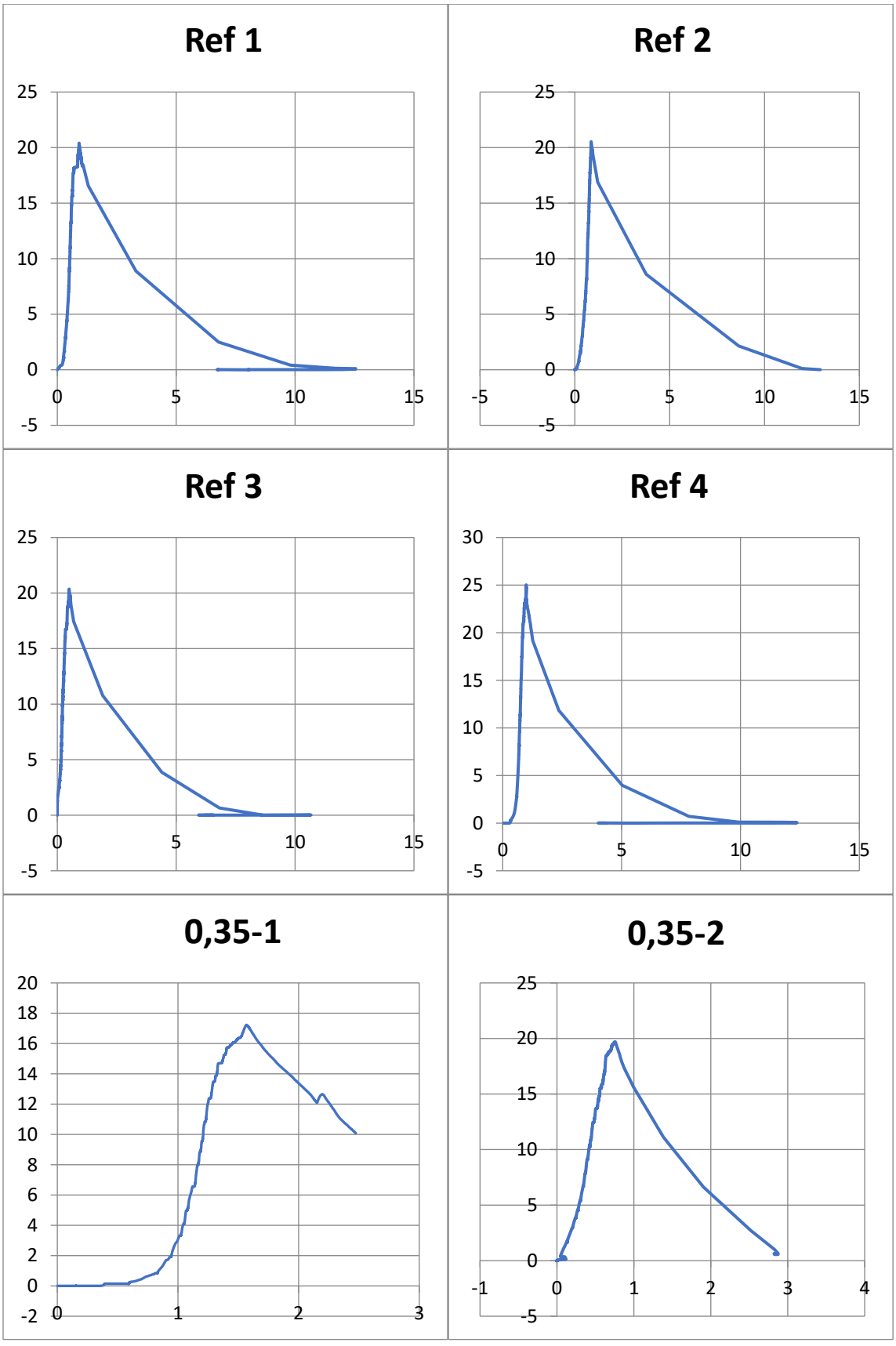

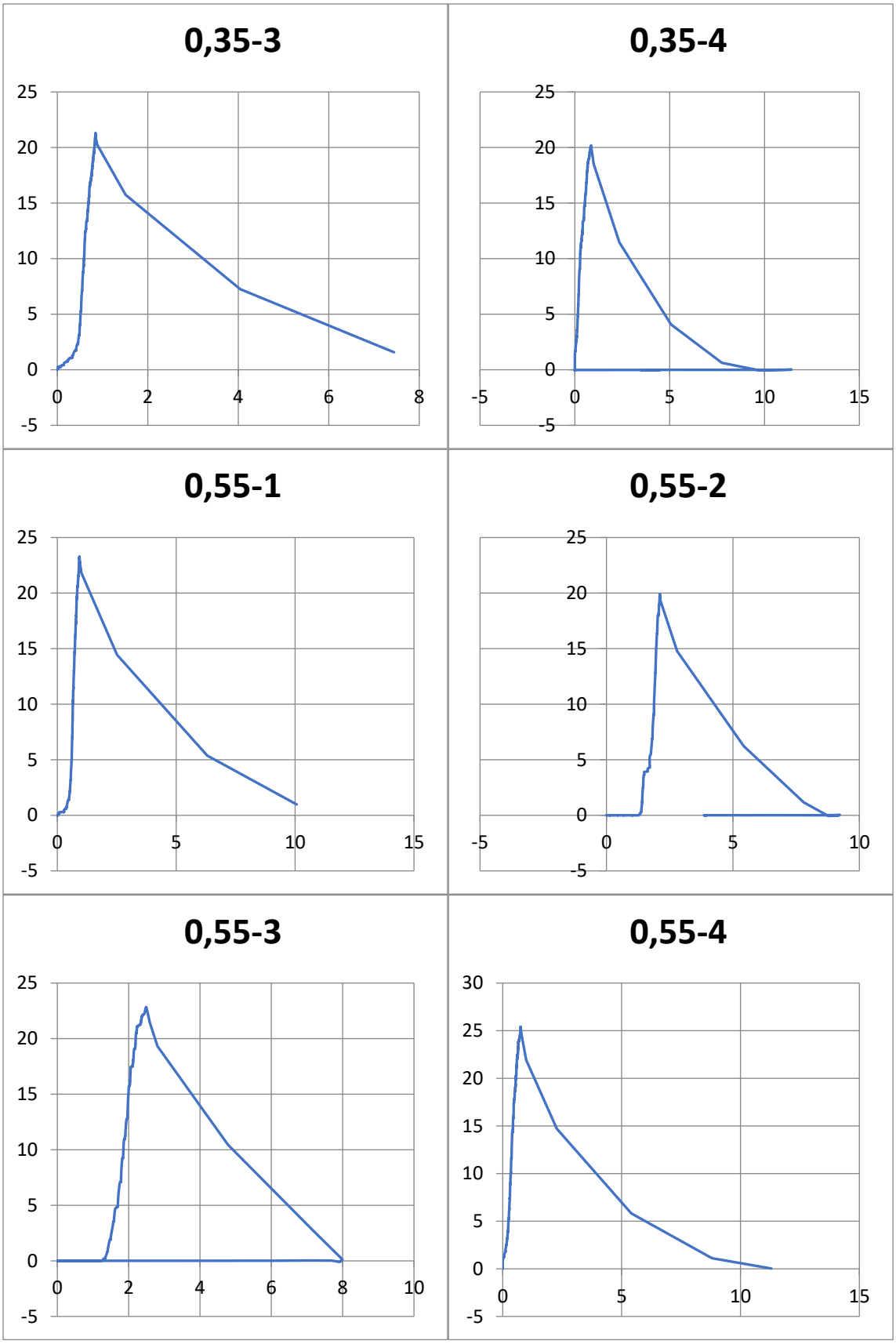
0,35-3
0,35-4
0,55-1
0,55-2
0,55-3
0,55-4

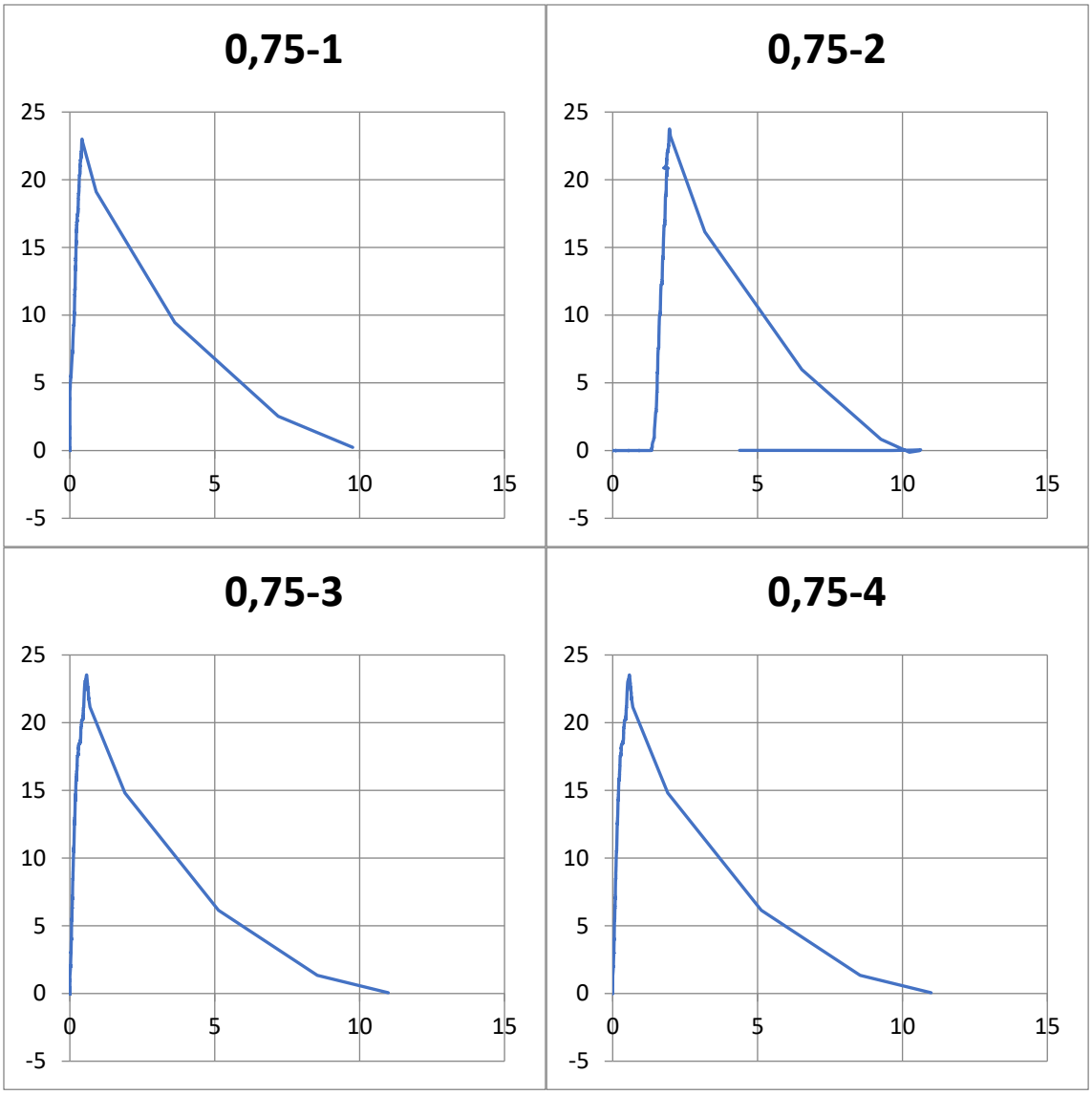
0,75-1
25
20
15
10
5
0
-5
0
5
10
15
0,75-2
25
20
15
10
5
0
-5
0
5
10
15
0,75-3
25
20
15
10
5
0
-5
0
5
10
15
0,75-4
25
20
15
10
5
0
-5
0
5
10
15

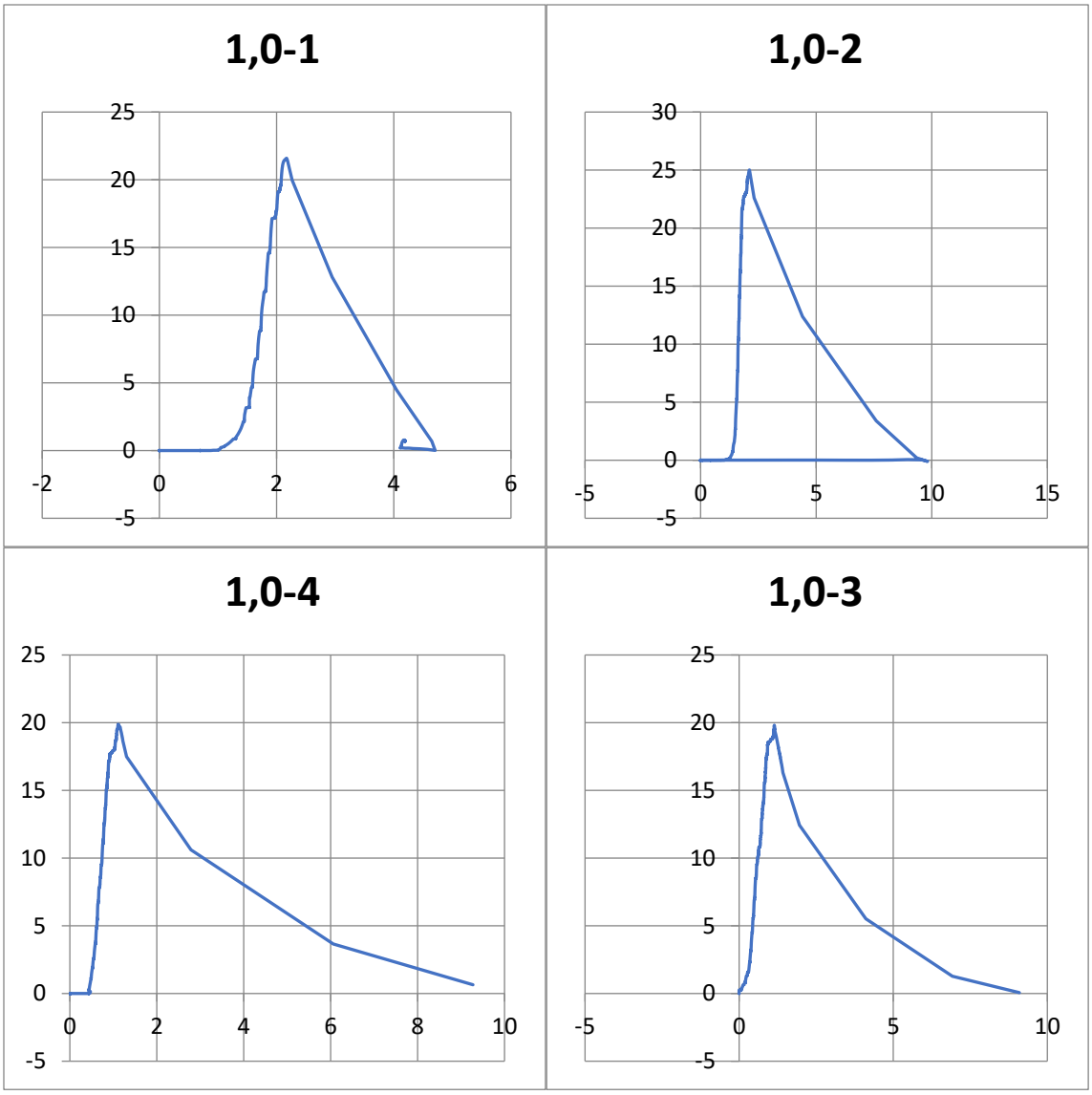
1,0-1
25
20
15
10
5
0
-5
-2
0
2
4
6
1,0-2
30
25
20
15
10
5
0
-5
-5
0
5
10
15
1,0-4
25
20
15
10
5
0
-5
0
2
4
6
8
10
1,0-3
25
20
15
10
5
0
-5
-5
0
5
10

Test Batch 4 (3 day binary)

This batch was recreated, the figures are from the second creation due to a complete failure to record the deformation data in the first iteration of the batch. However, the first iteration still has a UCS result which are taken into consideration.

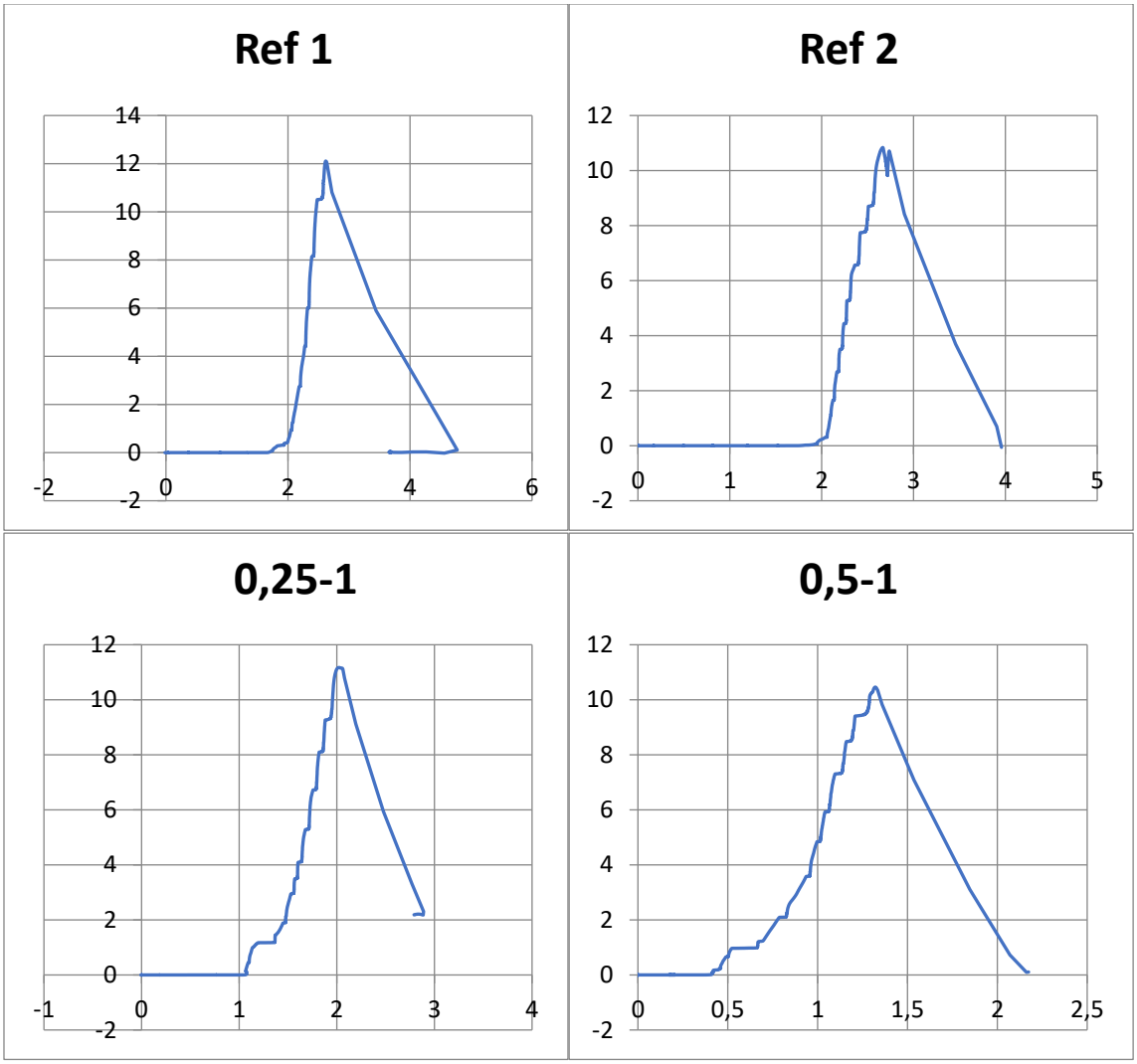

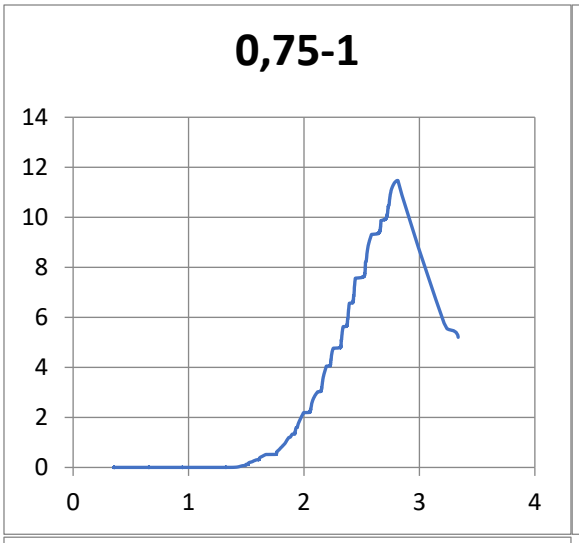

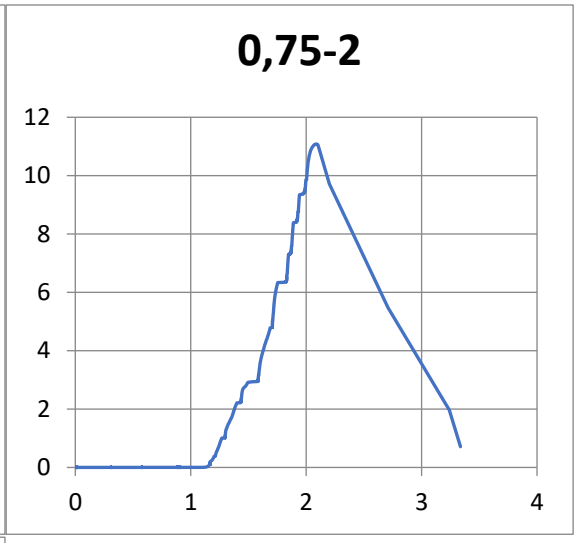

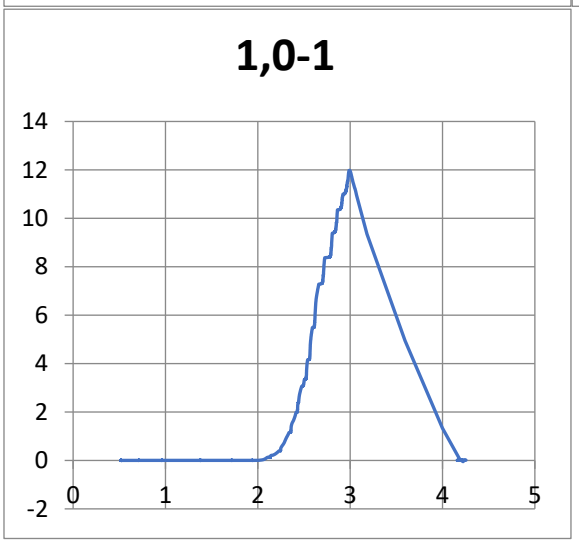

Test Batch 4 (7 day binary)

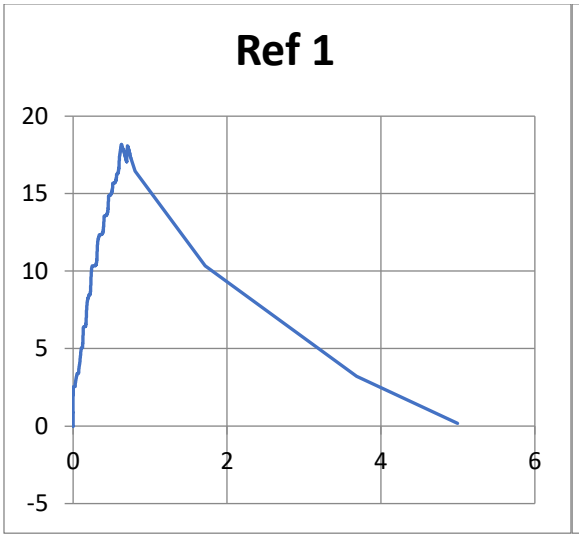

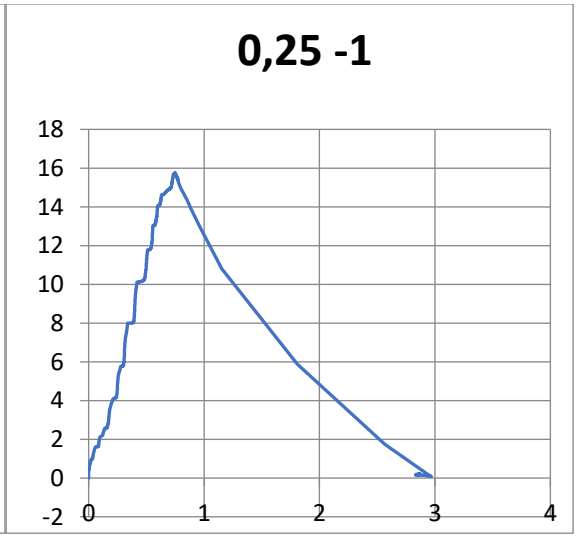

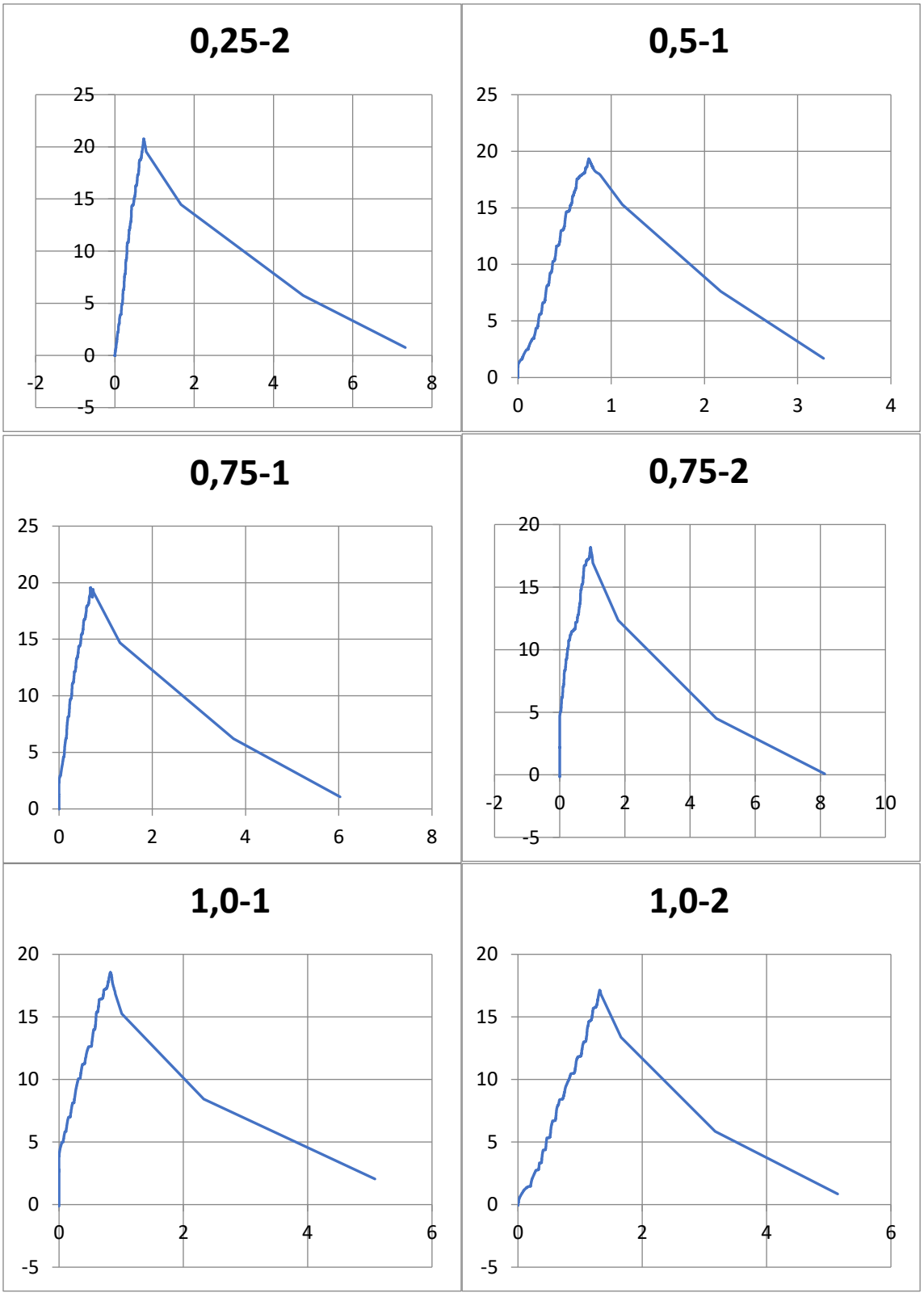
0,25-2
0,5-1
0,75-1
0,75-2
1,0-1
1,0-2

Test Batch 6 (28 day binary)

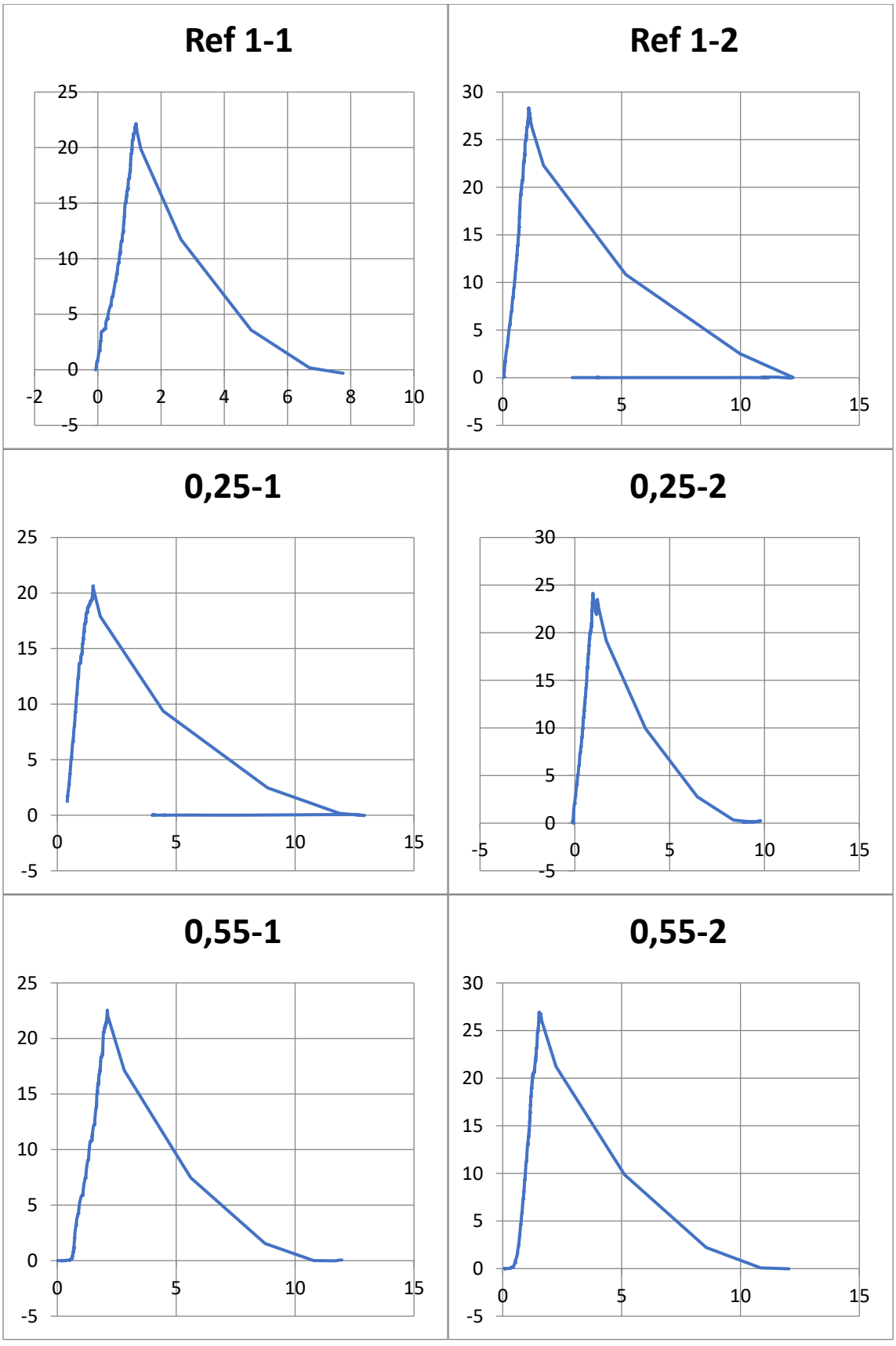

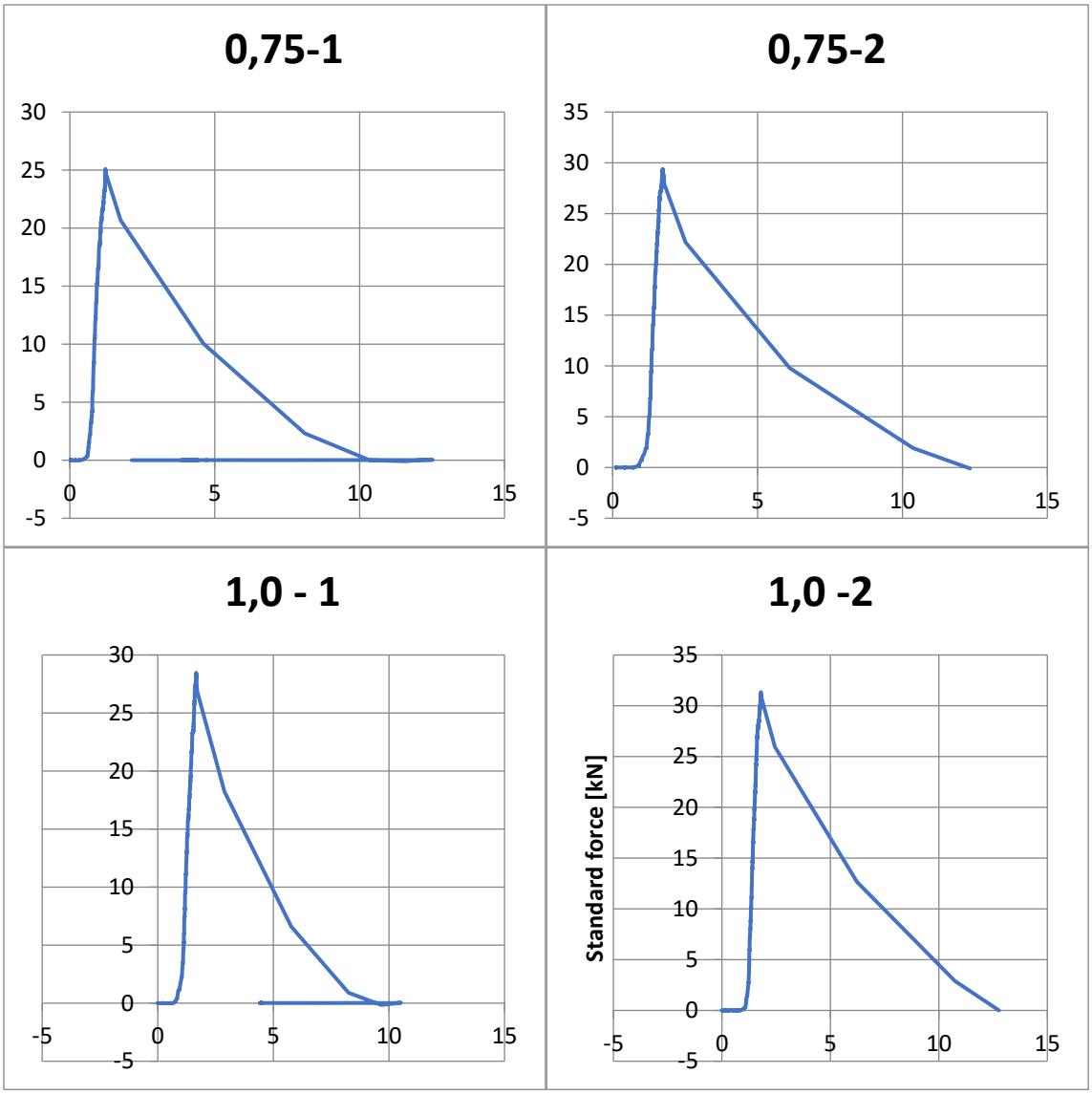
0,75-1
30
25
20
15
10
5
0
-5
0
5
10
15
0,75-2
35
30
25
20
15
10
5
0
-5
0
5
10
15
1,0 - 1
30
25
20
15
10
5
0
-5
-5
0
5
10
15
1,0 -2
Standard force [kN]
35
30
25
20
15
10
5
0
-5
-5
0
5
10
15

Test batch 7 (Ternary blend 3 day)

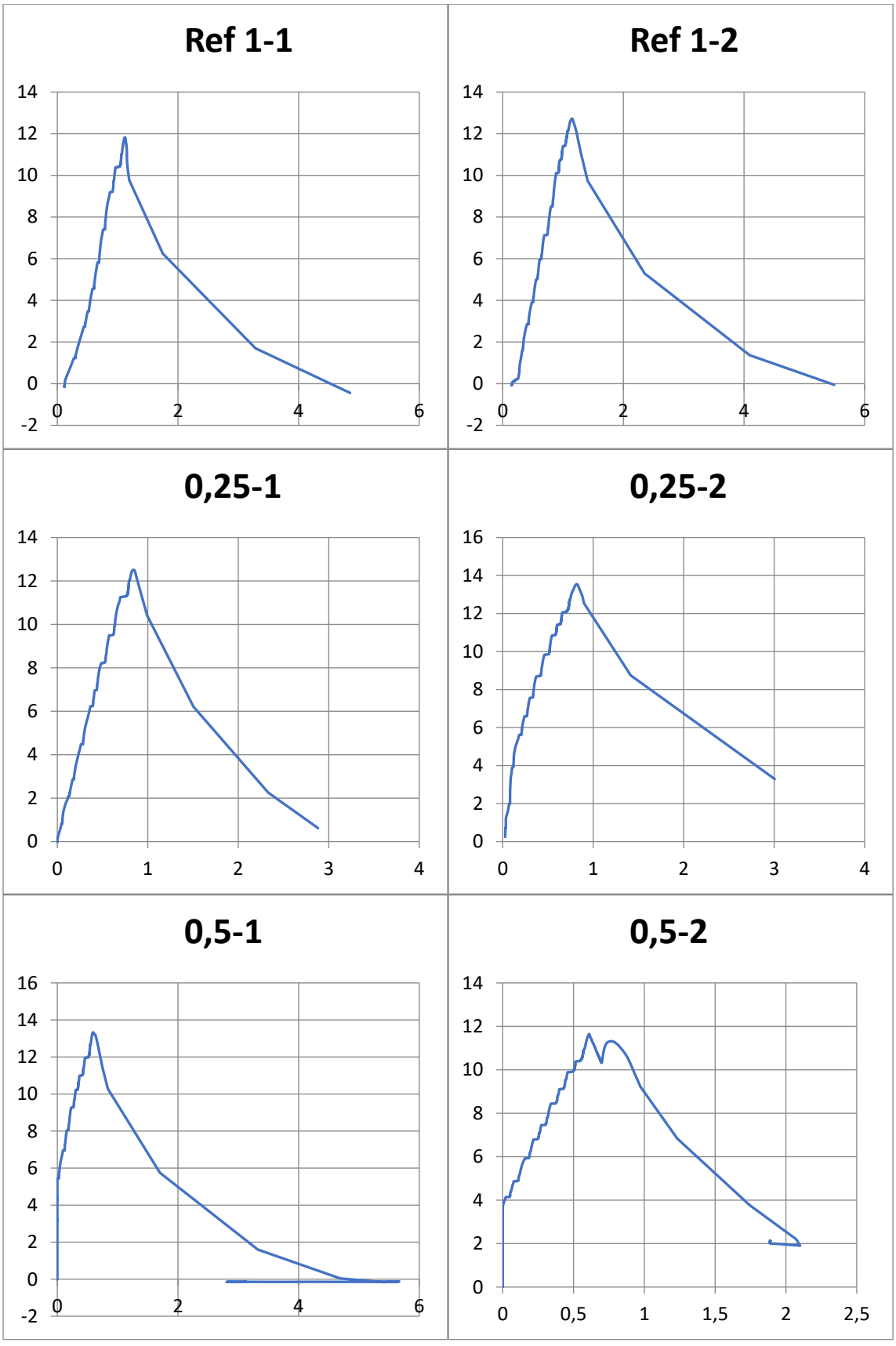

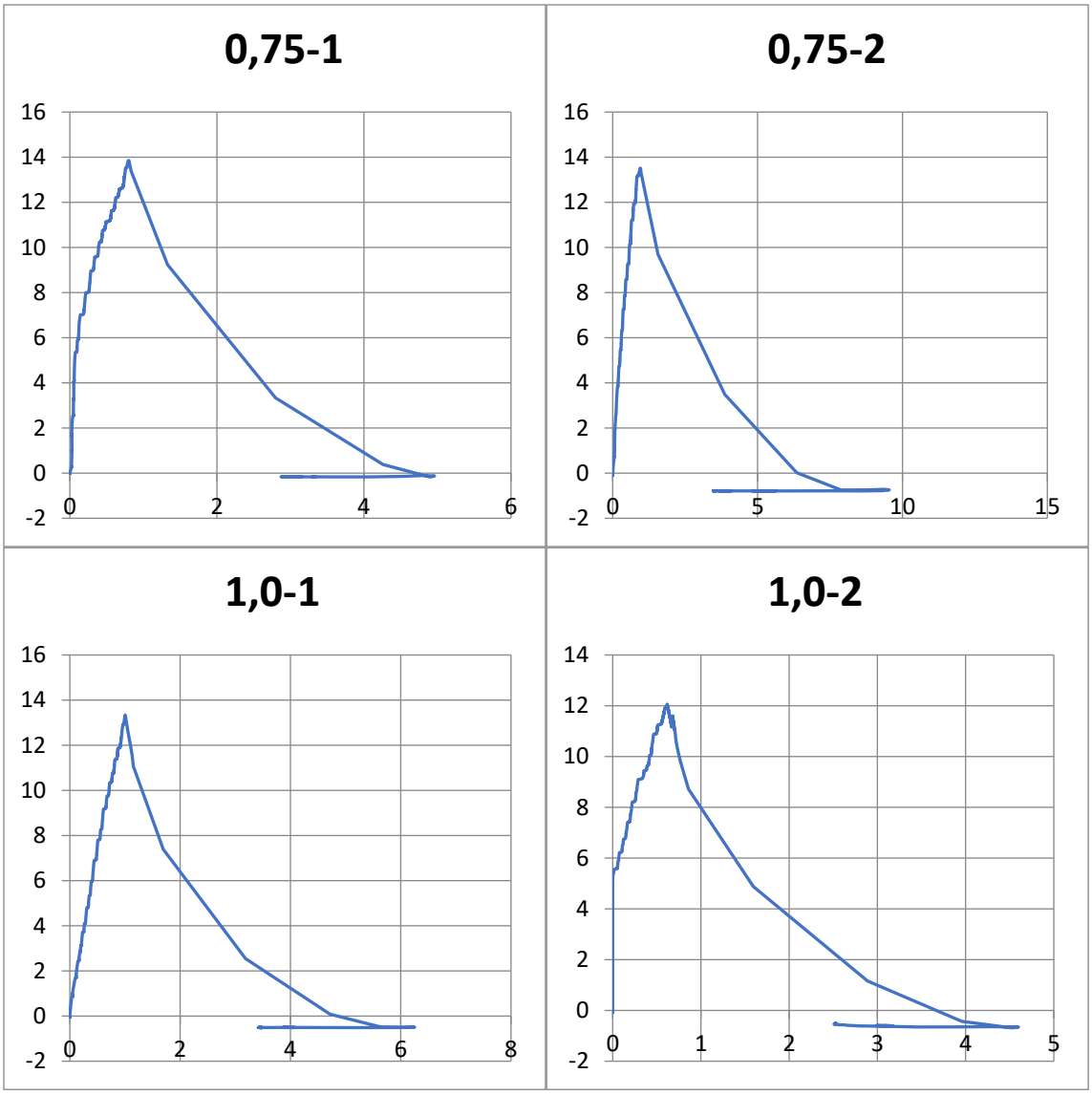
0,75-1
16
14
12
10
8
6
4
2
0
-2
0
2
4
6
0,75-2
16
14
12
10
8
6
4
2
0
-2
0
5
10
15
1,0-1
16
14
12
10
8
6
4
2
0
-2
0
2
4
6
8
1,0-2
14
12
10
8
6
4
2
0
-2
0
1
2
3
4
5

Test batch 8 (ternary blend 7 day)

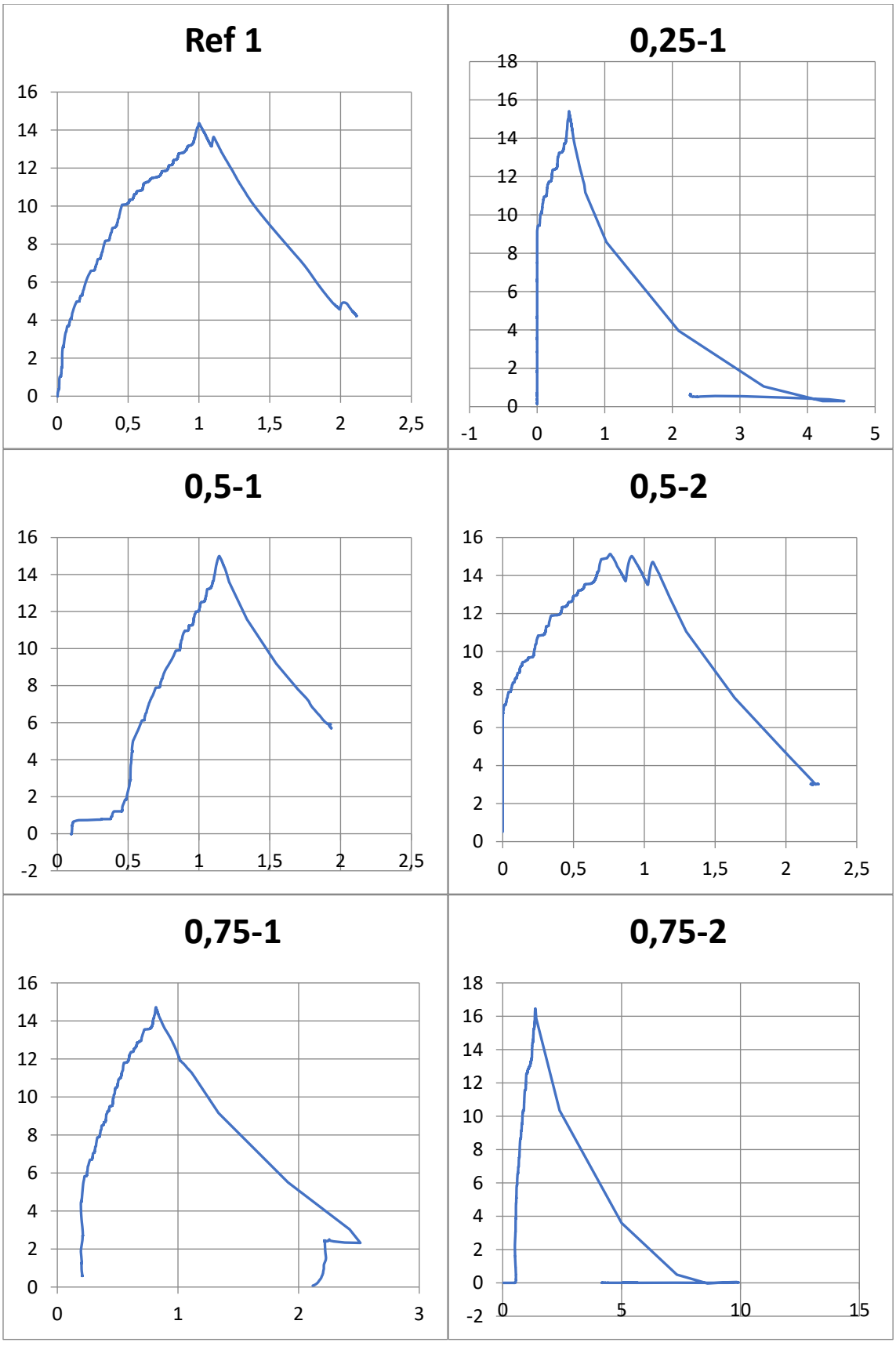

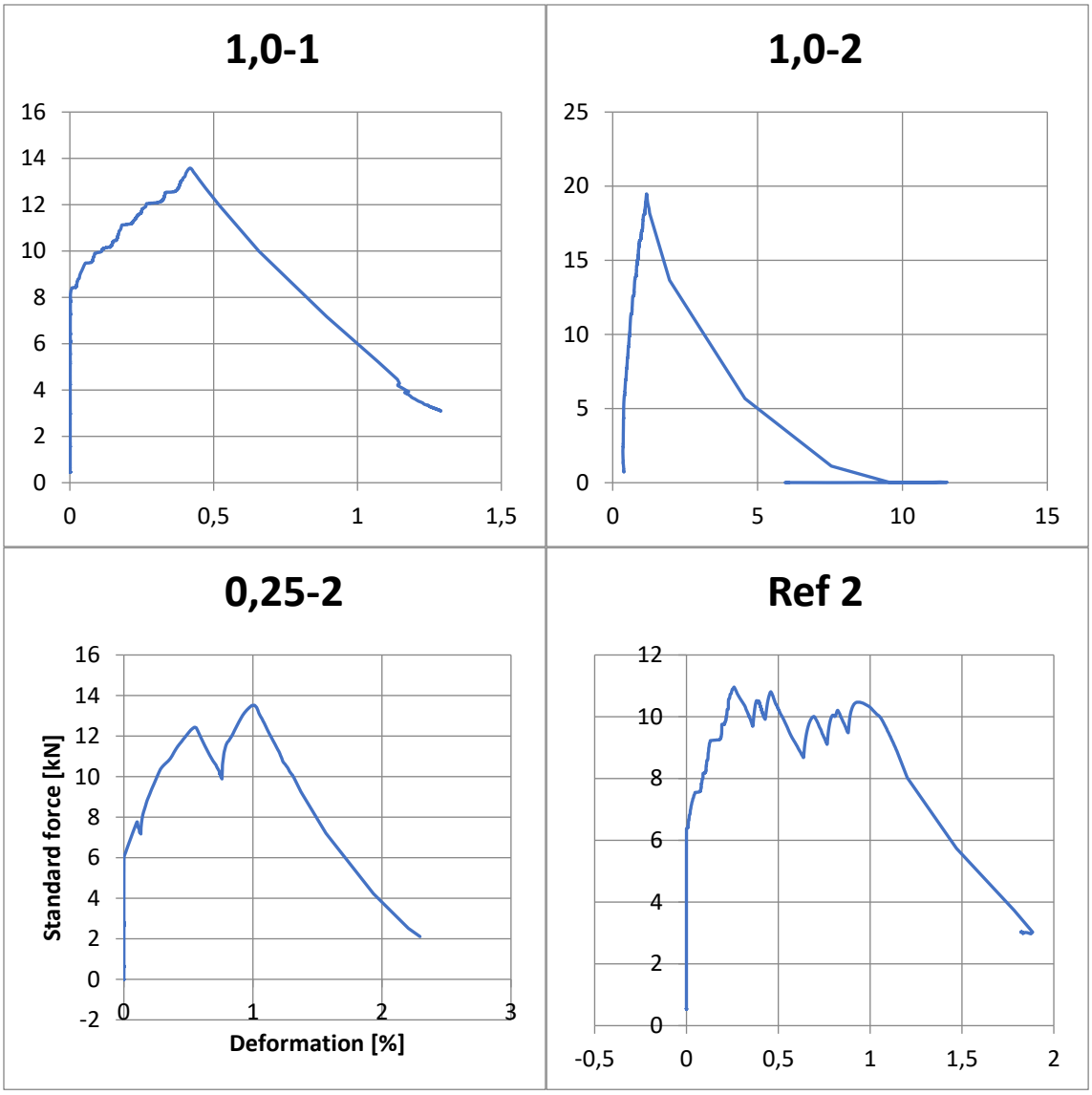
1,0-1
16
14
12
10
8
6
4
2
0
0
0,5
1
1,5
1,0-2
25
20
15
10
5
0
0
5
10
15
0,25-2
Standard force [kN]
16
14
12
10
8
6
4
2
0
-2
0
1
2
3
Deformation [%]
Ref 2
12
10
8
6
4
2
0
-0,5
0
0,5
1
1,5
2

Test Batch 9 (ternary blend 28 day)

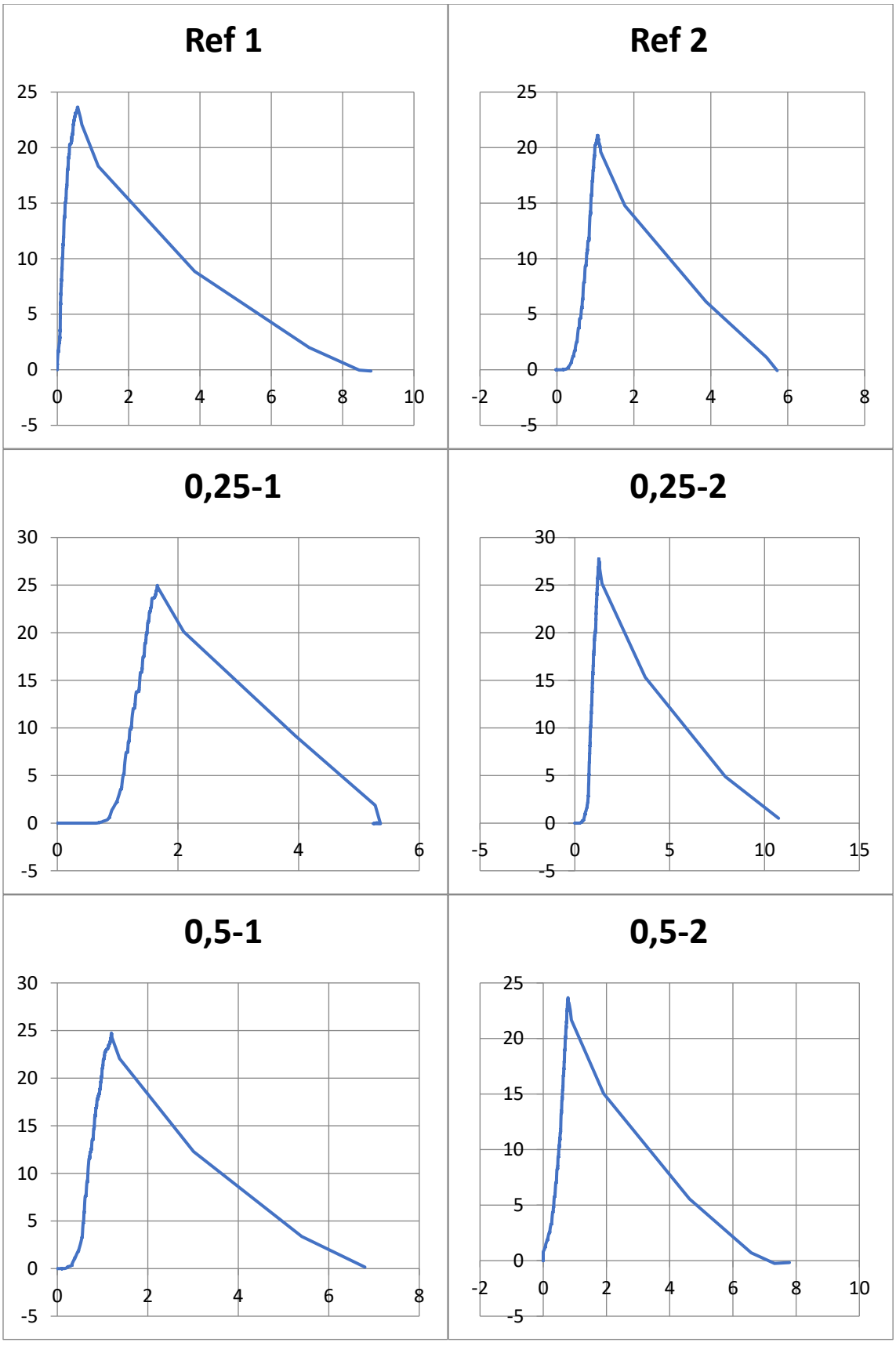

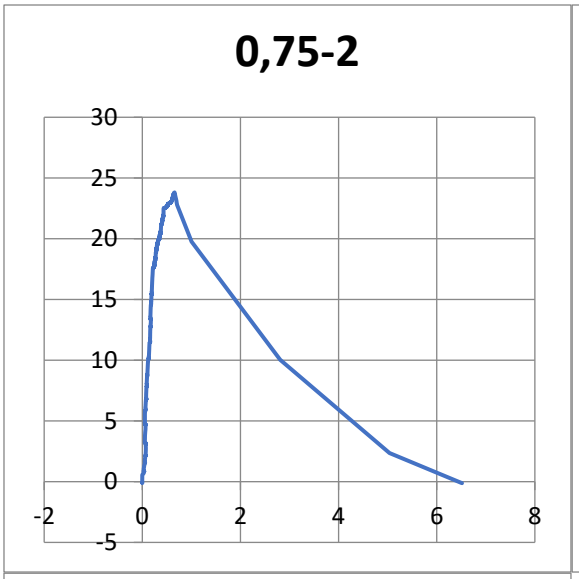
0,75-2
30
25
20
15
10
5
0
-5
-2
0
2
4
6
8

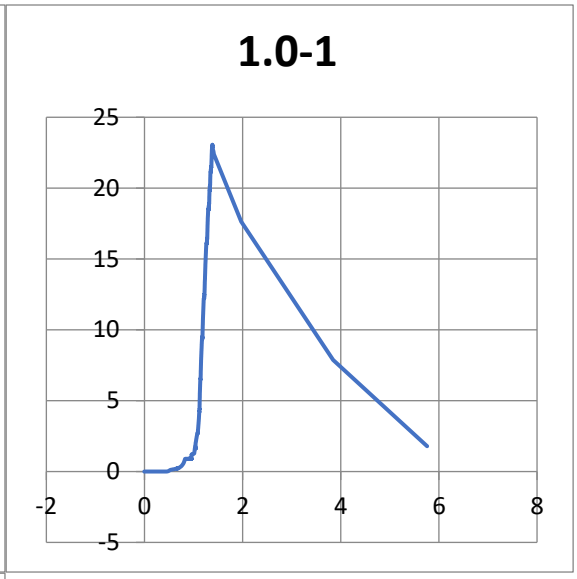
1.0-1
25
20
15
10
5
0
-5
-2
0
2
4
6
8

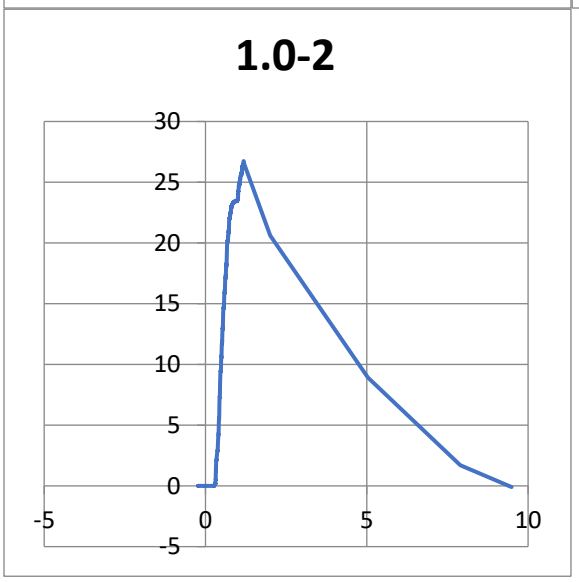
1.0-2
30
25
20
15
10
5
0
-5
-5
0
5
10

Test Batch 10 (FA 3 days)

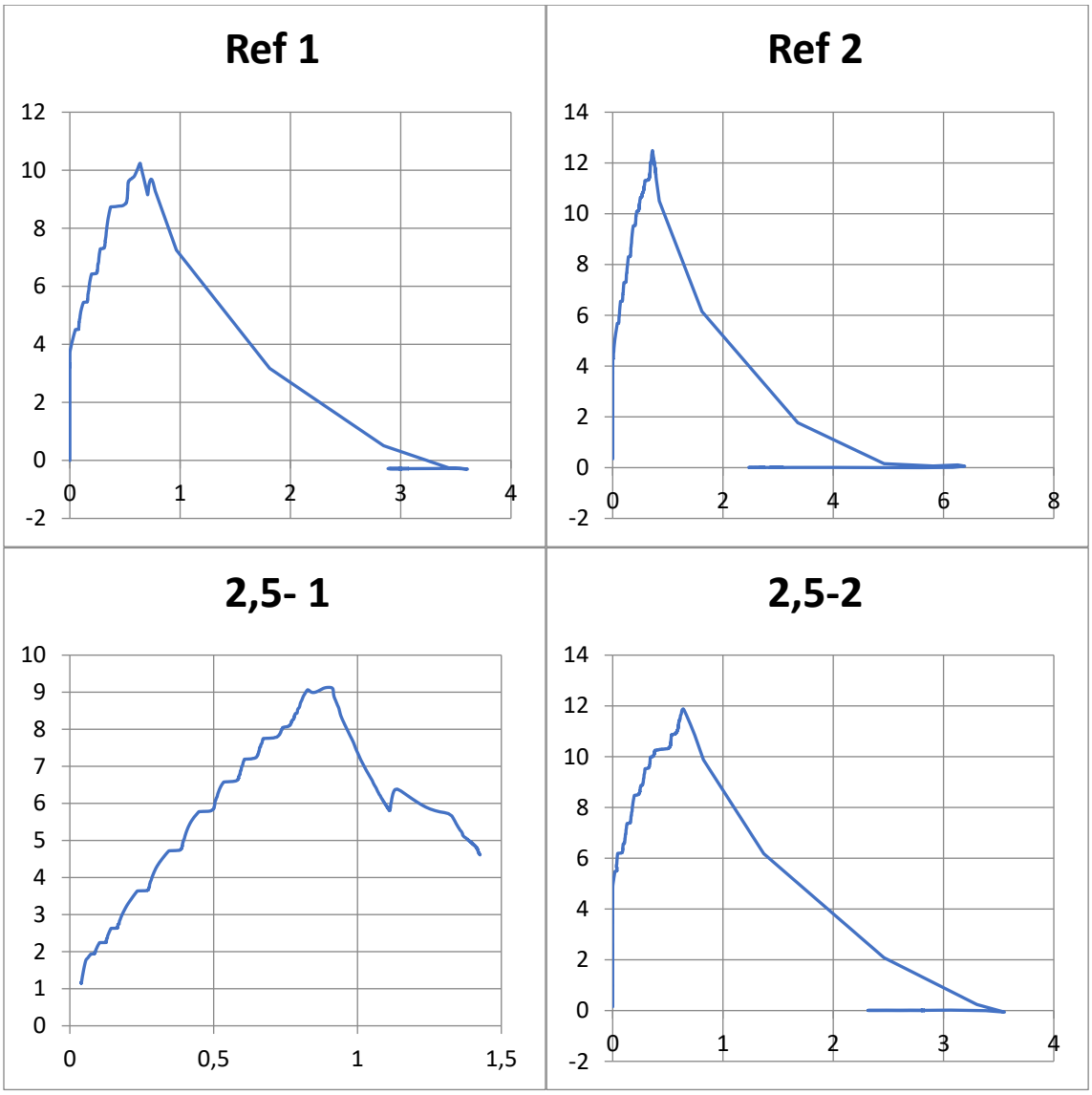

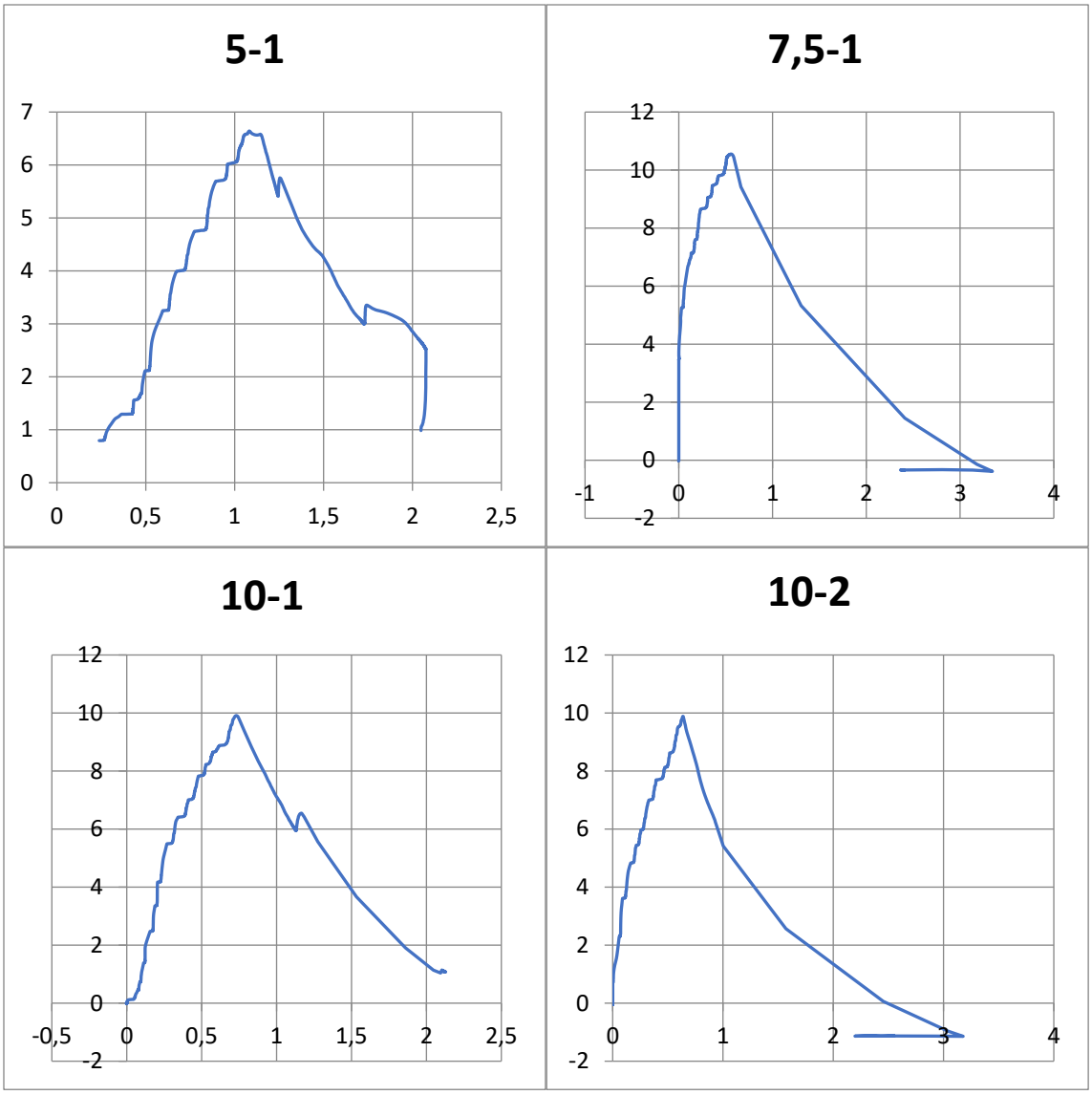
5-1
7,5-1
10-1
10-2

Test Batch 11 (FA 7 day)

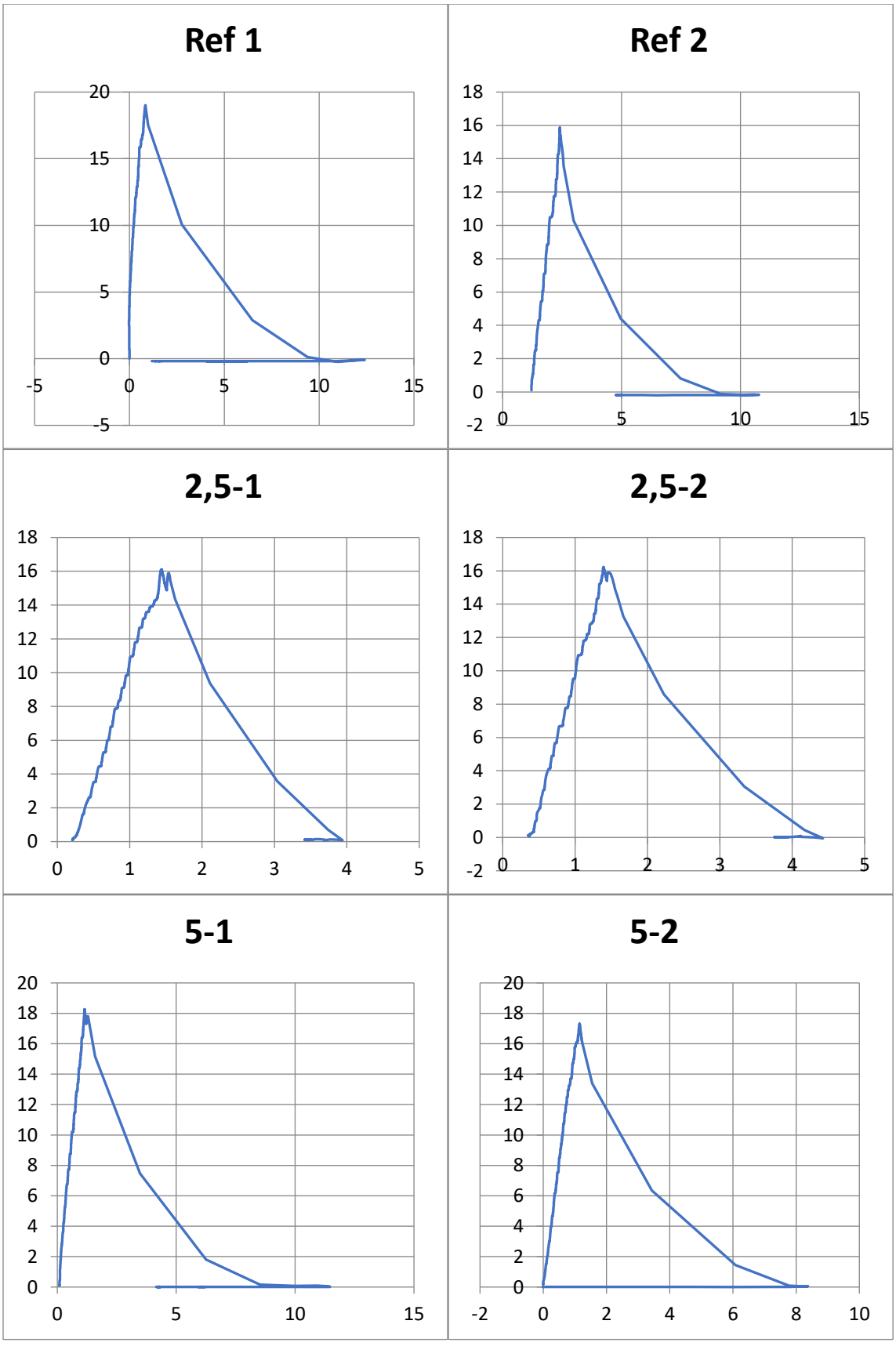

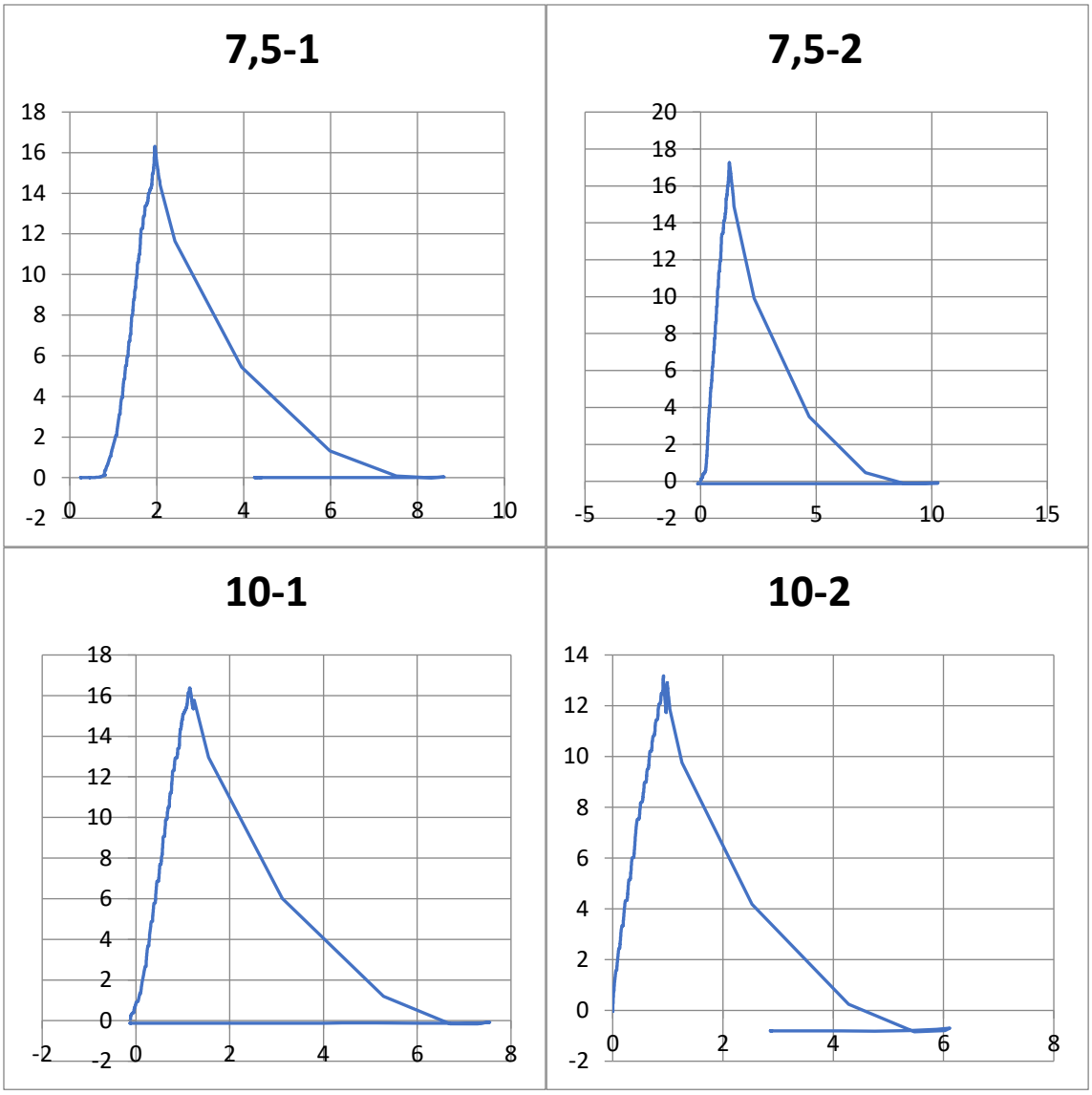
7,5-1
18
16
14
12
10
8
6
4
2
0
-2
0
2
4
6
8
10
7,5-2
20
18
16
14
12
10
8
6
4
2
0
-2
-5
0
5
10
15
10-1
18
16
14
12
10
8
6
4
2
0
-2
-2
0
2
4
6
8
10-2
14
12
10
8
6
4
2
0
-2
0
2
4
6
8

Test batch 12(Fly ash 28 day)

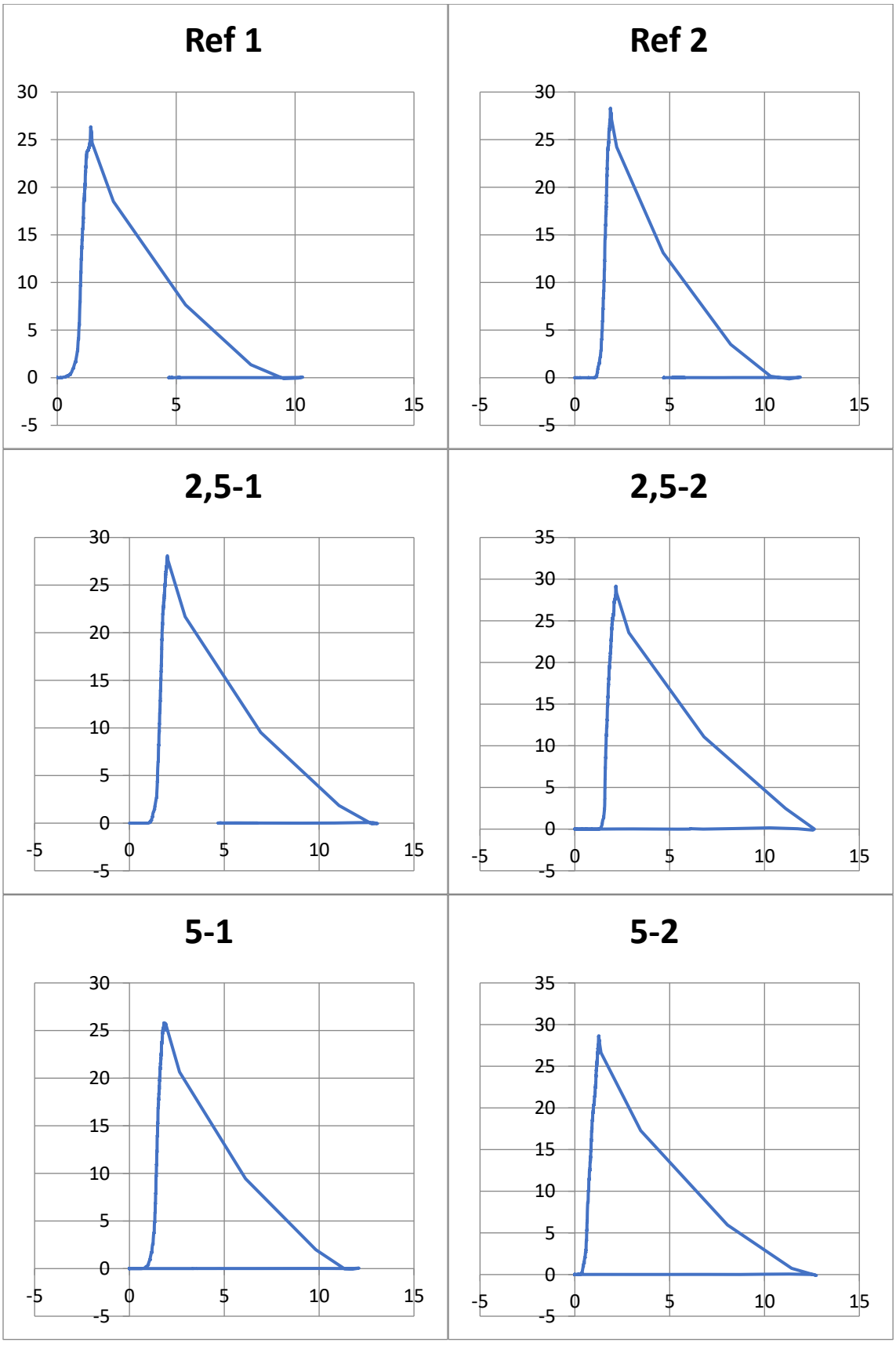

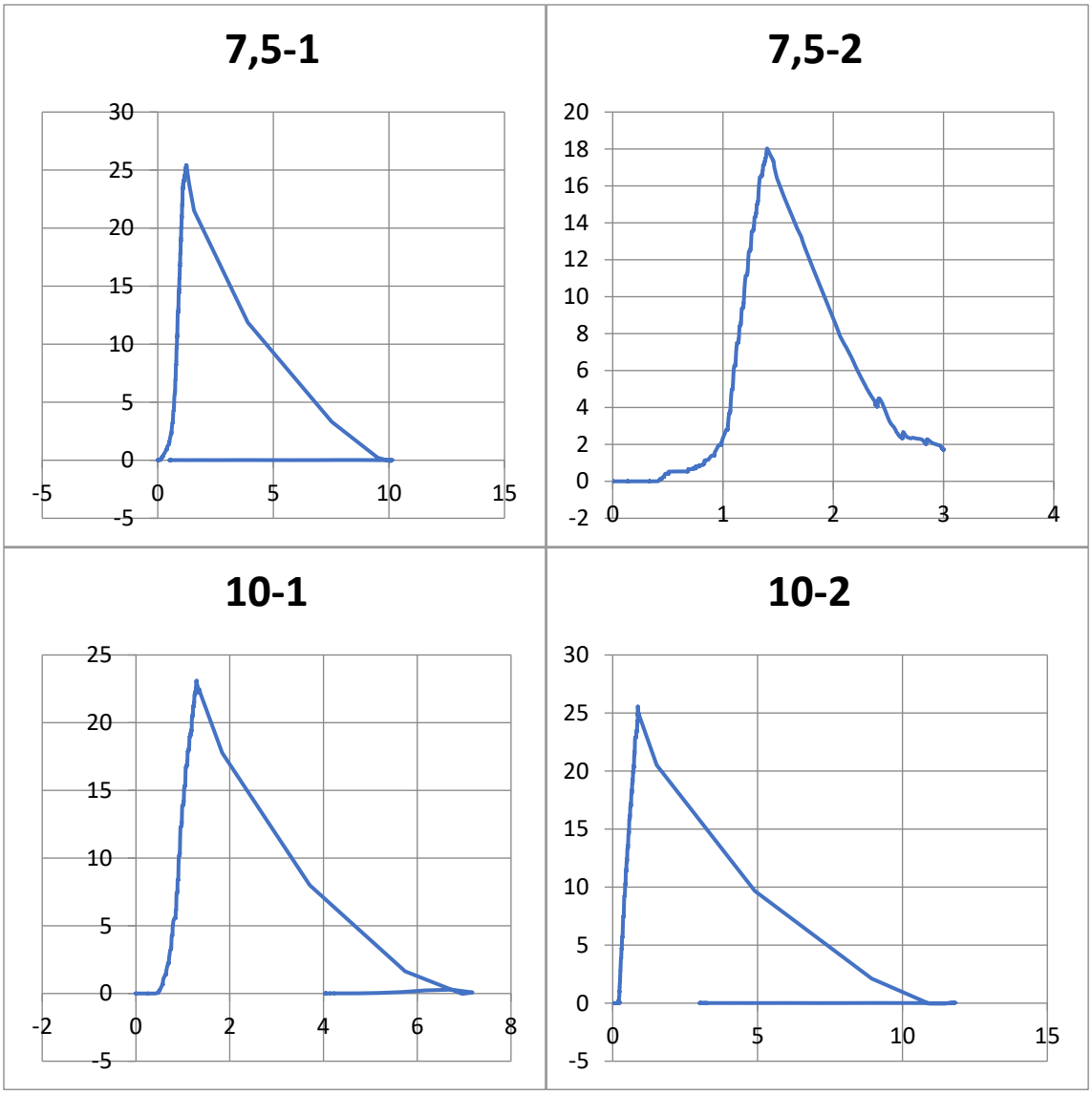
7,5-1
30
25
20
15
10
5
0
-5
-5
0
5
10
15
7,5-2
20
18
16
14
12
10
8
6
4
2
0
-2
0
1
2
3
4
10-1
25
20
15
10
5
0
-5
-2
0
2
4
6
8
10-2
30
25
20
15
10
5
0
-5
0
5
10
15

Test batch 13(FA + SiO_2 3 day)

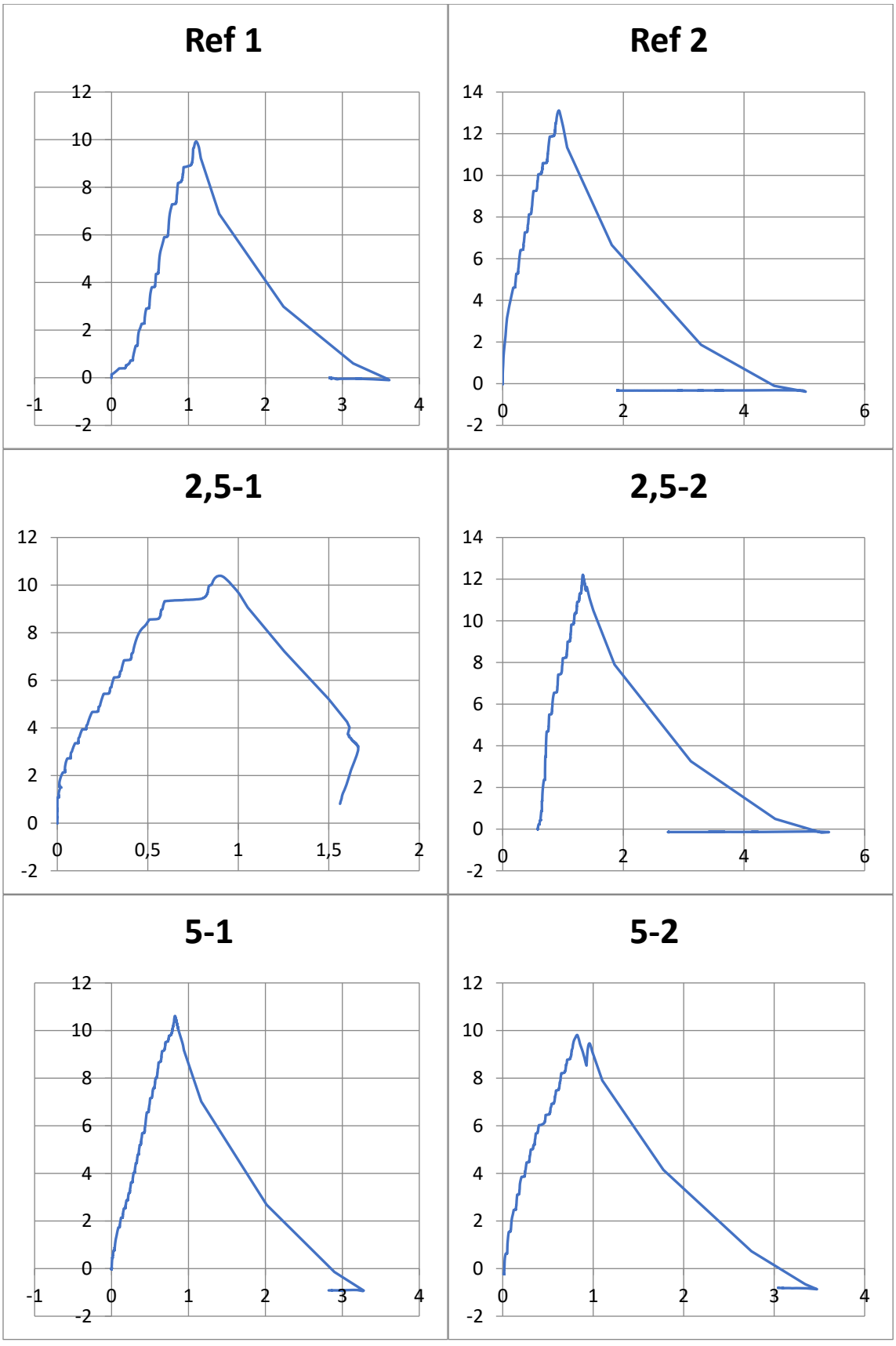

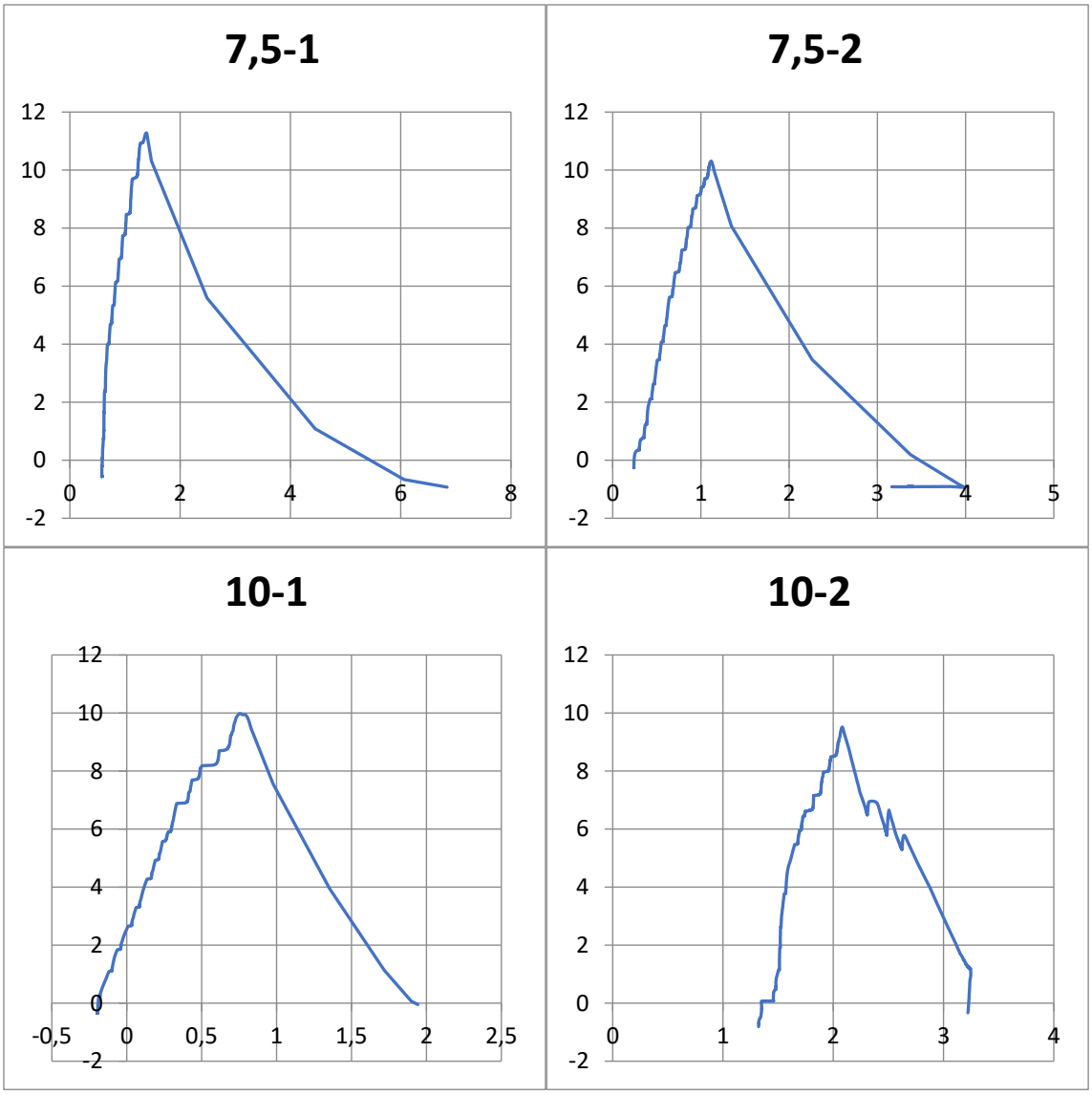
7,5-1
12
10
8
6
4
2
0
-2
0
2
4
6
8
7,5-2
12
10
8
6
4
2
0
-2
0
1
2
3
4
5
10-1
12
10
8
6
4
2
0
-2
-0,5
0
0,5
1
1,5
2
2,5
10-2
12
10
8
6
4
2
0
-2
0
1
2
3
4

Test Batch 14 (7 day FA + SiO_2 blend)

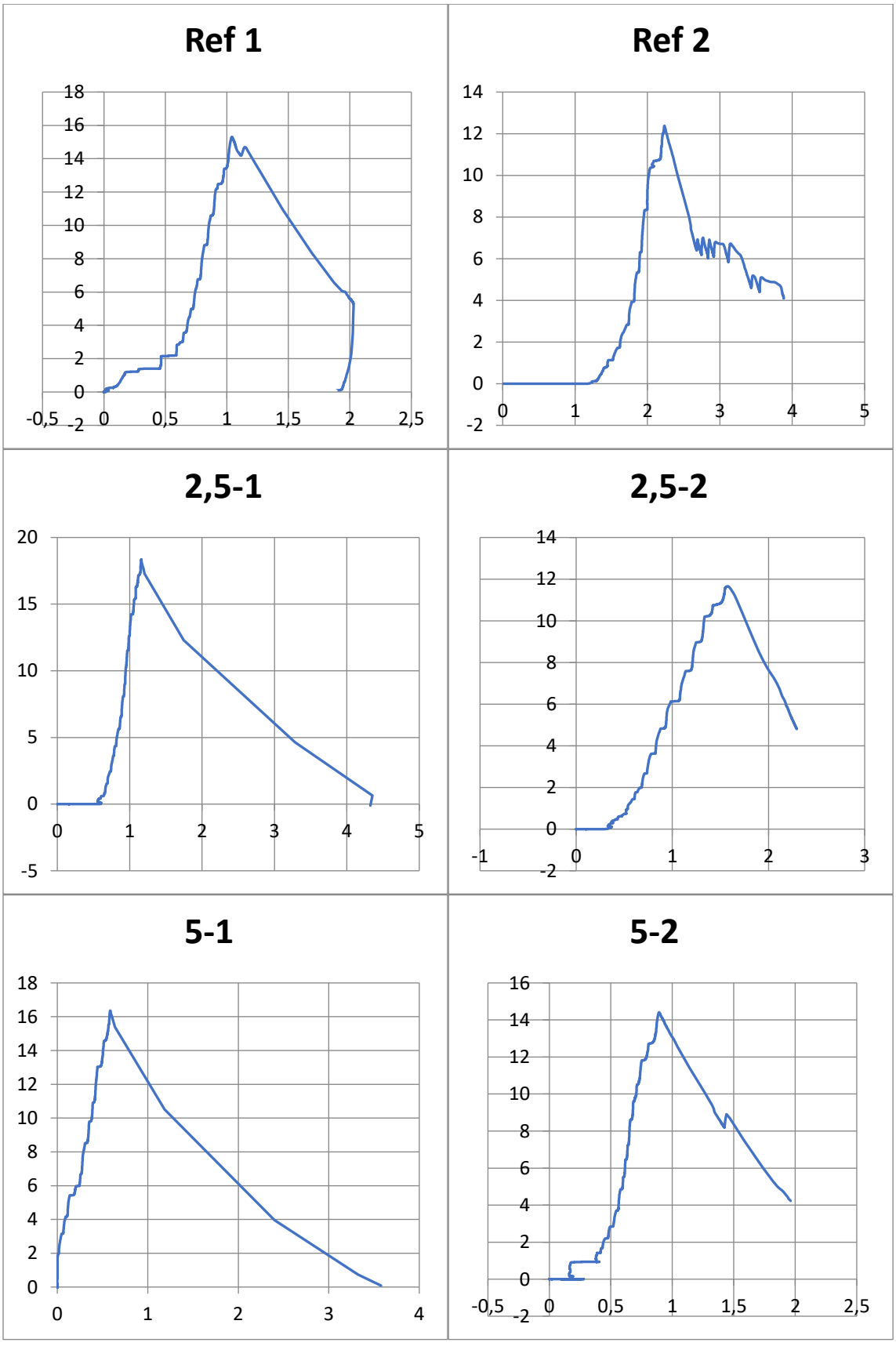

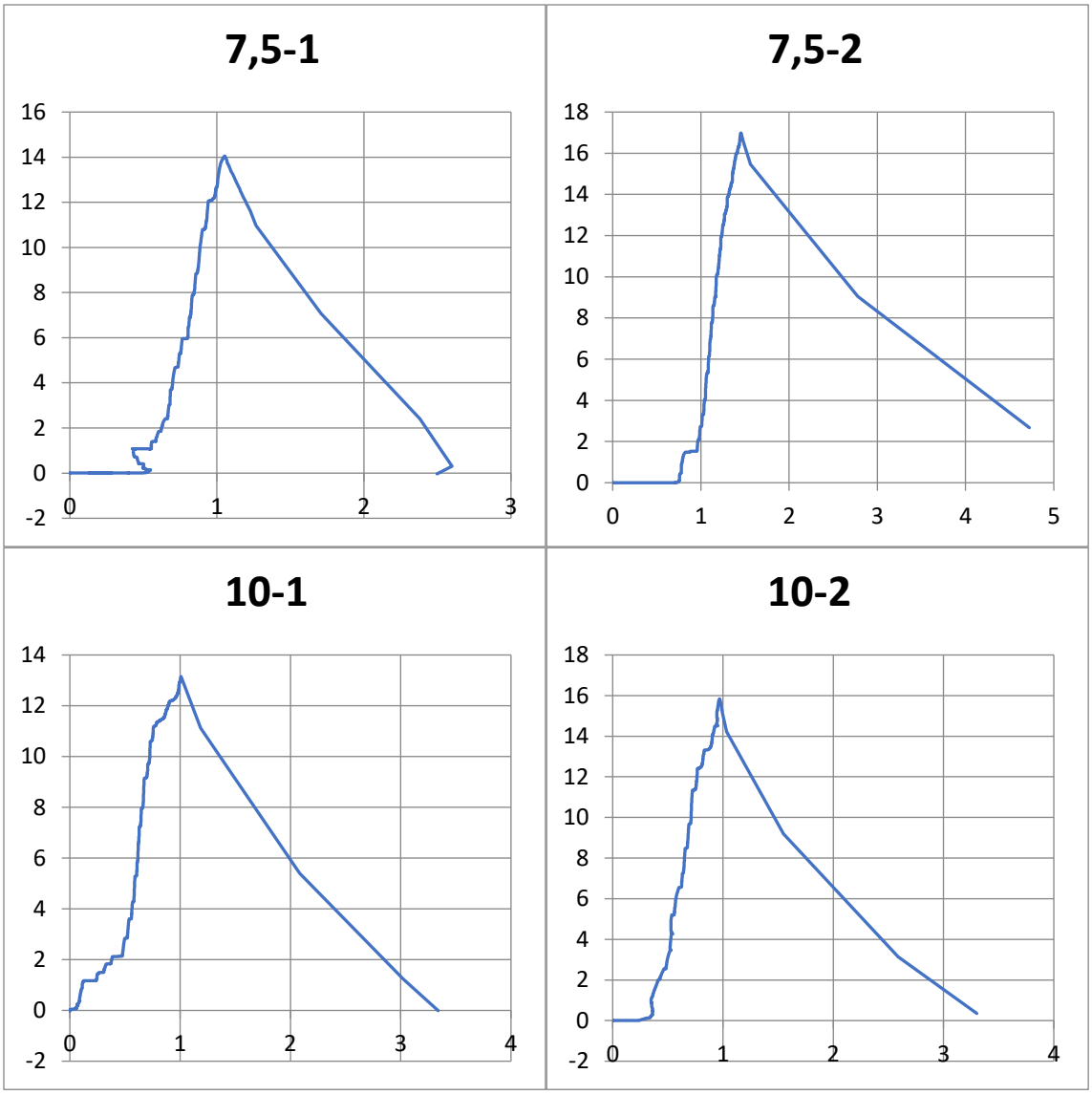
7,5-1
16
14
12
10
8
6
4
2
0
-2
0
1
2
3
7,5-2
18
16
14
12
10
8
6
4
2
0
0
1
2
3
4
5
10-1
14
12
10
8
6
4
2
0
-2
0
1
2
3
4
10-2
18
16
14
12
10
8
6
4
2
0
-2
0
1
2
3
4

Test Batch 15(28 day FA+SiO_2)

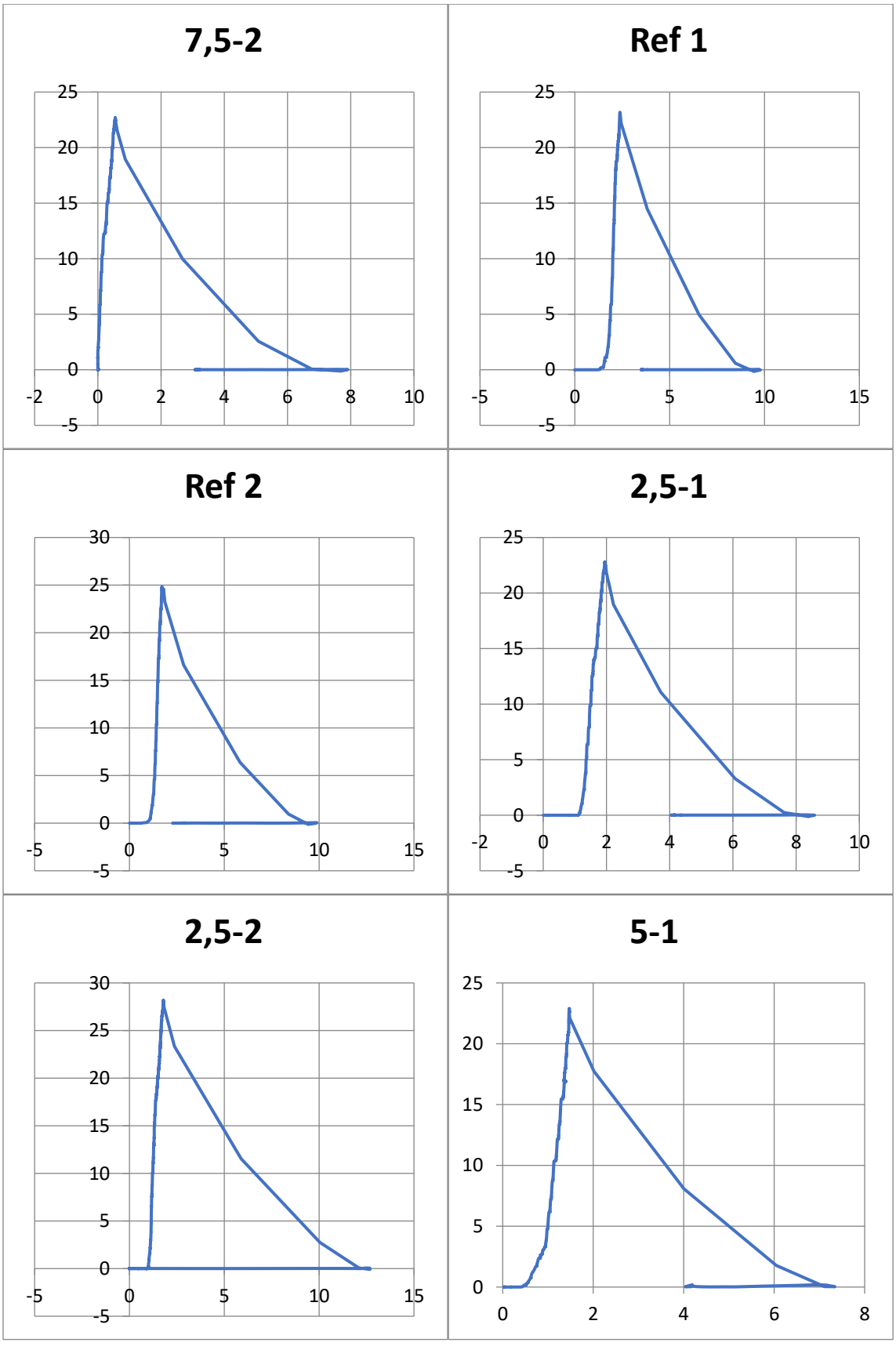

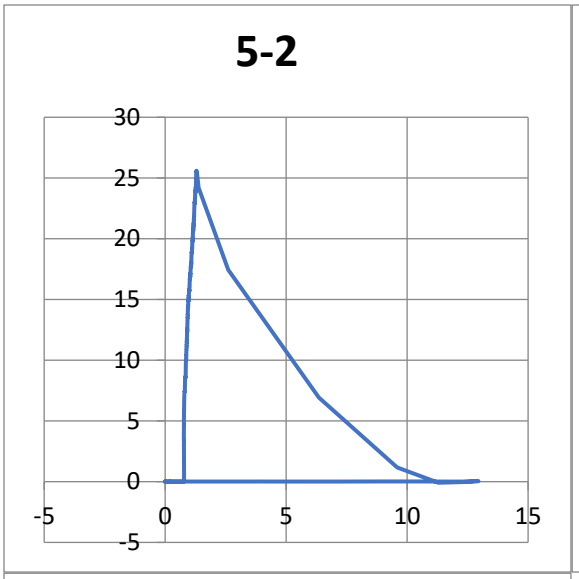
5-2
30
25
20
15
10
5
0
-5
-5
0
5
10
15

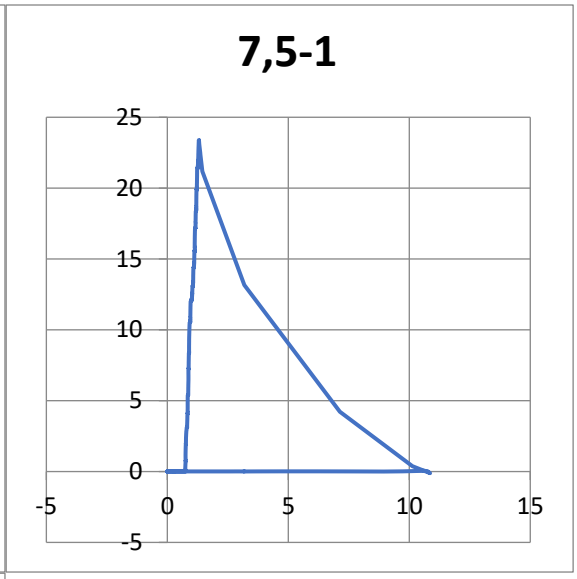
7,5-1
25
20
15
10
5
0
-5
-5
0
5
10
15

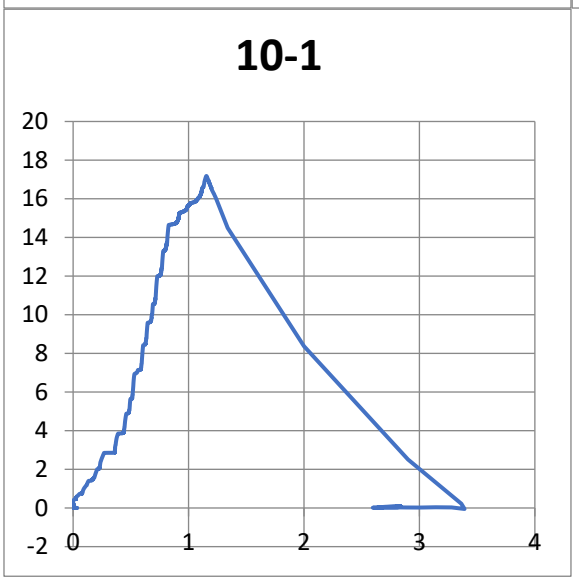
10-1
20
18
16
14
12
10
8
6
4
2
0
-2
0
1
2
3
4

Appendix C – Non-destructive values

Appendix C contains raw data like OD, Length, Mass etc. obtained before destructive testing of the specimens. These values are used to calculate M-modulus and compressional wave velocity

Test Batch 1

Plug #	OD, mm	Length, mm	Mass, g	Volume, m^3	Sonic, µs	Density, kg/m^3	Velocity, m/s	Modulus of Elasticity(M), GPa
ref 1-1	33,01	64,83	105,32	5,54826E-05	22,5	1898	2881	15,8
ref 1-2	33,01	64,73	104,918	5,5397E-05	21,9	1894	2956	16,5
0.35-1	33,01	64,76	107,258	5,54227E-05	22,3	1935	2904	16,3
0.35-2	33,01	63,37	104,063	5,42331E-05	21,5	1919	2947	16,7
0.55-1	33,01	65,23	106,71	5,58249E-05	23,10	1912	2824	15,2
0,55-2	33,01	62,17	102,222	5,32061E-05	21,3	1921	2919	16,4
0.75-1	33,01	60,83	101,097	5,20594E-05	20,2	1942	3011	17,6
0.75-2	33,01	60,9	101,562	5,21193E-05	19,7	1949	3091	18,6
1.0-1	33,01	64,63	105,22	5,53115E-05	21,1	1902	3063	17,8
1.0-2	33,01	62,04	96,732	5,30949E-05	21,8	1822	2846	14,8

Test batch 2

Plug #	OD, mm	Length, mm	Mass, g	Volume, m^3	Sonic, µs	Density, kg/m^3	Velocity, m/s	Modulus of Elasticity(M), GPa
ref 1-1	33,01	64,49	106,54	5,51916E-05	22,5	1930	2866	15,9
ref 1-2	33,01	63,44	105,729	5,4293E-05	21,9	1947	2897	16,3
0.35-1	33,01	63,64	103,547	5,44642E-05	22,3	1901	2854	15,5
0.35-2	33,01	62,64	102,652	5,36084E-05	21,5	1915	2913	16,3
0.55-1	33,01	64,49	106,326	5,51916E-05	23,10	1926	2792	15,0
0,55-2	33,01	63,87	105,411	5,4661E-05	21,3	1928	2999	17,3
0.75-1	33,01	62,78	102,846	5,37282E-05	20,2	1914	3108	18,5
0.75-2	33,01	66,83	108,828	5,71943E-05	19,7	1903	3392	21,9
1.0-1	33,01	65,02	106,846	5,56452E-05	21,1	1920	3082	18,2
1.0-2	33,01	64,71	105,823	5,53799E-05	21,8	1911	2968	16,8

Test batch 3

Plug #	OD, mm	Length, mm	Mass, g	Volume, m^3	Sonic, µs	Density, kg/m^3	Velocity, m/s	Modulus of Elasticity(M), GPa
ref 1-1	33,01	67,45	107,7	5,77249E-05	19,6	1866	3441	22,1
ref 1-2	33,01	66,62	107,03	5,70145E-05	19,4	1877	3434	22,1
0.35-1	33,01	67,25	105,31	5,75537E-05	19,6	1830	3431	21,5
0.35-2	33,01	67,48	108,3	5,77505E-05	19	1875	3552	23,7
0.55-1	33,01	67,64	107,49	5,78875E-05	19,90	1857	3399	21,5
0,55-2	33,01	67,32	108,14	5,76136E-05	20,1	1877	3349	21,1
0.75-1	33,01	67,24	106,4	5,75451E-05	19,3	1849	3484	22,4
0.75-2	33,01	67,57	108,18	5,78276E-05	19,2	1871	3519	23,2
1.0-1	33,01	67,56	107,16	5,7819E-05	20,4	1853	3312	20,3
1.0-2	33,01	67,22	108,31	5,7528E-05	19,7	1883	3412	21,9

Test batch 4

Plug #	OD, mm	Length, mm	Mass, g	Volume, m^3	Sonic, µs	Density, kg/m^3	Velocity, m/s	Modulus of Elasticity(M), GPa
ref 1-1	33,01	67,44	108,741	5,77163E-05	23,1	1884	2919	16,1
ref 1-2	33,01	67,15	109,487	5,74681E-05	22,9	1905	2932	16,4
0.25-1	33,01	68,35	108,775	5,84951E-05	24	1860	2848	15,1
0.25-2	33,01	67,93	109,052	5,81357E-05	23,1	1876	2941	16,2
0.5-1	33,01	67,9	109,438	5,811E-05	22,50	1883	3018	17,2
0,5-2	33,01	67,24	109,365	5,75451E-05	23,3	1901	2886	15,8
0.75-1	33,01	68,18	110,663	5,83496E-05	22,8	1897	2990	17,0
0.75-2	33,01	67,63	110,295	5,78789E-05	22,5	1906	3006	17,2
1.0-1	33,01	67,85	110,317	5,80672E-05	22,4	1900	3029	17,4
1.0-2	33,01	67,22	107,089	5,7528E-05	22,4	1862	3001	16,8

Test batch 5

Plug #	OD, mm	Length, mm	Mass, g	Volume, m^3	Sonic, µs	Density, kg/m^3	Velocity , m/s	Modulus of Elasticity(M), GPa
ref 1-1	33,01	67,58	109,568	5,78361E-05	21,9	1894	3086	18,0
ref 1-2	33,01	67,58	110,183	5,78361E-05	22	1905	3072	18,0
0.25-1	33,01	67,43	108,634	5,77077E-05	21,3	1882	3166	18,9
0.25-2	33,01	67,57	110,589	5,78276E-05	21,1	1912	3202	19,6
0.5-1	33,01	67,48	109,743	5,77505E-05	21,50	1900	3139	18,7
0,5-2	33,01	66,92	108,965	5,72713E-05	21,1	1903	3172	19,1
0.75-1	33,01	67,72	109,478	5,79559E-05	21,5	1889	3150	18,7
0.75-2	33,01	67,5	109,999	5,77677E-05	21,8	1904	3096	18,3
1.0-1	33,01	68,99	111,356	5,90428E-05	22,1	1886	3122	18,4
1.0-2	33,01	67,77	109,338	5,79987E-05	22	1885	3080	17,9

Test batch 6

Plug #	OD, mm	Length, mm	Mass, g	Volume, m^3	Sonic, µs	Density, kg/m^3	Velocity, m/s	Modulus of Elasticity(M), GPa
ref 1-1	33,01	67,3	107,76	5,75965E-05	20,5	1871	3283	20,2
ref 1-2	33,01	67,52	108,62	5,77848E-05	20	1880	3376	21,4
0.25-1	33,01	67,4	108,05	5,76821E-05	20,5	1873	3288	20,2
0.25-2	33,01	67,65	108,81	5,7896E-05	20,2	1879	3349	21,1
0.5-1	33,01	67,18	106,91	5,74938E-05	21,50	1860	3125	18,2
0,5-2	33,01	67,45	109,65	5,77249E-05	20,3	1900	3323	21,0
0.75-1	33,01	67,41	106,7	5,76906E-05	21,4	1850	3150	18,4
0.75-2	33,01	67,43	108,92	5,77077E-05	20,3	1887	3322	20,8
1.0-1	33,01	67,23	107,59	5,75366E-05	20,5	1870	3280	20,1
1.0-2	33,01	67,58	107,67	5,78361E-05	20,6	1862	3281	20,0

Test Batch 7

Plug #	OD, mm	Length, mm	Mass, g	Volume, m^3	Sonic, µs	Density, kg/m^3	Velocity, m/s	Modulus of Elasticity(M), GPa
ref 1-1	33,01	69,13	112,566	5,91626E-05	24,5	1903	2822	15,1
ref 1-2	33,01	67,56	111,914	5,7819E-05	22,9	1936	2950	16,8
0.25-1	33,01	69,13	114,58	5,91626E-05	23,7	1937	2917	16,5
0.25-2	33,01	67,35	111,545	5,76393E-05	22,8	1935	2954	16,9
0.5-1	33,01	67,62	111,707	5,78703E-05	22,90	1930	2953	16,8
0 5-2	33,01	68,64	113,551	5,87433E-05	23,5	1933	2921	16,5
0.75-1	33,01	67,17	110,389	5,74852E-05	22,9	1920	2933	16,5
0.75-2	33,01	67,47	111,333	5,7742E-05	23,2	1928	2908	16,3
1.0-1	33,01	67,51	110,563	5,77762E-05	22,9	1914	2948	16,6
1.0-2	33,01	67,85	111,128	5,80672E-05	23,3	1914	2912	16,2

Test batch 8

Plug #	OD, mm	Length, mm	Mass, g	Volume, m^3	Sonic, µs	Density, kg/m^3	Velocity, m/s	Modulus of Elasticity(M), GPa
ref 1-1	33,01	68,37	111,92	5,85122E-05	20,4	1913	3351	21,5
ref 1-2	33,01	68,42	111,49	5,8555E-05	20,9	1904	3274	20,4
0.25-1	33,01	68,38	110,22	5,85208E-05	20,5	1883	3336	21,0
0.25-2	33,01	68,32	111,42	5,84694E-05	20,5	1906	3333	21,2
0.5-1	33,01	67,01	109,42	5,73483E-05	19,20	1908	3490	23,2
0,5-2	33,01	68,14	112,45	5,83154E-05	20,5	1928	3324	21,3
0.75-1	33,01	67,85	109,59	5,80672E-05	19,8	1887	3427	22,2
0.75-2	33,01	68,29	110,37	5,84437E-05	19,9	1888	3432	22,2
1.0-1	33,01	68,48	111,75	5,86064E-05	20,9	1907	3277	20,5
1.0-2	33,01	67,73	110,83	5,79645E-05	20,1	1912	3370	21,7

Test batch 9

Plug #	OD, mm	Length, mm	Mass, g	Volume, m^3	Sonic, µs	Density, kg/m^3	Velocity, m/s	Modulus of Elasticity(M), GPa
ref 1-1	33,01	67,66	109,3	5,79046E-05	19,2	1888	3524	23,4
ref 1-2	33,01	66,74	106,12	5,71172E-05	20,1	1858	3320	20,5
0.25-1	33,01	67,34	108,44	5,76307E-05	19,3	1882	3489	22,9
0.25-2	33,01	67,18	108,82	5,74938E-05	19,2	1893	3499	23,2
0.5-1	33,01	67,21	108,79	5,75195E-05	19,20	1891	3501	23,2
0,5-2	33,01	67,56	109,26	5,7819E-05	19,3	1890	3501	23,2
0.75-1	33,01	66,95	107,28	5,7297E-05	19,4	1872	3451	22,3
0.75-2	33,01	67,07	108,92	5,73996E-05	19,9	1898	3370	21,6
1.0-1	33,01	67,74	108,47	5,7973E-05	19,3	1871	3510	23,0
1.0-2	33,01	67,67	109,78	5,79131E-05	19,6	1896	3453	22,6

Test batch 10

Plug #	OD, mm	Length, mm	Mass, g	Volume, m^3	Sonic, µs	Density, kg/m^3	Velocity, m/s	Modulus of Elasticity(M), GPa
ref 1-1	33,01	69,56	113,153	5,95306E-05	24,1	1901	2886	15,8
ref 1-2	33,01	67,81	110,338	5,8033E-05	23,7	1901	2861	15,6
2.5-1	33,01	66,8	108,059	5,71686E-05	23,6	1890	2831	15,1
2.5-2	33,01	69,72	113,44	5,96676E-05	24,5	1901	2846	15,4
5-1	33,01	67,37	107,387	5,76564E-05	24,20	1863	2784	14,4
5-2	33,01	67,1	108,827	5,74253E-05	23,7	1895	2831	15,2
7.5-1	33,01	67,2	109,348	5,75109E-05	24,1	1901	2788	14,8
7.5-2	33,01	68,12	110,318	5,82983E-05	24,3	1892	2803	14,9
10-1	33,01	67,81	109,089	5,8033E-05	23,7	1880	2861	15,4
10-2	33,01	67,34	109,712	5,76307E-05	23,7	1904	2841	15,4

Test batch 11

Plug #	OD, mm	Length, mm	Mass, g	Volume, m^3	Sonic, µs	Density, kg/m^3	Velocity, m/s	Modulus of Elasticity(M), GPa
ref 1-1	33,01	67,85	110,521	5,80672E-05	20,1	1903	3376	21,7
ref 1-2	33,01	67,31	110,269	5,7605E-05	19,3	1914	3488	23,3
2.5-1	33,01	67,63	109,402	5,78789E-05	20	1890	3382	21,6
2.5-2	33,01	67,55	109,099	5,78104E-05	20,2	1887	3344	21,1
5-1	33,01	67,45	108,844	5,77249E-05	19,40	1886	3477	22,8
5-2	33,01	67,77	109,963	5,79987E-05	20	1896	3389	21,8
7.5-1	33,01	67,67	109,193	5,79131E-05	20,1	1885	3367	21,4
7.5-2	33,01	67,61	109,322	5,78618E-05	20,1	1889	3364	21,4
10-1	33,01	67,47	109,108	5,7742E-05	20,1	1890	3357	21,3
10-2	33,01	67,44	108,28	5,77163E-05	20,3	1876	3322	20,7

Test batch 12

Plug #	OD, mm	Length, mm	Mass, g	Volume, m^3	Sonic, µs	Density, kg/m^3	Velocity, m/s	Modulus of Elasticity(M), GPa
ref 1-1	33,01	67,25	108,76	5,75537E-05	18,6	1890	3616	24,7
ref 1-2	33,01	67,35	109,63	5,76393E-05	19,1	1902	3526	23,6
2.5-1	33,01	67,41	109,73	5,76906E-05	18,8	1902	3586	24,5
2.5-2	33,01	66,45	108,88	5,6869E-05	18,2	1915	3651	25,5
5-1	33,01	67,24	109,33	5,75451E-05	18,80	1900	3577	24,3
5-2	33,01	66,94	108,49	5,72884E-05	18,9	1894	3542	23,8
7.5-1	33,01	67,39	107,77	5,76735E-05	20,1	1869	3353	21,0
7.5-2	33,01	67,15	108,4	5,74681E-05	19,6	1886	3426	22,1
10-1	33,01	67,08	106,51	5,74082E-05	19,7	1855	3405	21,5
10-2	33,01	67,38	108,33	5,7665E-05	19,5	1879	3455	22,4

Test batch 13

Plug #	OD, mm	Length, mm	Mass, g	Volume, m^3	Sonic, µs	Density, kg/m^3	Velocity, m/s	Modulus of Elasticity(M), GPa
ref 1-1	33,01	67,45	106,003	5,77249E-05	24,7	1836	2731	13,7
ref 1-2	33,01	67,63	108,483	5,78789E-05	23,7	1874	2854	15,3
2.5-1	33,01	68,08	108,352	5,8264E-05	23,4	1860	2909	15,7
2.5-2	33,01	67,27	109,606	5,75708E-05	23,4	1904	2875	15,7
5-1	33,01	67,67	109,472	5,79131E-05	23,70	1890	2855	15,4
5-2	33,01	67,11	108,195	5,74339E-05	24,1	1884	2785	14,6
7.5-1	33,01	67,08	108,554	5,74082E-05	23,1	1891	2904	15,9
7.5-2	33,01	67,19	108,431	5,75023E-05	23,8	1886	2823	15,0
10-1	33,01	67,3	109,23	5,75965E-05	23,9	1896	2816	15,0
10-2	33,01	65,45	105,849	5,60132E-05	22,9	1890	2858	15,4

Test batch 14

Plug #	OD, mm	Length, mm	Mass, g	Volume, m^3	Sonic, µs	Density, kg/m^3	Velocity, m/s	Modulus of Elasticity(M), GPa
ref 1-1	33,01	67,08	105,72	5,74082E-05	20,9	1842	3210	19,0
ref 1-2	33,01	66,9	107,21	5,72542E-05	22	1873	3041	17,3
2.5-1	33,01	67,2	106,964	5,75109E-05	21,7	1860	3097	17,8
2.5-2	33,01	67,45	107,46	5,77249E-05	22,1	1862	3052	17,3
5-1	33,01	67,34	107,264	5,76307E-05	21,80	1861	3089	17,8
5-2	33,01	67,42	107,18	5,76992E-05	22	1858	3065	17,4
7.5-1	33,01	67,17	105,198	5,74852E-05	22,1	1830	3039	16,9
7.5-2	33,01	67,44	106,463	5,77163E-05	22,4	1845	3011	16,7
10-1	33,01	67,37	103,659	5,76564E-05	22,8	1798	2955	15,7
10-2	33,01	67,72	107,934	5,79559E-05	23	1862	2944	16,1

Test batch 15

Plug #	OD, mm	Length, mm	Mass, g	Volume, m^3	Sonic, µs	Density, kg/m^3	Velocity, m/s	Modulus of Elasticity(M), GPa
ref 1-1	33,01	67,27	108,69	5,75708E-05	18,6	1888	3617	24,7
ref 1-2	33,01	67,24	108,15	5,75451E-05	18	1879	3736	26,2
2.5-1	33,01	67,41	107,59	5,76906E-05	18,6	1865	3624	24,5
2.5-2	33,01	66,45	109,25	5,6869E-05	18,3	1921	3631	25,3
5-1	33,01	67,24	107,52	5,75451E-05	19,00	1868	3539	23,4
5-2	33,01	66,94	108,69	5,72884E-05	18,8	1897	3561	24,1
7.5-1	33,01	67,39	106	5,76735E-05	18,2	1838	3703	25,2
7.5-2	33,01	67,15	108,05	5,74681E-05	18,8	1880	3572	24,0
10-1	33,01	67,08	104,9	5,74082E-05	17,8	1827	3769	26,0
10-2	33,01	67,38	106,93	5,7665E-05	18,7	1854	3603	24,1

Appendix D – Miscellaneous pictures

This section includes miscellaneous pictures snapped during this thesis

The picture below shows a compromised cement specimen. This would occur from time to time

The picture below shows 42 cement plugs curing, each specimen is carefully labelled.

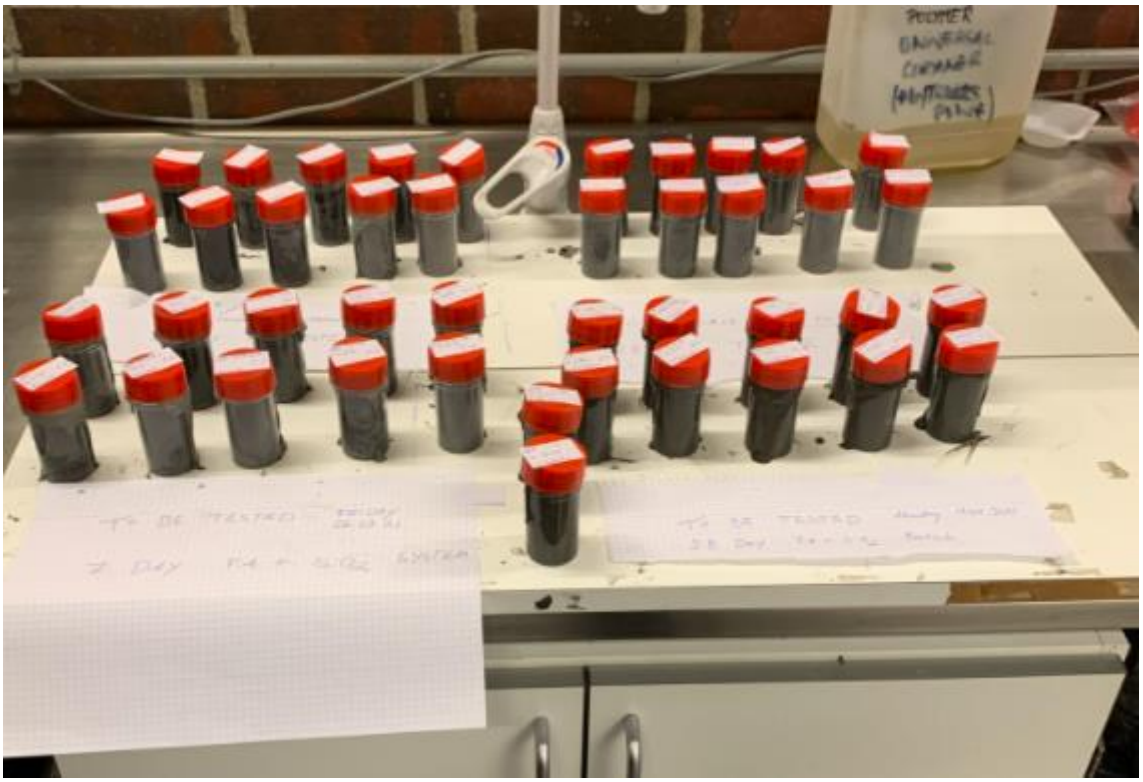

The picture below also shows 10 specimens waiting for their testing day

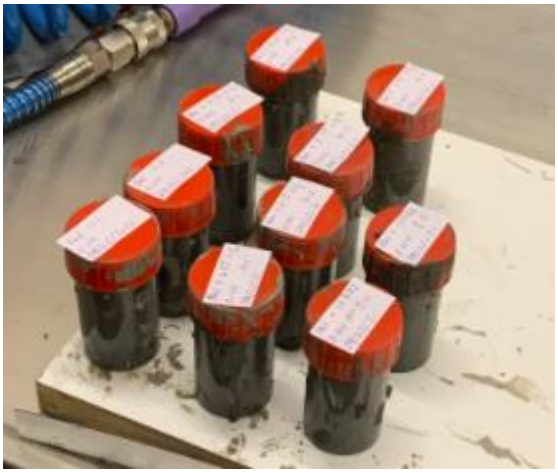

The picture below shows 10 plugs after being levelled on top, and retrieved from their plastic mould